AD NUMBER
AD876023
LIMITATION CHANGES
TO: **Approved for public release; distribution is unlimited.**
FROM: **Distribution: Further dissemination only as directed by Air Force Space and Missile Systems Organization, SMYSE, Norton AFB, CA 92409, AUG 1970, or higher DoD authority.**
AUTHORITY
samso, usaf ltr, 28 feb 1972

SAMSO-TR-70-367

Technical Report
Re-entry System Environmental Protection (RESEP)
Advanced 3D Fabrication Techniques

Final Report

By

A R. Hirasuna
M. L. Damoth
N. M. Harrington
J. R. Stetson
"et al"

Philco-Ford Corporation
WDL Division
Newport Beach, California

Prepared for

Space and Missile Systems Organization
Deputy for Re-entry Systems
Air Force Systems Command
Norton Air Force Base, California

August 1970

SAMSO-TR-70-367

Technical Report
Re-entry System Environmental Protection (RESEP)
Advanced 3D Fabrication Techniques

Final Report

By

A. R. Hirasuna
M. L. Damoth
N. M. Harrington
J. R. Stetson
"et al"

August 1970

PHILCO Ford
Philco-Ford Corporation
WDL Division
Newport Beach, Calif. • 92663

FOREWORD

The technical information reported here has been developed by the Western Development Laboratories Division (WDL) of Philco-Ford Corporation, Newport Beach, California, under Contract F04701-68-C-0183.

The work was sponsored by the Space and Missile Systems Organization, Air Force Systems Command, Norton Air Force Base, California. The Air Force Project Officer was Capt. T. W. Swartz. Mr. S. R. Breshears of Aerospace served as principal technical monitor for the Air Force and he was assisted by Messrs. D. L. Robbins and M. E. Schwartz.

The program management was performed by Mr. D. B. Linde, A(3D)FT Program Manager and the technical effort was conducted under the direction of Mr. Mr. A. R. Hirasuna, A(3D)FT Program Engineer. The development of this Final Report and the technology advancement achieved under A(3D)FT are also attributable to the following Philco-Ford personnel: Mr. T. M. Place (Materials Development), Messrs. N. M. Harrington and R. L. Hagen (Structures), Messrs. J. R. Stetson and E. T. Miyazawa (Thermodynamics), Messrs. H. B. Thoeni and M. L. Damoth (Materials Applications), and Mr. J. H. Zickgraf (Electrical Design).

The principal subcontractors who participated include Fiber Materials, Inc. (Mr. W. L. Lachman), Southern Research Institute (Mr. S. Starrett), Avco Corporation (Messrs. J. L. Duggan and H. E. Hoercher), Dynatech (Mr. R. P. Tye), and MIT Laboratory for Insulation Research (Mr. W. B. Westphal).

This report has been reviewed and approved by:

Mr. R. Q. Jenkins
Contracting Officer
Space and Missile Systems Organization
Norton Air Force Base, California

ABSTRACT

This final report is the culmination of a 16 week effort, the Advanced 3D Fabrication Techniques Program (A(3D)FT), executed by Philco-Ford Corporation. The fundamental objective of A(3D)FT was to prove the feasibility of fabricating a relatively large, cone-frustum shaped, ablative, antenna window from a 3D quartz yarn reinforced, silica material. This material, AS-3DC, is a further development of AS-3DX which was developed on previous programs. AS-3DX antenna windows are small and fabricated from simple, block-shape billets. The large, cone-frustum-shaped, antenna windows developed here represent a substantial advance in the state of the art.

The program objectives were successfully fulfilled. Three full-scale AS-3DC frusta were woven, impregnated, machined, and the resulting parts characterized. The data indicate a superior ceramic antenna window material would ultimately result. Areas for improvement were identified and recommendations made for any subsequent development of the material.

This report documents all the tasks which were accomplished. A design data package is included. The design data are representative of AS-3DC in its initial phase of development and improvement is a certainty for subsequent AS-3DC frusta.

 Page iv Intentionally Left Blank

CONTENTS

CONTENTS - (Continued)

ILLUSTRATIONS

ILLUSTRATIONS - (Continued)

ILLUSTRATIONS - (Continued)

APPENDIX IV - (Continued)

TABLES

SECTION 1

PROGRAM SUMMARY

This section summarizes all the work performed on the Advanced 3D Fabrication Techniques Program, A(3D)FT, which was contracted to Philco-Ford by SAMSO/ABRES. The effort extended over a 16 week period commencing in March 1970.

1.1 OBJECTIVES

The primary objective of the A(3D)FT Program was to prove the feasibility of fabricating a full-scale, 3D, quartz-reinforced, silica-cone frustum using the colloidal-silica impregnation process, developed for AS-3DX.

Tasks required to accomplish this objective are:

- Scale up AS-3DX colloidal silica impregnation process.
- Determine optimum cone-frusta weave construction.
- Weave and impregnate three full-scale cone frusta.
- Fully characterize the resulting material.

1.2 BACKGROUND

Approximately 4 years ago SAMSO/ABRES began developing antenna window systems which are hardened against a relatively severe nuclear environment. This was primarily implemented through a series of programs* awarded to Philco-Ford. In addition, Philco-Ford was awarded a related development program** by AFML. The combination of these two efforts resulted in a very promising antenna-window material for hardened applications designated AS-3DX. The companion impregnation process which was developed is designated the "AS process". AS-3DX is an orthogonal, 3D, quartz-reinforced, silica, antenna-window material for fuzing applications fabricated from small block billets. The material's exceptional performance characteristics warrant classifying it as a developmental breakthrough. It is strong and can withstand high-stress wave-response loading emanating from impulsive loads. It can be readily formed and machined to desired shapes. The thermal properties are good from the standpoint of heatshield requirements and the electrical properties are good from the standpoint of antenna window requirements. Since the material is a pure quartz/silica composite no carbon containing organic compounds are present, hence, good rf transmission properties are ensured during ablation.

---

*RESEP I - Task 6
RESEP II - HAWD (Hardened Antenna Window Development)
**Hardened Antenna Window Program (HAW)

To date, all the AS-3DX windows have been of small size consistent with fuze antenna requirements and fabricated from simple block billet shapes. The combination of properties of AS-3DX warrant evolving it into other applications. Several applications exist which require much larger and much more complex shaped antenna windows. The objective of the current A(3D)FT program is to prove the feasibility of extending the AS-3DX process to the fabrication of large windows in a cone frustum configuration.

The new variation designated AS-3DC has the same material composition as the AS-3DX but differs in the construction of the reinforcement weave. The preform billet is woven directly into the cone frustum shape. It is a much more difficult and complex task to weave the frusta as opposed to the simple block billets for AS-3DX. The directional distribution of yarns differs from AS-3DX and is consistent with cone frustum requirements. Because of their small dimensions, the response of the blocks to re-entry and nuclear environments is essentially one dimensional and in the radial direction. With the larger AS-3DC frustum parts, the longitudinal and circumferential directions are of predominant importance and consequently more yarns are distributed in these two directions.

1.3 SIGNIFICANT RESULTS

The program objectives listed previously were fulfilled. Three full-scale, 3D frusta were successfully woven, impregnated, and subsequently characterized. Figure 1 is a photographic sequence capturing various points along the manufacturing process. Figure 2 indicates the approximate final dimensions of the parts.

The three frusta developed are all representative of "first time" parts; the total program duration including weaving, impregnating, machining, testing, and data evaluation was 16 weeks. Consequently, all three frusta were woven within a short space of time which disallowed any feedback information for perfecting the weave. The first opportunity to inspect the weave through the thickness was when the specimens were being cut from the first frustum. By this time the weaving on the third frustum was nearly complete. Considering the large developmental step in going from the small block billet fuze windows to the large cone frustum shape windows, these "first time" parts were of good quality.

Extensive mechanical testing was performed in all three orthogonal directions, as well as at elevated temperatures up to 1800°F. The data indicate that AS-3DC will ultimately have exceptional strength and consistency of data when compared to other ceramic materials. In general, the compressive strength ranged from about 10 to 20 ksi in all three orthogonal directions. Some data were measured below the nominal 10 ksi level, but all were specimens from the underdense center portion of the frusta discussed below. The axial tensile strength ranges from about 4 to 7 ksi which is extremely good data for a ceramic. The circumferential tensile strength was about 2 ksi, a lower level than was anticipated. All the hoop tensile rings were from the overdense ends of the frusta which is described below. The data imply that

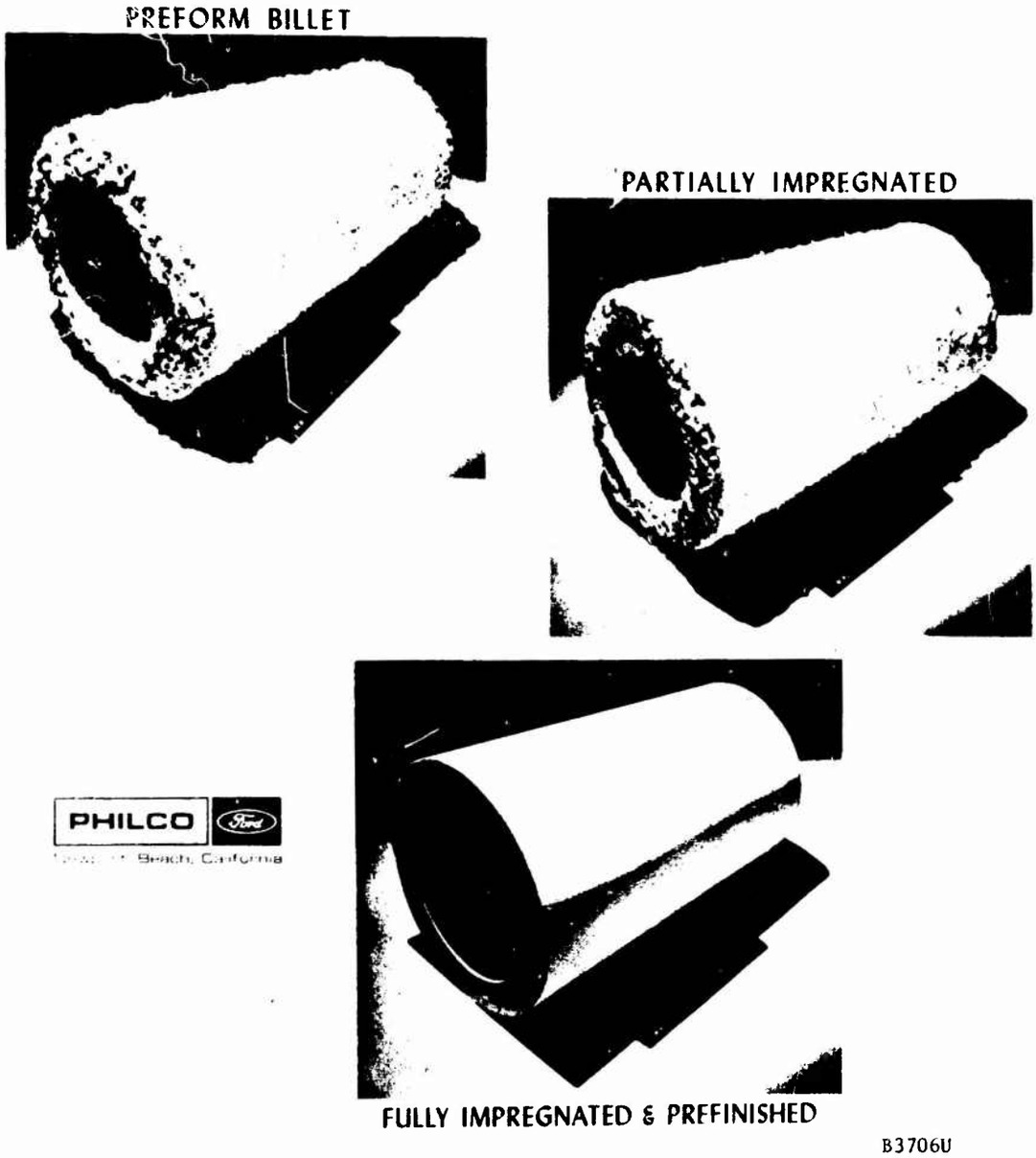

FIGURE 1. AS-3DC FABRICATING SEQUENCE

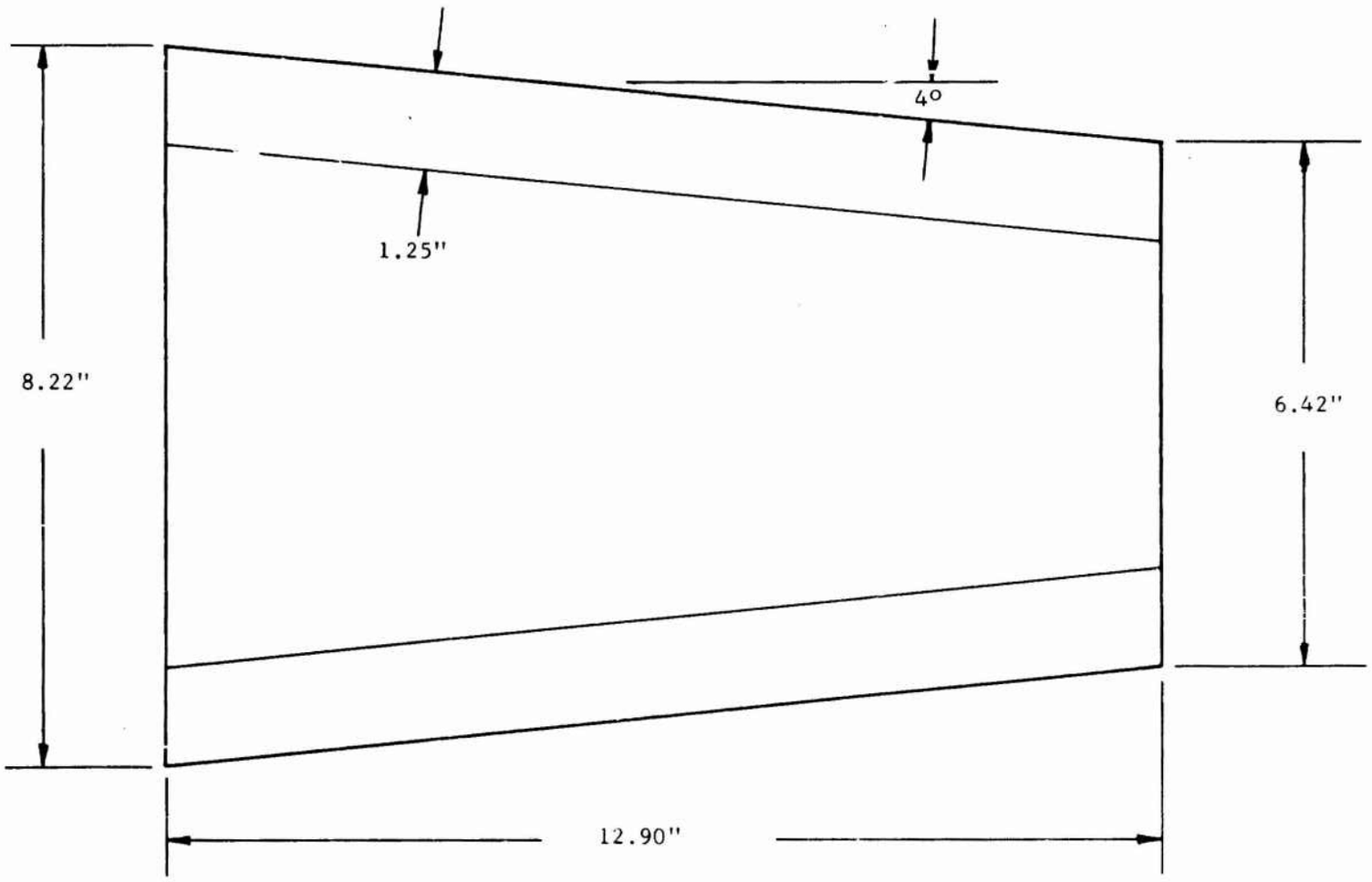

B3707U

FIGURE 2. APPROXIMATE AS-3DC FINISHED FRUSTUM DIMENSIONS

if the weave density is lowered to a more optimum value, substantially greater circumferential tensile strengths will be achieved. Values lower than the 2 ksi number were also measured; however, prior to the tests it was anticipated that they would be low because of obvious gross waviness in the circumferential yarns.

The data show that AS-3DC has good electrical properties for antenna window applications and good thermal properties with respect to heatshield requirements. AS-3DC is essentially the same material, i.e., quartz yarn and silica, as AS-3DX from the electrical and thermal standpoints, this is for all practical purposes substantiated by the data.

Thorough examination of the AS-3DC frusta was performed in an attempt to correlate the test data with identifiable characteristics of the weave or the impregnated part. The preform billet was woven to an average density of about 1 gm/cc and the final impregnated parts had an average density of about 1.65 gm/cc as anticipated. It was concluded that the impregnation process is almost completely perfected for these large parts; however, the weaving process requires some improvement.

Perfection of the weave is of primary importance, since the preform billet forms the foundation for the part. Flaws in the preform billet carry through as weakensses in the final part. As previously mentioned, the quality of the woven preforms were very good for "first time" conical parts. However, two problem areas did exist with the weave. There were problems with the density of the weave and straightness of the yarns. A significant variation in density existed in the preform billets. Measurements indicate that the frusta were overdense at either end and underdense in the middle. The straightness problems arose in maintaining the alignment of the axials and the ring shape of the circumferentials. At the upper portion of the frusta some axials moved out of the orthogonal pattern as viewed from their ends. Since the circumferentials are threaded between the axials they are bent from a perfect circle by the displaced axials. There was also a problem with straightness of the circumferentials in the other plane. This can be visualized by picturing a wavy doughnut which cannot lie flat on a surface.

These two weave problems were discussed at length with the Philco-Ford subcontractor, Fiber Materials, Inc., and the remedies appear to be relatively simple. The overdense weave can be altered at will to the desired density. The underdense weave results from loom limitations and is the same problem experienced by Fiber Materials, Inc., with cylinders. The same modifications which were made on the cylinder looms can be made on the frusta looms. The axial yarn misalignment occurred near the upper portion of the frusta where the partial internal mandrel did not extend. A full length mandrel can be used to give more positive position control along the full length of the axials. The final problem, circumferential waviness, tends to originate in the overdense portions of the frusta. A weave flaw cannot be accommodated in the tightly packed yarns and it compounds into a larger and larger wave as the weaving proceeds toward the small end of the frustum. The combination of reducing the density to the optimum level, so that small lumps can be

accommodated and not passed on to the succeeding layer, and specific attention to this problem on the part of the loom operator should remedy it. It appears highly probable that these improvements can substantially enhance the already good characteristics of AS-3DC.

1.4 RECOMMENDATIONS

The measurements taken on the A(3D)FT Program demonstrate the potential of the AS-3DC material. Aspects of the frusta were identified which warrant attention and improvement in any future development of the material. The following are the related recommendations:

(1) Specify the local weave density by defining the required number of layers of circumferential and radial yarns per unit axial length as a function of axial station.

(2) Modify frustum loom(s) to enable weaving a more dense middle portion.

(3) Use a full length internal mandrel to provide positive position control of the axials along their full length.

(4) Pay specific attention to maintaining well aligned, taut, and straight circumferentials.

(5) Adjust sintering temperature to correspond to the purity level to minimize the material's hygroscopicity.

(6) Address the potential of weave variations which may provide substantial additional strength improvement.

SECTION II

AS-3DC FRUSTUM CHARACTERISTICS

This section reports the characteristics and the observations of the three silica/quartz frusta developed on this program. These are the first conical billets of this large size which have been woven by Fiber Materials, Inc., using this particular 3D, orthogonal-weave technique. All three frusta are representative of "first time" parts, since the contract required quick execution which precluded the feedback of information to improve the second and third frusta.

2.1 WOVEN PREFORM BILLET

The frusta were woven with J. P. Stevens 300-4/4 quartz yarn. The preform billet cone frusta were approximately 14 inches long, 9 inches in OD at the large end and 1.75 inches thick with a 4 degree cone angle and an average density about 1.0 gm/cc. The exact dimensions of each billet are shown in Figure 3.

The weave construction is illustrated in Figure 4. The distribution of 300 4/4 yarns is as follows: 8 in the circumferential direction, 4 in the radial direction, and from 16 to 22 in the axial direction going from the ID to the OD. This variation compensates for the pie wedge effect. The yarns are positioned on 1/8 inch centers at the large end of the frustum.

Considering the state of development of these preform frusta billets, the quality of the parts was good. The preforms were woven almost precisely to the 4 degree specification. The general density level was in the desired regime resulting in a good stiff preform. However, there are two definite problem areas which require improvement. There was a rather wide density variation of the woven part along its length. The extremes, the overdense and the underdense portions, resulted in weakened parts. The other problem area pertains to straightness of the yarns. The problem primarily centers about the straightness of the circumferential hoops. These problems are discussed in greater detail in the following paragraphs. The feedback of these observations alone, will provide substantial improvement of any future conical parts.

It is difficult to obtain the local density at a given point in the woven preform. However, a good means of obtaining the relative density is available through measurement of the impregnated specimens cut from the frusta. The amount of silica matrix which is impregnated in a part is directly dependent on how much yarn is in the part. Consequently, the density variation of the woven billet is implied by the density variation of the final impregnated part. Figure 5 shows the approximate density variation observed in the impregnated AS-3DC frusta. Either end was in the 1.7 to 1.8 gms/cc regime, while the

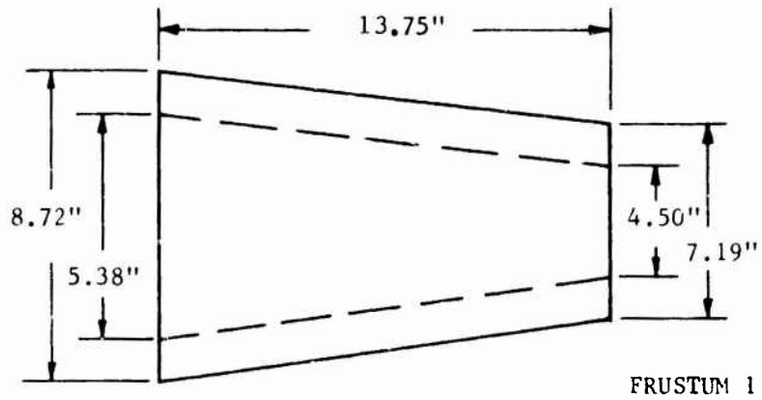

ρ = 64.3 LB/FT^3

FRUSTUM 1

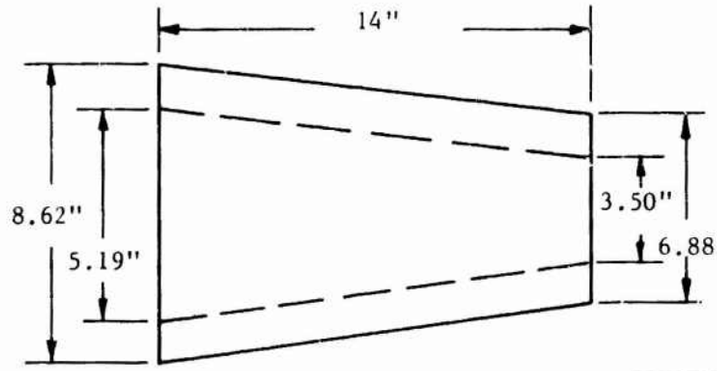

ρ = 62.0 LB/FT^3

FRUSTUM 2

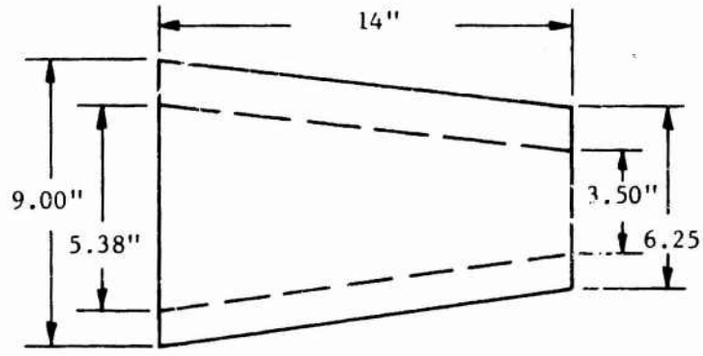

ρ = 65.0 LB/FT^3

FRUSTUM 3

B3708U

FIGURE 3. WOVEN FRUSTUM PREFORM DIMENSIONS

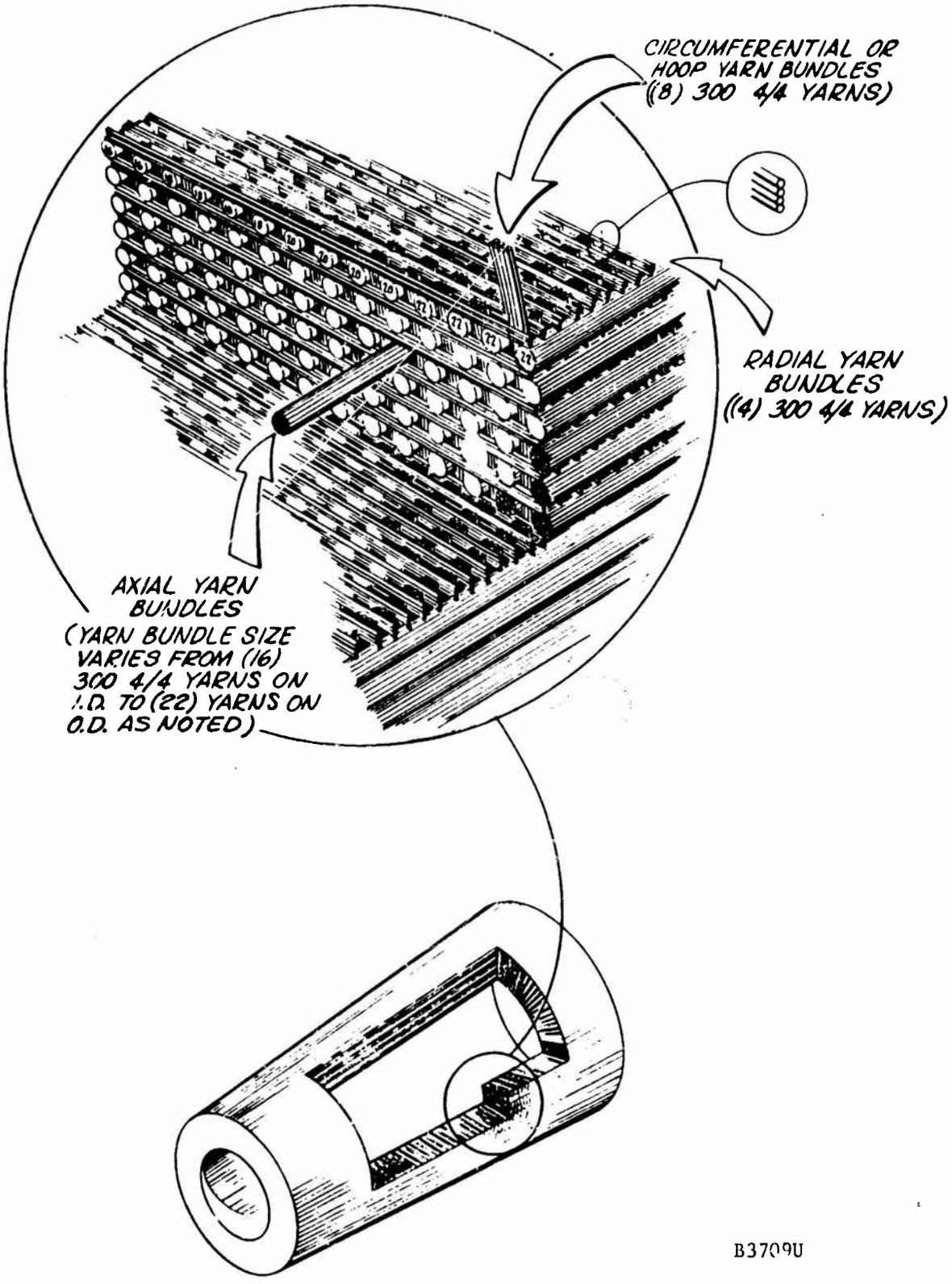

FIGURE 4. FRUSTUM CONSTRUCTION DETAILS

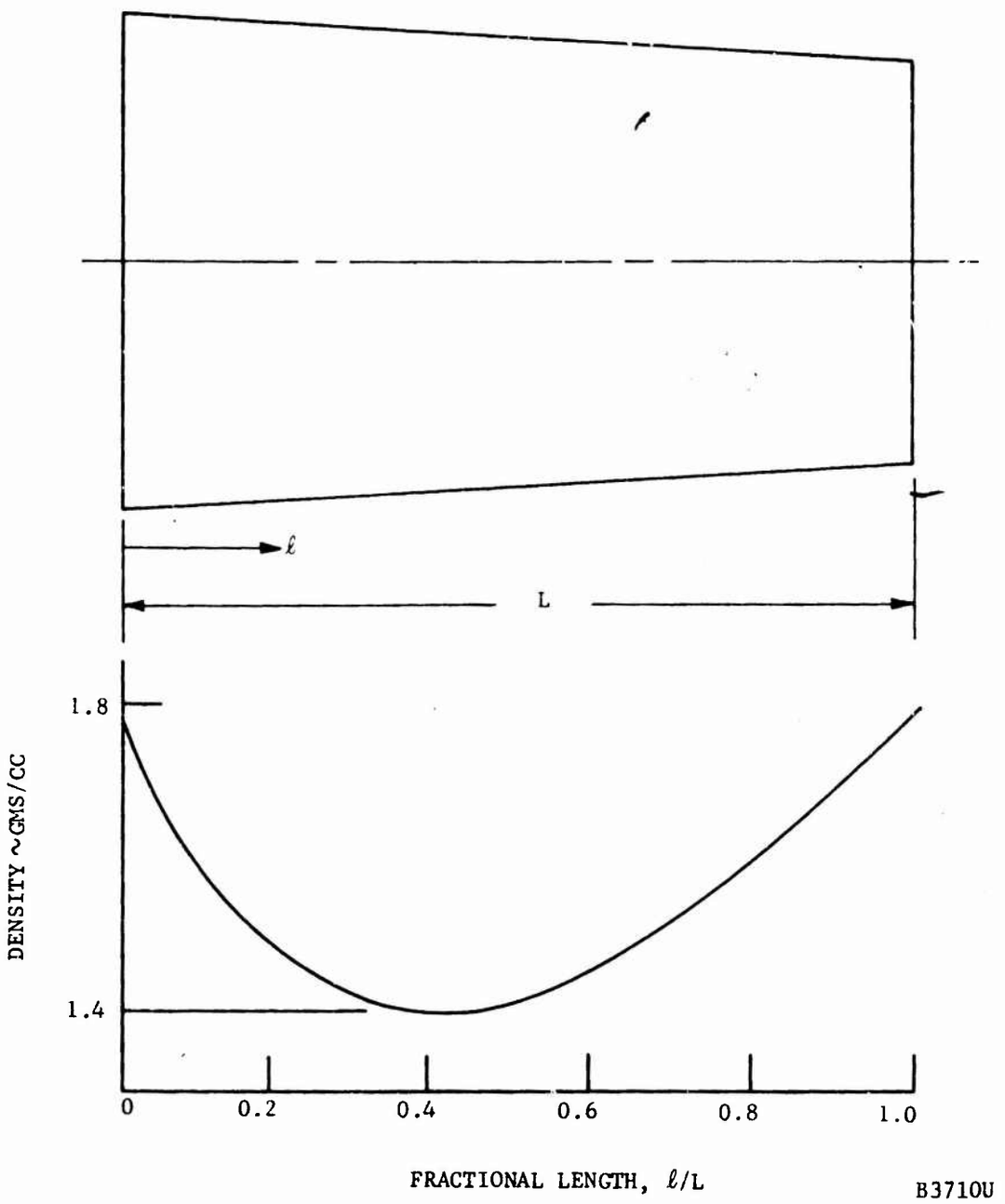

FIGURE 5. APPROXIMATE DENSITY VARIATION OF IMPREGNATED FRUSTA

mid portion was as low as about 1.4 gms/cc. It is desirable to have the entire part at a density of about 1.60 to 1.65 gms/cc.

As previously mentioned, both the underdense and the overdense portions of the frusta were weakened. It appears that the weakness in the underdense material results simply from insufficient amount of yarn. The reason for the weakness in the overdense material is much more obscure. Inspection of the fractures in the overdense material indicates that greater strength potential exists. The fractures are typical brittle fractures characterized by the break occurring over a short length of material. The optimal construction of the material produces tensile fractures which are jagged and splintered and occur over 1/2 to 1 inch of the material Photographs of the two classes of breaks are in Section 4, Figures 27 and 28.

The overdense regions can be identified from the outside of the frusta. The density variation is a direct result of the tightness to which the layers of circumferential and radial yarns are packed in the axial direction. It is apparent by inspection that the circumferential hoop layers are closer together at either end of the frusta than they are in the middle. Figure 6 illustrates the probable effects resulting from overcompaction in the overdense regions. The overdense material gives typical brittle characteristics as indicated previously. In the development of the AS process, it was noted that the material acted in this manner if the part is too completely filled with the silica matrix. Void cells are an inherent characteristic of a 3D orthogonal weave. These void cells continue to exist in a good quality AS part. The voids are filled if the yarns are so closely woven that the cells are small. The part then tends to act more like a typical brittle homogeneous ceramic. In depth inspection of the overdense regions of the AS-3DC frusta revealed complete closure of the void cells, implying that stronger parts are available through a less compact weave. In addition to this effect, there is the distinct possibility of additional weakening phenomena resulting from the overcompaction. Keeping in mind that the overcompaction is accomplished by physically pushing down of the radial and circumferential yarns, the higher compaction implies a greater amount of working of the yarns. There is a distinct possibility that this greater amount of working results in significant mechanical damage or fraying of the yarns. It also follows that the greater the degree of compacting, the more likely the yarns will be forced to fill and conform to the void cells. This results in an inter-yarn waviness of the yarns which is obviously undersirable. When a particular set of yarns is pulled the kinks will straighten first before stressing the yarns and in the process break the silica matrix. The maximum strength occurs when the yarns are stressed and broken simultaneous with the break-up of the silica matrix.

The other basic problem stated previously pertains to straightness of the circumferential hoop yarns. This problem is illustrated in Figure 7. From the end view, A-A, of the small end of the frusta it is apparent that the axial yarns have moved from their orthogonal pattern. This occurs only toward the small end of the frusta. It results from the fact that the doughnut-shaped, cross-sectional area is decreasing towards the small end of the frusta. The same amount of axials are woven into the area resulting

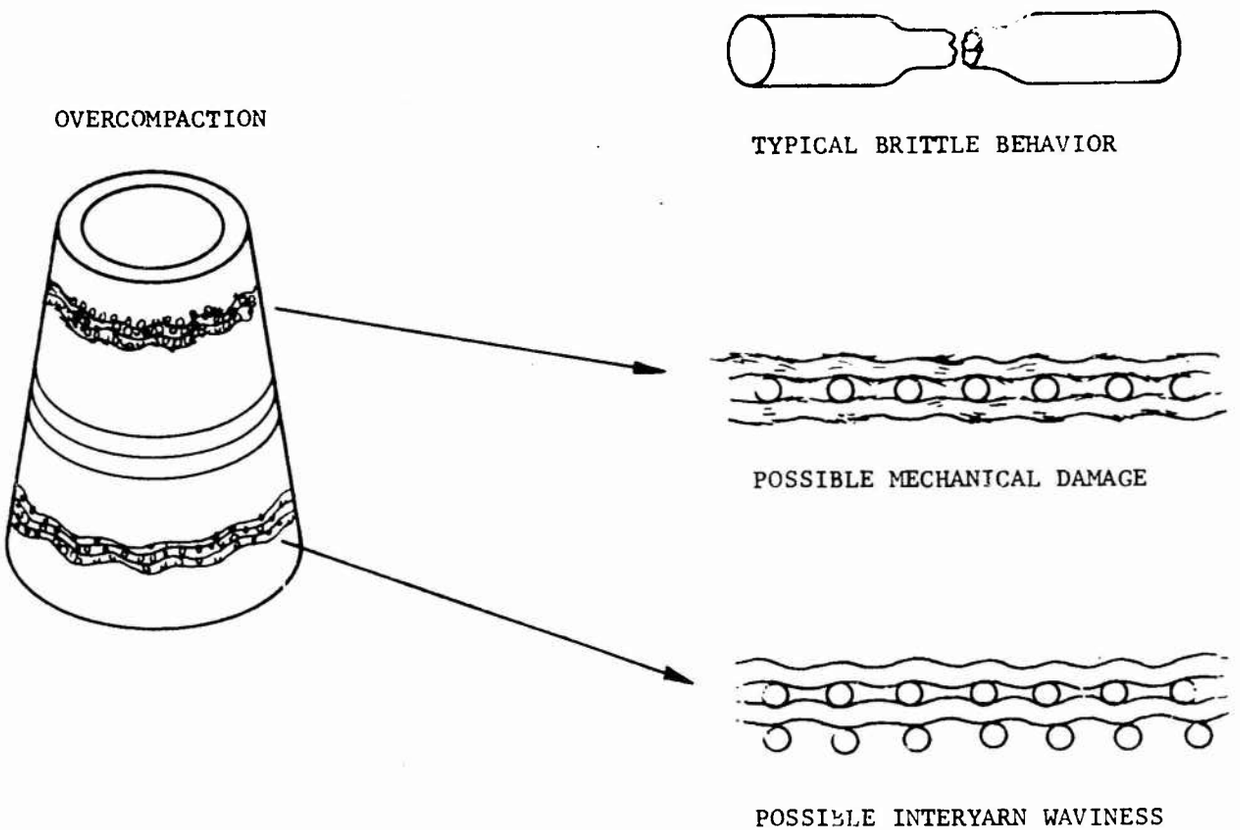

FIGURE 6. PROBABLE EFFECTS OF OVERCOMPACTION

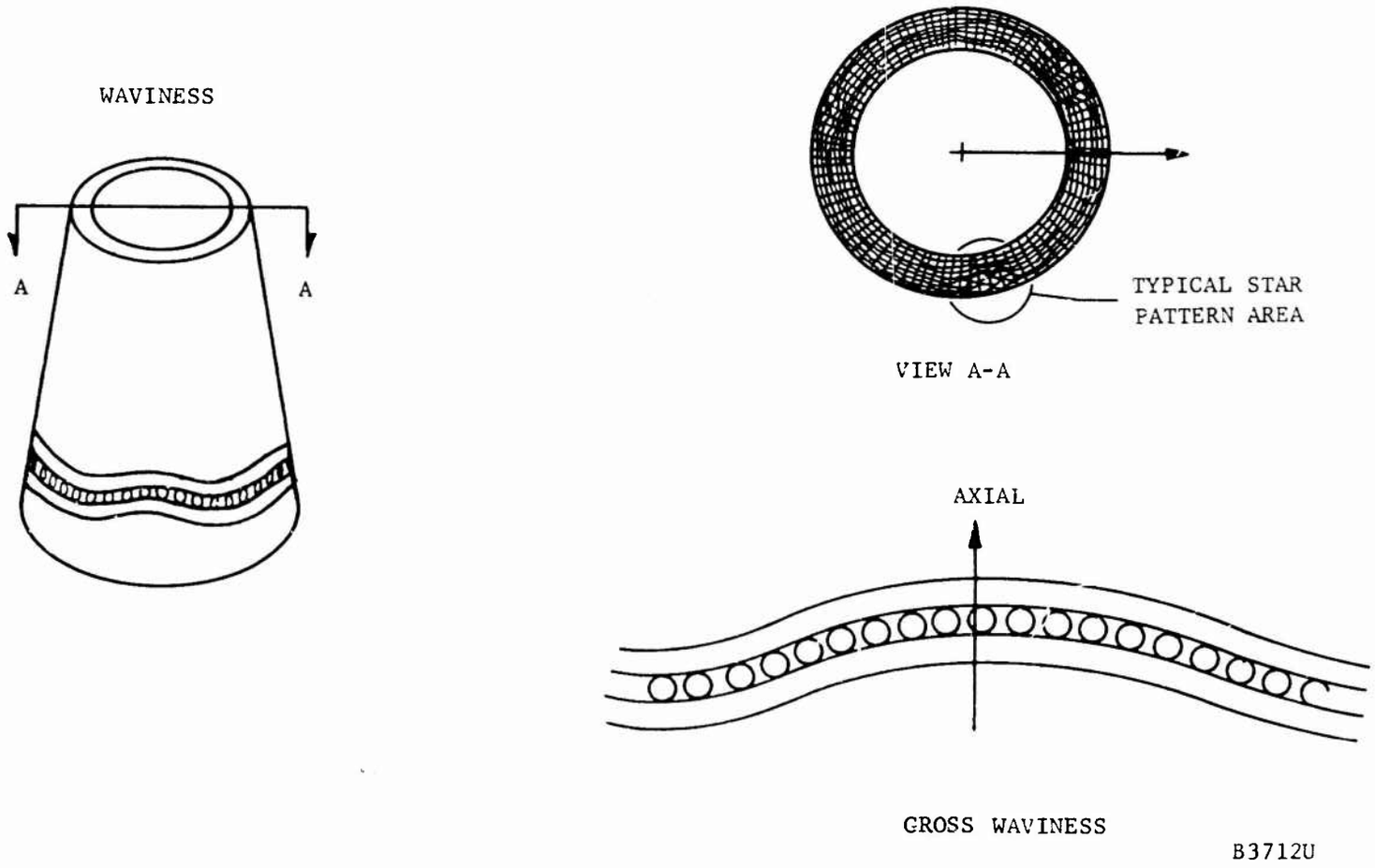

FIGURE 7. WAVINESS OF CIRCUMFERENTIAL YARNS

in crowding at the smaller end. The crowding causes the axials to squirm out of place as is observed. A photograph showing this is Figure 25, Paragraph 4.2. This movement of the axials forces kinks in the circumferentials which are threaded between them. The bending of the axials is slight enough such that the axial strength is probably not reduced, however, the circumferential hoop strength probably is. Looking at the side of the frustum it is apparent that a gross waviness of the circumferentials exists. This phenomenon primarily exists toward the ends where the material is overdense. Figures 24 and 26 of Paragraph 4.2 show this waviness in the hoop tensile specimens. It is apparent from the location of the fractures that this waviness does result in weak points.

The preceding is a detailed description of the observations made which are associated with the two basic weave problems: weave density and yarn straightness. These problems were discussed at length with Fiber Materials, Inc., and the remedies are relatively simple. The general question of weave density would be covered by a more specific specification in the future. An analysis was performed and a methodology identified which provides a definite means by which to specify the weave density. Equations were derived which define the number of layers of circumferential/radial yarns per unit axial length required to maintain a constant weave density. Figure 8 gives the results for the AS-3DC frusta. The layer count decreases towards the smaller end to compensate for the decreasing doughnut-shaped, cross-sectional area. The weave density which is represented by this curve is the same value which exists in the forward midsection of the No. 1 frustum. This section exhibited consistently high strengths. There is no problem in reducing the count in the overdense portions of the frusta to meet the desired layer count. However, raising the count in the underdense portions will require loom modifications. The same problem, underdense weave in the midsection, was experienced by Fiber Materials, Inc., with cylinders and was corrected. The same modifications made on the cylinder looms can be made on the frusta looms. The yarn straightness problem is related to the weave density. The waviness of the hoops, in the plane parallel to the ends of the frusta, occurs primarily in the overdense regions of the weave. A perturbation in the tightly compacted weave is passed on to the subsequent layer in a compounding manner. Reducing the weave density to the optimum level will provide a greater capability for accommodating the perturbations and not allowing them to compound. Hence, by eliminating the overdense weave through specification in combination with directing the loom operator's attention to this specific problem, the waviness of the circumferential hoop in the plane parallel to the ends of the frusta, should be eliminated. The final aspect of yarn straightness is associated with maintaining the parallelism of the axials at the small ends of the frusta. The three frusta on this contract were built with a partial internal mandrel which just covered a fraction of the large end. Future frusta would be made with a full length internal mandrel which would provide positive position control along the full length of the axials.

Because of the schedule and scope constraints of this program it was necessary to choose a single weave configuration and characterize the resulting part. The opportunity remains to use the knowledge gained on this program as a stepping stone to investigate weave variations which may substantially increase the strength of the part. An obvious area of investigation is to determine

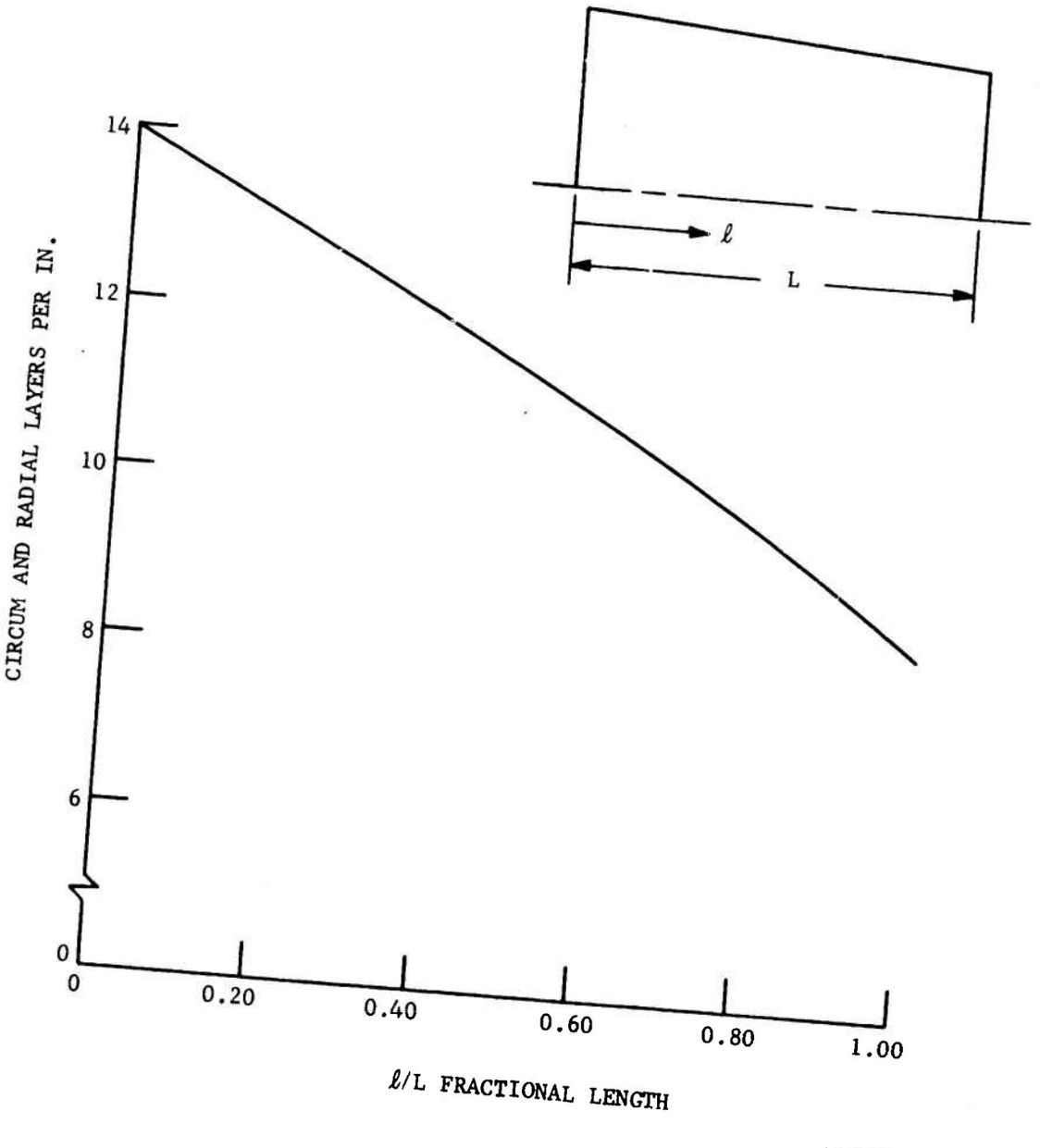

FIGURE 8. AS-3DC WEAVE REQUIREMENTS

the precise weave specification which maximizes the strength of the basic weave configuration used. Details of concern include density considerations and the straightness of the circumferential yarns. Other potential alternatives have also become apparent. They require changes to the basic weave configuration. Presently all the circumferential yarns are continuous over the length of the frusta and the transition to the subsequent layer is along a single cone ray. The information generated on this program was insufficient to determine if this method of transition has a weakening effect on the frusta or if another method is stronger. This question is especially important as it relates to the circumferential tensile strength of the frusta. The other potential weave alternative involves experimenting with the yarn distribution in each of the orthogonal directions, and the yarn size and center to center dimension. A good understanding of the extent of the effect of these variations does not exist.

2.2 FINAL IMPREGNATED AS-3DC FRUSTA

The three AS-3DC frusta were impregnated with a high-purity colloidal silica. The unique impregnation process is the result of substantial development under the SAMSO RESEP II-HAWD and AFML HAW Programs. The process used on this program is exactly the same as previously developed except for the scaling up required for the larger frustum parts. It begins with heat cleaning of the preform billet to remove any organics which may exist. Then the standard cycle of vacuum impregnation and curing at elevated temperatures is applied. Prior to the completion of the impregnation, the part is machined to the desired dimensions. It is then reimpregnated until it achieves the target density of about 1.64 gms/cc. A final finishing impregnation using a glass slurry is applied to fill any surface voids which exist producing a smooth surface.

The AS-3DC part can be readily machined using standard ceramic techniques. These include drilling, grinding, and sawing using diamond tooling and distilled water as a coolant.

The three AS-3DC frusta were built to generally conform to the dimensions shown on Figure 2. However, since the frusta were going to be cut up into characterization specimens, it was not critical to conform precisely to these dimensions. Consequently, the first two were finished such that a minimum amount of material was removed. The No. 3 frustum was finished such that all surface blemishes and end tie offs were removed. The exact dimensions of each of the machined frusta are given in Figure 9. Also indicated are the final average densities of the fully impregnated parts. The achieved densities conform closely to the target of 1.64 gms/cc.

The characterization data confirm that the impregnation or AS process is almost fully perfected even for these larger parts. However, the electrical data indicate one minor adjustment for future parts. There is a complex relationship between the purity of the material, the sintering temperature, and the materials hygroscopic properties. A more hygroscopic material or one that more readily absorbs and retains water is more lossy because of the water content. Since the AS-3DC parts were more pure than AS-3DX, about 50 to 100 ppm of Na versus about 160 ppm of Na, the balance was tipped toward

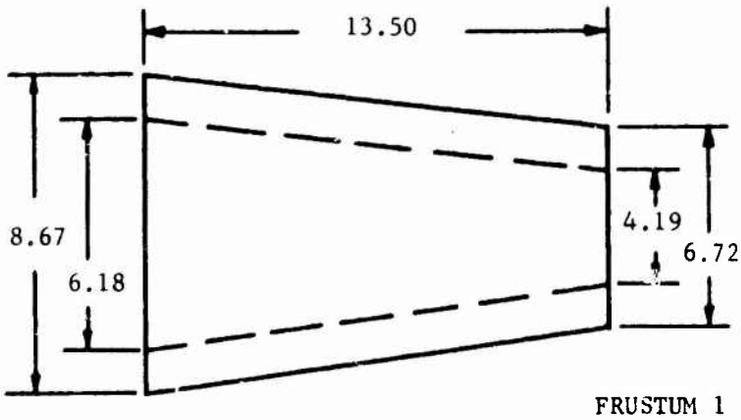

ρ = 102.9 LB/FT^3
1.65 GM/CC

FRUSTUM 1

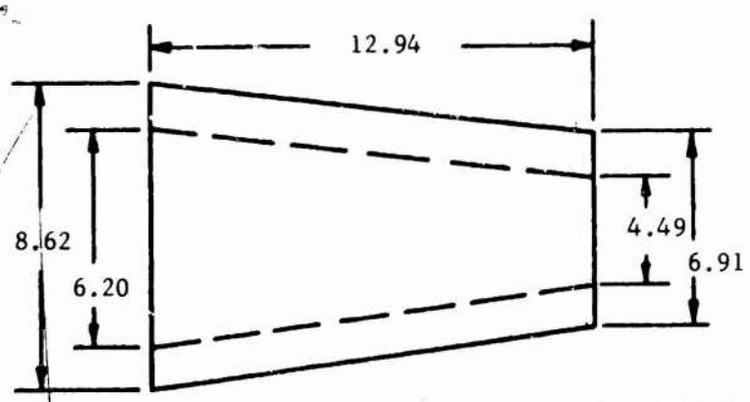

ρ = 100.5 LB/IT^3
1.61 GM/CC

FRUSTUM 2

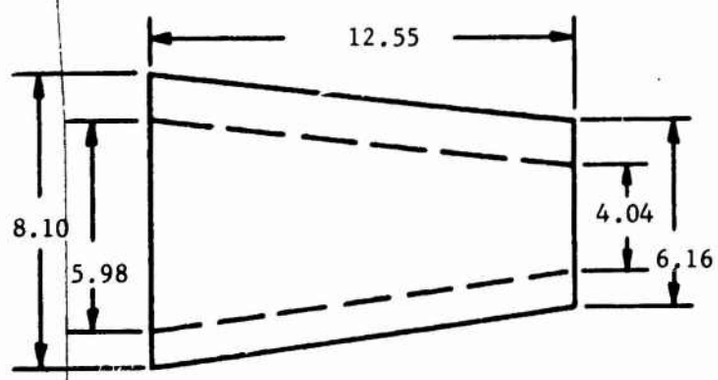

ρ = 105.5 LB/FT^3
1.69 GM/CC

FRUSTUM 3

B3714U

FIGURE 9. IMPREGNATED AND MACHINED AS-3DC FRUSTUM DIMENSIONS

TABLE I. QUARTZ PREFORM BILLET ANALYSES

Element/ Compound	Frustum 1[a]	Frustum 2[b]		Frustum 3[c]	
	Side and End	Side[d]	End[d]	Side	End
SiO_2	Remainder	Remainder	Remainder	Remainder	Remainder
MgO, %	0.0021	0.0023	0.0045	0.0028	0.0026
Fe_2O_3, %	0.0070	0.0093	0.020	0.017	0.019
Al_2O_3, %	0.0059	0.031	0.023	0.010	0.0064
CuO, %	0.00014	0.00016	0.00014	0.00028	0.00023
Ag_2O, %	0.00031	-	-	0.00014	0.00011
CAO, %	0.0020	0.0020	0.0040	0.0026	0.0022
Cr_2O_3, %	0.0016	0.00050	0.0054	0.0025	0.0021
B_2O_3, %	-	0.011	0.048	-	-
ZrO_2, %	-	0.032	0.025	-	-
NiO, %	-	0.00030	0.0010	0.0015	0.0014
Sodium, ppm	Not Detected Less than 5.0	94.	330.	50.	87.
Barium, ppm	Not Detected Less than 5.0	Not Detected Less than 3.0	54.	Trace Less than 2.0	Trace Less than 2.0
Lithium, ppm	Not Detected Less than 2.0	Not Detected Less than 1.0	Trace Less than 2.0	Trace Less than 0.50	Trace Less than 0.50
Potassium, ppm	Not Detected Less than 5.0	Not Detected Less than 4.0	Not Detected Less than 8.0	Not Detected Less than 2.0	Not Detected Less than 2.0
Strontium, ppm	1.2	0.19	3.1	0.37	0.65

Notes: (a) Reference 1.
(b) Reference 2.
(c) Reference 3.
(d) Samples taken after one impregnation cycle.

TABLE II. IMPREGNATED AS-3DC FRUSTA ANALYSES

Element/ Compound	Frustum 1		Frustum 2		Frustum 3
	Mid Section[a]	Aft Section[b]	Mid Section[c]	Aft Section[b]	
SiO_2	Remainder	Remainder	Remainder	Remainder	Not Analyzed
MgO, %	0.0012	0.0021	0.0021	0.0014	
Fe_2O_3, %	0.0086	0.016	0.011	0.012	
Al_2O_3, %	0.020	0.022	0.013	0.027	
CuO, %	0.00037	0.00061	0.00016	0.00033	
TiO_2, %	0.0022	0.0020	0.0027	0.0037	
ZrO_2, %	-	0.0031	0.0020	0.0019	
CAO, %	0.0013	0.0021	0.0013	0.0021	
Cr_2O_3, %	-	-	0.00057	-	
Ag_2O, %	-	0.00036	-	0.000077	
Sodium, ppm	120.	91.	58.	46.	
Barium, ppm	Trace Less than 2.0	4.6	3.0	3.2	
Lithium, ppm	Not Detected Less than 0.50	Not Detected Less than 0.50	Not Detected Less than 0.50	Not Detected Less than 0.50	
Potassium, ppm	Not Detected Less than 2.0	Not Detected Less than 2.0	Not Detected Less than 2.0	Not Detected Less than 2.0	
Strontium, ppm	1.8	0.78	0.36	0.52	

Notes: (a) Reference 4.
(b) Reference 5.
(c) Reference 6.

a more hygroscopic material. This is reflected in the electrical properties and is discussed in Section 6. A change in the sintering temperature is indicated to compensate for the higher purity. These relationships were investigated in the AFML HAW Program and no change in mechanical properties is expected due to the required change in sintering temperature.

2.3 CHEMICAL PROPERTIES

Arc spectrographic analyses were performed on the preform billet and the finished AS-3DC parts to determine the contamination level. The No. 1 preform billet was exceptionally clean with no detectable Na. Higher levels of impurity occurred on the subsequent two billets. The finished AS-3DC parts had about 100 ppm for frustum No. 1 and about 50 ppm for frustum No. 2. Frustum No. 3 was not analyzed. The analyses for the preform billet and the finished frusta are reported on Tables I and II. The letter reports are in Appendix VII. They indicate a substantial improvement over the AS-3DX which is at the 160 ppm level. Additional improvement can be expected in the future with further development of the process.

A factor which may be related to the difference in contamination level of the No. 1 preform billets as opposed to the No. 2 and No. 3 preform billets is the yarn. Two batches of yarn were used to weave the three frusta. No. 1 was woven completely from 300 4/4 yarn shipped directly from France. Part of the No. 2 and all of the No. 3 used yarn from another source which they braided into 300 4/4 yarn. The reason the impregnated No. 1 frustum shows a higher Na content than No. 2 is due to a lower purity silica solution. Because of schedule constraints, more residence time prior to final ion exchange was available for the solution for the No. 2 frustum which allowed more of the Na to become available. Hence, it was purified to a greater degree.

The spectroanalysis detectability level was less precise for the No. 1 quartz preform sample than for the other samples. The method used by Pacific Spectrochemical, Inc., is to analyze the ash resulting from an acid distillation process. For the quartz yarn the ash is approximately 0.06 percent by weight. To achieve a 1 to 2 ppm detectability level of contaminants, 10 mg of ash are required. The amount of starting material was underestimated for the first sample analyzed, resulting in about 3.24 mg of ash and a 5 ppm detectability level. However, the 5 ppm detectability level is also fine enough to serve the objectives of this contract.

SECTION III

TEST MATRIX AND CHARACTERIZATION SPECIMENS

This section provides an overview of the entire scope of the characterization testing. Included are data pertaining to the tests in general, testing conditions, and specifics associated with the test specimens.

Shown in Table III is a summary of the characterization tests which were performed on the frusta. Included in the table are the total number of specimens tested, test temperature, test facility, and specimen configuration.

Figures 10 and 11 indicate the individual cutting locations of each specimen from frusta 1 and 2, respectively. The frusta are least dense in the middle and most dense at the ends, so specimens undergoing identical test conditions were taken from these two general positions wherever possible. This provided data to observe the effect of density on the characteristics. The rings for the hoop tensile tests were cut from either end of both frusta 1 and 2. This was necessary in order to assure that sufficient length would remain from which to cut the axial tensile and flexural specimens. The dash lines indicate additional material which was provided to facilitate the machining of the specimens. Also shown in Figures 10 and 11 are the individual bulk densities of the specimens.

TABLE III. TEST MATRIX

Test	No. of Specimens and Test Temperature						Test Facility	Specimen Configuration
	Total No.	RT	500 F	1000 F	1500 F	2000 F		
Ablation Turbulent	4	-	-	-	-	-	Avco 10 mw arc jet	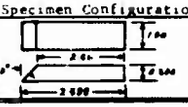
Thermal								
Specific Heat	1	1 →					Dynatech	
Thermal Cond	1	1 →					Dynatech	
Thermal Exp	1	1 →					Philco-Ford	
Mechanical								
Axial Flex and Mod	13	4	3	3	3	-	SoRI	
Axial Tensile and Mod	10	4	3	3	-	-	SoRI	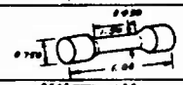
Axial Comp and Mod	16	4	3	3		3(a)	SoRI	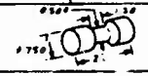
Circum Comp and Mod (Hoop)	4	4	-	-	-	-	Philco-Ford	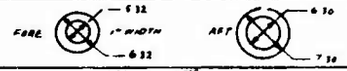
Circum Comp and Mod	16	4	3	3	3	3(a)	SoRI	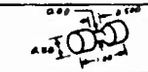
Radial Comp and Mod	4	4	-	-	-	-	Philco-Ford	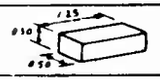

(a) At 1800 F.

TABLE III. TEST MATRIX - (Continued)

Test		No. of Specimens and Test Temperature: Total No.	RT	500 F	1000 F	1500 F	2000 F	Test Facility	Specimen Configuration
Electrical — Dielectric Constant and Loss Tangent	X-Band	1	1					Mass Inst of Tech Cambridge, Mass	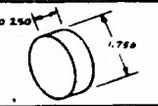
	VHF	2	2					Mass Inst of Tech Cambridge, Mass	
Density		Almost all specimens	-	-	-	-	-	Philco-Ford Newport Beach, California	
Chemical Properties		3(b) 4(c)	-	-	-	-	-	Pacific Spectrochemical, Inc. Los Angeles, California	Remnants
X-Ray	Cones	12(d)	-	-	-	-	-	Philco-Ford Newport Beach, California	
	Specimens	All specimens	-	-	-	-	-	Philco-Ford Newport Beach, California	
Microwave Attenuation		4 samples	2 Measurements per day over 5 days	-	-	-	-	Philco-Ford Newport Beach, California	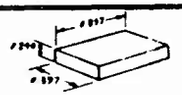

(b) Yarn samples on as received preform.

(c) Samples of finish impregnated frustum (2 per frustum).

(d) Minimum of 4 per frustum, 90 degrees apart.

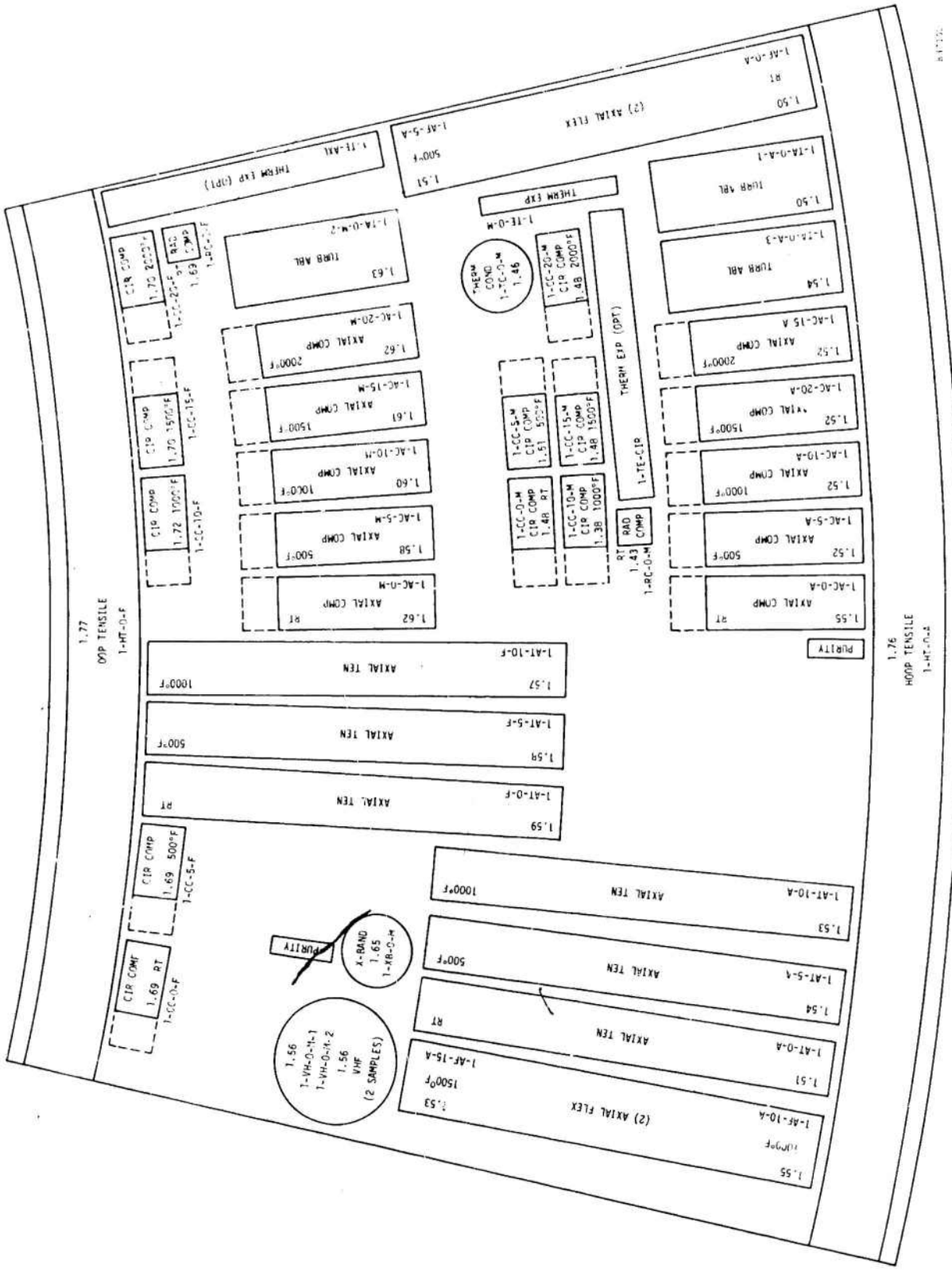

FIGURE 10. FRUSTUM 1 CUTTING DIAGRAM

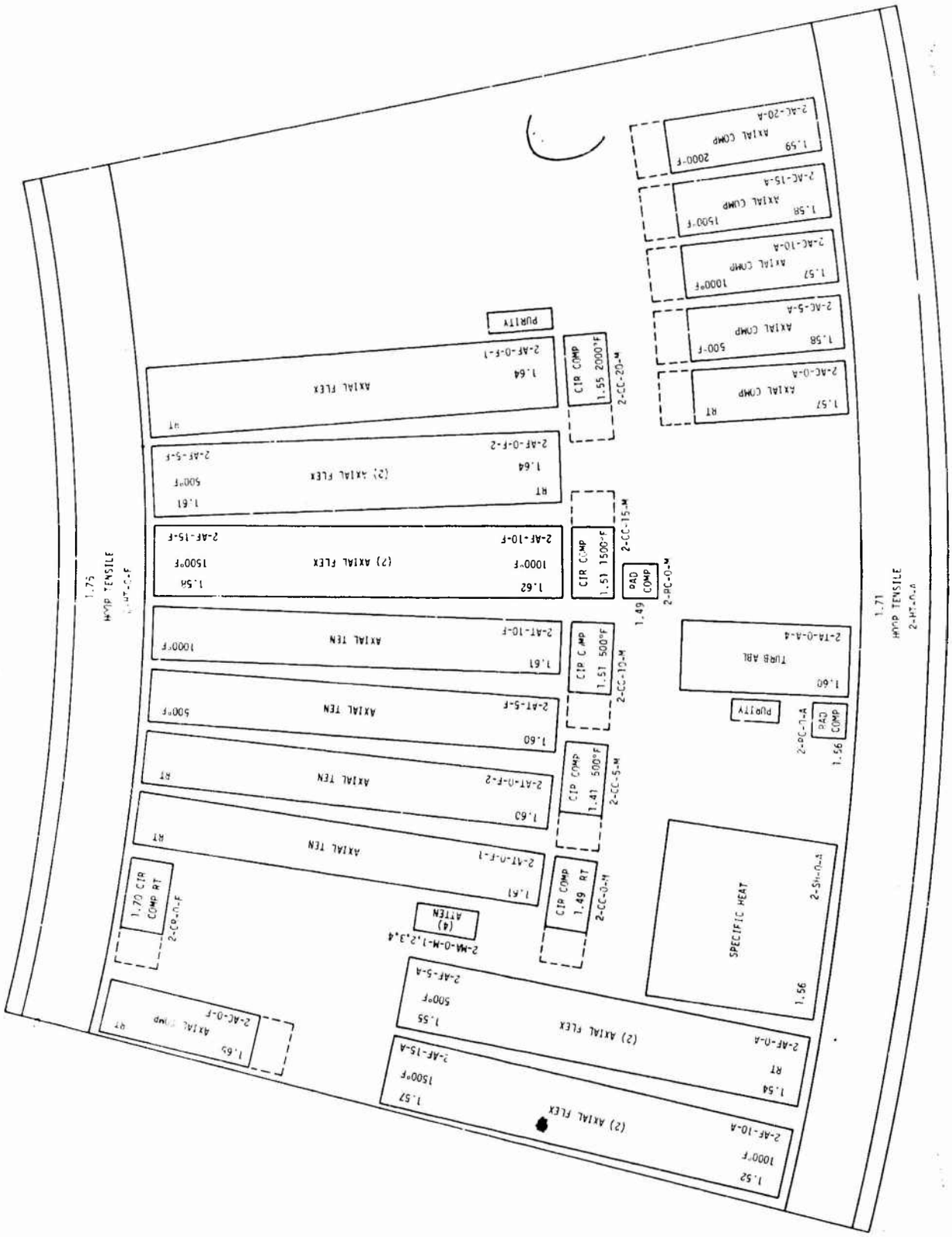

FIGURE 1'. FRUSTUM 2 CUTTING DIAGRAM

SECTION IV

MECHANICAL PROPERTIES

A total of 63 AS-3DC test specimens were fabricated for the matrix of mechanical property tests shown in Table III. Of these, 55 specimens were scheduled for testing at Southern Research Institute (SoRI) and the remaining 8 specimens were to be tested in-house.

4.1 SoRI TESTS

The following SoRI mechanical property tests were planned:

- 13 axial flexure tests.
- 10 axial tension tests.
- 16 axial compression tests.
- 16 circumferential compression tests.

Test specimen configurations and test apparatus details are contained in Appendix III.

4.1.1 AXIAL FLEXURE TESTS

All 13 axial flexure specimens were tested successfully. The following room temperature values were obtained (average of four specimens):

- Flexural strength, 4000 psi.
- Flexural modulus, 1.86×10^6 psi.

The test data points for strength and modulus are shown in Figures 12 and 13, respectively. The data show a definite trend of increasing flexural strength with temperature. However, the flexural modulus appears to remain constant over the test temperature range. The average strength and modulus of the four specimens from frustum No. 1 are quite close to the average values for either set of specimens from frustum No. 2.

4.1.2 AXIAL TENSION TESTS

All ten axial tension specimens were tested successfully. The following room temperature values were obtained (average of four specimens):

- Tensile strength, 4480 psi.
- Tensile modulus, 2.99×10^6 psi.

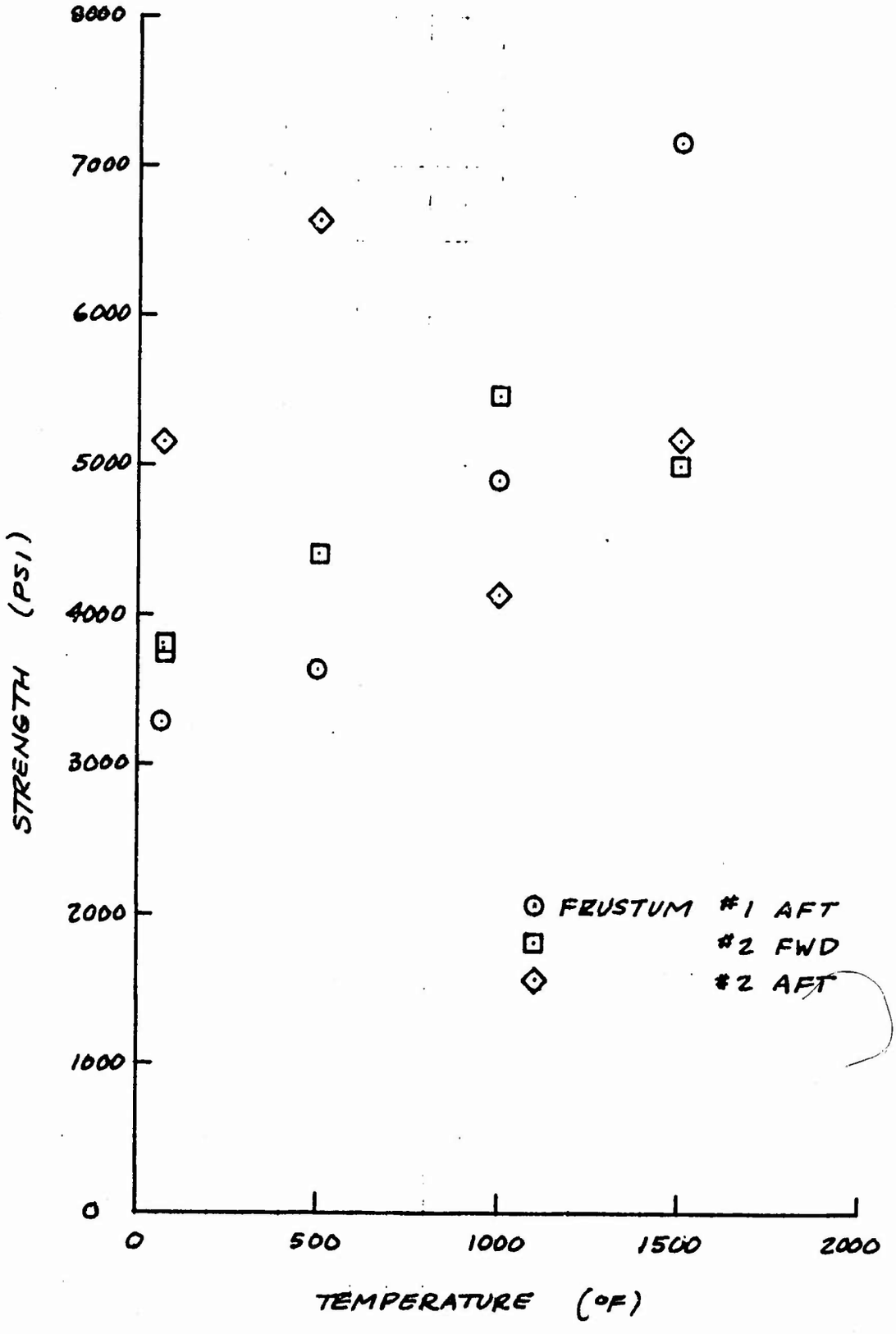

B3717U

FIGURE 12. AS-3DC AXIAL FLEXURAL STRENCTH

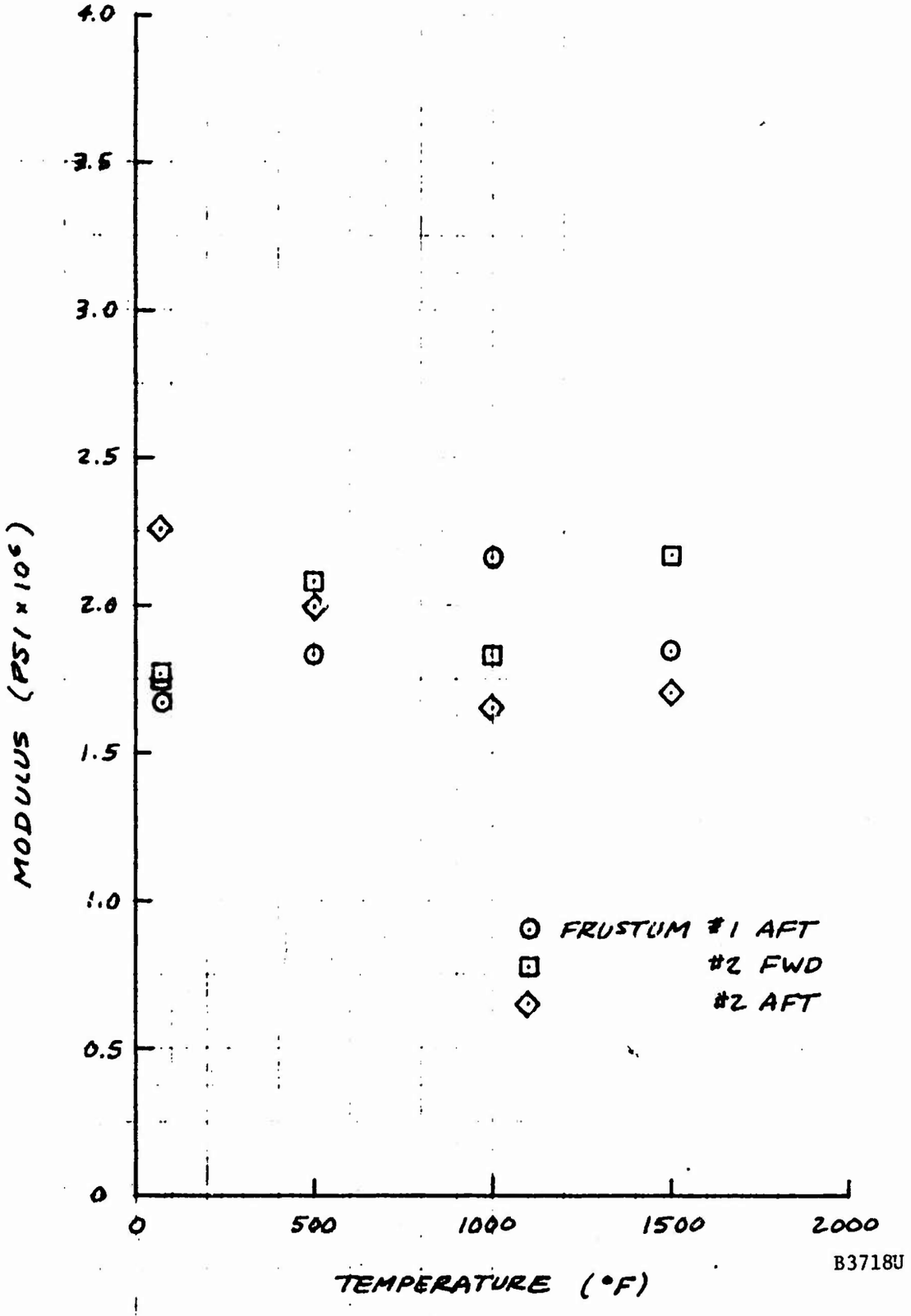

FIGURE 13. AS-3DC AXIAL FLEXURAL MODULUS

The test data points for strength and modulus are shown in Figures 14 and 15, respectively. The data indicate that tensile strength increases with temperature, while tensile modulus remains about constant. The average strength of the specimens taken from the aft end of frustum No. 1 is almost equal to the average strength for specimens from the forward end of frustum No. 2. However, the average strength of specimens from the forward end of frustum No. 1 is considerably higher (44 percent greater than frustum No. 2).

These values are probably lower than the actual strengths in that it is extremely difficult to prevent bending of the specimens caused by non-homogeneity especially inherent in a composite material. This is critical to brittle materials as opposed to ductile materials, since with ductile materials yielding occurs and accommodates any inconsistencies. Bending did occur as was substantiated by strain flags which were observed to move together while the tensile force was continuing to pull them apart.

4.1.3 AXIAL COMPRESSION TESTS

Of the 16 axial compression specimens tested, 14 were successful. Two test attempts at 2000°F were unsuccessful because of rapid shrinkage of the test specimens as the test temperature was approached. The shrinkage was caused by exceeding the sintering temperature of AS-3DC (about 1800°F). To avoid this problem, subsequent specimens scheduled for testing at 2000°F were tested at 1800°F.

The following room temperature properties were obtained (average of four specimens):

- Compressive strength, 13,310 psi.
- Compressive modulus, 2.55×10^6 psi.

The test data points for strength and modulus are shown in Figures 16 and 17, respectively. The data indicate that compressive strength increases with temperature, while modulus remains relatively constant. The average strengths for specimens taken from the mid and aft regions of frustum No. 1 are nearly equal. However, the average strength of the test specimens from frustum No. 1 aft is 18 percent higher than the average strength of the comparable specimens from frustum No. 2 aft.

4.1.4 CIRCUMFERENTIAL COMPRESSION TESTS

Of the 16 circumferential compression specimens tested, 14 were successful. Specimen 2-CC-0-M was broken in handling, so specimen 2-CC-20-M was tested at room temperature in its place. Specimen 2-CC-5-M was broken while being installed in the test machine, so it was not tested.

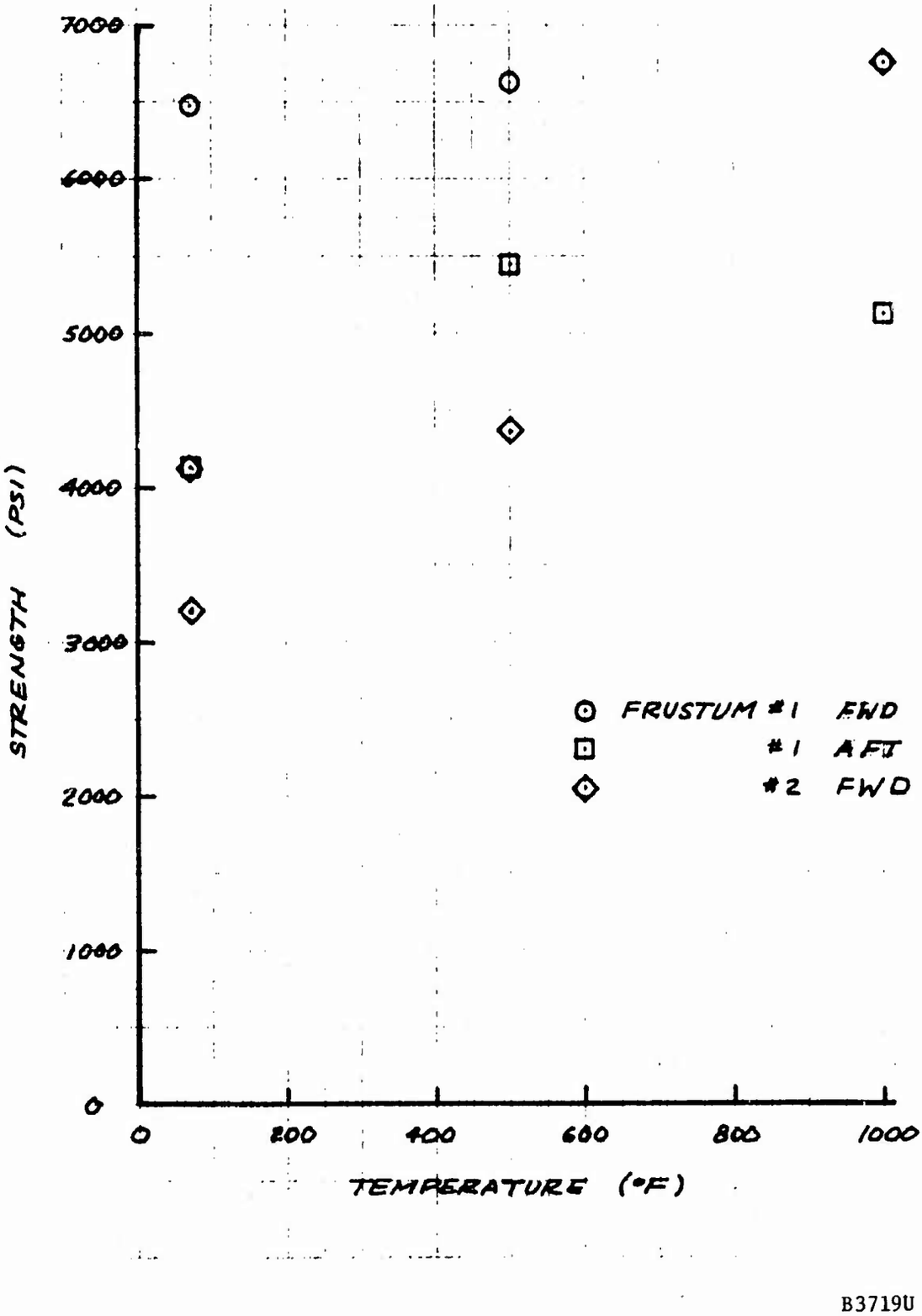

B3719U

FIGURE 14. AS-3DC AXIAL TENSILE STRENGTH

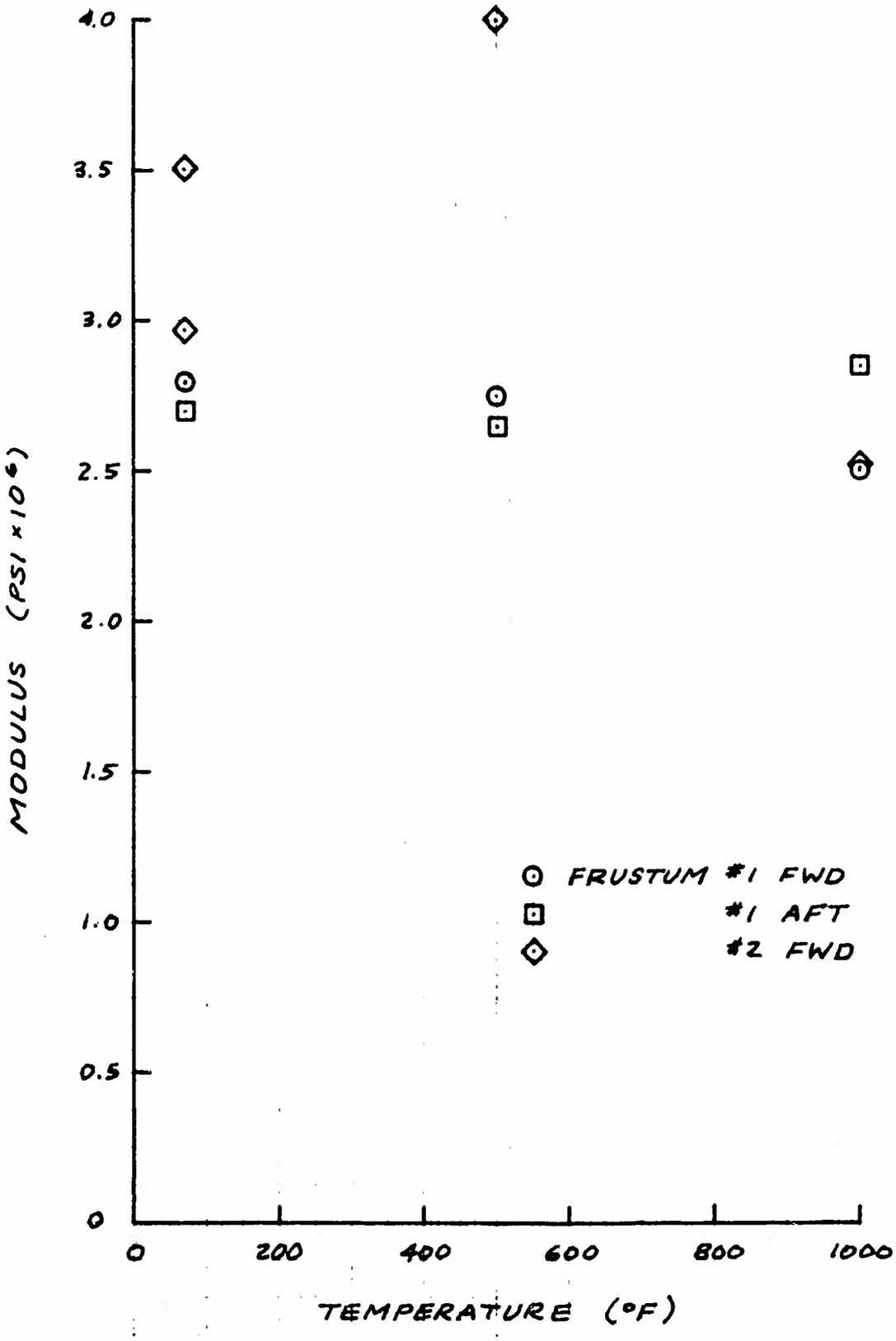

B3720U

FIGURE 15. AS-3DC AXIAL TENSILE MODULUS

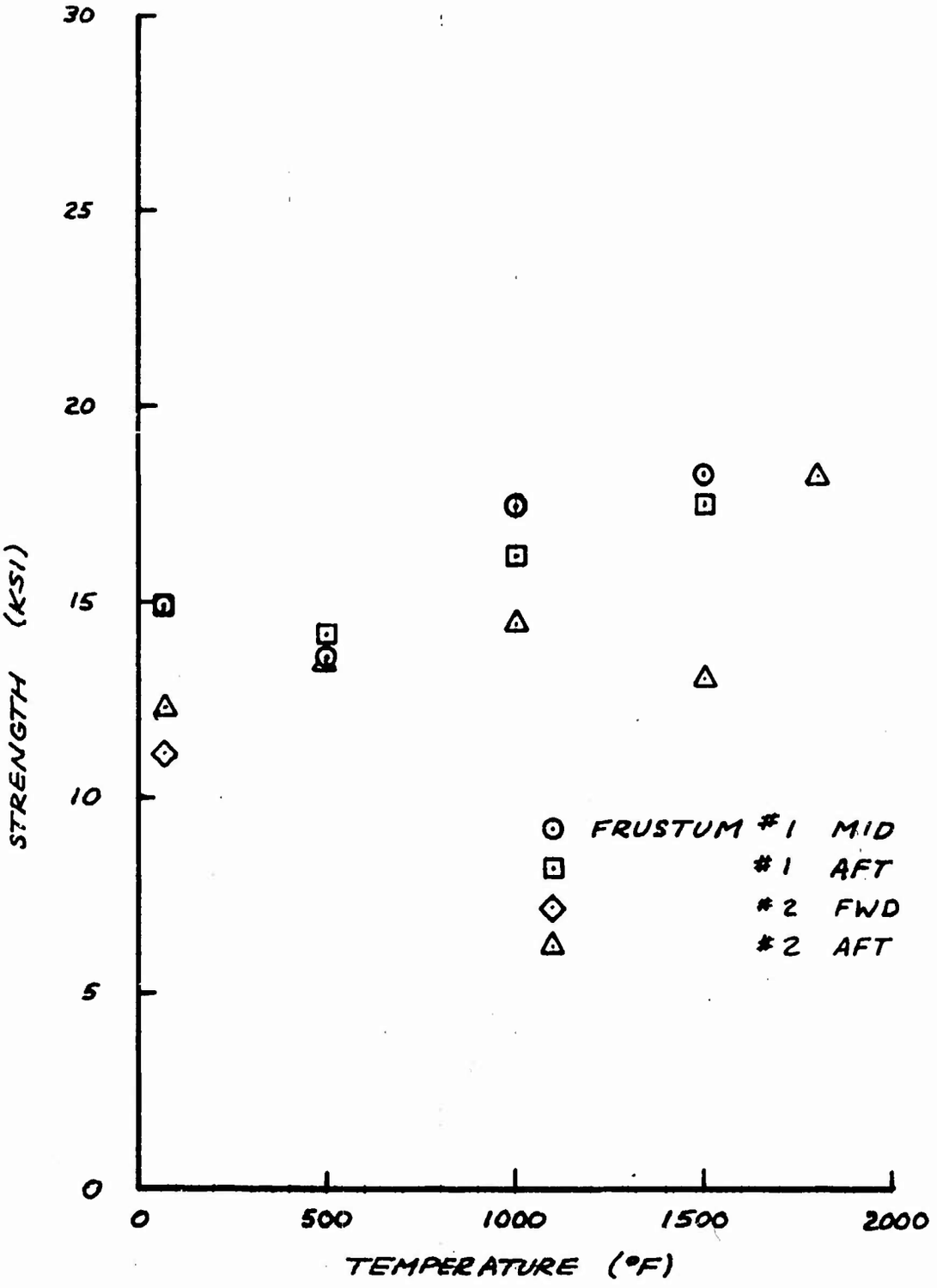

B3721U

FIGURE 16. AS-3DC AXIAL COMPRESSIVE STRENGTH

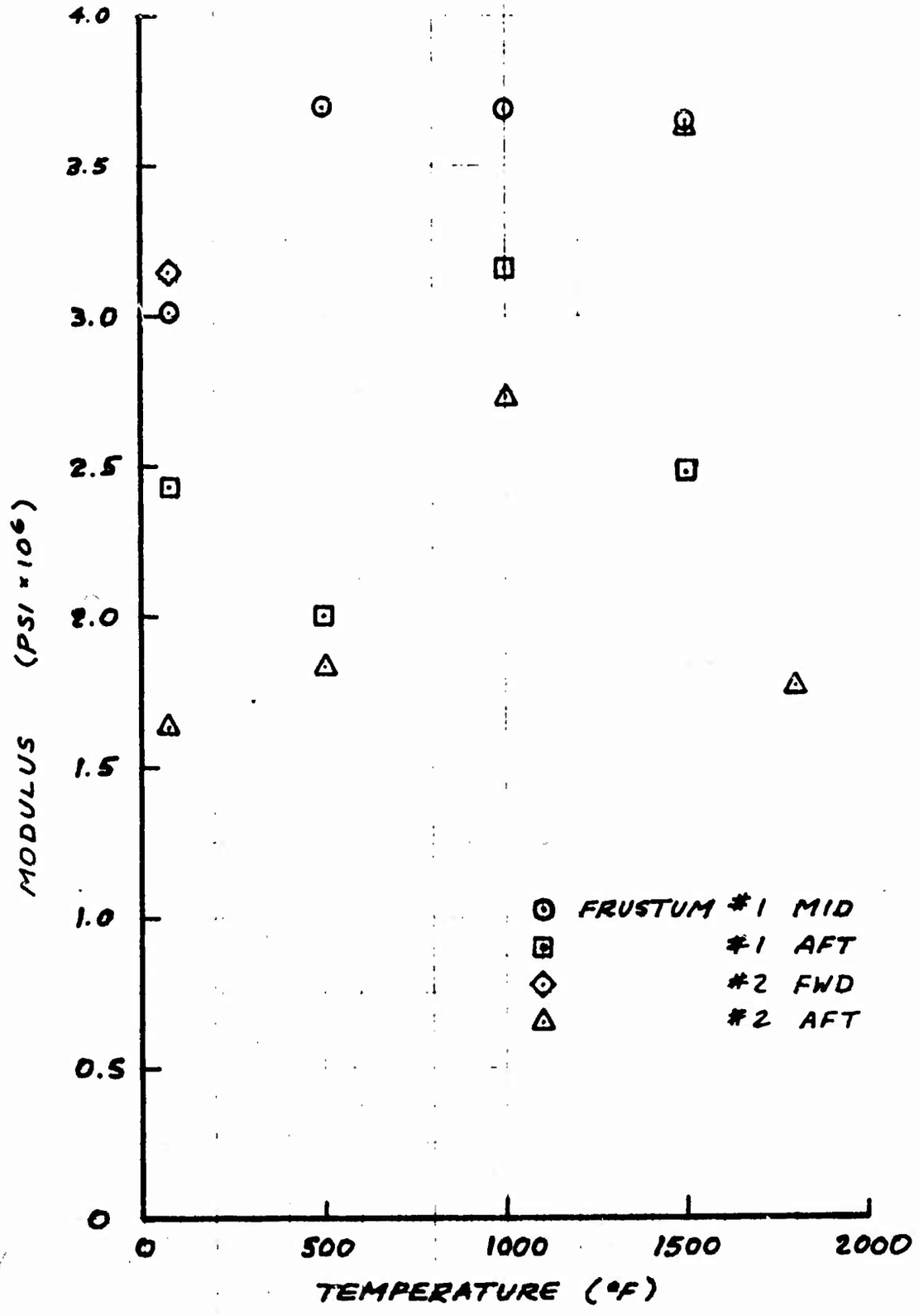

B3722U

FIGURE 17. AS-3DC AXIAL COMPRESSIVE MODULUS

The following room temperature properties were obtained:

- Compressive strength, 8830 psi (average of four specimens).
- Compressive modulus, 3.25×10^6 psi (average of three specimens).

The test data points for strength and modulus are shown in Figures 18 and 19, respectively. The data show that compressive strength increases with temperature, whereas modulus appears to decrease. Specimens taken from the forward region of frustum No. 1 are significantly stronger than specimens taken from the underdense mid region, 74 percent stronger on the average. A full discussion of the frustum characteristics is contained in Section 2.

Specimens from frustum No. 2 showed considerable scatter. A possible explanation for this behavior is shown in the radiograph for these specimens reproduced in Figure 20. The figure shows that specimen 2-CC-5-M, which failed while being installed in the test machine, has badly skewed circumferential fibers. As might have been expected the corner chipped off. Specimen 2-CC-10-M, which failed at 2670 psi has a flaw in the weave. Since this flaw covers a relatively large fraction of the test specimen cross section, the strength value obtained is not representative of the bulk material. For comparison note specimens 2-CC-15-M and 2-CC-20-M which failed at 14,200 psi and 10,700 psi, respectively. Both specimens have relatively straight, flaw-free fiber structures.

4.2 IN-HOUSE TESTS

4.2.1 HOOP TENSILE TESTS

Two forward and two aft hoop tensile specimens shown in Figure 21 were to be tested by applying a uniform internal pressure with a torodial rubber bladder contained between the specimen and the test fixture shown schematically in Figure 21. The test setup is shown in Figure 22.

The instrumentation consisted of four pairs of axial and hoop strain gauges located at 90 degree intervals around the outer periphery of the specimens. The loads were increased in 100 psi increments and the strains were recorded at each increment until failure occurred.

Table IV provides a summary of applied loads and resulting stresses, strain gauge data, and computed material properties. Figure 23 indicates the stress strain curve resulting from averaging the four hoop gauges on each specimen.

The specimens were visually and radiographically examined prior to the test. Photographs were taken prior to and after failure. Based on the pretest visual inspection, it was apparent that the circumferential yarn waviness would result in low strengths. Consideration was given to not testing the defective parts; however, it was decided to test them to determine how badly the strength was impaired by the waviness. For this reason the data are not considered to be representative of future AS-3DC frusta.

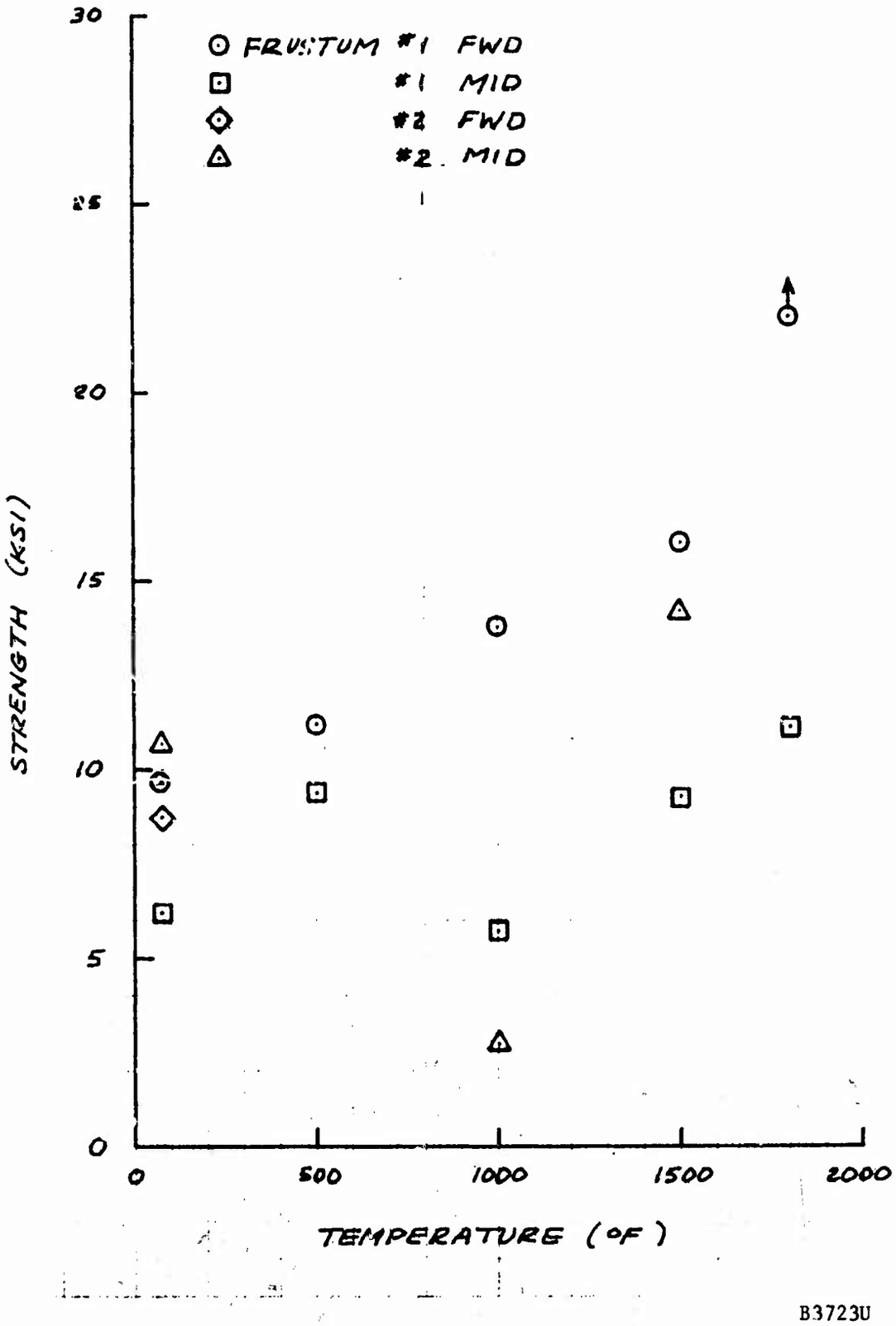

FIGURE 18. AS-3DC CIRCUMFERENTIAL COMPRESSIVE STRENGTH

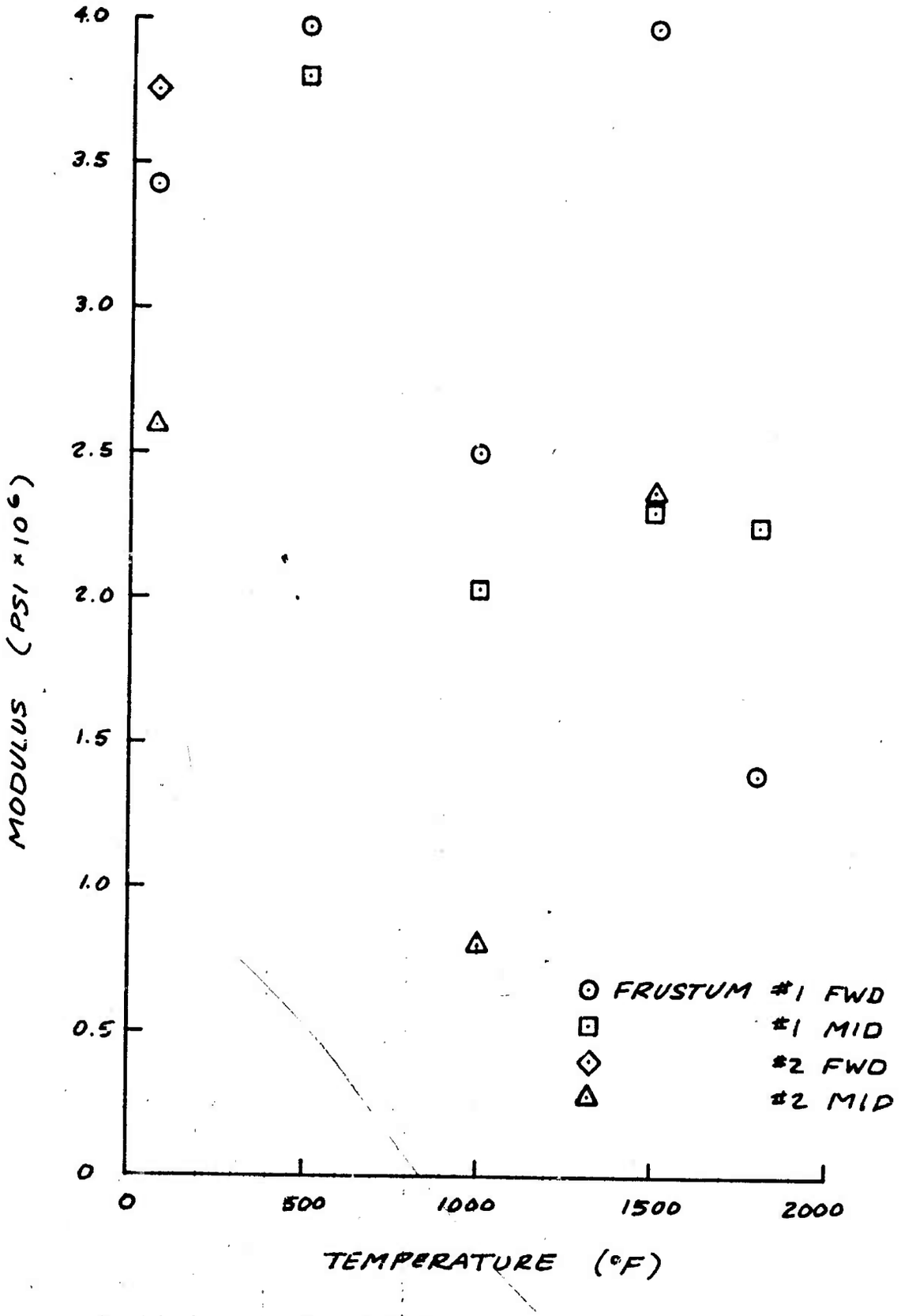

B3724U

FIGURE 19. AS-3DC CIRCUMFERENTIAL COMPRESSIVE MODULUS

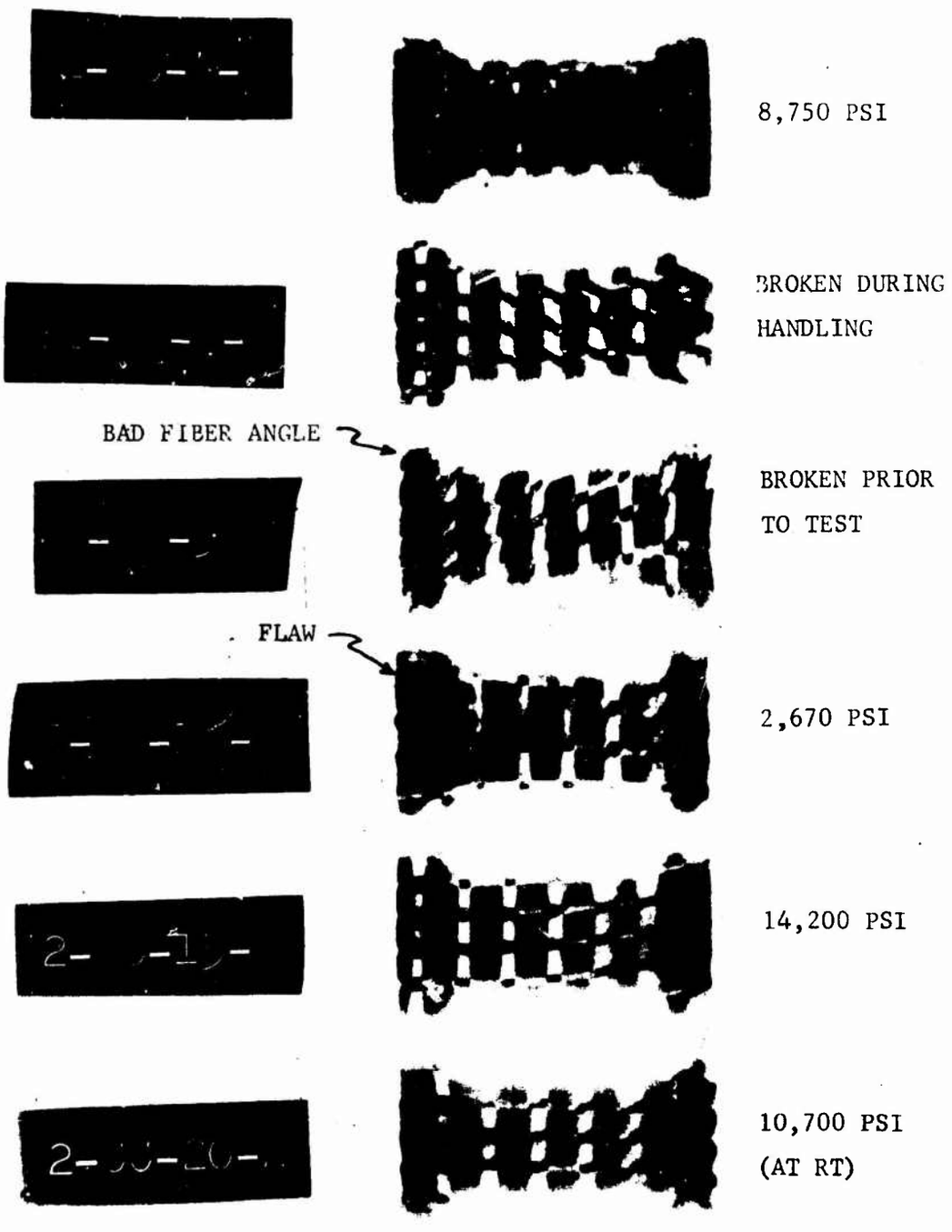

FIGURE 20. X-RAY PHOTOGRAPH OF CIRCUMFERENTIAL COMPRESSION SPECIMENS FROM FRUSTUM NO. 2

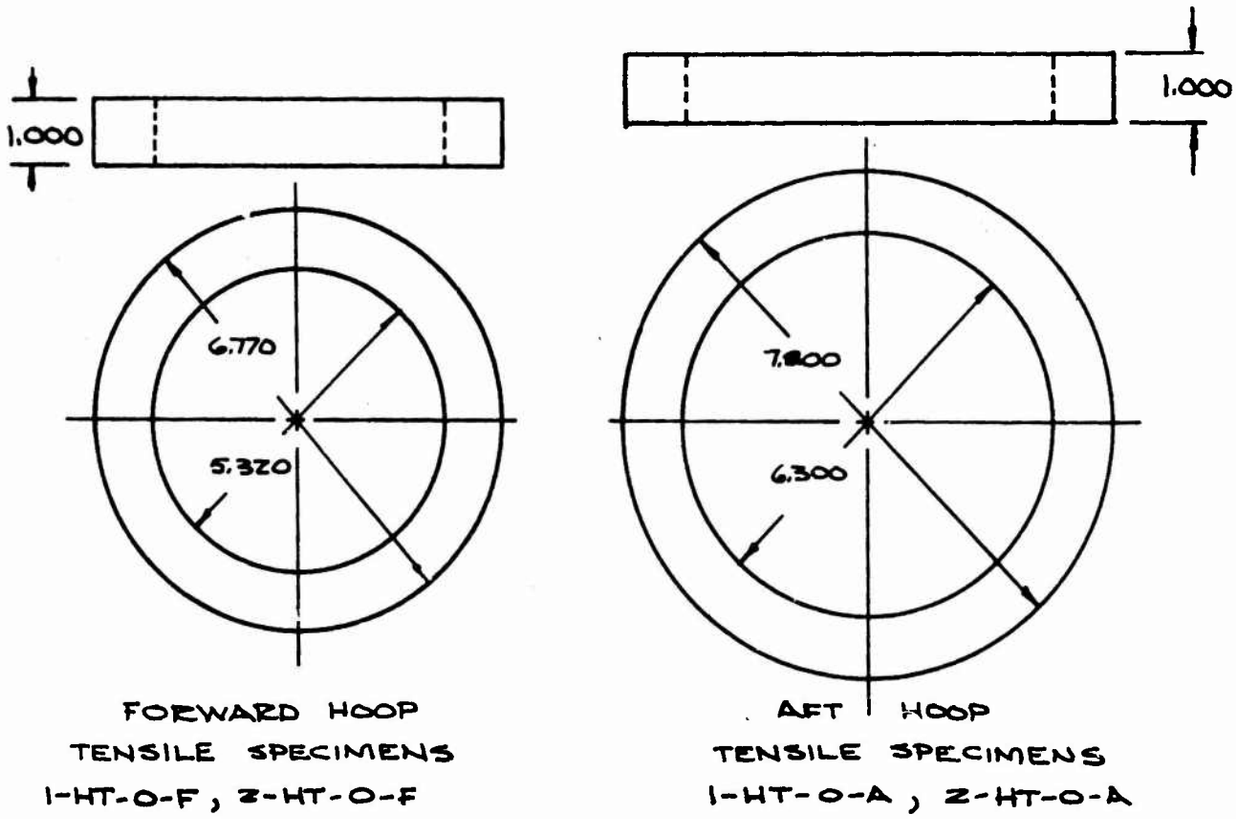

FIGURE 21a. HOOP TENSILE SPECIMENS

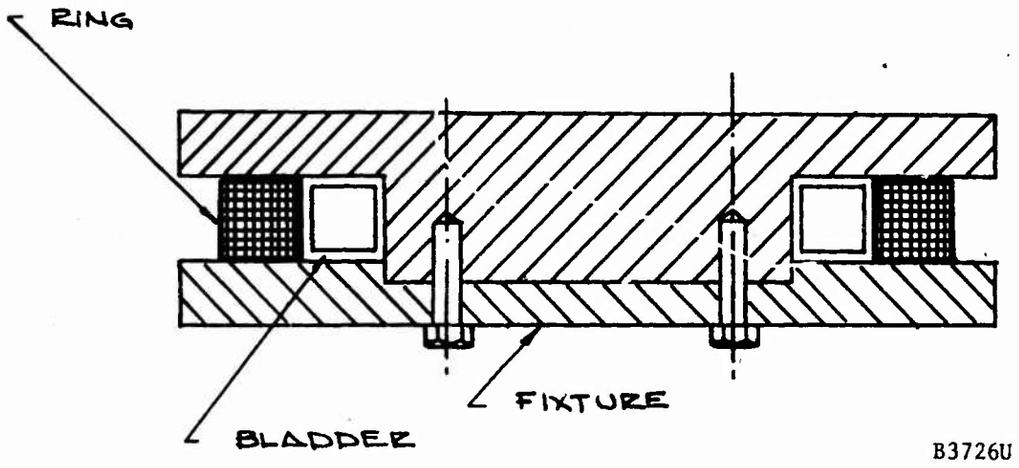

FIGURE 21b. TEST FIXTURE

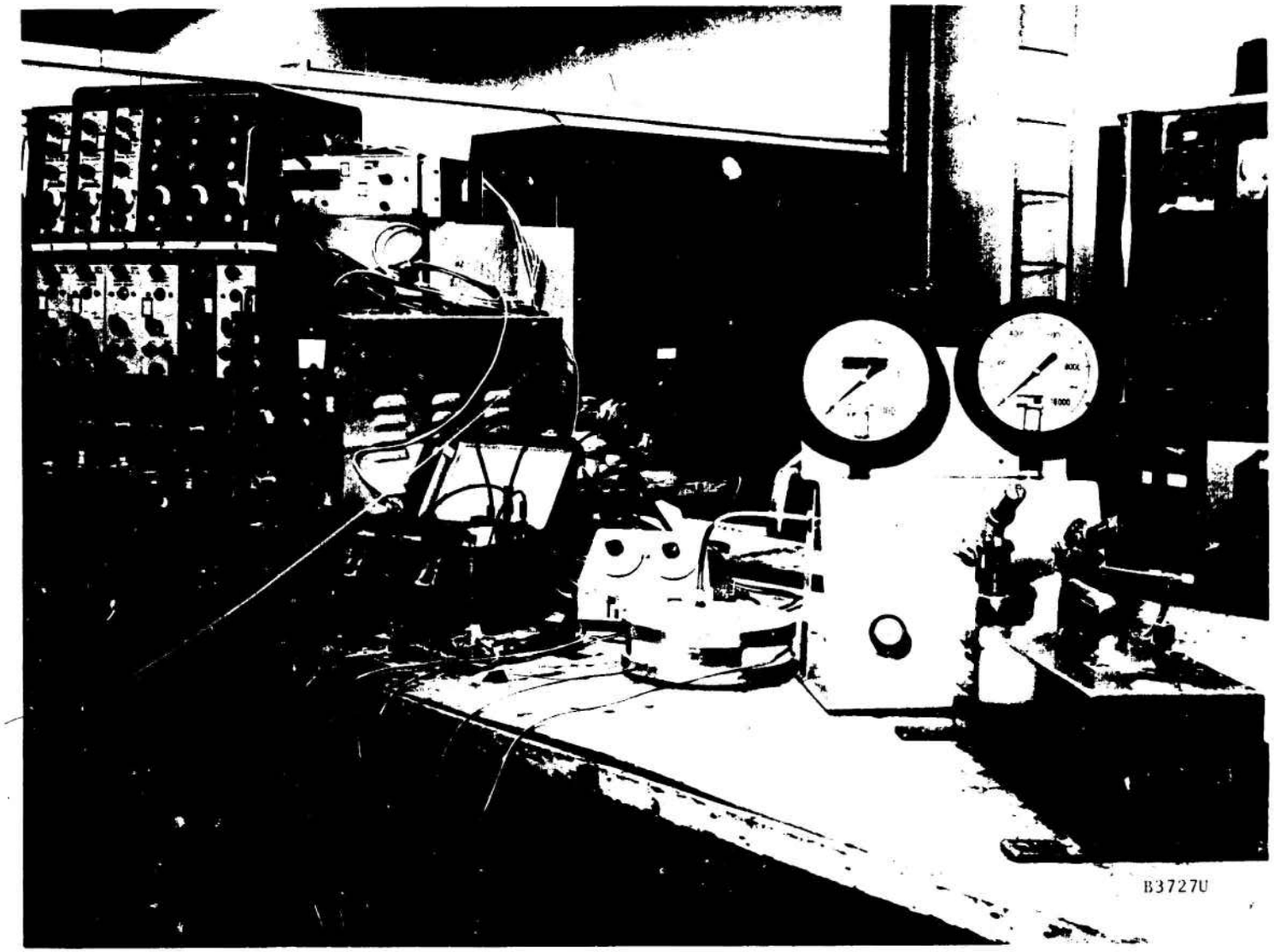

FIGURE 22. HOOP TENSILE TEST SETUP

TABLE IV. AS-3DC HOOP TENSILE SPECIMENS

Specimen Number / Properties		Bladder Pressure (psi)	Outer Hoop Stress (psi)	Inner Hoop Stress (psi)	Strain Gauge Date — Strain (μ inch/inch)							
					1 Axial	2 Hoop	3 Axial	4 Hoop	5 Axial	6 Hoop	7 Axial	8 Hoop
1-HT-O-A		100	375	475	9.86	98.34	3.25	155.62	6.78	122.00	12.69	374.40
$Ex10^{-6}$ (psi) Average	3.30	200	751	951	19.73	199.96	12.98	281.44	20.33	237.23	19.04	587.35
σ_{ult} (psi)	1307	275 @ Failure										
ν Range	0.04 to 0.07											
2-HT-O-A		100	375	475	6.51	134.39	9.78	133.08	0	124.13	-6.44	112.18
$Ex10^{-6}$ (psi) Average	3.07	200	751	951	16.28	285.18	22.83	252.85	10.36	254.98	3.22	218.30
σ_{ult} (psi)	2138	300	1226	1426	22.80	452.36	35.88	382.60	17.27	389.18	16.10	328.97
ν Range	0.04 to 0.09	400	1501	1901	16.28	586.76	45.66	492.39	24.17	503.25	25.76	422.96
		450 @ Failure										
1-HT-O-F		100	323	423	3.33	114.34	3.23	154.82	6.61	166.36	3.24	84.51
$Ex10^{-6}$ (psi) Average	2.63	200	646	846	6.67	238.49	12.90	286.58	9.92	336.11	9.71	214.18
σ_{ult} (psi)	1903	300	969	1269	20.00	372.44	16.13	451.28	13.22	560.18	12.94	358.42
ν Range	0.03 to 0.04	400	1291	1692	23.33	529.25	19.35	635.74	13.22	828.38	12.94	520.15
		450 @ Failure										
2-HT-O-F		Specimen failed at less than 100 psi bladder pres										

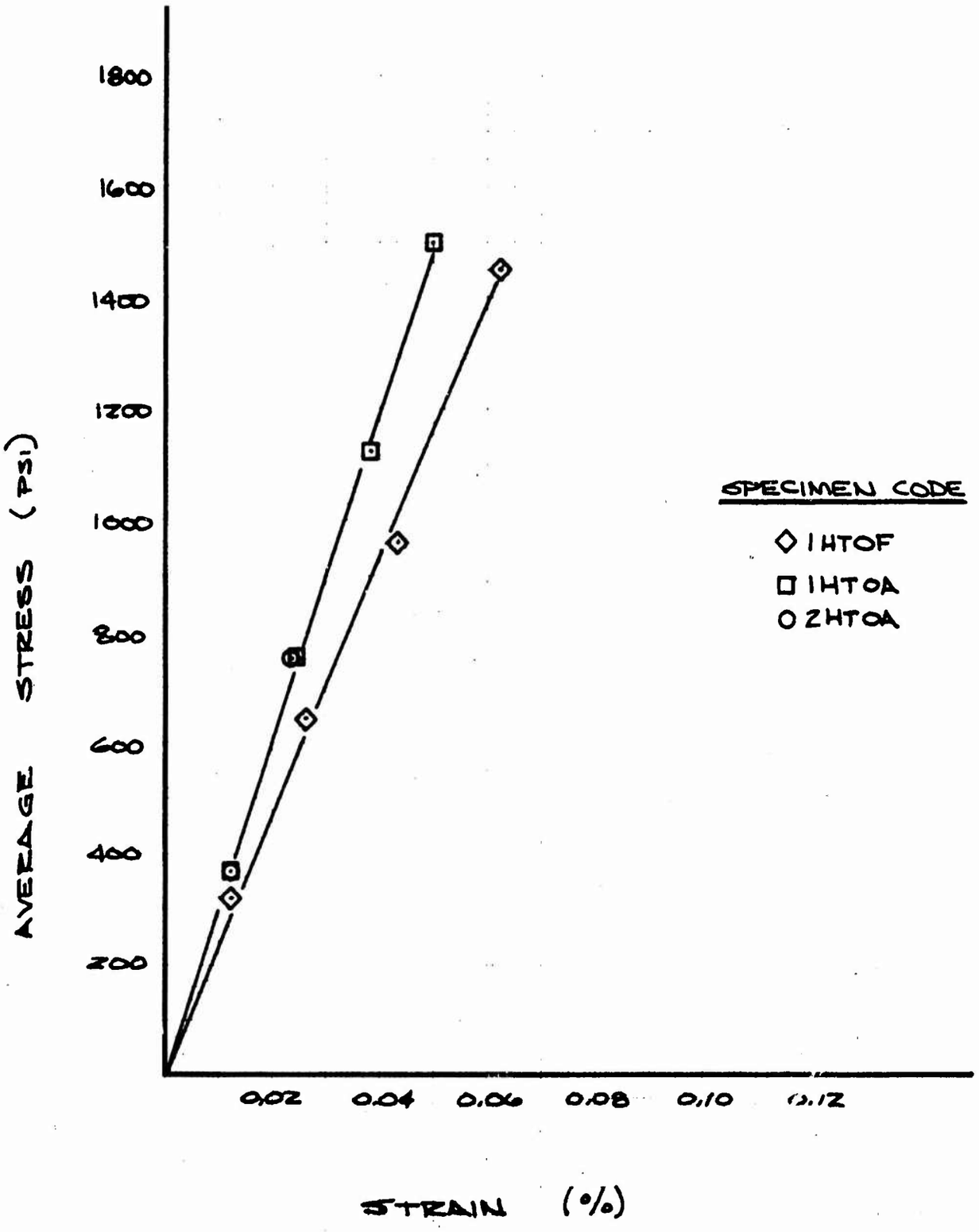

B3738U

FIGURE 23. AVERAGE STRESS VERSUS STRAIN AS-3DC HOOP TENSILE SPECIMENS

Specimen 2-HT-0-F shown in Figure 24 failed while exercising the strain gauges at a bladder pressure of less than 100 psi which corresponds to an inner fiber stress level below 423 psi. The figure indicates axial variations in circumferential fiber directions in excess of 55 degrees.

Specimen 1-HT-0-A which failed at the second lowest inner fiber stress of 1307 psi exhibited high strain readings at hoop gauge No. 8 relative to the three remaining hoop gauges by over a factor of 2.5. The failure occurred within 1 inch of the center of the No. 8 gauge.

Specimen 1-HT-0-F which failed at an inner fiber stress of 1903 psi exhibited a predominance of star patterns evidenced in Figure 25. A discontinuity in the radial fiber pattern adjacent to the fracture surface is also apparent in the previously mentioned figure. The circumferential fiber direction variation is illustrated in Figure 26.

Specimen 2-HT-0-A achieved the highest ultimate strength, 2138 psi. This specimen exhibited the most uniform fiber orientations of the four specimens, as shown in Figure 27. The yarn alignment was good in all three orthogonal directions. This was the only hoop specimen which was anticipated to yield good results based on the pretest observations. The results are not as high as anticipated, however, based on inspection of the fracture substantial improvement is expected with minor refinements. This subject is fully discussed in Paragraph 2.1.

4.2.2 RADIAL COMPRESSION TESTS

Four radial compression specimens were tested in an Instron tensile test machine with the crosshead travel set at 0.05 inch per minute. A continuous record of the applied load was made. The specimen configuration and the resulting ultimate loads and stresses are shown in Table V. The two weakest specimens, 1-RC-0-M and 2-RC-0-M, exhibited erratic load traces which were probably indicative of end crushing of the specimens. It should also be noted that these specimens were from the underdense midsections of the frusta.

4.3 CONCLUSIONS AND RECOMMENDATIONS FOR IMPROVING MECHANICAL PROPERTIES

4.3.1 CONCLUSIONS

The following general conclusions have been reached based on the test data and examination of the test specimens:

- Axial direction properties are much more consistent than circumferential properties, i.e., they exhibit less scatter.

- In general, the axial fibers in the conical frusta are relatively straight and parallel, whereas the circumferential fibers deviate in places as much as 50 to 60 degrees from the true circumferential direction. It is felt that this is the primary reason for the

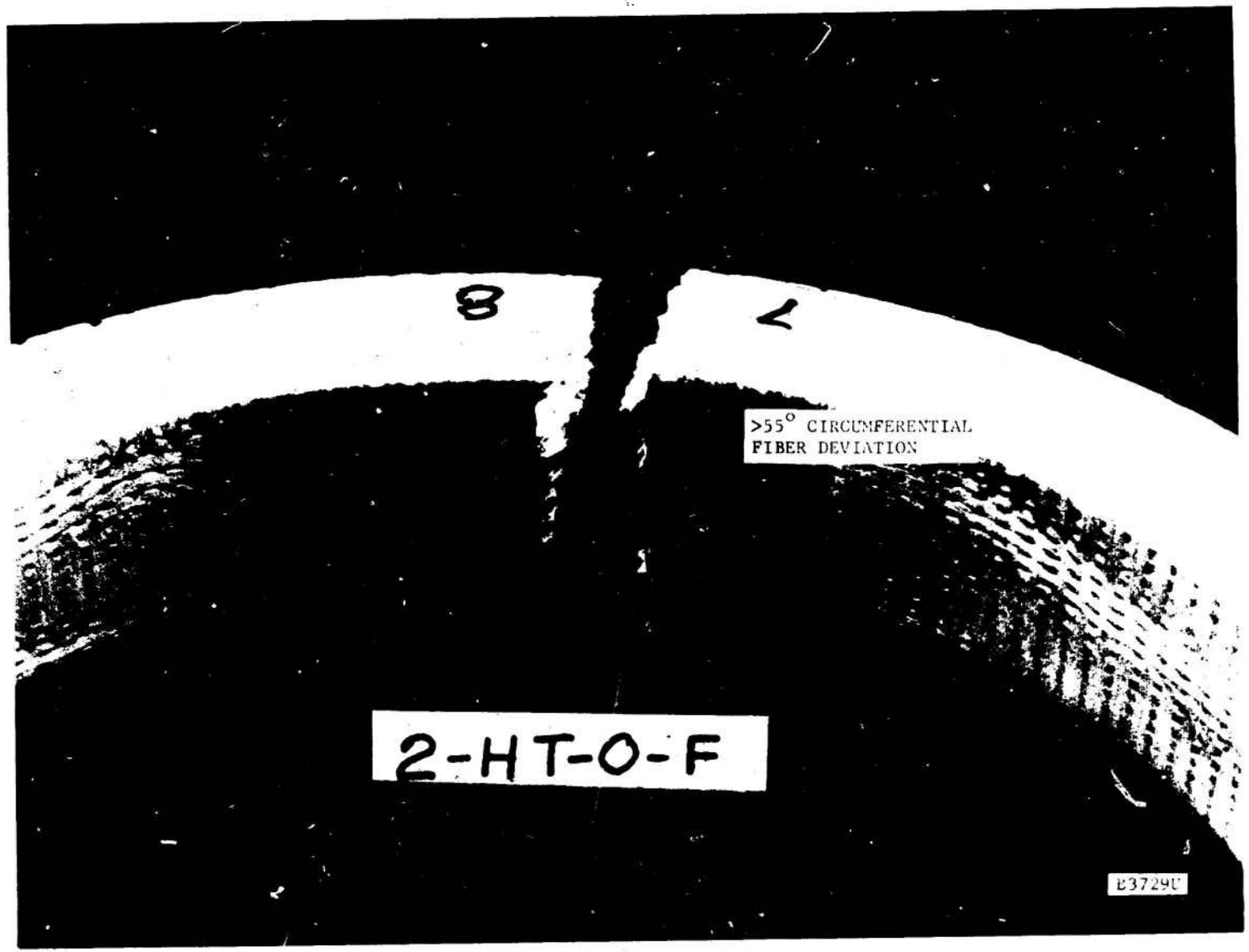

FIGURE 24. HOOP TENSILE FAILURE SHOWING CIRCUMFERENTIAL FIBER DEVIATION

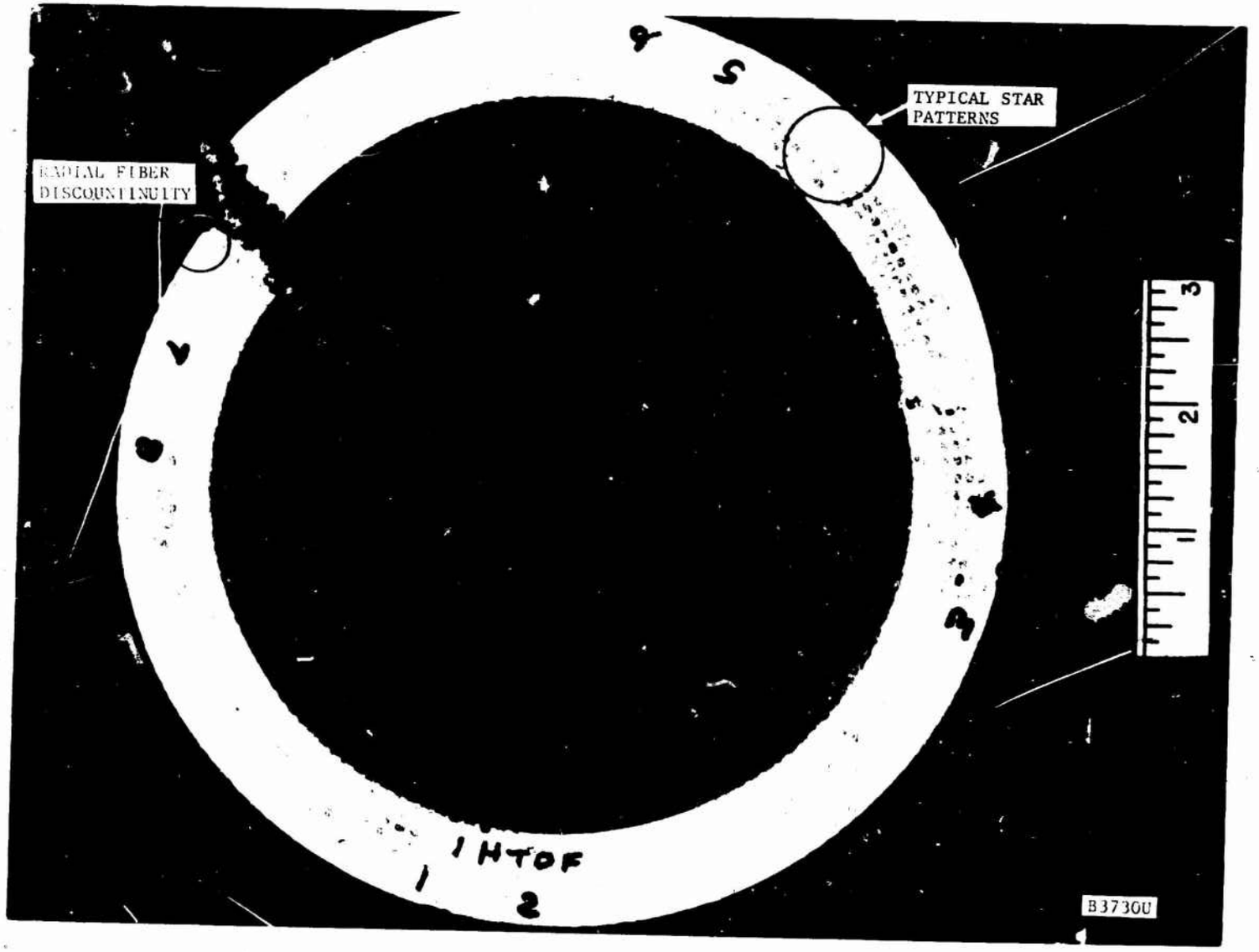

FIGURE 25. HOOP TENSILE FAILURE

FIGURE 26. HOOP TENSILE FAILURE SHOWING FIBER DEVIATION

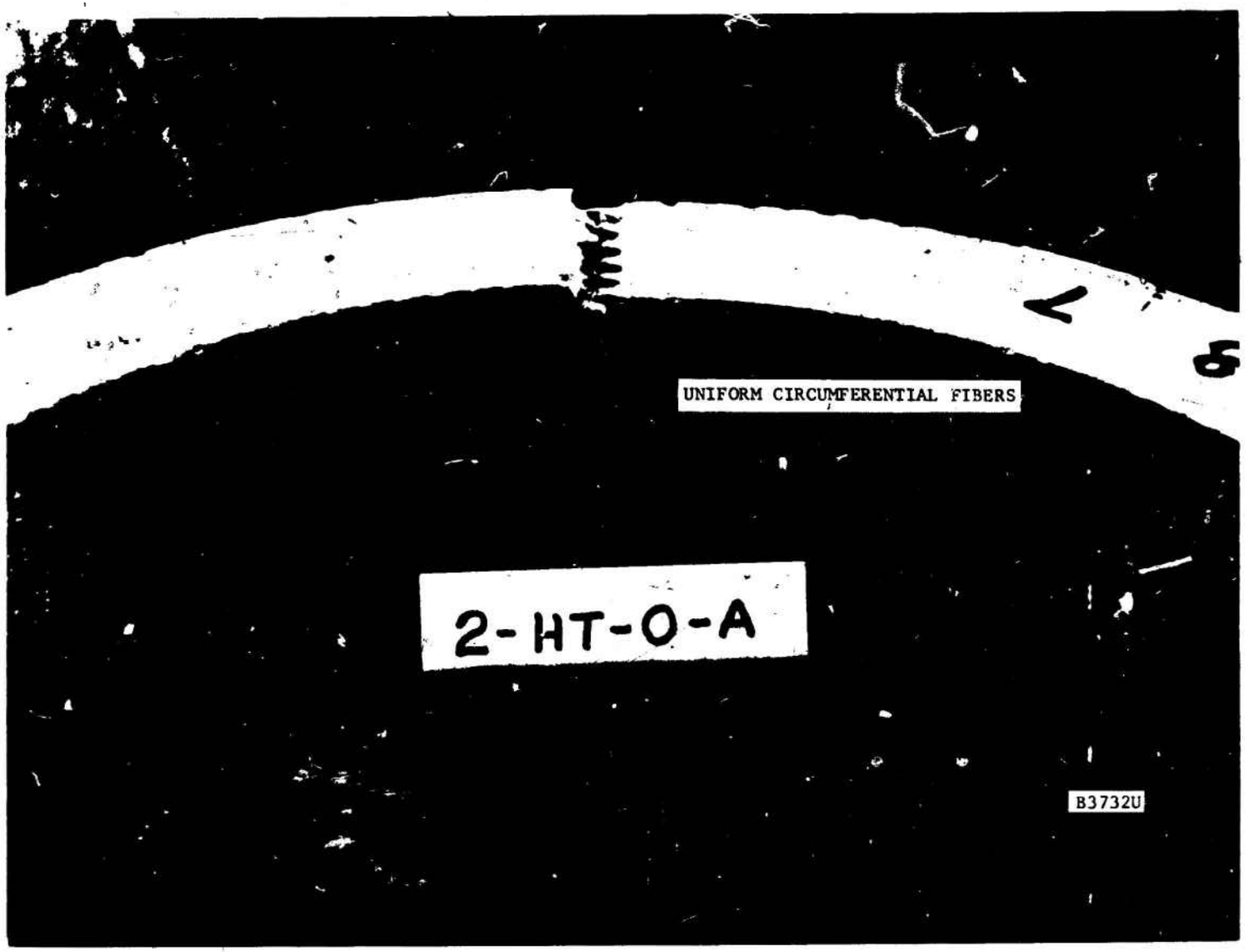

FIGURE 27. HOOP TENSILE FAILURE

TABLE V. RADIAL COMPRESSION DATA

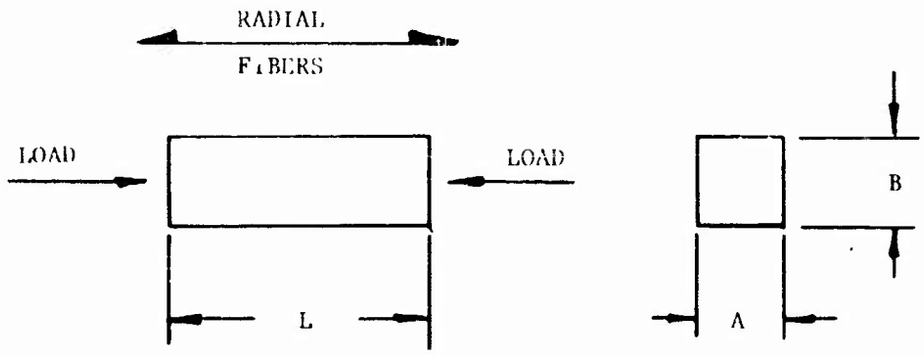

RADIAL COMPRESSION SPECIMENS

Specimen Number	A (in.)	B (in.)	L (in.)	Area ($in.^2$)	Ultimate Load (lb)	Ultimate Stress (psi)
1-RC-O-M	0.4995	0.499	0.996	0.249	1020	4,096
1-RC-O-F	0.501	0.501	0.993	0.251	3470	13,824
1-RC-O-M	0.5015	0.489	0.964	0.245	1750	7,143
2-RC-O-A	0.4985	0.4925	0.998	0.246	2400	9,756

greater scatter in the circumferential direction properties.

- Strength increases with temperature while modulus remains relatively constant.

- Properties for the forward portion of frustrum No. 1 are generally superior.

4 3.2 RECOMMENDATIONS FOR MATERIAL IMPROVEMENT

It is felt that the strength values and associated variability measured in the current test program are quite reasonable for a new composite brittle material in its early development phase. There are two material fabrication factors which are recommended for further investigation with the objective of increasing the mechanical properties and improving their repeatability.

(1) It is recommended that techniques be investigated for improving the "straightness" of the circumferential fibers in the weaving process. It is felt that large variations in the direction of the circumferential fiber was a major factor in the observed scatter.

(2) It is recommended that variations in "fiber packing" and resulting material density be investigated further. At both extremes of the frusta the circumferentials were tightly packed, the silica matrix completely filled the voids between fibers, and the resulting material density exceeded 1.7 gm/cc. It has been observed in previous work with quartz-silica materials (Reference 7) that under these conditions the fiber reinforced material behaves like a homogeneous brittle material such as slip cast fused silica. Fracture planes are flat, showing little evidence of fiber action, and strength values are low. This behavior was exhibited by the circumferential tension specimens.

When the fibers are less tightly packed, the voids between fibers do not fill completely, and the resulting density is between 1.50 and 1.60 gm/cc. Under these conditions the fracture surfaces are very jagged, showing strong evidence of desirable individual fiber breakage. Resulting material strengths are higher. Most of the axial tension specimens exhibited fibrous fractures. Figure 28 is a photograph of a typical fractured tensile specimen. It is theorized (Reference 7) that the looser weave and the voids in the matrix permit the fibers to move, and therefore distribute the load, whereas in the higher density material the fibers are more restrained against moving.

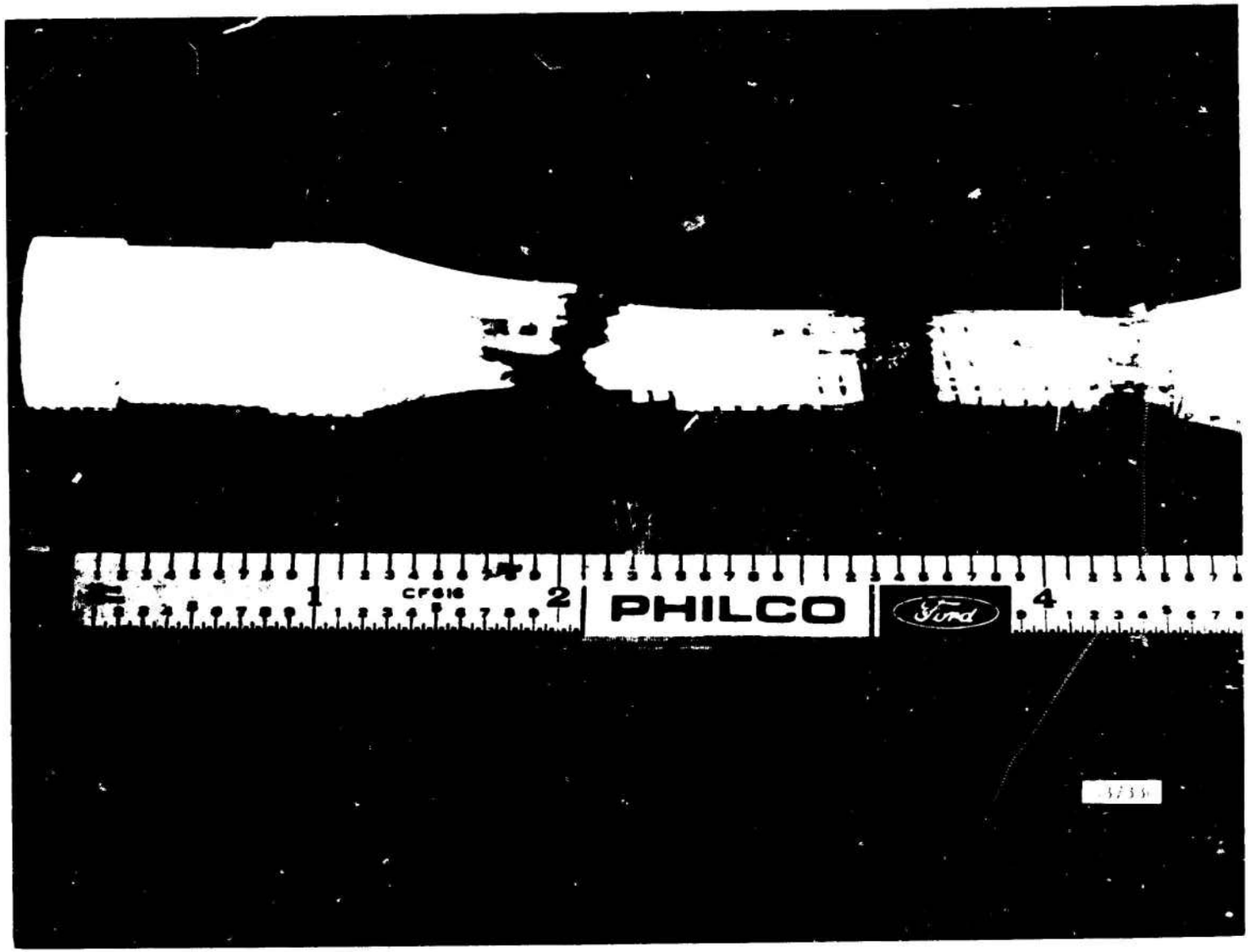

FIGURE 28. TYPICAL FIBROUS FRACTURE

An attempt was made to correlate axial tensile and compressive strengths with density. The results are shown in Figures 29 and 30. Since the density range is not very wide, and the results are influenced by weaving imperfections, the trend with density is not conclusive. It appears possible that the strength might decrease with density. Further work is recommended to determine the effects of fiber spacing and related material density.

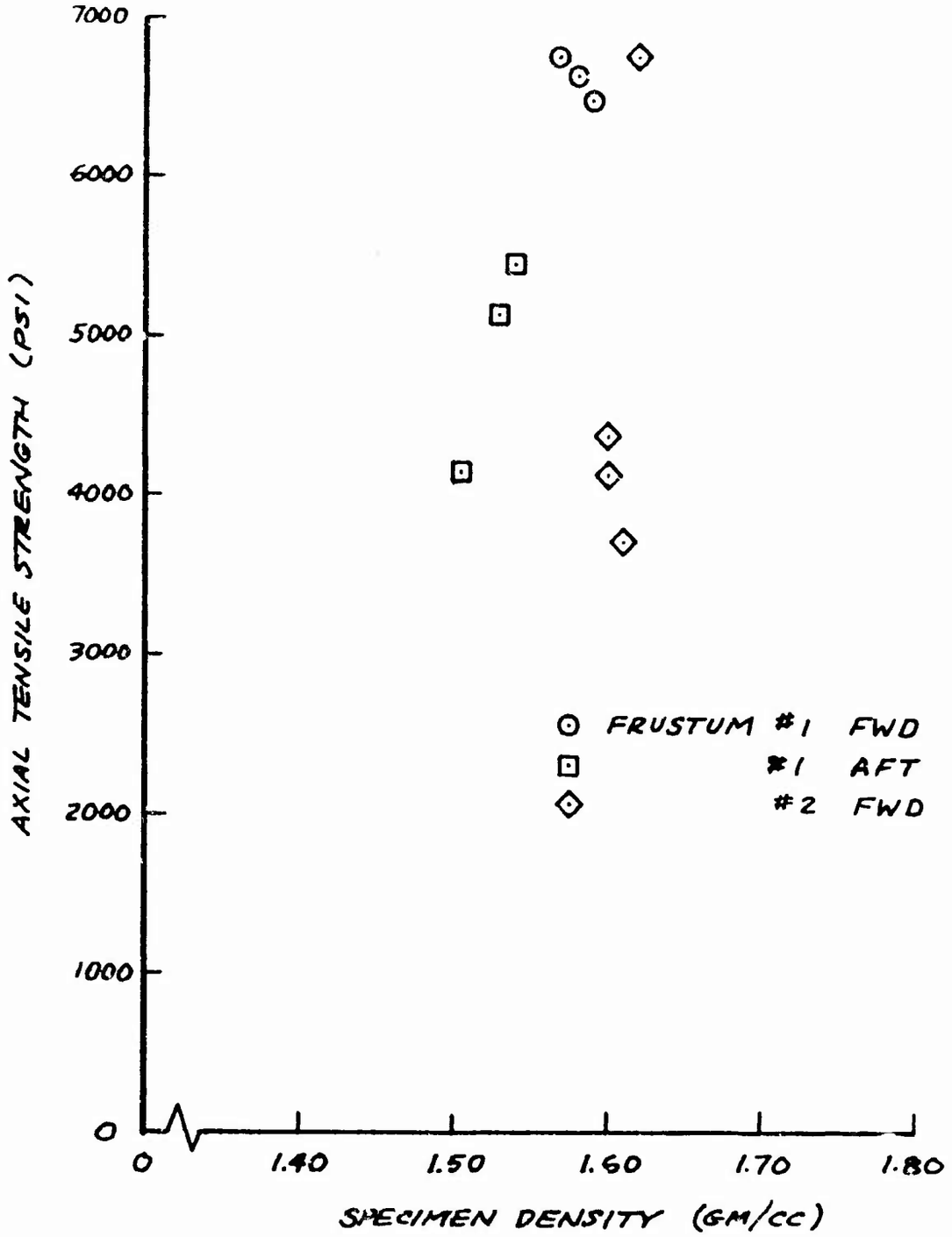

B3734U

FIGURE 29. AS-3DC AXIAL TENSILE STRENGTH VERSUS DENSITY

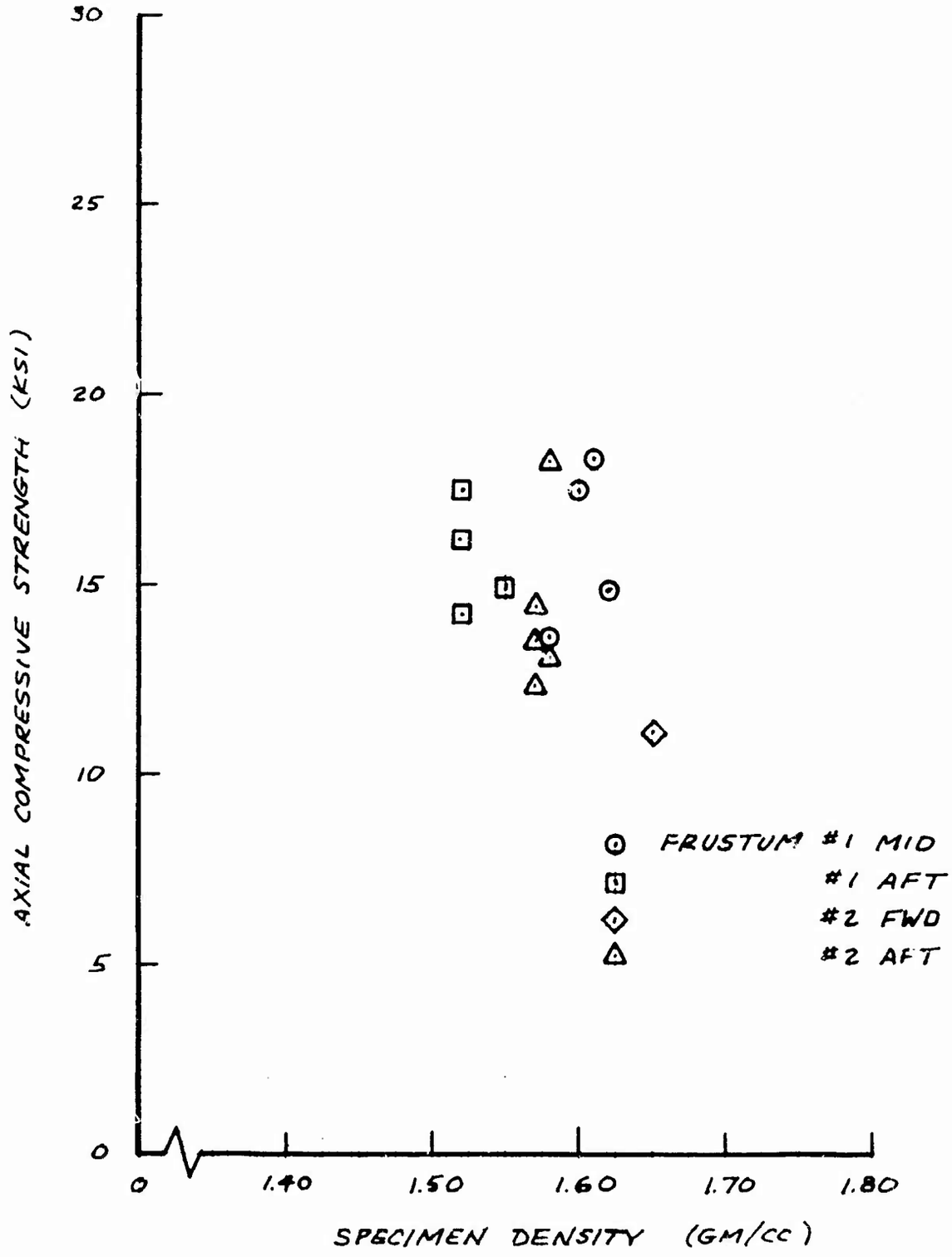

FIGURE 30. AS-3DC AXIAL COMPRESSIVE STRENGTH VERSUS DENSITY B3735U

SECTION V

THERMAL PROPERTIES

Characterization of the thermal properties of AS-3DC were carried to the extent necessary to provide high-confidence, preliminary-design data. Turbulent heat of ablation, thermal conductivity, heat capacity, and thermal expansion were measured.

5.1 TURBULENT HEAT OF ABLATION

Four AS-3DC specimen models were tested at two different flow conditions in the Avco 10 MW plasma arc heater. The objectives of the tests were: (1) to measure the effective heat of ablation in turbulent flow, (2) to determine the fraction of ablated material that is vaporized, and (3) to determine the material backface temperature response caused by thermal conduction and thermal radiation transmittance, if any, through the radial quartz fibers. Each test model included a specimen of AS-3DC material bonded to a phenolic-silica model holder. The four AS-3DC specimens were cut from selected locations within the first two cone frusta. Three of the ablation specimens were cut from regions of differing density in the first frustum, while the fourth specimen was cut from a similar, high-density region from the second frustum. A cutting plan was prepared (Section III) and each specimen was identified as to its location and density within each frustum. The identification of each specimen, its density, and the associated test model number and test condition are given in Table VI.

Two models were tested at one condition and two at a second condition as shown in Table VII. Both test conditions were representative of the turbulent heating and enthalpy values for a typical re-entry trajectory. The models were mounted such that the leading edge was flush with the rectangular nozzle exit plane with the flat model surface at an angle of either 10 or 15 degrees to the flow. The models were supplied by Philco-Ford to fit the model holder of the arc-jet subcontractor, Avco Corporation. The test time was kept constant at 10 seconds between all models to give comparative results.

A heat flux calibration of each test condition was performed with a calorimeter model of the same external shape as the test specimens. The calibration tests were performed at the same plenum pressure and enthalpy conditions as for the model tests. Photographs of the calibration model and the calibration results are shown in the Subcontractor Data Report (Appendix III).

Instrumentation for each test model included two backface thermocouples and three backface calorimeters. The thermocouples were mounted in slots machined in the phenolic silica base material such that the thermocouples lay behind and in contact with the AS-3DC material when bonded to the base. The leads were potted in place with Saureisen cement and the junctions were made to contact the backface of the AS-3DC by bending of the junction bead. The thermocouples were 28 gage fiberglass-covered, chromel-alumel wires.

TABLE VI. TURBULENT Q* TEST SPECIMENS

Model Number	Specimen Number	Density	Test Condition
AS-1	1-TA-0-A-1	1.50	AFT-1
AS-2	1-TA-0-M-2	1.63	AFT-1
AS-3	1-TA-0-A-3	1.54	AFT-2
AS-4	2-TA-0-A-4	1.60	AFT-2

TABLE VII. TURBULENT WEDGE ABLATION TEST CONDITIONS

Condition	AFT-1	AFT-2
Surface Heat Flux, Btu/ft^2-sec (Average)	850	1050
Total Enthalpy, Btu/lb	4000	8300
Exit Mach Number	2.5	2.0
Model Wedge Angle, degree	15	10
Exposure Time, seconds	~10	~10
Number of Models	2	2
Surface Pressure, atmospheres (Average)	1.82	1.13
Surface Shear PSF (Average)	58	40

Three oxygen-free, high-conductivity, copper calorimeters, 0.188-inch diameter by 0.100-inch long, were used to measure the AS-3DC backface radiation in each specimen. Each calorimeter had a coating of high emissivity PT404A paint on the surface viewing the AS-3DC backface. The calorimeter response was measured by 28 gauge chromel-constantan thermocouples with junction staked into the backface of the calorimeter. A 0.032-inch thickness of Fiberfax paper was used to insulate the calorimeter from the surrounding phenolic silica base. The calorimeters were recessed 0.030-inch into the phenolic silica to preclude conduction from the AS-3DC backface, thus permitting only radiation to be measured by the calorimeters.

Additional external instrumentation was used to measure model surface temperature, total surface radiation, the recession profile (from a series of still photographs). The pyrometer and total radiation thermopile were sighted as closely as possible to the center of the model surface with the sight diameter made as small as was practicable (about 0.1 inch). Color motion pictures were taken of each test at a film speed of 100 frames per second. The "f-stop" setting of the camera allowed observation of as much ablation mechanism detail as possible. Still photographs (black and white) of the test setup and of the models before and after each test were taken (see Appendix IV).

5.1.2 RESULTS

One heat flux and pressure calibration was made for each test condition. The average heat flux determined for each of the conditions is given in Table VII. Average surface pressures are also given in Table VII. The heat flux distribution for each of the conditions is shown in Figure 31. Additional details of the calibration results are given in the Subcontractor's Data Report (Appendix IV).

Each of the four AS-3DC models was tested for 10 seconds. The test results are summarized in Table VIII; pretest and post-test photographs of the specimen are shown in Appendix IV. A visual inspection of each model and of the films revealed moderate flow of the softened quartz caused by the arc-plasma flow impingement on the test specimen at an angle of approximately 10 to 15 degrees. The models tested at the lower heat flux condition showed a darker surface appearance because of apparent deposition of a carbonaceous-looking "soot" from the arc-jet electrodes. The deposits were similar to those observed in previous antenna window ablation tests (Reference 8).

5.1.3 ANALYSIS

The post-test analysis included the calculation of effective heats of ablation, Q*, and comparison with theory for quartz. The Q* values calculated for each of these tests on AS-3DC are given in Table VIII. Figure 32 shows the heat of ablation as a function of enthalpy difference for AS-3DC and for AS-3DX based on previous antenna window tests (Reference 8).

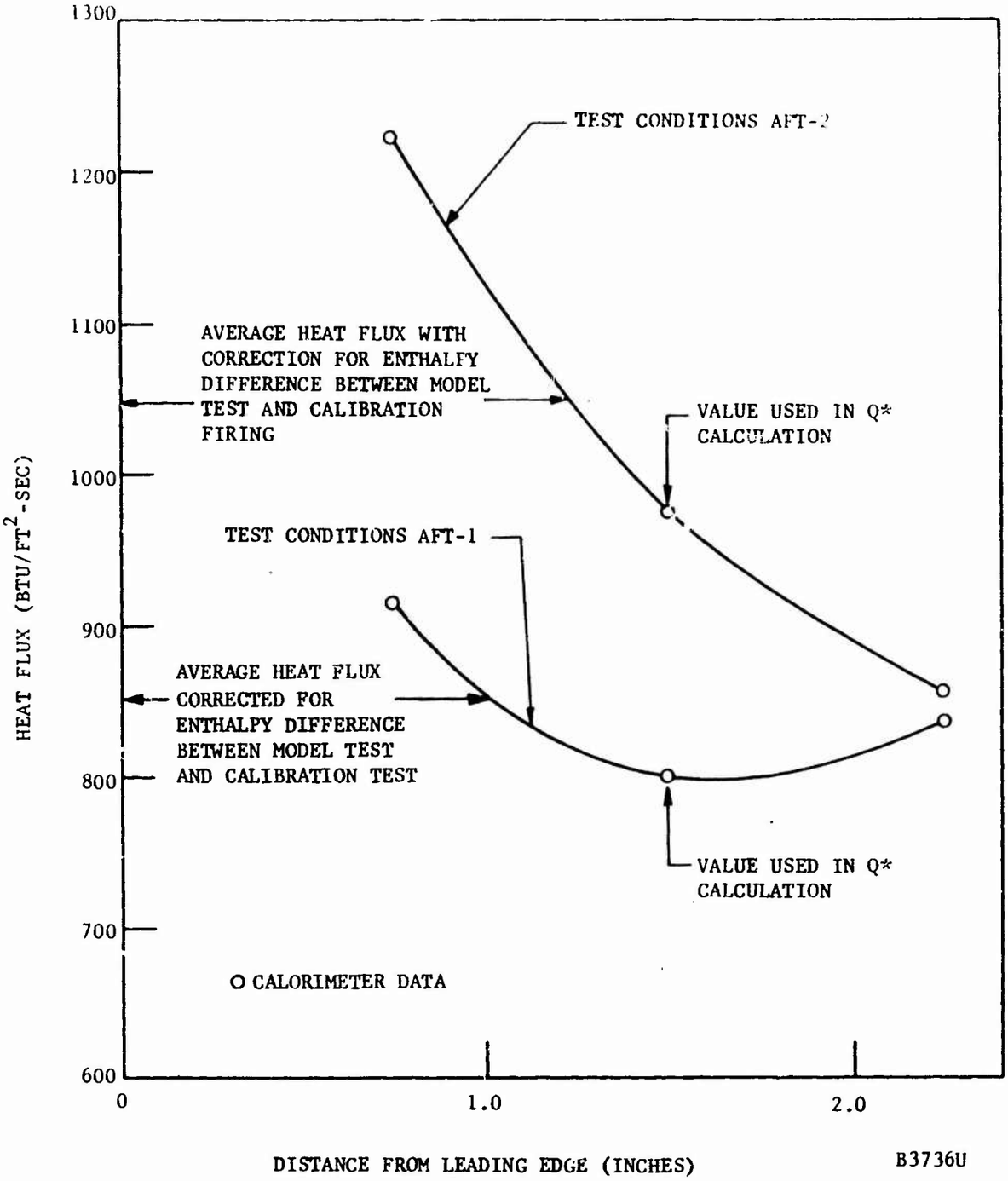

FIGURE 31. CALIBRATED HEAT FLUX VARIATION ALONG THE MODEL SPECIMEN CENTERLINE

TABLE VIII. SUMMARY - AS-3DC TEST DATA

Model	Run No.	Q_{cw} (1) (Btu/ft^2-sec)	T_T (2) (^oF)	Q_{rad} (3) (Btu/ft^2-sec)	H_o (Btu/lb)	τ_w Lb/ft^2	Q* (4) Btu/lb	$\bar{\gamma}$ (5) (CM^{-1})	A_R/A_T (6)
AS-1	9116	850	4650	70	4000	58	4000	30.2	0.145
AS-2	9117	850	4510	65	4000	58	4960	34.9	0.1162
AS-3	9122	1050	4900	85	8300	40	6000	30.3	0.1455
AS-4	9123	1050	4880	87	8300	40	6020	30.9	0.1320

NOTES:
(1) Average heat flux value across specimen.
(2) True surface temperature at shutdown.
(3) Measured surface radiation.
(4) Q* calculation based on measured Q_{cw} at 1.50-inch from leading edge (calibration firing) and Nikon profile camera recession rates.
(5) Based on view factor, F, = 0.74 and calorimeter emissivity, ϵ = 0.90.
(6) Ratio of radial fiber bundles area to total specimen surface area.

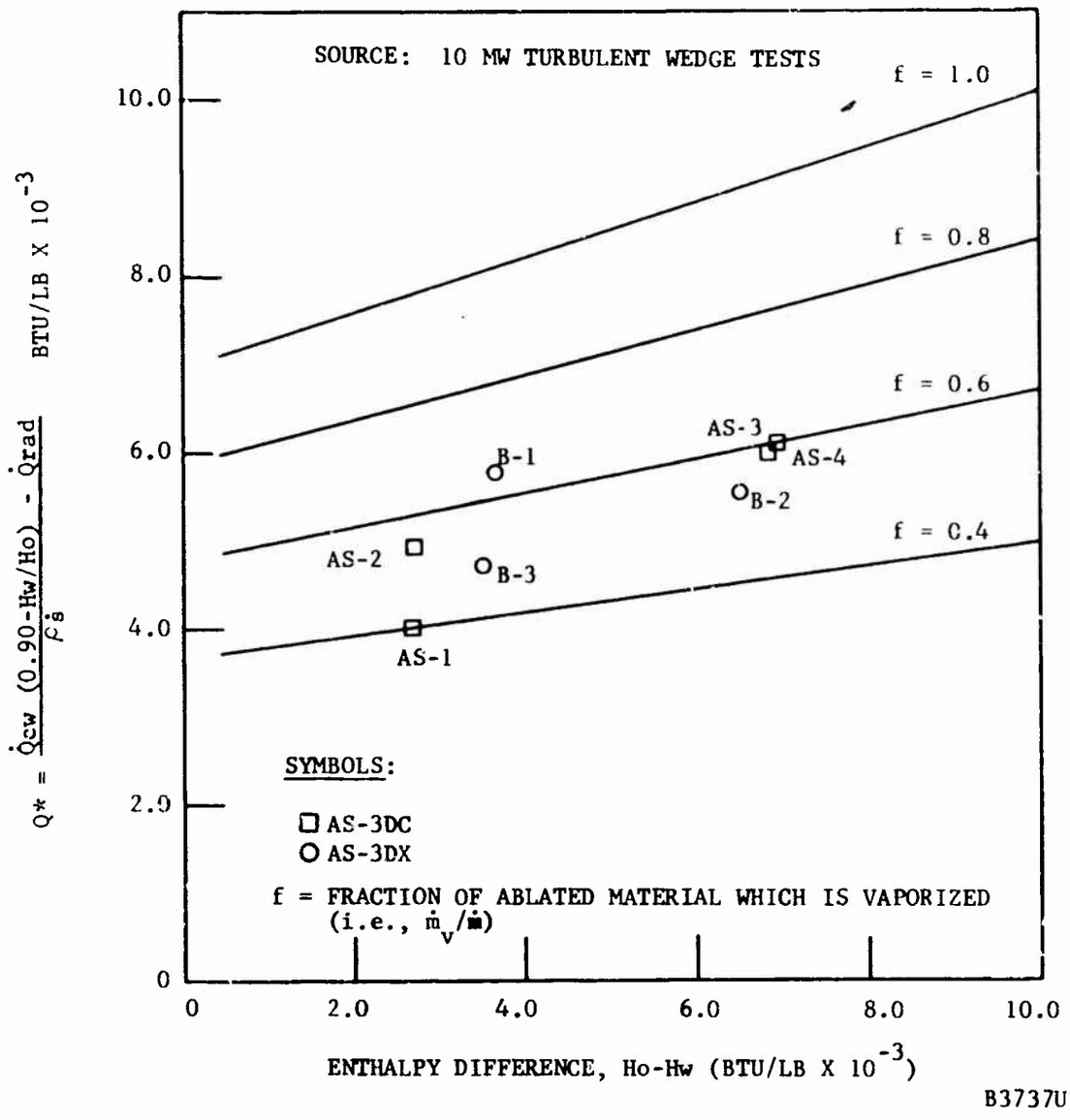

FIGURE 32. EFFECTIVE HEAT OF ABLATION VERSUS ENTHALPY DIFFERENCE FOR AS-3D MATERIALS

The net effective heat of ablation for the AS-3DC was calculated from the relationship:

$$Q^*_{net} = \frac{\dot{Q}_{cw}(0.90-H_w/H_o)-\dot{Q}_{rad}}{\rho \dot{S}}$$

where

Q^*_{net} = net effective heat of ablation, Btu/lb.

$\dot{Q}_{cw}$ = average measured cold wall heat flux, Btu/ft^2-sec.

H_w = surface enthalpy based on measured true surface temperature, Btu/lb.

H_o = free stream total enthalpy - based on an energy balance in the arc-jet plenum, Btu/lb.

$\dot{Q}_{rad}$ = total surface radiation (from the Eppley thermopile), Btu/ft^2-sec.

ρ = material density, lb/ft^3.

$\dot{S}$ = surface recession rate, ft/sec (based on Nikon Camera profile measurements).

Since the Q* values were calculated for the recession measured by the Nikon Camera, the correct heat flux at the camera location was required. Figure 31 shows the axial variation for the calibration firings. The heat flux 1.50 inches from the leading edge was used in the Q* calculation. The true surface temperature of the quartz window was calculated based on the measured surface brightness temperature and a spectral emissivity of 0.5 at the wavelength of the pyrometer (0.8μ). The hot-wall heating rate correction factor, $(0.90-H_w/H_o)$, was used to be consistent with previous Q* data (References 8 and 9). This factor adjusted the measured cold-wall heat rates to account for a combination of turbulent-flow boundary layer recovery, enthalpy losses to the expansion nozzle, and hot-wall heating rate.

The calculated Q* values shown in Figure 32 as a function of enthalpy are also compared with theoretical Q* values calculated with the fraction of ablated material that is vaporized, f_v, as a parameter. The theoretical Q* calculations used the thermodynamic and thermochemical properties of quartz given in Reference 10. From the results shown in Figure 32 the fraction of ablated quartz that was vaporized was determined to be from 0.40 to 0.60.

A comparison of the dependence of vaporization fraction on material density and on the percentage radial fiber area is shown in Figure 33 and 34, respectively. Note that there appears to be an increasing trend of vaporization fraction with increasing density. However, the comparison of vaporization fraction with percent of radials was not conclusive.

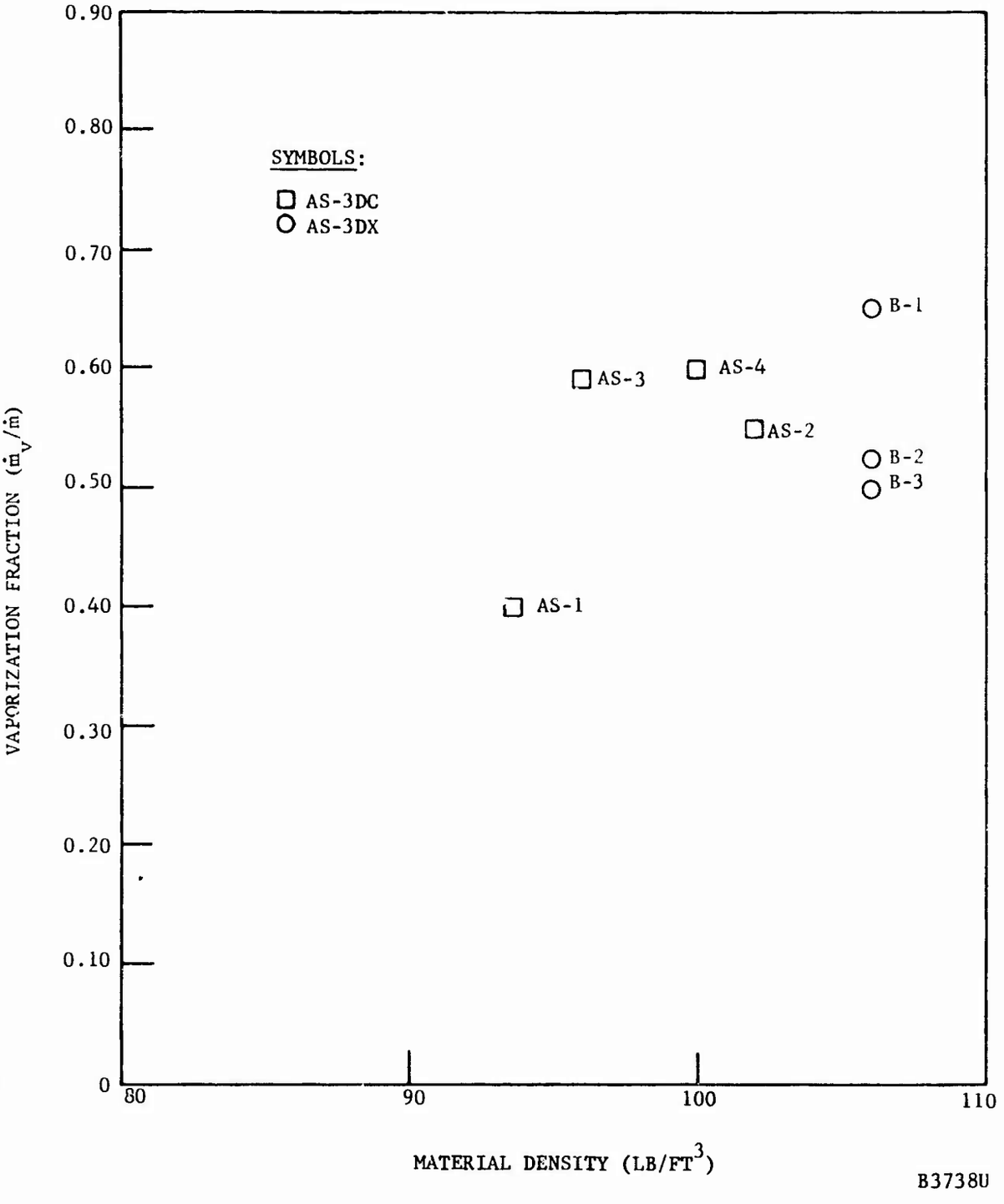

FIGURE 33. VAPORIZATION FRACTION VERSUS MATERIAL DENSITY FOR AS-3D TEST SPECIMENS

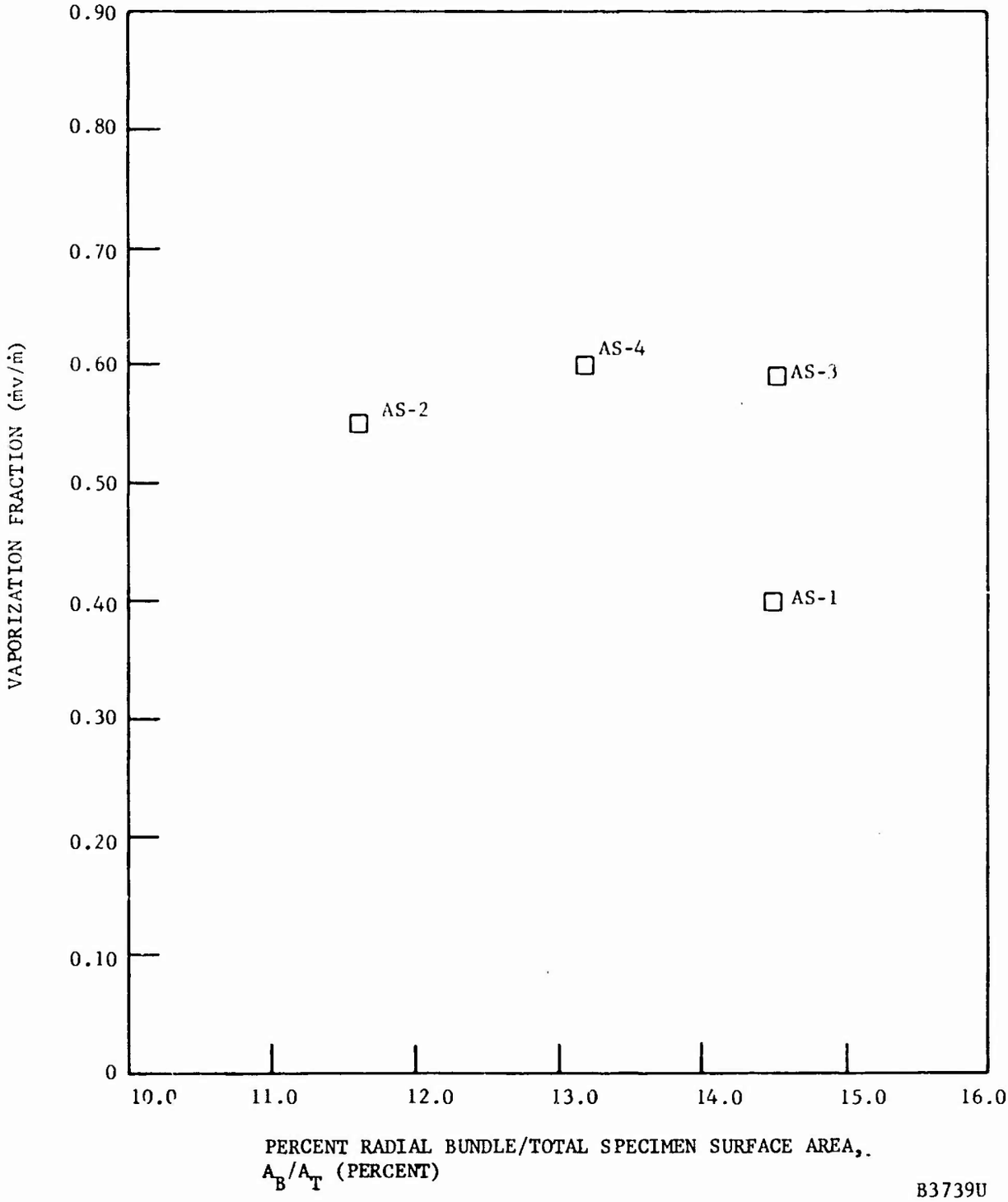

FIGURE 34. VAPORIZATION FRACTION VERSUS PERCENTAGE RADIAL FIBER SURFACE AREA ON AS-3DC

The measured thermocouple and calorimeter trace data are given in Figures 35 and 36 for models AS-1 through AS-4, respectively. The measurements also are compared in Figures 35 and 36 with pretest surface and backface predictions for approximately the same test conditions. Note that both surface and backface temperature measurements are in good agreement with pretest prediction. The higher-than-predicted surface temperature measurements for models AS-3 and AS-4 are the result of higher than predicted total enthalpy and surface heat flux (cf. Table VII).

The thermal radiation through the AS-3DC models was calculated from backface calorimeter histories for each model. The equivalent backface radiation flux was calculated from the calorimeter measurements using the following expression:

$$\dot{Q}_{cal} = \dot{Q}_{rad,\ b} = \rho c \left(\frac{\delta}{12}\right)\frac{\Delta T}{\Delta \tau}$$

where

ρ = calorimeter density (558 lb/ft^3)

c = calorimeter heat capacity (0.092 Btu/lb^{o}F)

δ = calorimeter thickness (0.100 inch)

ΔT = temperature rise, ^{o}F

$\Delta \tau$ = time, seconds

The backface radiant flux, $\dot{Q}_{rad,b}$, can be related to the measured radiation flux from the hot surface by the expression:

$$\dot{Q}_{rad,\ b} = e^{-\bar{\gamma}\Delta X}\ F\epsilon\ \dot{Q}_{rad,\ surface}$$

where

ΔX is the thickness of the AS-3DC

F is the view factor of calorimeter relative to the surface (0.72)

ϵ is the emissivity of the calorimeter (0.9)

$\bar{\gamma}$ is the mean radiation absorption coefficient

This expression assumes a thin, radiating surface layer and a uniform absorption coefficient within the AS-3DC that is independent of wavelength. The mean absorption coefficient then was calculated from the above relation. The results are summarized in Table III, which indicates a mean absorption coefficient of from 30.2 to 34.9 cm^{-1}. Note that there is a correlation between measured $\bar{\gamma}$ and the percentage of radial fiber area (A_R/A_T). For example, the specimen with the lowest percentage of radials (AS-2) has the highest absorption coefficient.

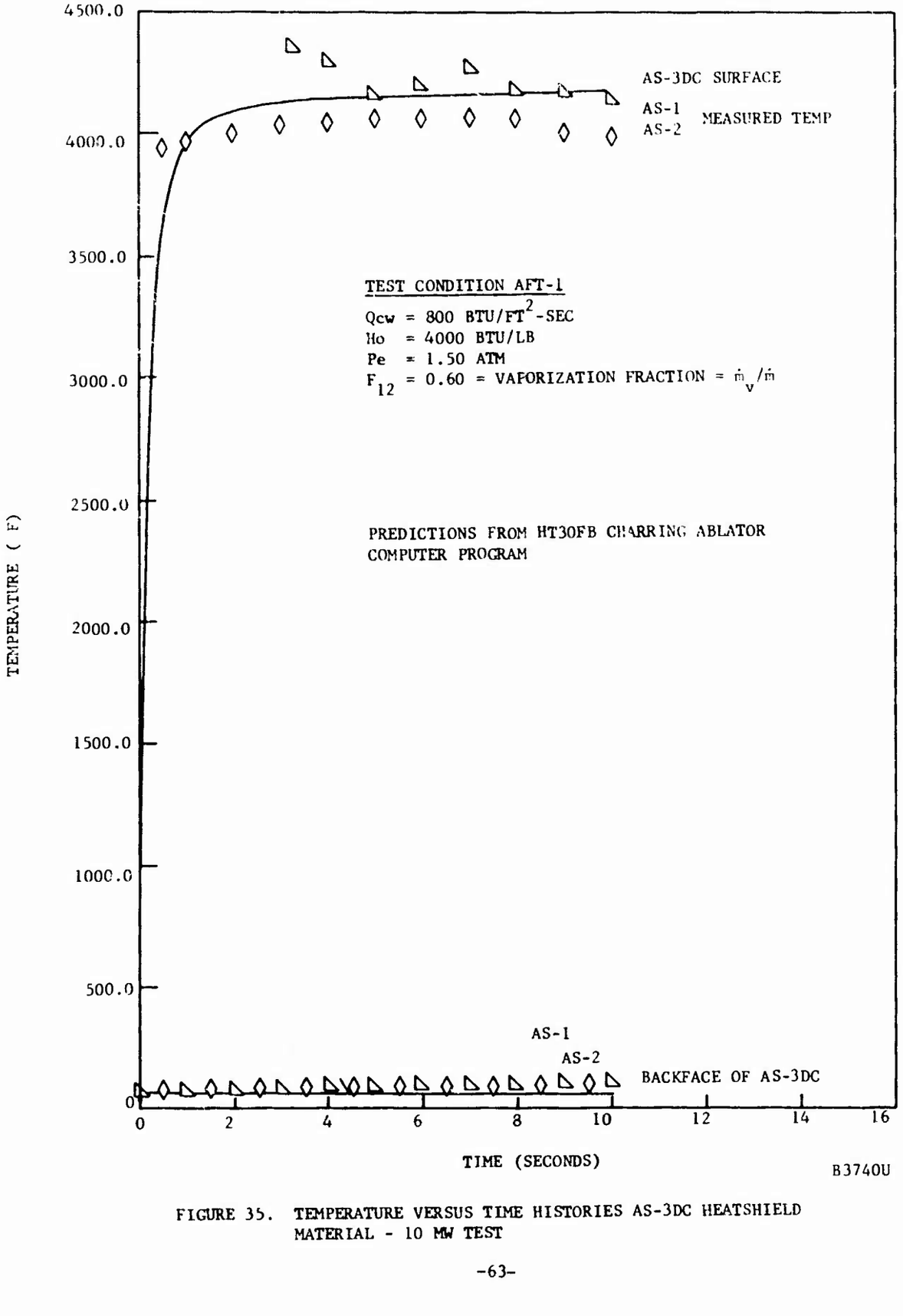

FIGURE 35. TEMPERATURE VERSUS TIME HISTORIES AS-3DC HEATSHIELD MATERIAL - 10 MW TEST

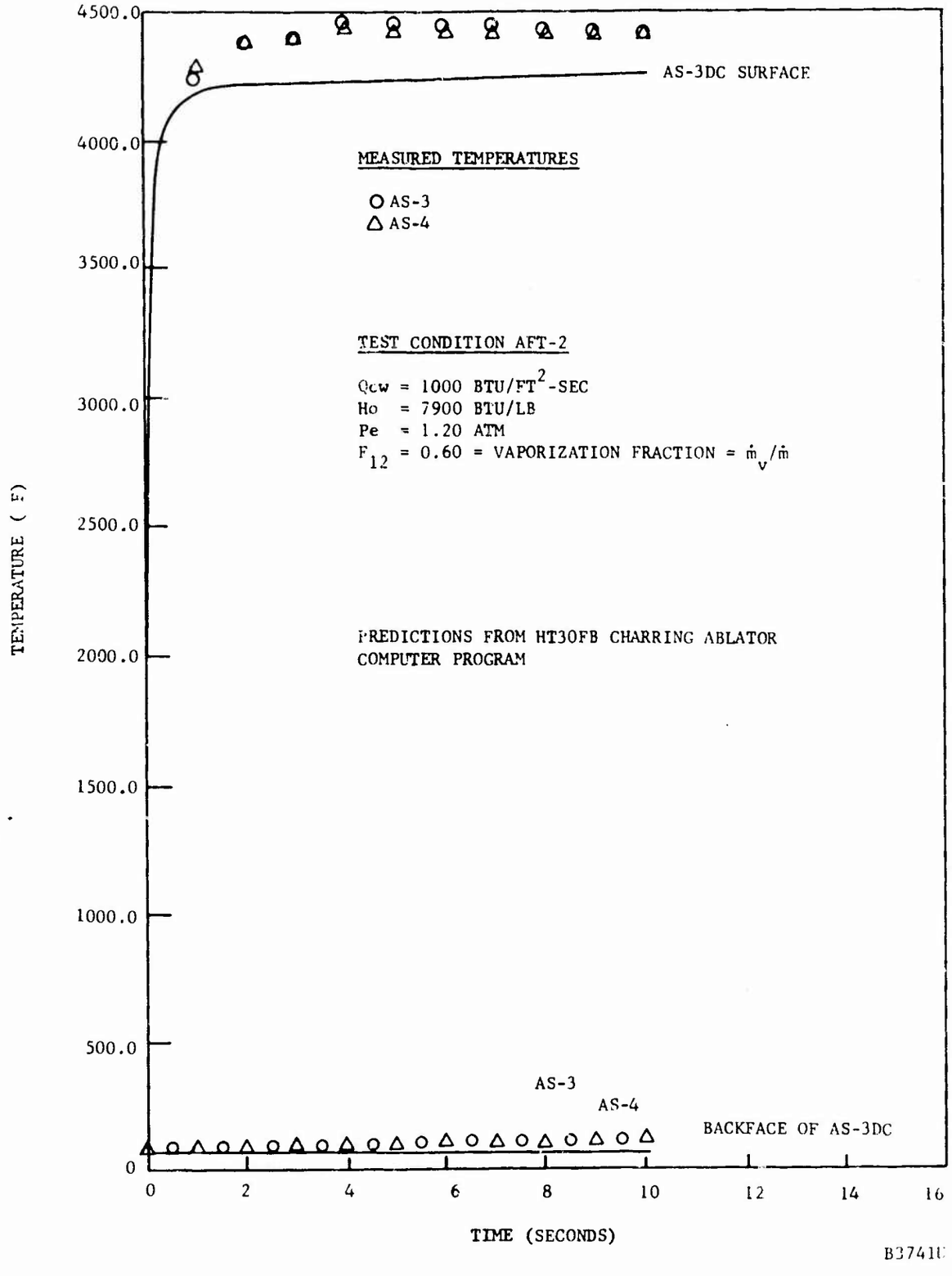

FIGURE 36. TEMPERATURE VERSUS TIME HISTORIES AS-3DC HEATSHIELD MATERIAL - 10 MW TEST

5.1.4 CONCLUSIONS

The following conclusions were made based on the results of the 10 mw tests on the AS-3DC test specimens:

(1) The calculated vaporization fraction, f_v, for the AS-3DC material varied from 0.40 to 0.60. The calculated effective heat of ablation, Q*, of the AS-3DC material is similar to AS-3DX and varied from Q* = 4000 to 6020 Btu/lb, depending upon enthalpy potential.

(2) The data indicated that the vaporization fraction f_v, increased with density; however, the dependence of f_v on the percent of radial fibers was inconclusive.

(3) The data indicated a very small radiation "shine-through" contribution with calculated effective absorption coefficients ranging from $\bar{\gamma}$ = 30.2 to 34.9 cm^{-1} and depending upon the percentage of radials. However, this radiation contribution should have only a small effect on the backface temperature of full-scale configurations.

(4) The backface temperature measurements indicated that, excluding the very small radiation shine-through effect, the thermal conductivity is similar to that of AS-3DX (less than 0.5 Btu/ft hr deg at room temperature).

5.2 THERMAL CONDUCTIVITY AND HEAT CAPACITY

The thermal conductivity and heat capacity were measured from room temperature to 1100°C (2010°F). One specimen was provided for each measurement. The thermal conductivity was measured by the comparative "cut-bar" method using a 1 inch diameter by 1 inch thick cylindrical specimen. The axial direction of the test cylinder corresponded to the radial fiber direction of the frustum. Heat capacity was measured by a combination of adiabatic and drop calorimeter methods. The former method used a 2-1/2 by 2-1/2 by 0.5 inch rectangular specimen for data up to 350°C. From 300°C to 1100°C data points were obtained by the latter method using the thermal conductivity cylinder as the test specimen. All tests were performed by Dynatech Corporation, Cambridge, Mass. The subcontractor test results and report are given in Appendix V.

The measured thermal conductivity curve is shown in Figure 37. Curves for AS-3DX, fused silica, and 3DQP are shown for comparison. The conductivity of AS-3DC was found to be from 20 to 50 percent higher than for AS-3DX. In addition, the increased curvature of the AS-3DC curve at the higher temperatures suggests a greater thermal radiation contribution than was observed for AS-3DX. There were two factors that may have influenced the

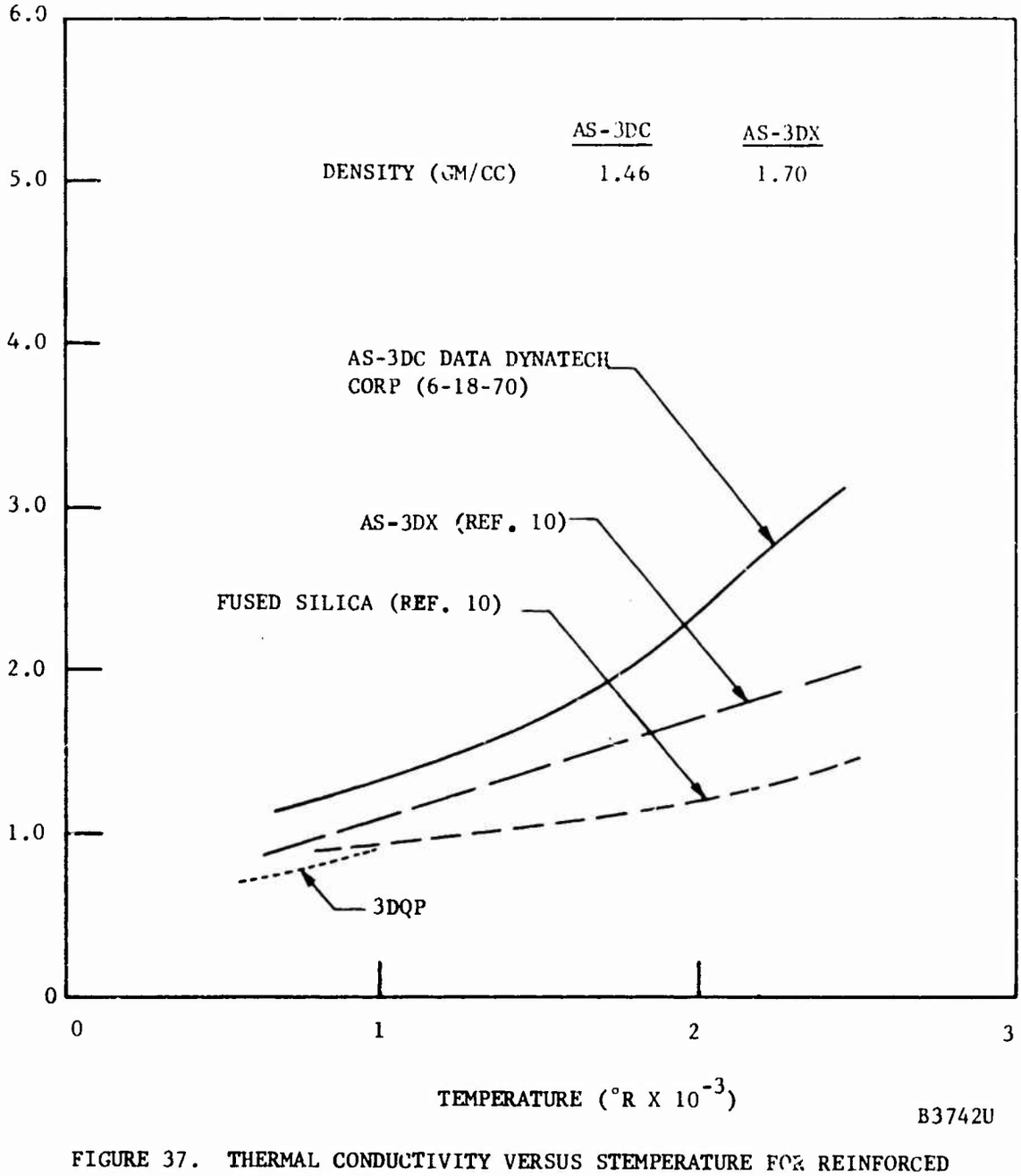

FIGURE 37. THERMAL CONDUCTIVITY VERSUS STEMPERATURE FOR REINFORCED QUARTZ MATERIALS

the data differences between AS-3DC and AS-3DX: (1) the AS-3DC specimen density was 1.46 versus 1.70 for AS-3DX, and (2) the AS-3DC data were obtained from a "cut-bar" specimen, whereas the AS-3DX data were a combination of guarded hot plate results and comparative flat plate results on a larger size specimen (2-1/2 by 2-1/2 by 0.5 inch). In any event, the conductivity of the AS-3DC material is not so high that it does not perform well as an insulator. This is substantiated by the thermal ablation tests in the 10 mw arc. The heat loads applied are roughly equivalent to an IRBM trajectory and with 1/2 inch of material, the temperature rise at the backface, shown in Figures 35 and 36, was negligible.

Figure 38 shows the measured specific heat curve for AS-3DC compared with an average curve for fused silica. (The heat capacity for AS-3DX was not measured as a function of temperature.) There is very good agreement between the curves for AS-3DC and fused silica.

5.3 THERMAL EXPANSION

The thermal expansion was measured on one sample from room temperature to 1000°C by the Aeronutronic Materials Laboratories. A Leitz dilatometer was used with a specimen length of 50 mm and a cross section of 0.25 cm^2 in a 7940 fused silica sample holder. This run and the results are indistinguishable from a previous test of AS-3DX (Reference 10). The coefficient of thermal expansion was determined to be

$$\alpha = 5.6 \times 10^{-7}/^{\circ}C (25^{\circ} \text{ to } 7000^{\circ}C)$$

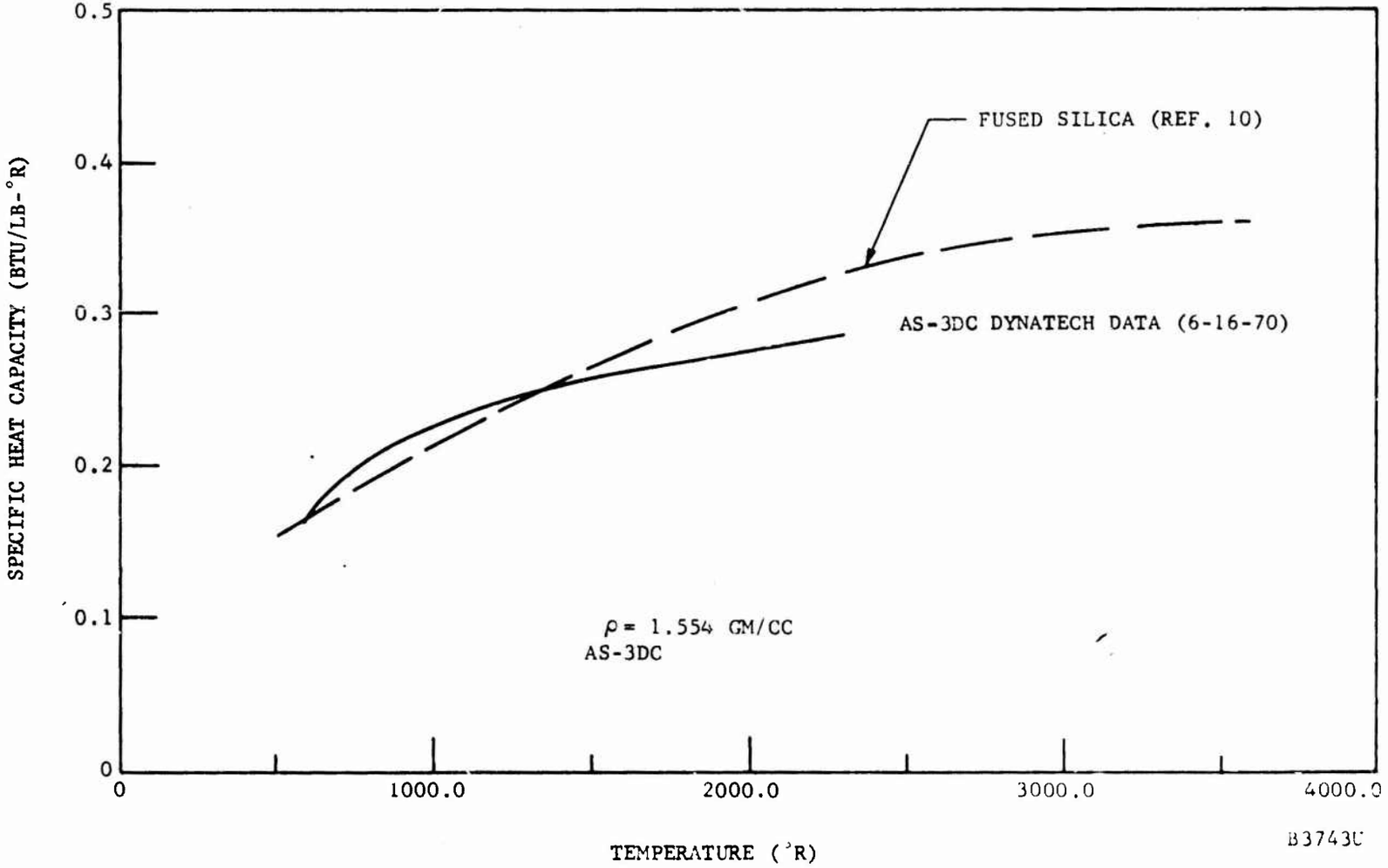

FIGURE 38. SPECIFIC HEAT CAPACITY OF SEVERAL QUARTZ-TYPE MATERIALS

SECTION VI

ELECTRICAL PROPERTIES

The electrical properties of the AS-3DC material which were measured on this program were relative permittivity, loss tangent, and microwave attenuation. The first two properties were measured at the Laboratory for Insulation Research, MIT; microwave attenuation measurements were made in the Philco-Ford antenna lab.

6.1 MIT MEASUREMENTS

Relative permittivity (K) and loss tangent (tan δ) measurements on AS-3DC were made at five frequencies from 0.1 MHz to 8520 MHz. In addition, the measured data were extrapolated to provide information at a sixth frequency. At the highest frequency, 8520 MHz, data were taken at elevated temperatures; at all other frequencies data were taken at room temperature only. The samples were taken from the center section of the first frustum. The data are shown in Table IX. Figure 39 compares the temperature dependence of the electrical properties of AS-3DC and AS-3DX at X-band. The relative permittivities of both materials are almost identical and are insensitive to temperature. The loss tangent of AS-3DC is lower than that of AS-3DX at all temperatures; this is due to the fact that AS-3DC is the purer material. This difference in purity is not due to an inherent difference, rather, it results from further development of the AS process which would be incorporated in all future AS parts including AS-3DX. The loss tangent of each material decreases with increasing temperature up to 350°C or 450°C. This unusual characteristic is the result of loss of chemically bound water absorbed by the material. The loss tangent of AS-3DC decreases considerably more than that of AS-3DX because AS-3DC had absorbed more water than AS-3DX. This conclusion follows from the results of work performed by Philco-Ford on the AFML HAW Contract. On the HAW Program it was found that a relationship exists between purity, sintering temperature, and hygroscopicity, or ability to absorb moisture. In particular, Reference 11 contains data which show that for constant sintering temperature, hygroscopicity increases with purity. Other data in this document show that increasing the sintering temperature decreases the hygroscopicity. Since AS-3DC and AS-3DX had the same sintering temperature, AS-3DC (the purer material as indicated) absorbed more moisture. When the materials were heated, the absorbed water was gradually driven off causing a decrease in both loss tangents. Since AS-3DC lost more water than AS-3DX, its loss tangent decreased more. At sufficiently high temperatures, higher than 100°C since the water is chemically bound, all the water is driven off and the loss tangents increase with temperature in the normal manner. After the last elevated temperature measurement (at 972°C) was made, an additional measurement at room temperature was made. The loss tangent after the temperature run was 0.00042 compared to a value of 0.00169 before the temperature run. The lower value and the dashed curve on Figure 39 indicate the true loss tangent of AS-3DC at room temperature without moisture. Thus, the AS-3DC measurements are superior to AS-3DX, but a higher sintering temperature must be used to

TABLE IX. ELECTRICAL PROPERTIES OF AS-3DC

Sample	Condition	Freq MHz	Temp °C	Permittivity K	Loss Tangent tan δ
1-XB-0-M	As received, face 1 up	8520	25	2.919	0.0062
(density 1.653 g/cc)	As received, face 2 up		25	2.956	0.0064
	After vacuum bake 80°C for 10 days				
	face 2 up		25	2.938	0.00162
	face 1 up		25	2.895	0.00169
			115	2.89	0.0012
			246	2.89	0.0006
			357	2.90	0.0005
			438		0.0006
			535		0.0008
			608		0.0010
			710		0.0014
			805		0.0020
			908		0.0026
			972		0.0028
			1000	*	0.0031*
			25	2.89	0.00042
1-VH-0-M-1	As Received	0.1	25	2.779	0.00046
(density 1.536 g/cc)		1.0		2.777	0.00083
		10.0		2.777	0.00064
		75.0		2.775	0.00135
		180.0		2.772*	0.0017*
	After vacuum bake 18 hours at 80°C	10.0	25	2.77	0.00046
		75.0		2.77	0.00091
		180.0		2.77	0.00115*
1-VH-0-M-2	As received	0.1		2.722	0.00049
		10.0		2.720	0.00059
		75.0		2.72	0.00130
		180.0		2.72*	0.0017*
	After vacuum bake 18 hours at 80°C	75.0		2.72	0.00064
		180.0		2.72*	0.00085*

*Extrapolated values

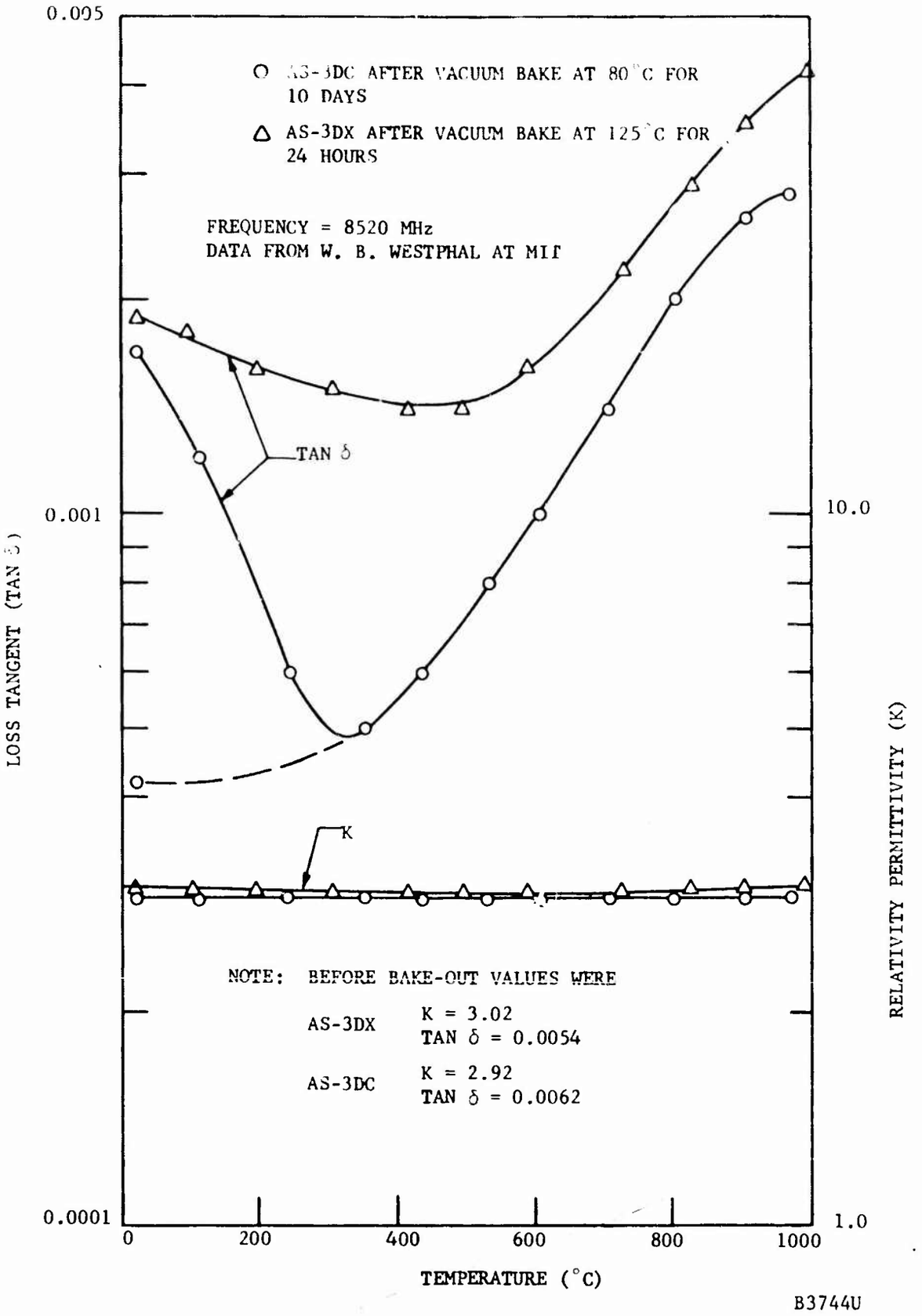

FIGURE 39. TEMPERATURE DEPENDENCE OF ELECTRICAL PROPERTIES.

prevent degrading of this performance by moisture absorption. This improvement reflects an advance in the development of the AS process and is characteristic of any future AS parts, not AS-3DC alone.

Figure 40 presents room temperature electrical properties and the influence of test frequency. The measurements were made on specimens which contained some hygroscopic water, hence the loss tangent is somewhat higher than that on Figure 39.

6.2 IN-HOUSE MEASUREMENTS

Microwave attenuation measurements were made at a frequency of 10 GHz to determine the effects of water absorption on attenuation. Four samples, approximately 0.9 by 0.4 by 0.25 inch each, were machined from the midsection of the second frustum to fit in RG52/U waveguide. The samples were baked at 160°C for 16 to 20 hours and then weighed and measured for attenuation. Two of the samples (Nos. 3 and 4) were then soaked in distilled water for 10 minutes, after which all four samples were again weighed and measured. Weight and attenuation measurements were repeated twice a day as the wet samples dried under ambient conditions. The dry samples were used as references to monitor changing ambient conditions. All attenuation measurements were made after reflection losses were tuned out. Weight and attenuation as functions of time are shown in Figures 41 and 42. These figures also show similar data for the AS-3DX material for comparison. The density of the AS-3DC samples was approximately 1.50 g/cc. Records of density were not available for the AS-3DX. The AS-3DC material dried to its terminal attenuation and weight values in about 20 hours after soaking, compared to about 24 hours for AS-3DX. However, the terminal values are higher for AS-3DC; the residual water content produced an attenuation of 0.5 dB for the 1/4 inch sample (2 dB per inch) compared with 0.8 dB per inch in the baked out condition and 1.2 dB per inch in the ambient condition. These data substantiate that AS-3DC is more hygroscopic than AS-3DX because of its higher purity. Consequently, the retained hygroscopic water degraded the electrical performance of AS-3DC resulting in a more lossy material. This is true of the control sample as well, since the bake temperature of 160°C was not sufficient to drive off all the chemically bonded water. As mentioned, adjustments in the AS process should provide future AS materials which approach the loss tangent indicated by the dashed curve of Figure 39.

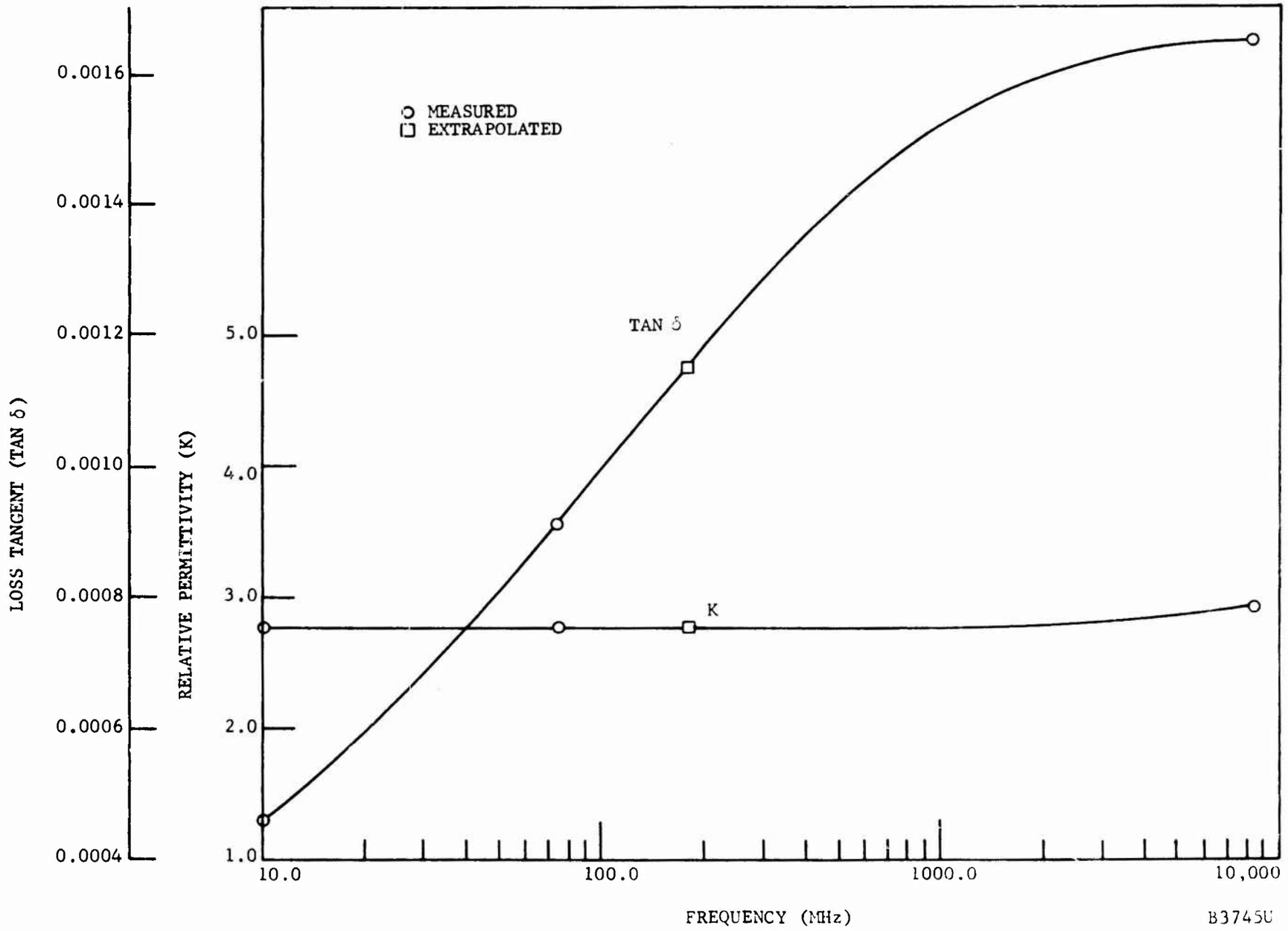

FIGURE 40. ELECTRICAL PROPERTIES OF AS-3DC MATERIAL AT 25°C WITH H_2O CONTAMINATION

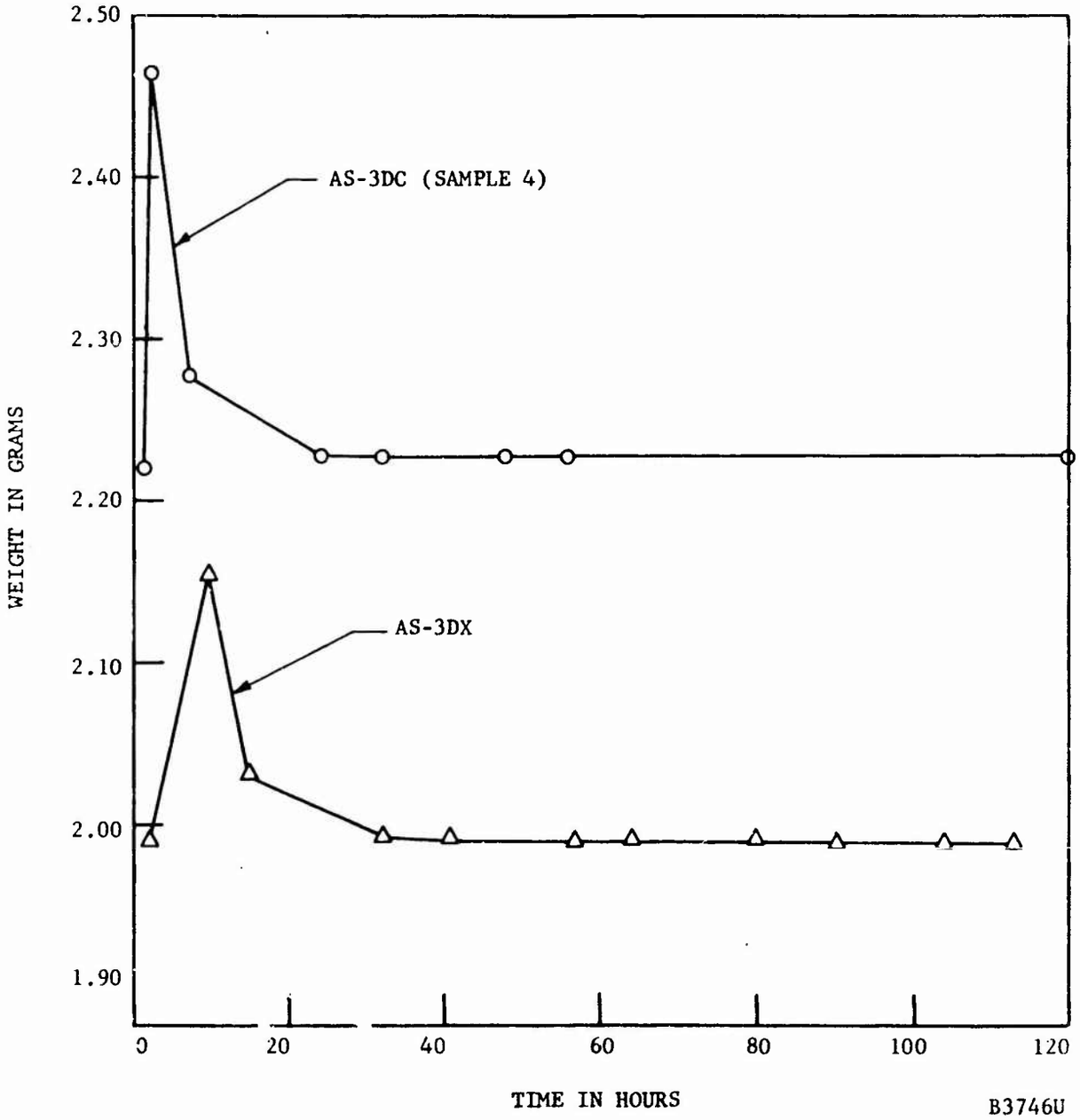

FIGURE 41. EFFECTS OF WATER ABSORPTION ON WEIGHT IN AS-3DX AND AS-3DC SPECIMENS

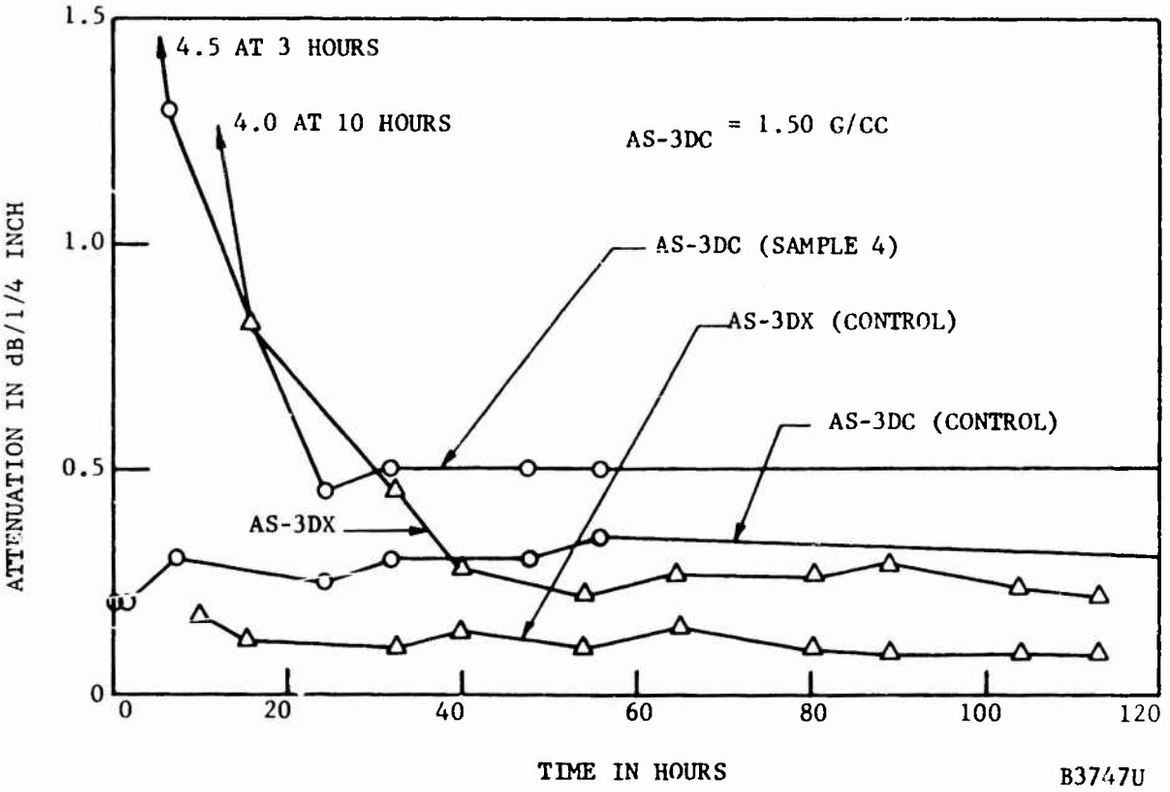

FIGURE 42. EFFECTS OF WATER ABSORPTION ON ATTENUATION IN AS-3DX AND AS-3DC SAMPLES

 Page -76- Intentionally Left Blank

APPENDIX I

AS-3DC ANTENNA WINDOW MATERIAL - DESIGN DATA

1.1 INTRODUCTION

This data package contains characteristics of AS-3DC antenna window material as measured on the Advanced 3D Fabrication Techniques (A(3D)FT) Program. Included are physical, chemical, mechanical, thermal, and electrical design data. The data are a conservative representation of AS-3DC especially from the standpoint of mechanical properties. The inevitable nonidealisms, where the test specimens do not accurately represent the material in application, resulted in lower than real results. For example, because of the nonhomogeneous nature of the AS-3DC quartz yarn/silica composite, it is virtually impossible to cut a tensile specimen from the frustum which has a center of strength coincident with the center of area of the test section. This causes bending and higher than indicated stresses on the part. The bending was substantiated. Strain flags were observed to move together while the tensile force was continuing to pull them apart. In addition, all specimens were cut from full sized frustum parts in an attempt to obtain representative data. This ensures that imperfections and weakness more prevalent in large parts and complex shapes are included. These and other facts lead to the conclusion that the data are conservative.

It is also important to note that AS-3DC represents a significant advance in the state of the art. Furthermore, these data represent AS-3DC in its initial phase of development as these were the first parts of this degree of difficulty ever built. Future parts would undoubtedly show an improvement.

1.2 PHYSICAL/CHEMICAL PROPERTIES

1.2.1 DENSITY PROPERTIES

Shown in Table I are the densities of AS-3DC woven preforms and impregnated frusta.

TABLE I. DENSITY PROPERTIES

Density	Preform	AS-3DC Frustum
gm/cc	0.95 - 1.15	1.60 - 1.65
lb/ft^3	59.3 - 71.8	100.0 - 103.0

1.2.2 CHEMICAL PROPERTIES

Shown in Table II are the representative chemical properties of the woven preforms and AS-3DC frusta.

TABLE II. CHEMICAL PROPERTIES

Preform		AS-3DC Frustum	
SiO_2, Wt (percent)	Trace Element Impurities	SiO_2, Wt (percent)	Trace Element Impurities
99.98	50 ppm*	99.95	155 ppm*

*Parts per million by weight of sodium equivalent. Includes sodium, barium, lithium, potassium, and strontium.

1.3 MECHANICAL PROPERTIES

These data are representative of AS-3DC early in the development cycle The mean values are fairly representative of the material; however, it is expected that these mean values would increase in future parts and the spread at a given measurement temperature would decrease. This is especially true of the circumferential and radial compression data. The circumferential tension data were not included in this data package because the data obtained are not representative. This point is discussed in Paragraph 4.2.

1.3.1 ROOM TEMPERATURE MECHANICAL PROPERTIES

See Table III.

1.3.2 ELEVATED TEMPERATURE MECHANICAL PROPERTIES

See Figures 1 through 4.

1.4 THERMAL PROPERTIES

1.4.1 HEAT OF ABLATION, Q*

See Figure 5.

1.4.2 THERMAL CONDUCTIVITY, k

See Figure 6. These data are considered to be tentative. They indicate a somewhat higher conductivity than anticipated.

1.4.3 SPECIFIC HEAT CAPACITY, C_p

See Figure 7.

1.4.4 THERMAL EXPANSION, α_T

$$\alpha_T = 5.6 \times 10^{-7} \text{ per } ^\circ\text{C} \quad 25 \lesssim T \lesssim 700^\circ\text{C}$$

TABLE III. SUMMARY OF ROOM TEMPERATURE MECHANICAL PROPERTIES

Material Direction	Type of Loading	Property (1)	Average Value	Range	Number of Specimens
Axial	Flexure	Strength	4,000	3,280-5,150	4
		Modulus	1.86	1.67-2.26	4
	Tension	Strength	4,480	3,200-6,470	4
		Modulus	2.99	2.70-3.50	4
	Compression	Strength	13,310	11,120-14,900	4
		Modulus	2.55	1.63-3.14	4
Circumferential	Compression	Strength	8,830	6,180-10,700	4
		Modulus	3.25	2.59-3.75	3
Radial	Compression	Strength	8,700	4,100-13,820	4

(1) Strength in psi
Modulus in 10^6 psi

1.5 ELECTRICAL PROPERTIES

1.5.1 RELATIVE PERMITTIVITY OR DIELECTRIC CONSTANT, k

See Figure 8.

1.5.2 LOSS TANGENT, tan δ

See Figure 8.

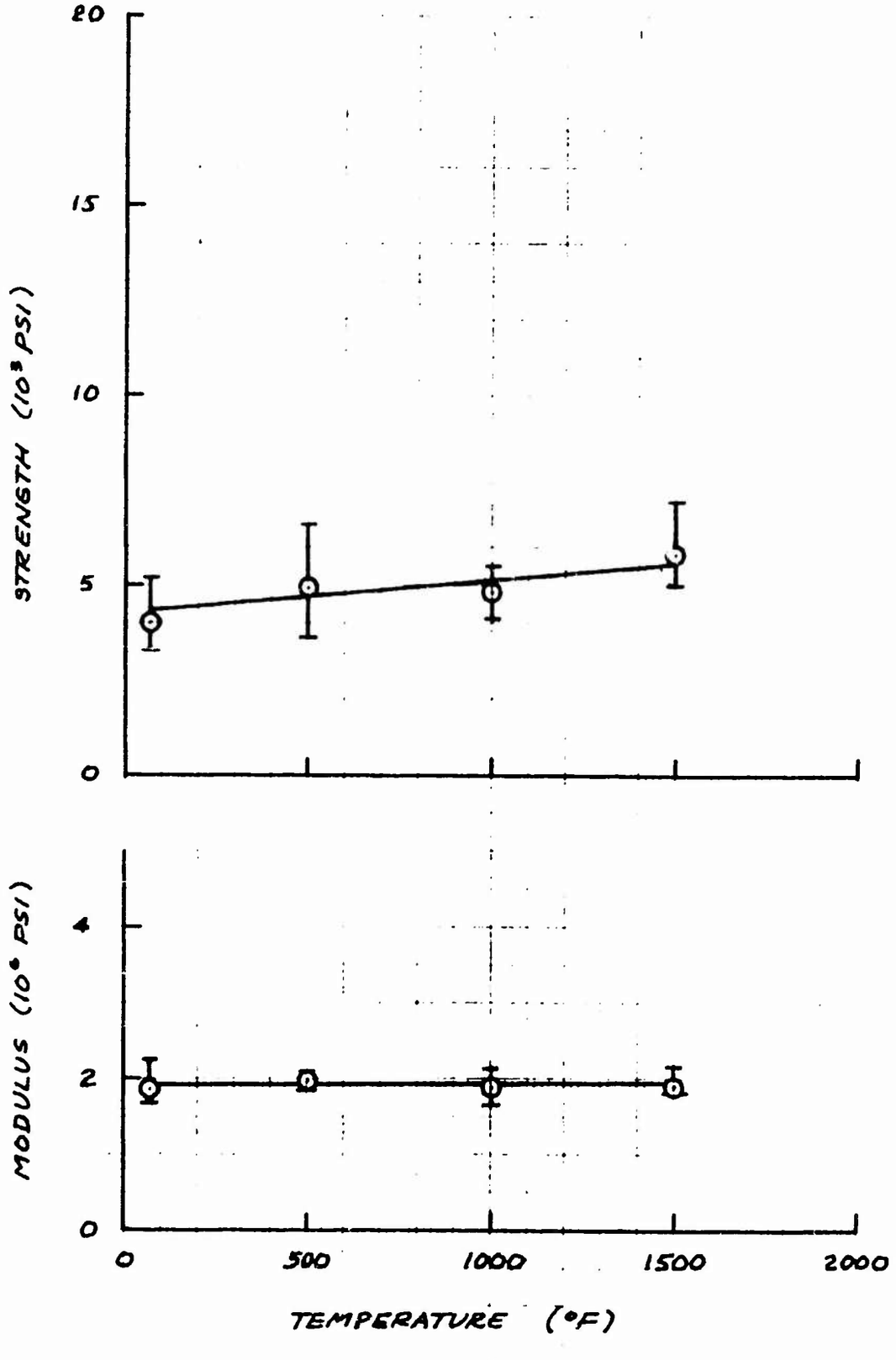

B3748U

FIGURE 1. AS-3DC AXIAL FLEXURAL PROPERTIES

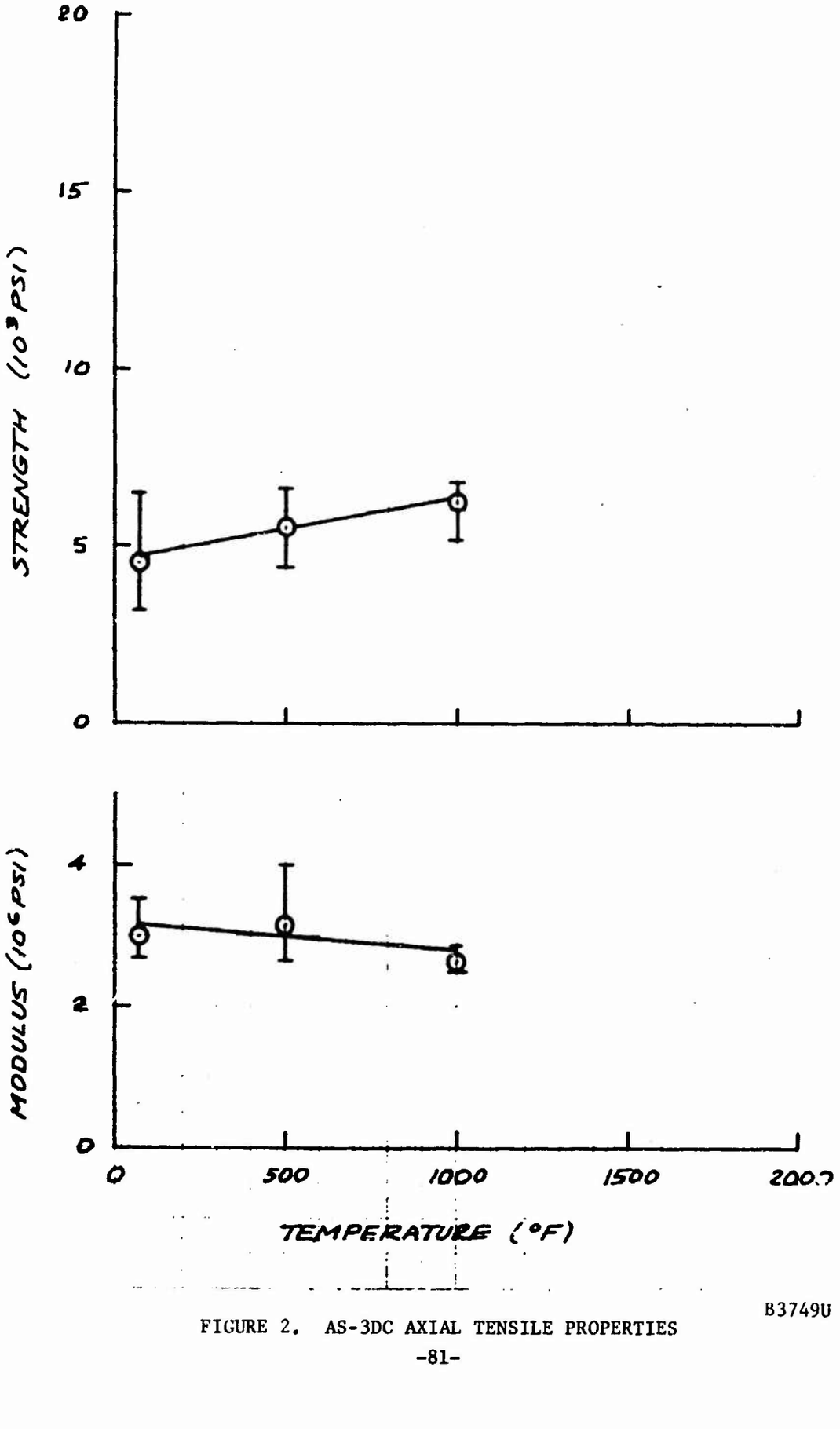

B3749U

FIGURE 2. AS-3DC AXIAL TENSILE PROPERTIES

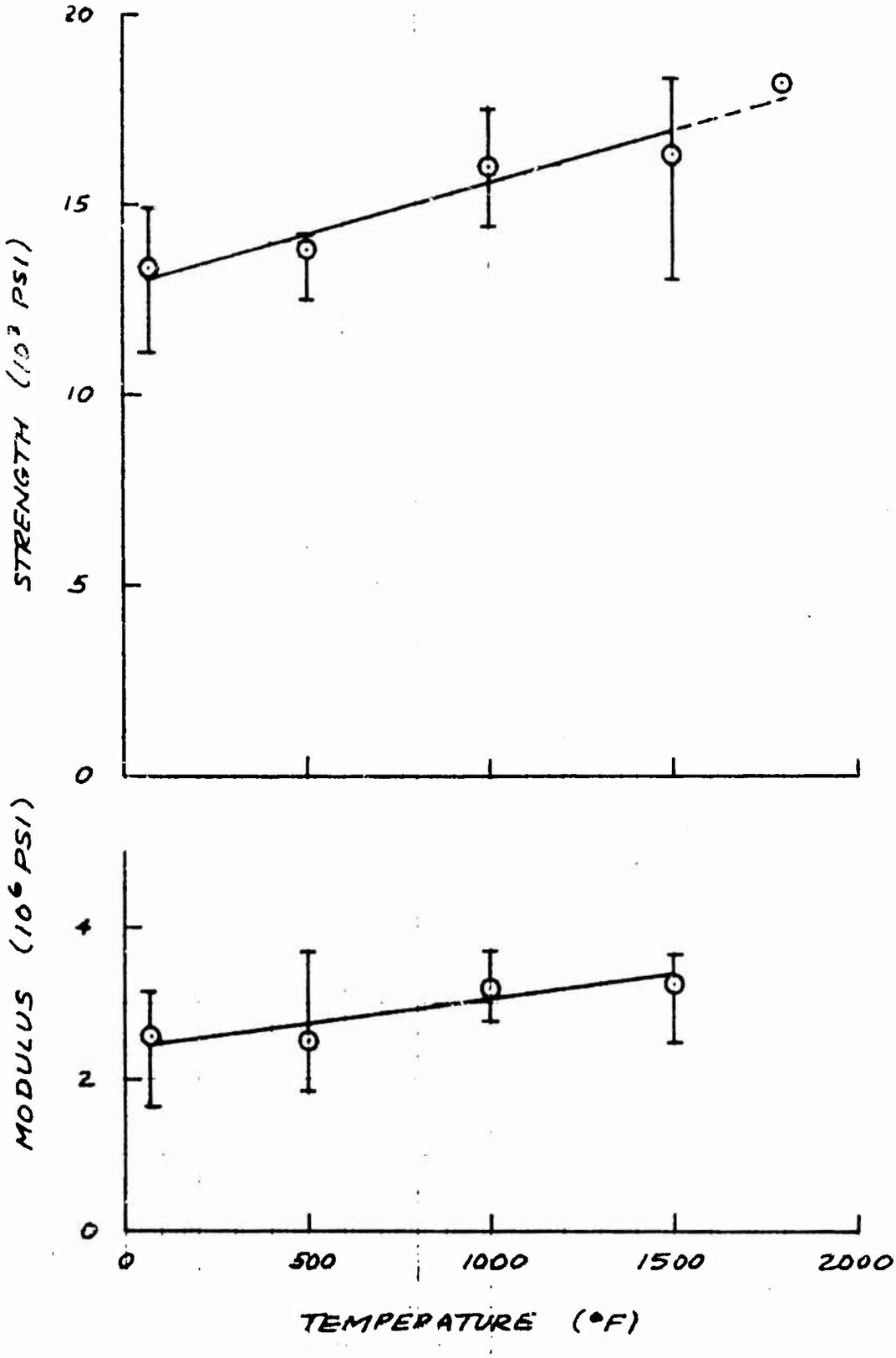

B3750U

FIGURE 3. AS-3DC AXIAL COMPRESSIVE PROPERTIES

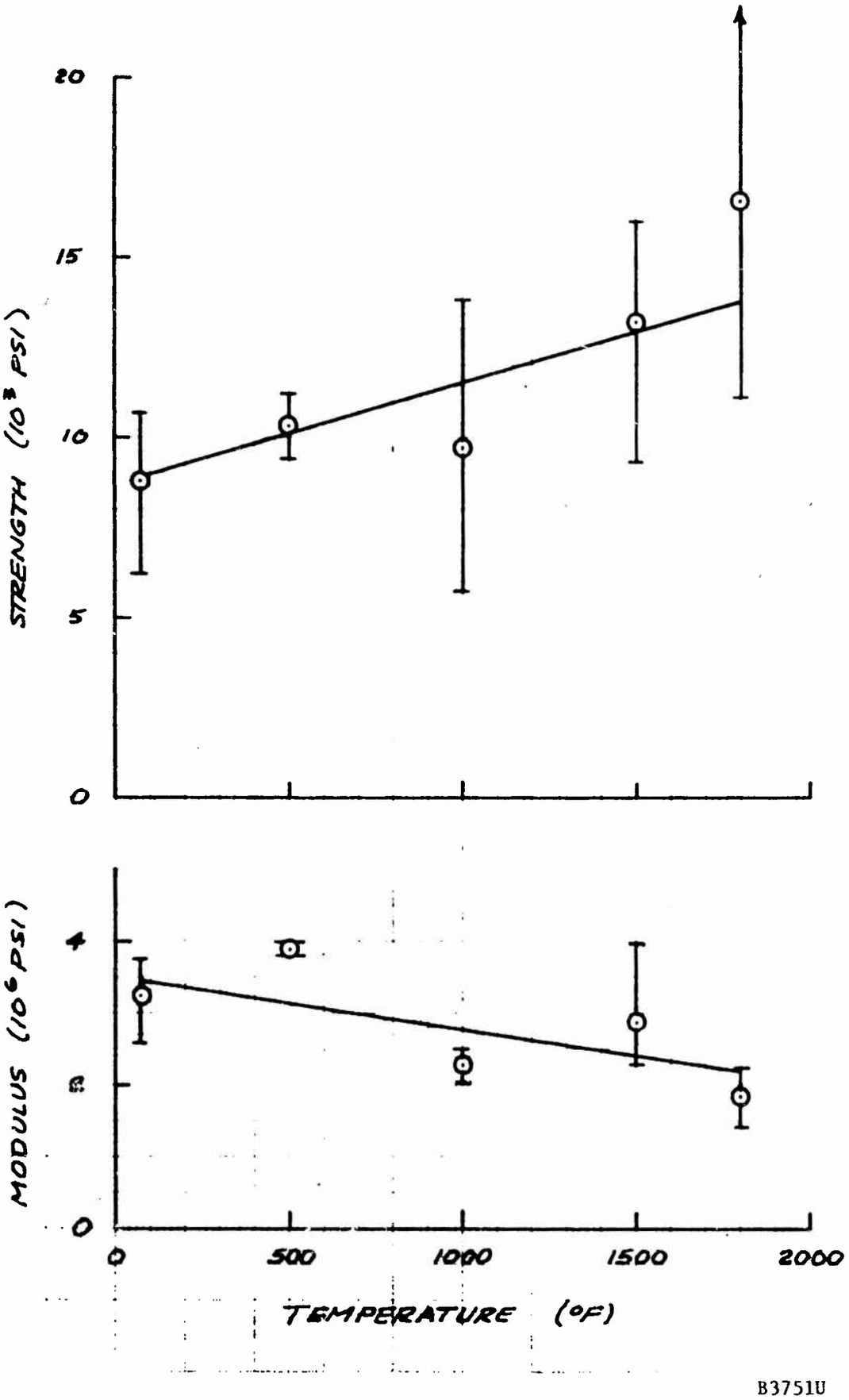

FIGURE 4. AS-3DC CIRCUMFERENTIAL COMPRESSIVE PROPERTIES

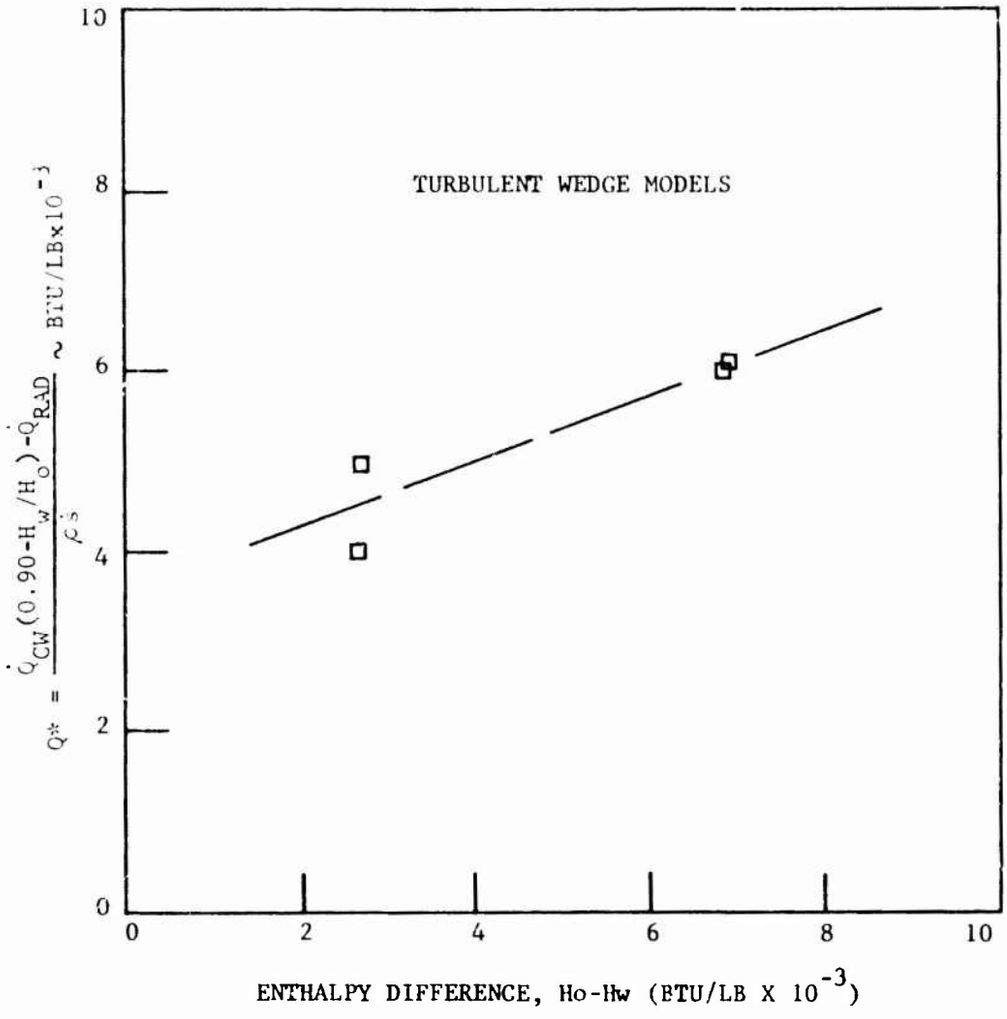

B3752U

FIGURE 5. EFFECTIVE HEAT OF ABLATION VERSUS ENTHALPY DIFFERENCE FOR AS-3DC MATERIALS TESTED IN AVCO CORPORATION 10 MW ARC-JET FACILITY

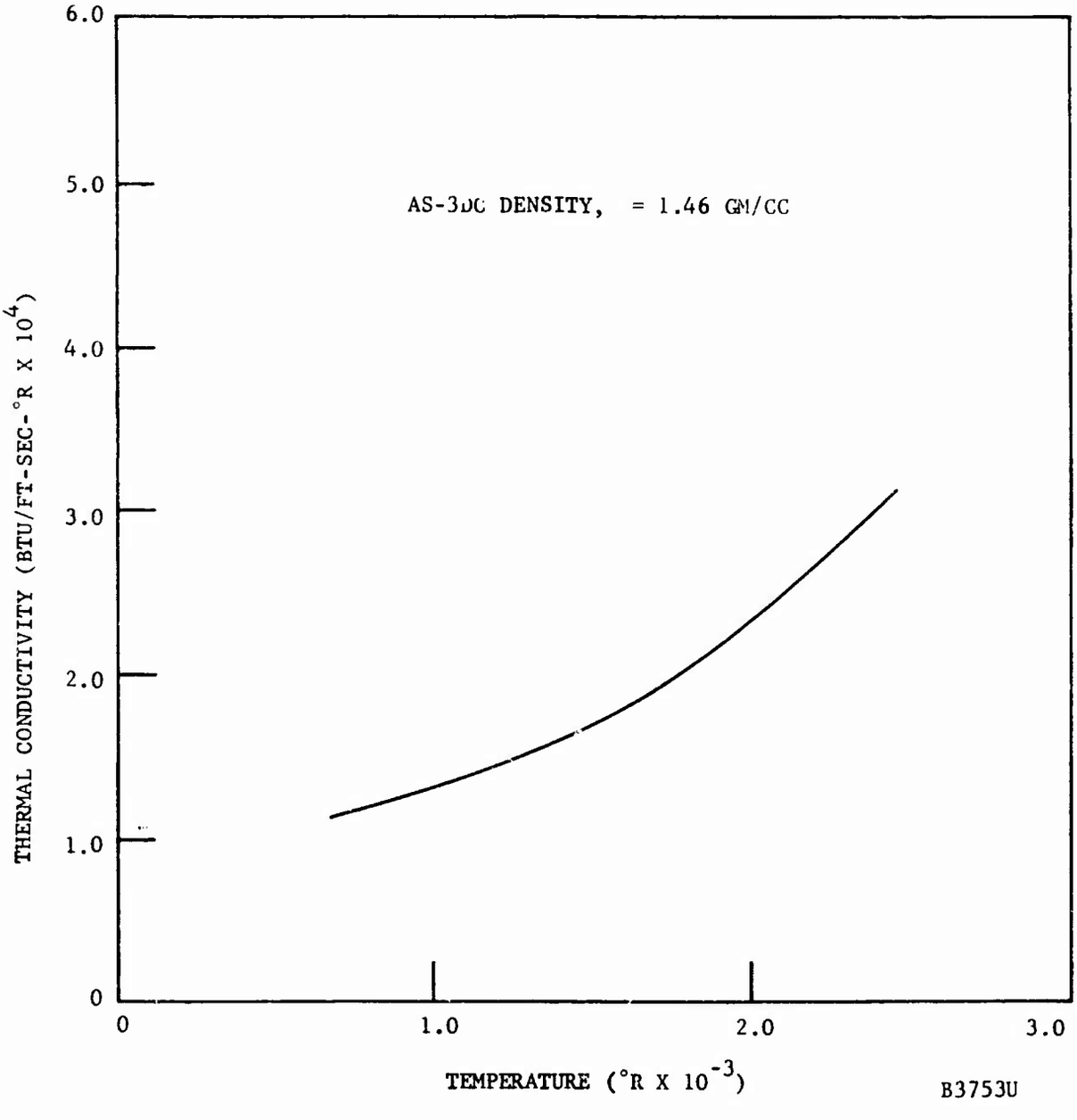

FIGURE 6. THERMAL CONDUCTIVITY VERSUS TEMPERATURE AS-3DC QUARTZ

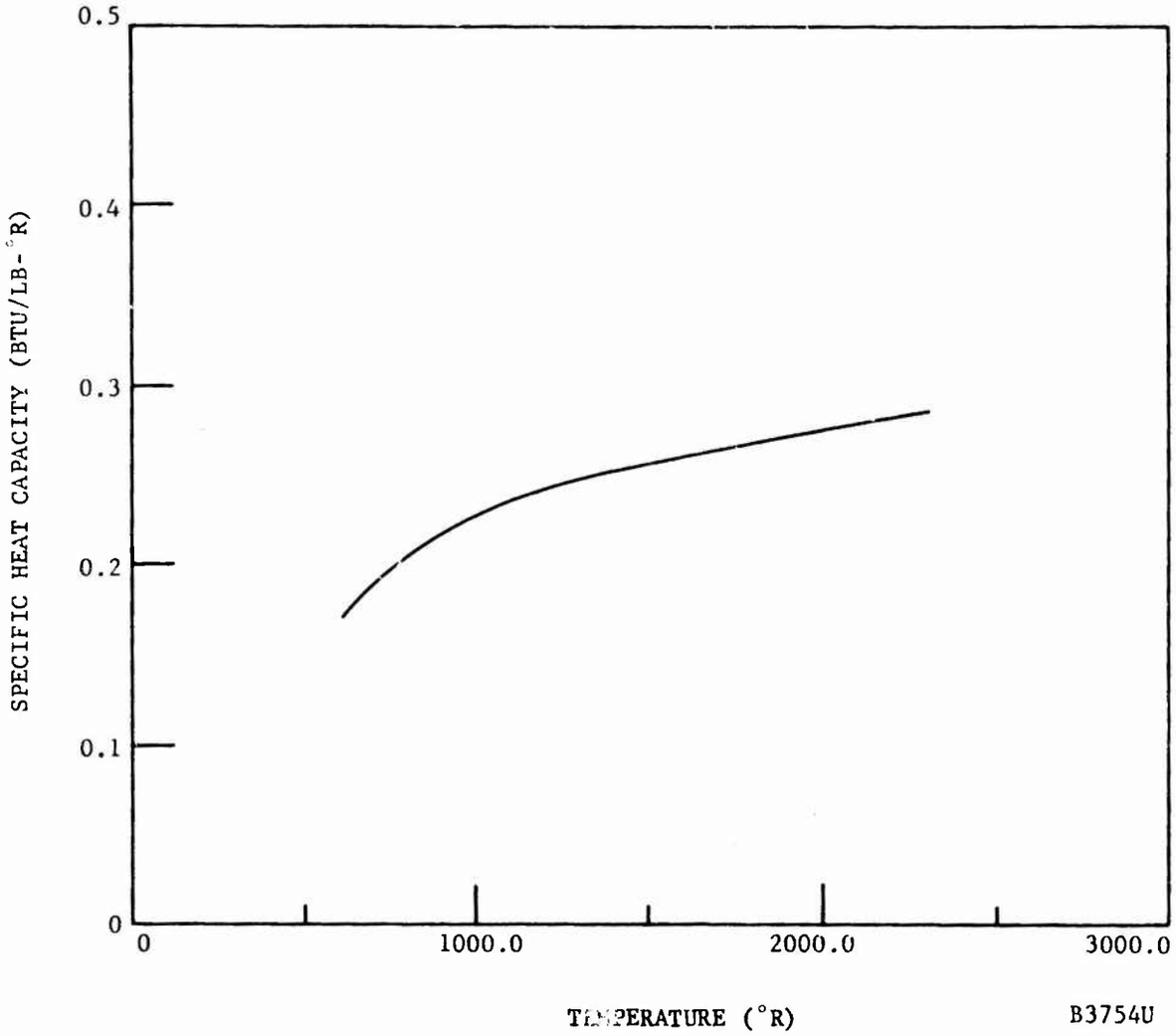

FIGURE 7. SPECIFIC HEAT VERSUS TEMPERATURE FOR AS-3DC QUARTZ

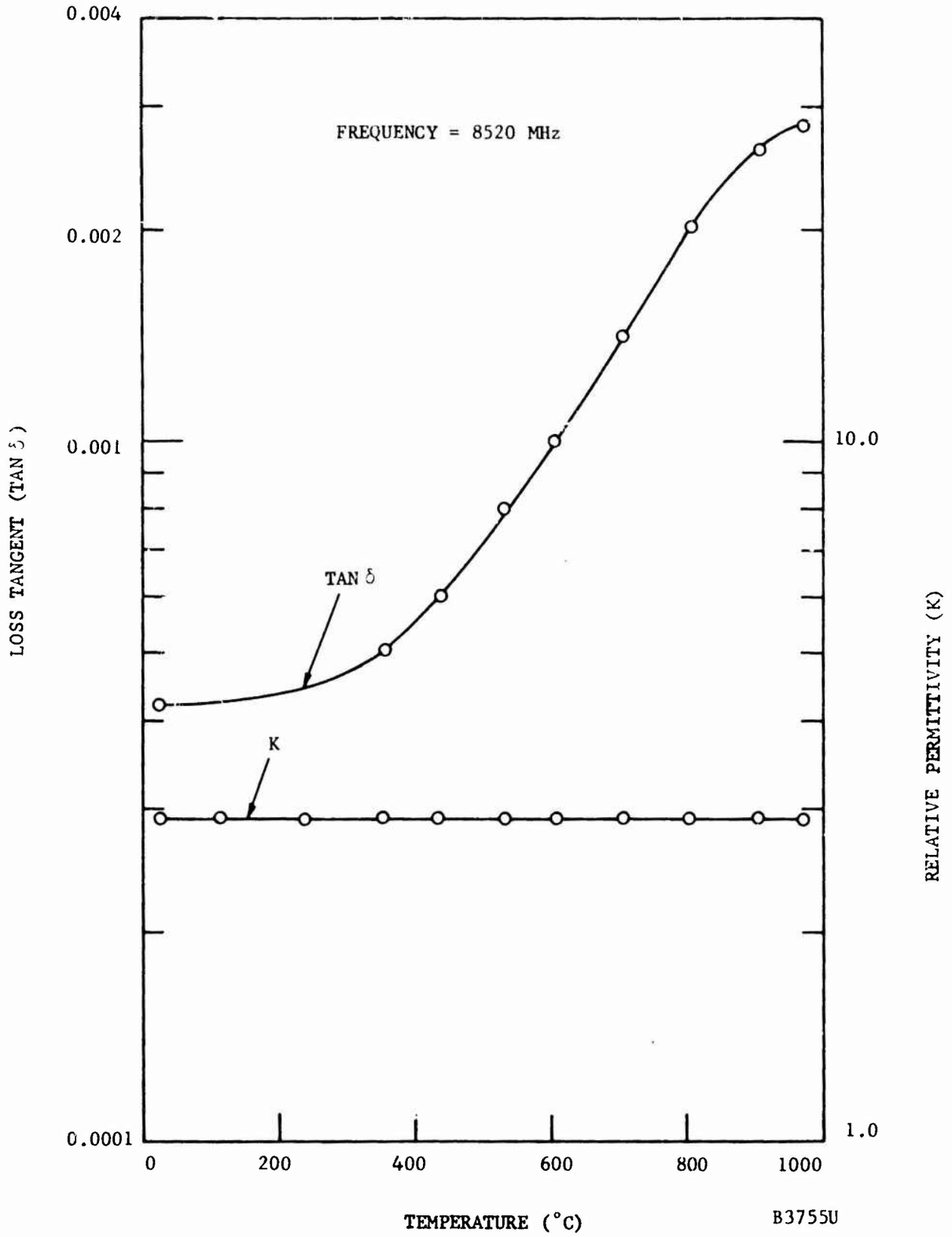

FIGURE 8. ELECTRICAL PROPERTIES VERSUS TEMPERATURE

APPENDIX II

3D QUARTZ CONE FRUSTUM PREFORM

1.0 SCOPE

1.1 This specification estsblishes the requirements for a three-dimensional orthogonally woven quartz pseudo-cone frustum preform.

1.2 Definition: "pseudo-cone frustum" implies thst the preform is woven as a cylinder and the conical configuration is formed during the weaving operation by successively tightening the circumferential yarns as the wesving progresses toward the small end of the frustum. A shape woven directly as a cone frustum would be referred to as a "true-cone frustum".

2.0 APPLICABLE DOCUMENTS

2.1 The following documents of the issue in effect at the time of invitation for bids form a part of this specification to the extent specified herein.

GOVERNMENT

Federal Test Method 406	Plastics: Methods of Testing
MIL-STD-453	Inspection, Radiographic

PHILCO-FORD

WDL 21-B03880 (App. VIII)	3D Quartz Conical Billet
SV-DB1549 (Ref. 10)	Quartz Yarn

3.0 REQUIREMENTS

3.1 Quartz Yarn Requirements.

3.1.1 The yarn utilized to weave the frustum shall be a quartz braiding yarn conforming to SV-DB1549.

3.1.2 No additional coatings, sizes, or binders shall be applied to the yarn.

3.2 Woven Frustum Requirements.

3.2.1 Construction, Size, and Shape. The frustum shall be constructed with yarns positioned in three orientations identified as the radial, circumferential, and axial directions. The weaving construction, yarn bundle count, and orientation shall conform to the requirements of Figure 1. The frustum preform shall be of sufficient size to assure that adequate material is available to remove the finish machined configuration shown on engineering drawing 21-B03880. Construction, size, and shape shall be determined by the test method described in 4.4.1. Since it is impractical to section the preform to determine weave construction, the supplier shall submit a letter of compliance certifying that the preform construction meets the requirements of this specification.

SIZE	CODE IDENT NO.	
A	26463	SV-DB1923
SCALE NONE	REV B	SHEET 2 OF

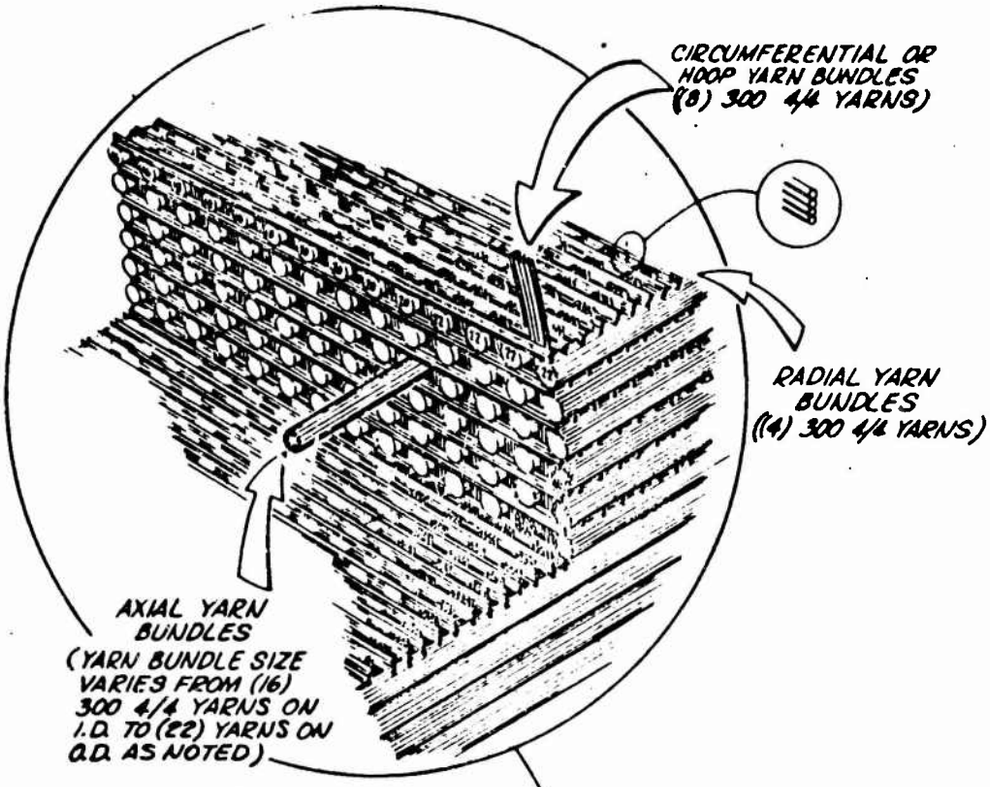

NOTE: AXIAL YARNS SHALL BE SPACED ON 1/8" CENTERS ON THE BASE ID AND ON 1/8" CENTERS FROM THE ID TO THE OD IN THE RADIAL DIRECTION.

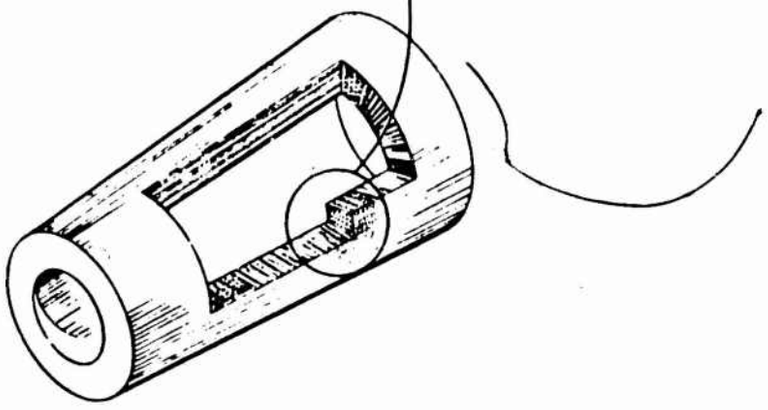

FIGURE 1
FRUSTUM CONSTRUCTION DETAILS

SIZE	CODE IDENT NO.	
A	26463	SV-DB1923
SCALE NONE	REV A	SHEET 3 OF

SRS-4041E (10/69)

3.2.2 Density. The bulk density of the woven frustum shall be a minimum of 58.0 lbs/ft^3 as determined by the test method identified in 4.4.2. There shall be the number of circumferential and radial yarn layers (±1 layer), as indicated on Figure 2, per inch of axial surface length.

3.2.3 Trace Element Impurities. The total concentration of trace element impurities collectively shall not exceed 50 parts per million of the sodium equivalent determined by use of the following weighting factors:

Trace Element	Weighting Factor
Lithium	2.30
Potassium	1.80
Sodium	1.00
Calcium	0.14
Strontium	0.12
Magnesium	0.025
Cesium	1.80
Barium	0.15
Aluminum	0.25

Purity shall be determined by the test method described in 4.4.3. The sample weight shall be a minimum of 15 grams and shall be selected at random from the frustum.

3.2.4 High Density Inclusions. The woven preform shall be radiographically inspected to assure that no metallic or other high density foreign inclusions are present. At least two longitudinal side view shots shall be taken of surface rays 90° apart. Radiographic inspection shall be accomplished in accordance with the requirements of 4.4.4.

3.2.5 Waviness of Circumferential Yarn Bundles. Circumferential yarn bundles shall be positioned parallel to the base of the frustum (see Figure 1). Waviness of a given winding of circumferential yarns shall not exceed 1/8" from its intended plane as pictorially illustrated in Figure 3. The rate of change of displacement of a circumferential yarn (axial to circumferential) from its intended plane shall not exceed 1. Yarn misalignment shall be determined by review of the x-ray films (see 4.4.4).

3.2.6 Yarn Bundle Displacement. Yarn bundles displaced more than 1/8" from their intended true position as a result of fixture indentations etc, shall not extend into the finished dimension configuration shown on engineering drawing number 21-B03880.

3.2.7 Tie Offs. The yarns shall be tied as necessary using quartz yarn. No other materials are acceptable. The tie offs shall be made outside of the finish machined dimension configuration shown on engineering drawing 21-B03880.

SIZE	CODE IDENT NO.	SV-DB1923	
A	26463		
SCALE NONE	REV B		SHEET 4 OF

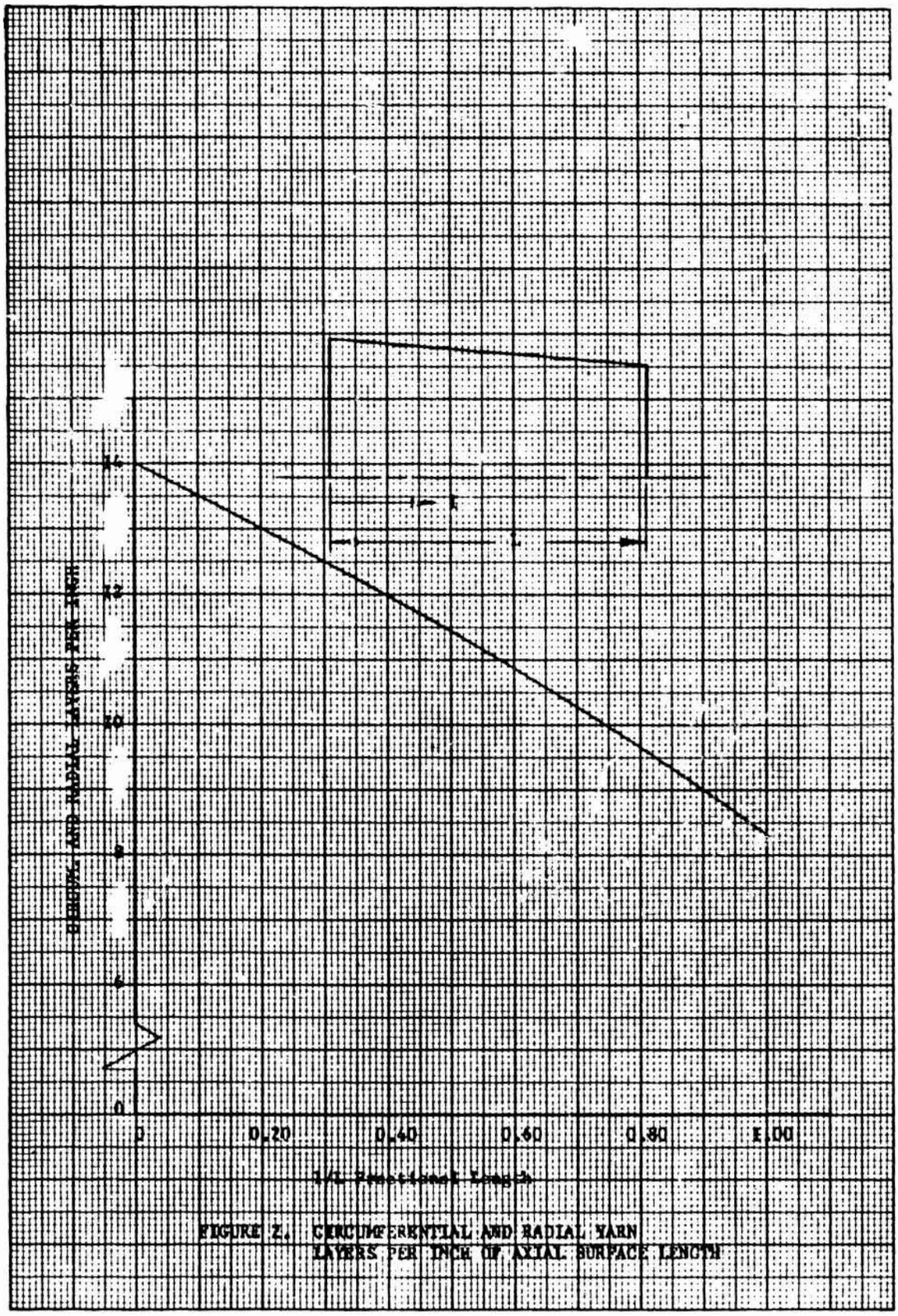

FIGURE 2. CIRCUMFERENTIAL AND RADIAL YARN LAYERS PER INCH OF AXIAL SURFACE LENGTH

REV A SV-DB1923 Sheet 5

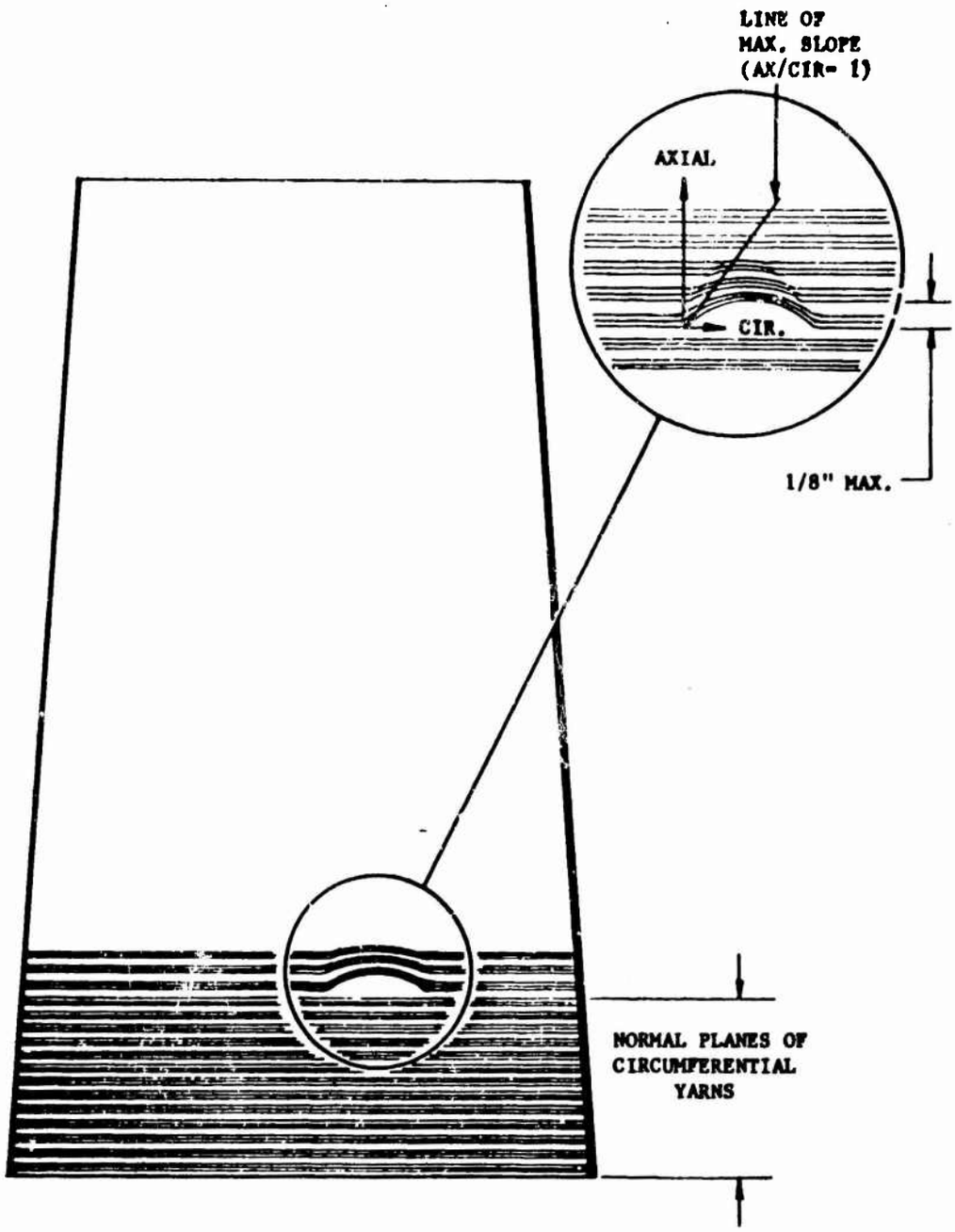

FIGURE 3. ALLOWABLE WAVINESS OF CIRCUMFERENTIAL YARNS

SIZE	CODE IDENT NO.	
A	26463	SV-DB1923
SCALE NONE	REV A	SHEET 6 OF

SRS-4041E (10/69)

3.2.8 Workmanship. The woven frustum shall show evidence of good workmanship and shall be free from dirt, stains, discolorations, or any other foreign material that could adversely affect the performance or purity of the component.

3.2.9 Handling. During and after the weaving operation, the frustum shall be handled in such a manner as to prevent damage and contamination. Plastic gloves placed over cotton gloves shall be worn by operators during the weaving operation.

NOTE: The frustum shall not be unnecessarily twisted, torqued, or otherwise distorted.

3.2.10 Further Processing. The frustum shall not be subjected to any further processing after removal from the loom, e.g., heat cleaning, ultrasonic cleaning, etc.

3.2.11 Packaging. The frustum shall be sealed in a clean polyethylene wrapper (or bag) and shall be suitably packaged in a cushioning material to prevent shipping damage.

3.2.12 Marking. No markings shall be applied directly onto the woven frustum. Markings shall be placed on the outside of the wrapping material.

4.0 QUALITY ASSURANCE PROVISIONS

4.1 Responsibility for Inspection. Unless otherwise specified by the contract or purchase order, the procuring activity shall be responsible for the performance of all inspection and test requirements as specified herein.

4.2 Supplier Qualification. The qualification of a suppliers product shall consist of meeting all the requirements specified in section 3.

4.3 Quality Conformance Tests. Each fabricated frustum shall be subjected to the following tests:

a. Frustum construction, size, and shape (see 4.4.1).

b. Density measurement (see 4.4.2).

c. Trace element impurities (see 4.4.3).

d. Radiographic analysis (see 4.4.4).

e. Frustum defects (see 4.4.5).

4.3.1 Rejection. Failure of the frustum to meet the quality conformance requirements shall cause rejection.

4.4 Test Methods.

4.4.1 Construction, Size, and Shape. Construction, size, and shape of the preform shall be determined by direct measurement and visual examination for compliance to the requirements of 3.2.1. (See requirement for vendor certification of weave construction in 3.2.1.)

SIZE	CODE IDENT NO.	
A	26463	SV-DB1923
SCALE NONE	REV A	SHEET 7 OF

SRS-4041E (10/69)

4.4.2 Density Measurement. The bulk density shall be determined in accordance with Federal Test Method STD-406, Method 5012, and shall meet the requirements of 3.2.2. The number of circumferential and radial yarns per inch shall be determined by direct measurement.

4.4.3 Trace Element Impurities. The presence of trace element impurities shall be determined by spectrographic analysis or by atomic absorption to check for conformance to the requirements of 3.2.3.

4.4.4 Radiographic Inspection. Radiographic inspection shall be accomplished in accordance with MIL-STD-453 to assure that the preform meets the requirements of 3.2.4 and 3.2.5.

4.4.5 Frustum Defects. The frustum shall be visually examined and measured to check for conformance to the requirements of 3.2.6, 3.2.7, and 3.2.8.

5.0 PREPARATION FOR DELIVERY

5.1 Packaging and Packing. Preforms shall be packed individually in a suitable container which will provide adequate protection against deformation, deterioration, physical damage, and contamination before, during, and after shipping.

5.2 Marking. In addition to any special marking required by the contract or purchase order, the shipping container shall be marked with the applicable purchase order number and any pertinent special handling notation.

6.0 NOTES

6.1 Ordering Data. Procurement documents shall specify, but not be limited to the following:

a. Title, number, and date of this specification.

6.2 Approved Material. On the date of issue of this specification, the following product and manufacturer has been approved:

Product

3D Quartz Pseudo-Cone Frustum

Manufacturer

Fiber Materials, Inc.
Broadway and Main Streets
Graniteville, Mass. 01829

SIZE	CODE IDENT NO.	
A	26463	SV-DB1923
SCALE NONE	REV A	SHEET 8 OF

SRS-4041E (10/69)

APPENDIX III

THE MECHANICAL PROPERTIES OF A THREE DIMENSIONAL COMPOSITE

INTRODUCTION

This is the final report to the Philco-Ford Corporation, Aeronutronic Division for work performed under Purchase Order G-70573 of Prime Contract FD4701-68-C-0183. The scope of work included tensile, compressive and flexural evaluations at room and elevated temperatures on a three dimensional silica composite supplied to Southern Research by Philco-Ford.

MATERIAL AND SPECIMEN PREPARATION

The material for this program was a three dimensional silica composite labeled AS3DC. The material was woven in a three dimensional weave with quartz fiber bundles and impregnated with a silica solution. Finished specimens were supplied to Southern Research by Philco-Ford. The material for the specimens had been extracted from conical frustums. Specimens were removed from both the axial (tension, compression and flexure) and circumferential (compression) directions. Each specimen was coded so that positive identification could be maintained throughout the program. The code (supplied by Philco-Ford) was as follows:

Frustum	Specimen	Temperature	Location	Number
1 - First Frustum	AF - Axial Flexure	0 - room temperature	F - Fore	1,2
2 - Second Frustum	AT - Axial Tension	5 - 500°F	M - Mid	
	AC - Axial Compression	10 - 1000°F	A - Aft	
	CC - Circumferential Compression	15 - 1500°F		
		20 - 2000°F		

Detailed cutting plans were not made available to Southern Research and therefore are not included in this report, however, some information on general location of the specimen was provided. The configurations of the tensile, compressive and flexural specimens used for the evaluations are shown in Figures 1, 2 and 3, respectively.

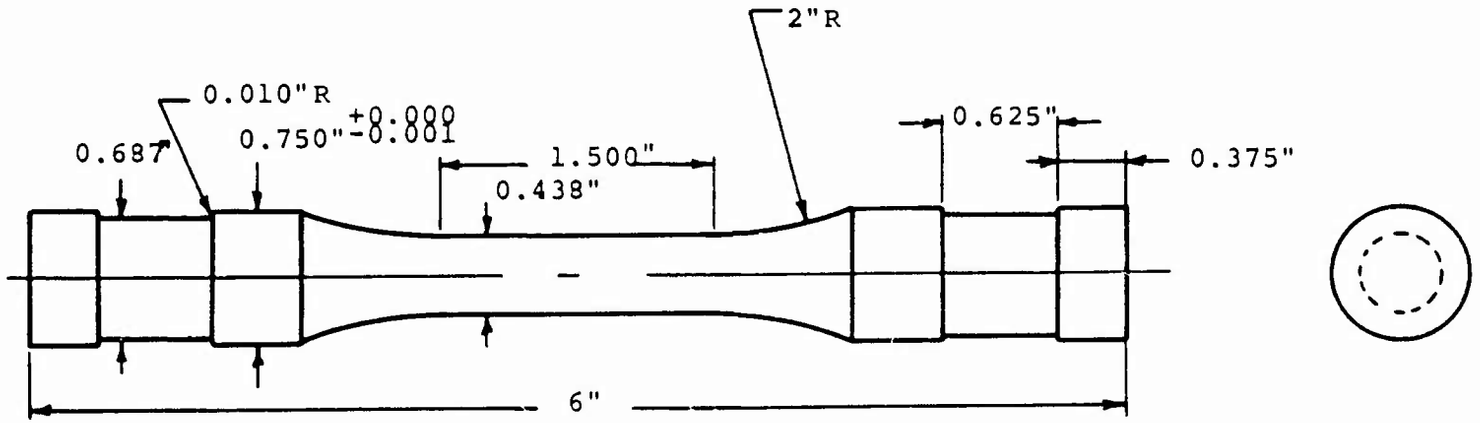

Notes:

1. All Dia True and Concentric to within 0.0005 inch
2. Both ends flat and perpendicular to ℄ to within 0.0005 inch
3. Do not undercut radii at tangent points
4. All dimensions are in inches. Tolerances are ±0.001 in. on Dia ±0.005 in. on length unless otherwise noted

Figure 1. Specimen Configurations for Tensile Evaluations in the Axial Direction

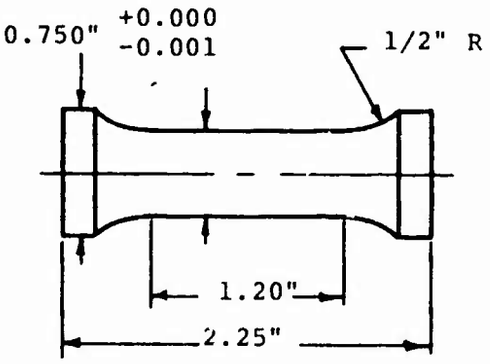

a. Axial Direction

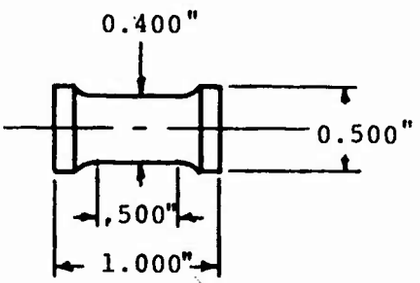

b. Circumferential Direction

Notes:

1. All Dia Must be True and Concentric to within 0.0005 in.
2. Both Ends Flat and Perpendicular to ℄ to within 0.0005 in.
3. Do Not Undercut Radii at Tangent Points. Contour Grind
4. Dimensions are in inches. Tolerances are ±0.001" on dia and ±0.005" on lengths unless otherwise noted.

Figure 2. Specimen Configuration for the Compressive Evaluations

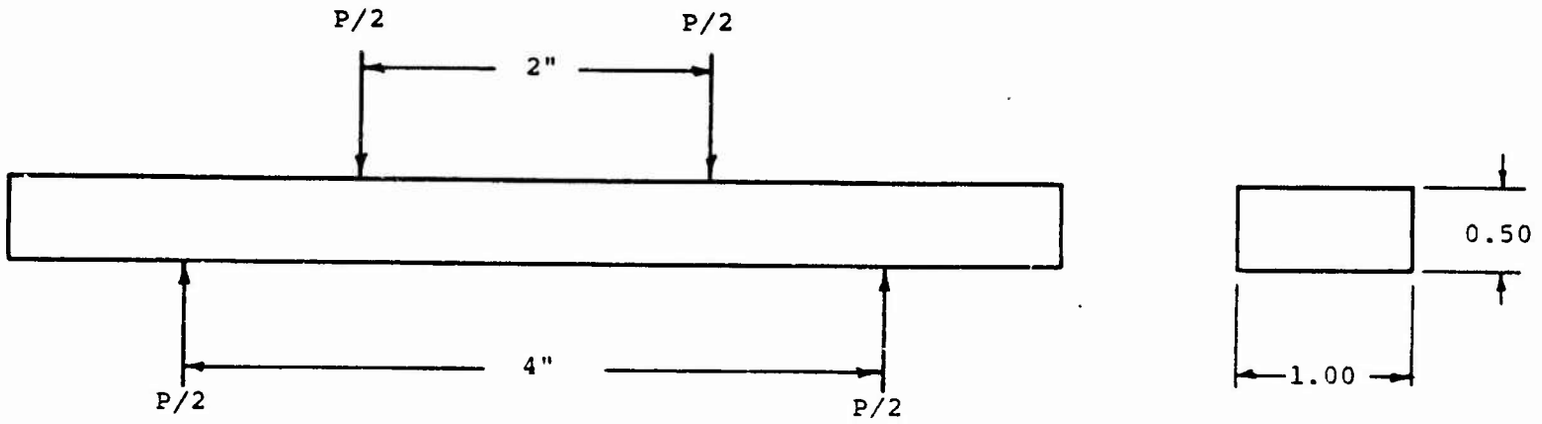

Figure 3. Schematic of Loading Setup for the Four-Point Flexural Evaluations

The compressive specimen shown in Figure 2 is not exactly the same as the configuration originially supplied by Philco-Ford. The original configuration had a major diameter of 0.625 in. and a gage diameter of 0.500 in. This configuration could have been used; however, there were no load train parts in-house that could be readily employed. To have used this configuration would have required machining all new load train parts. Since the time schedules were critical it was decided to alter the specimen configuration so that existing load trains could be used.

APPARATUSES AND PROCEDURES

Tension

The tensile evaluations were performed in a gas-bearing tensile facility. The tensile machine utilizes gas-bearing universals in the load linkage to prevent the introduction of unknown bending moments into the load train from crosshead motion and to allow continuous monitoring of the "straightness" of the load train.

A typical tensile facility is shown in the photograph in Figure 4 and in the schematic in Figure 5. The primary components are the gas-bearings, the load frame, the mechanical drive system, the 5500°F furnace, the optical strain analyzers, and associated instrumentation for measurement of load and strain. The load capacity is 15,000 pounds.

The load frame and mechanical drive system are similar to those of many good facilities. The upper crosshead is positioned by a small electric motor connected to a precision screw jack. This crosshead is stationary during loading and is moved only when assembling the load train. The lower crosshead is used to apply the load to the specimen through a precision screw jack chain driven by a variable speed motor and gear reducer.

Nonuniaxial loading, and therefore bending stresses, may be introduced in tensile specimens not only from (1) misalignment of the load train at the attachment to the crossheads, but also from (2) eccentricity within the load train, (3) unbalance of the load train, and (4) external forces applied to the load train by such items as electrical leads and clip-on extensometers. Although the bending moments from some of these sources may seem relatively slight, the resulting stress distortions are quite significant in the evaluation of the extremely sensitive brittle materials. Now consider each individually.

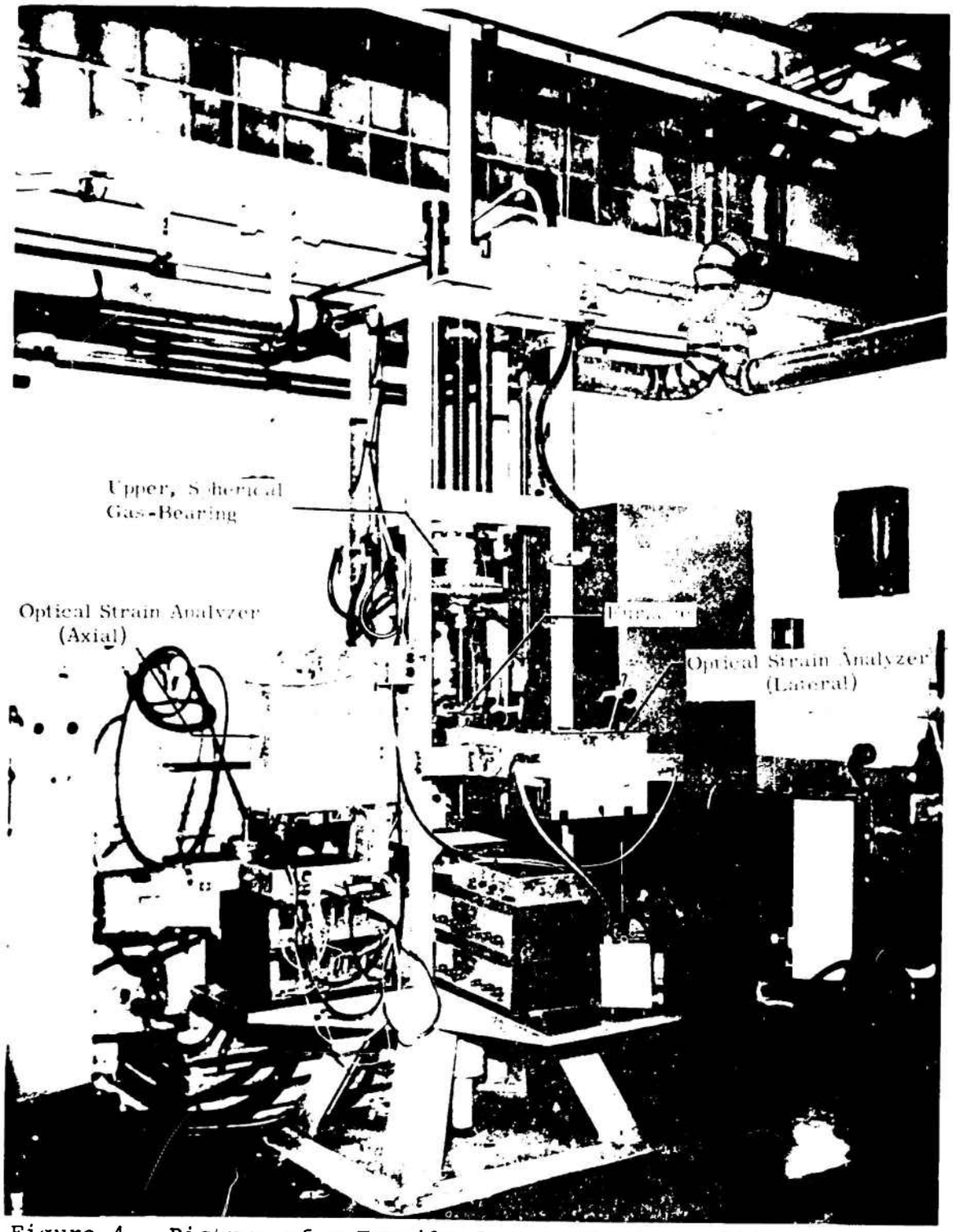

Figure 4. Picture of a Tensile Stress-Strain Facility

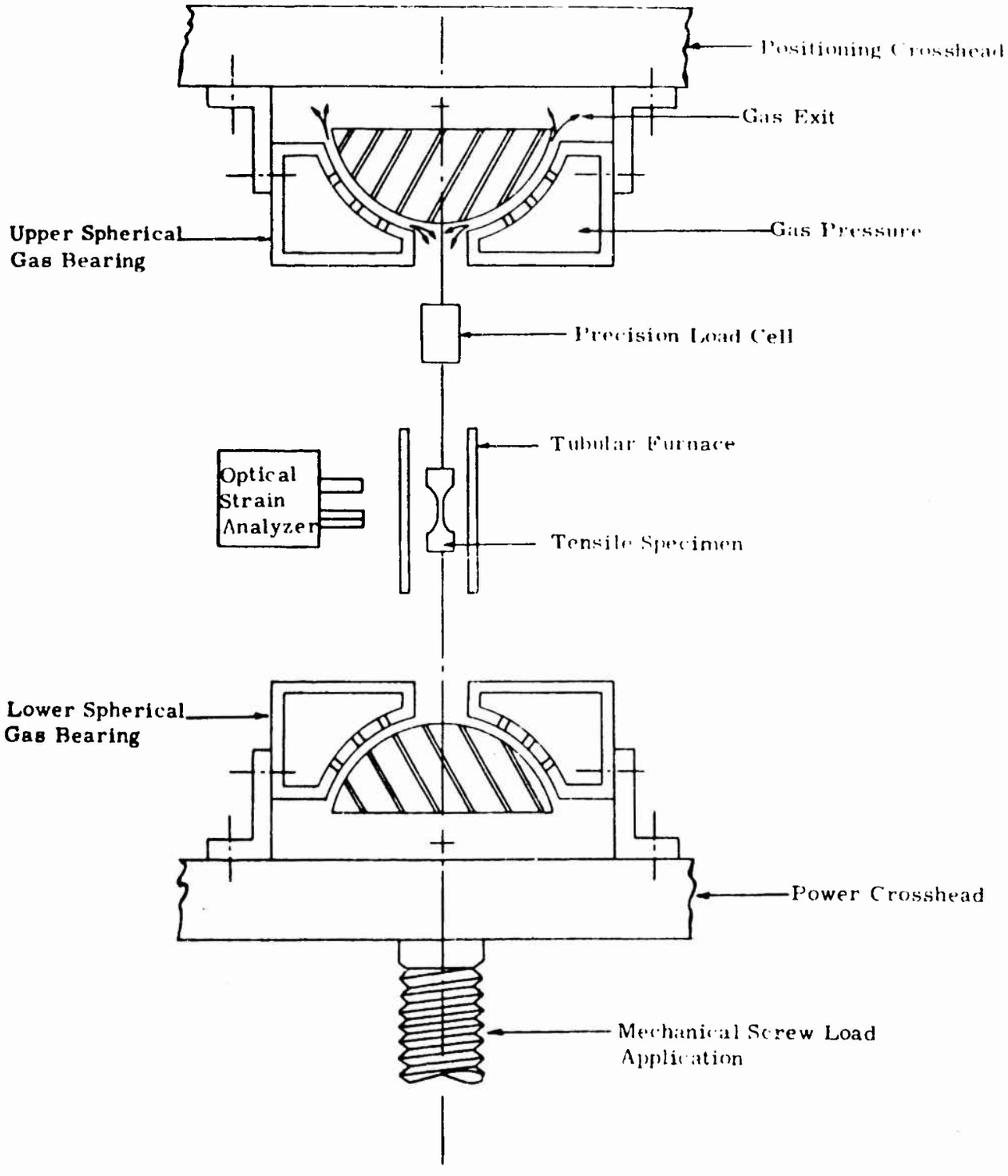

Figure 5. Schematic Arrangement of Gas-Bearing Universals, Specimen, Load Train and Grips

To confirm that the gas-bearings had eliminated nonuniaxial loading at the point of attachment of the load train to the crossheads, the frictional moment was determined at a load of 5000 pounds by measuring the torque required to produce initial motion within the system with the bearings in operation. This torque was found to be a maximum of 6.6×10^{-3} inch-pounds. The equation

$$M_O = \frac{2\mu P}{3} \left[\frac{R_2^3 - R_1^3}{R_2^2 - R_1^2} \right] \qquad (1)$$

was then applied to the system to calculate the kinetic friction where M_O was the resisting moment due to kinetic friction and μ represented the coefficient of kinetic friction. The calculated value of μ was then equal to a maximum of only 4.5×10^{-7}.

The classic equation

$$S = \frac{Mc}{I} \qquad (2)$$

was then employed to obtain the stress that could be induced in the specimen due to this bending moment. This value was 0.16 psi, or less than 0.002 percent of the tensile stress produced within a typical graphite specimen. These low values clearly indicate the elimination of problems of bending stress in the specimen imposed by misalignment at the crosshead attachments, either initially or during loading.

Emphasis in the design of the load train were placed on (1) large length-to-diameter ratios at each connection, (2) close sliding fits (less than 0.005 inch) of all mating connections, (3) the elimination of threaded connections, (4) the use of pin connections wherever possible, and (5) increasing the size of components to permit precise machining of all mating surfaces. All members were machined true and concentric to within 0.0005 inch, and the entire load train was checked regularly to ensure overall alignment following assembly of the individual members. This process ensures concentricity and no kinks in the system.

The problems of unbalance within the load train and of external forces applied to the load train have been explored and corrected. The entire load train is statically balanced to less than 0.01 inch-pound for normal operation.

The configuration of the tensile specimen has been shown in Figure 1. This specimen provides a relatively large L/D ratio in the gripping area to insure good alignment. All surfaces in the gripping area are cylindrical in order to make precision machining easier and repeatable from specimen to specimen. This specimen provides a uniform gage section which gives a definable volume of material under stress and permits accurate measurements of strain. The flags for the measurement of axial strain are positioned one inch apart so that unit strain is recorded directly.

The diameter of the gage section (0.438") was selected as a compromise. In order to insure gage breaks and keep the overall dimensions of the specimens within the limitations of the bulk material it was desirable to have a small gage section. However, the macrostructure required that the gage section be relatively large if representative data were to be obtained. Figure 6 shows an end-on view of Specimen 1-AT-10-F after fracture. Here it can be seen that approximately 10-11 axial fiber bundles were included in the gage section. If the unit cell in the transverse plane is measured as shown in the sketch below, there are about five unit cells in the cross-section.

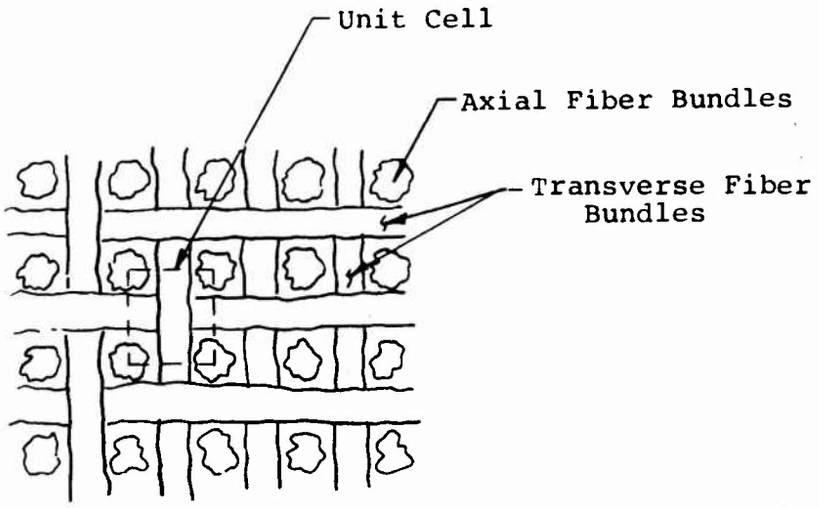

There is some doubt in our mind that a round specimen should be used for this material. Perhaps a square one would be better in that it could be extracted without cutting across cells. We also have not done enough work on this specific material to know the size effect of the gage dimensions whether round or square. Since tensile strengths were higher than flexural strengths the section used must not be too bad.

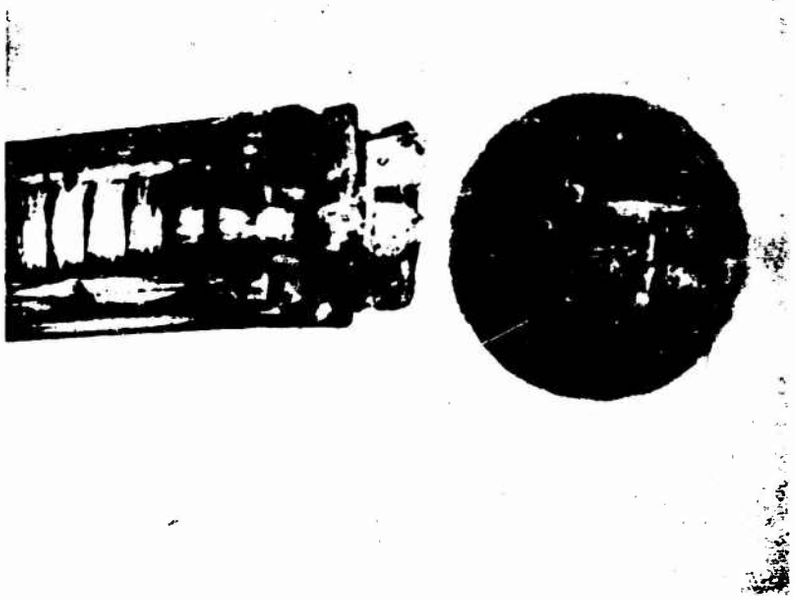

Figure 6. End-on View of Specimen 1-AT-10-F After Fracture

A schematic of the precision tensile grip is shown in Figure 7. The design is much like the jaws of a lathe head or the chuck of a drill motor made with precision. Observe from the figure the long surface contact of the mating parts and the close fits to establish precise alignment with the specimen. As the load is applied, the wedges maintain alignment to fracture.

Figure 8 is a sketch of the 5500°F furnace used for tension showing the basic components. The furnace consists of a resistively heated graphite element insulated from a water-cooled shell by thermatomic carbon. The furnace and specimen are purged with helium to provide an inert atmosphere. Ports with visual openings are provided on opposite sides of the furnace as a means of allowing the strain analyzers to view the gage flags on the specimen. Specimen temperatures are determined by optical pyrometers readings taken through another small sight port containing a sapphire window. A calibration curve was established for the loss through the sapphire window, and since the furnace cavity acts essentially as a blackbody, true temperature readings are obtained. Power is supplied to the heating element by means of a 25 KVA variable transformer.

Strain measurement consists of measuring optically the elongation between two flags, or targets, which are mounted on the specimen and separated initially by a predetermined gage length. The travel of the targets is measured by sensing the displacement of the image of the edge of the targets and then electromechanically following the image displacement. The relative travel of the two targets provides the strain. Readout is continuous and automatic on a millivolt recorder. A schematic of the analyzer is shown in Figure 9.

A brief summary of the mechanical motions of the components involved in monitoring the strain is helpful in understanding the detailed performance. A tracking telescope follows the upper target and carries a second telescope mounted on its carriage. The second telescope is capable of independent motion to follow the lower target. The relative displacement between the upper and lower telescope, as strain occurs, defines the strain. The system usually is operated so that the tracking telescope follows the upper target and the strain is monitored by the relative displacement of the aperture rather than the telescope following the lower target. With this procedure the maximum range is the maximum displacement available for the lower aperture, of about 1/8 inch, and the sensitivity is limited by the optics and the noise level of the detector. Using both telescopes, the range is about 3/4 inch.

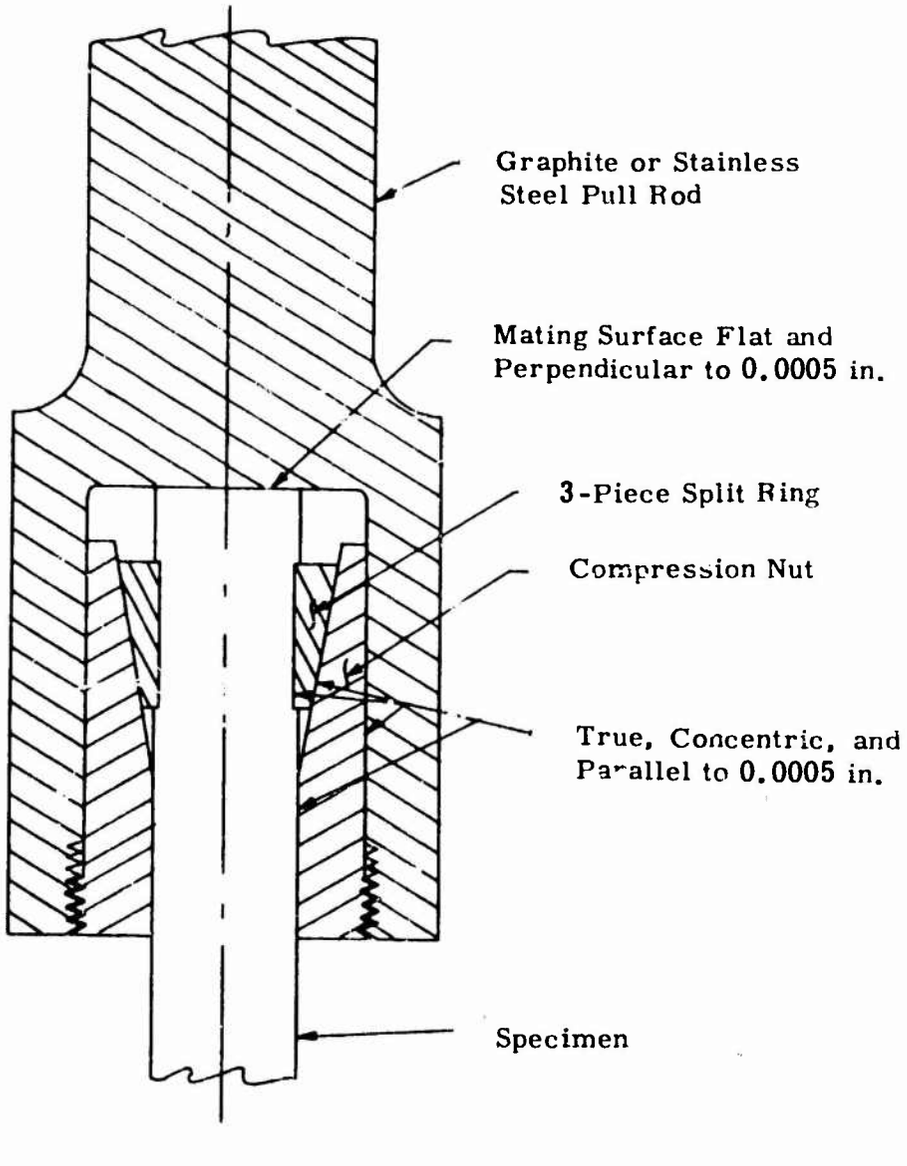

Figure 7. Precision collet grip for tensile specimens.

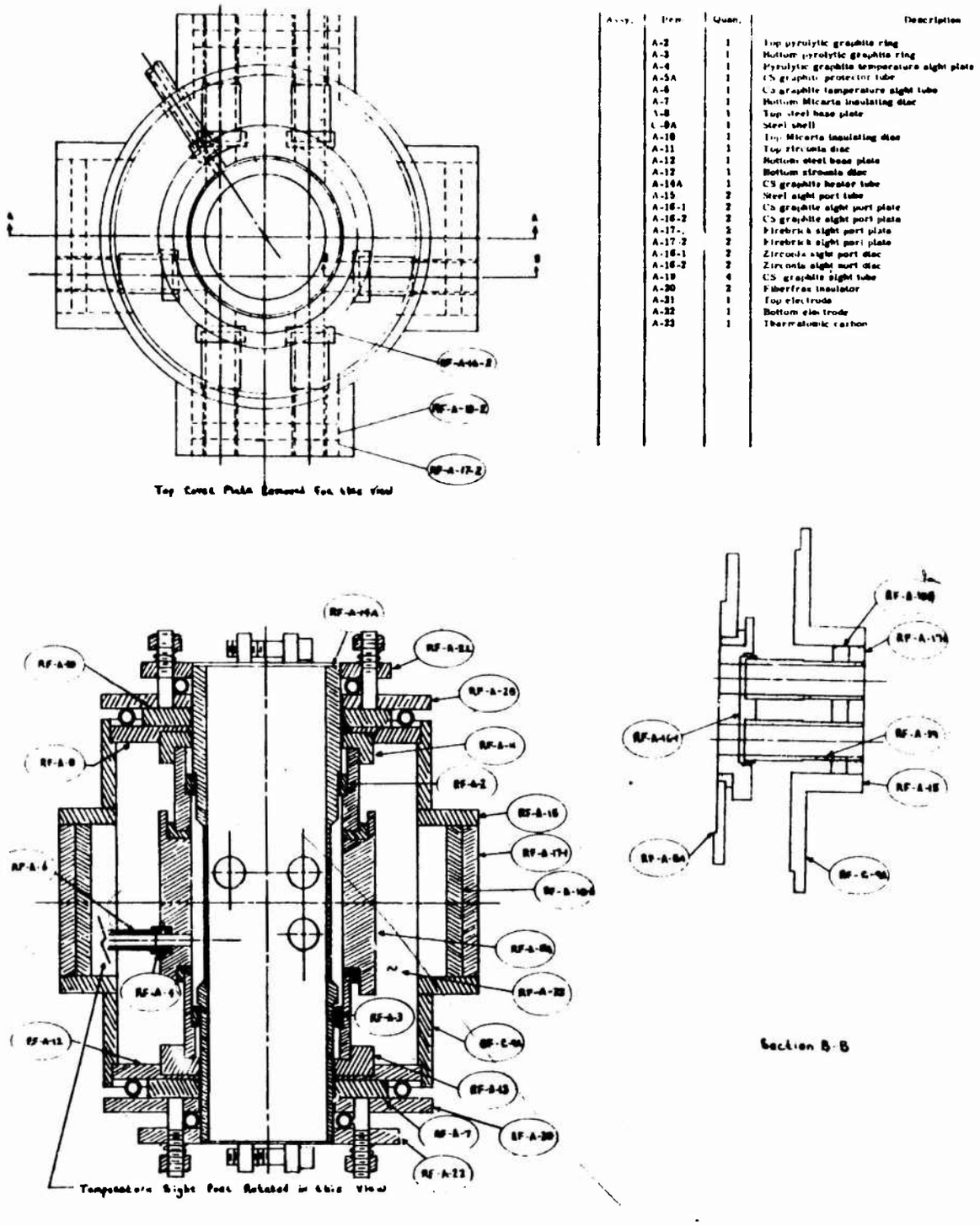

SOUTHERN RESEARCH INSTITUTE

Figure 8. Small 5500°F Graphite Resistance Furnace

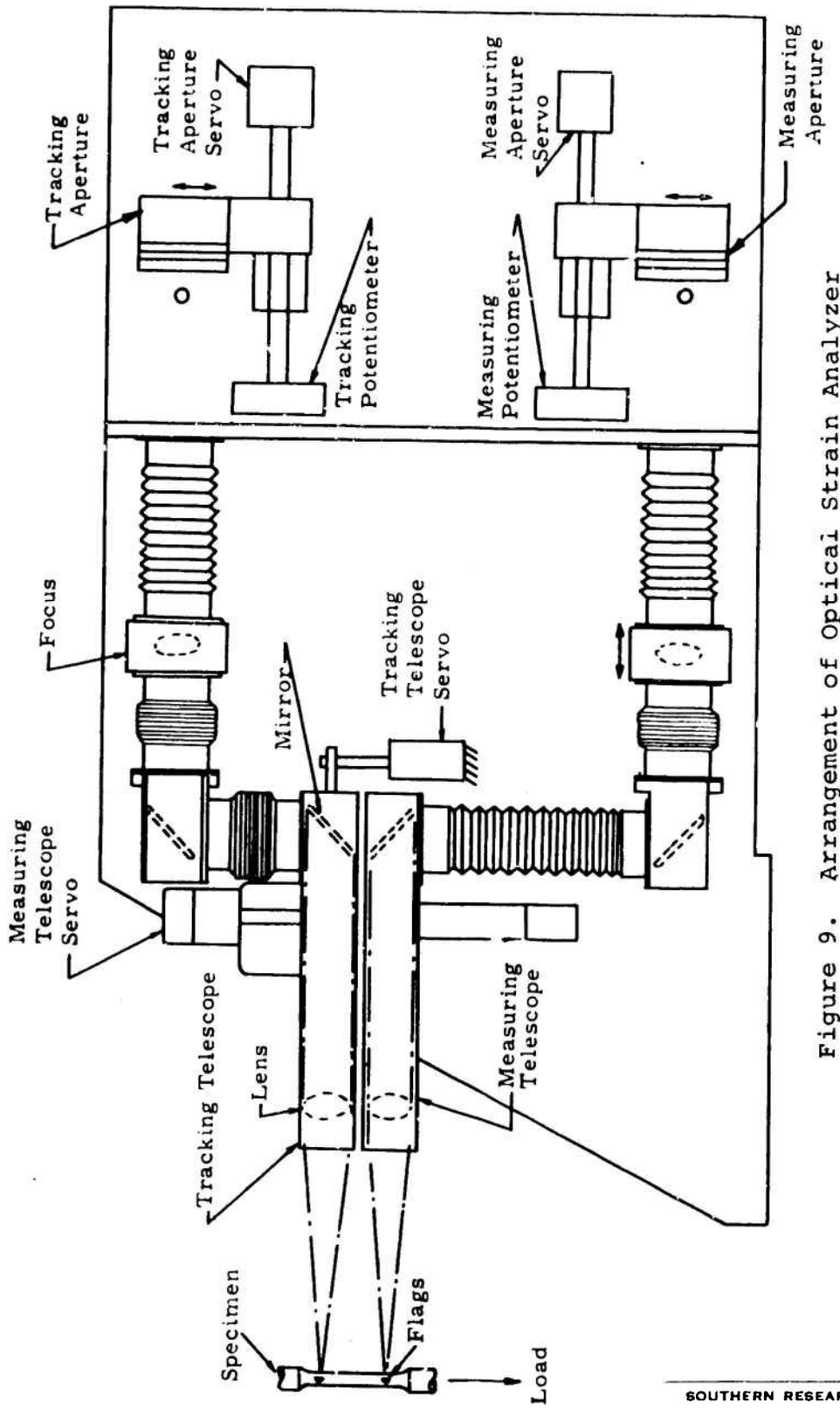

Figure 9. Arrangement of Optical Strain Analyzer

SOUTHERN RESEARCH INSTITUTE

To provide optical references on the specimens, targets are affixed to the test specimen, see Figure 10. When the specimen is heated to temperature, the targets are self-luminous and are observed optically. The optics view past the luminous targets into a cooled cavity in the opposite furnace wall. The self-luminous targets are then visible against a dark background. To obtain data below 2000°F, a light beam is directed from behind the flags providing a shadow image for the detection system.

The image of the flowing target is focused through a rotating shutter (chopper) and onto a rectangular aperture. Small slits in the aperture pass a portion of the upper and lower edges of the light beam. A photocell receives the light thus transmitted, and an electronic circuit detects whether the energy passed by the two slits is equal. A servo drives the apertures to let a balanced quantity of light pass through the two slits and thus maintains an optical null.

Calibrations of the analyzers are performed in various ways including absolute correlations to precision micrometers, strain gage extensometers, and direct plots of stress-strain for reference materials such as steel, plexiglas, magnesium and aluminum. Precision is within ±0.000020 inch.

Instrumentation includes primarily a stress-strain measurement system composed of a SR-4 Baldwin load cell, constant d. c. voltage power supply, two optical strain analyzers, and two X-Y recorders. Specimen temperature is monitored with an optical pyrometer. Stress (load) is measured by a commercial load cell. The cell receives a constant d. c. voltage input from the power supply and transmits a millivolt signal (directly proportional to load) to an X-Y recorder. Simultaneously, the optical strain analyzer measures the axial strain and transmits a millivolt signal (proportional to strain) to the X-Y recorders. Thus, a continuous plot of stress-axial strain is recorded.

Compression

The compressive evaluations were performed in a gas-bearing compressive facility. In a manner similar to the tensile facility, gas-bearing universals are utilized in the load train to prevent the introduction of unknown bending moments into the load train. The compressive apparatus is shown in the photograph in Figure 11 and in the schematic in Figure 12 and consists primarily of a load frame, gas bearings, load train, 50-ton screw jack, variable speed mechanical drive system, strain analyzers, 5500°F furnace and associated instrumentation for the measurements of load and strain.

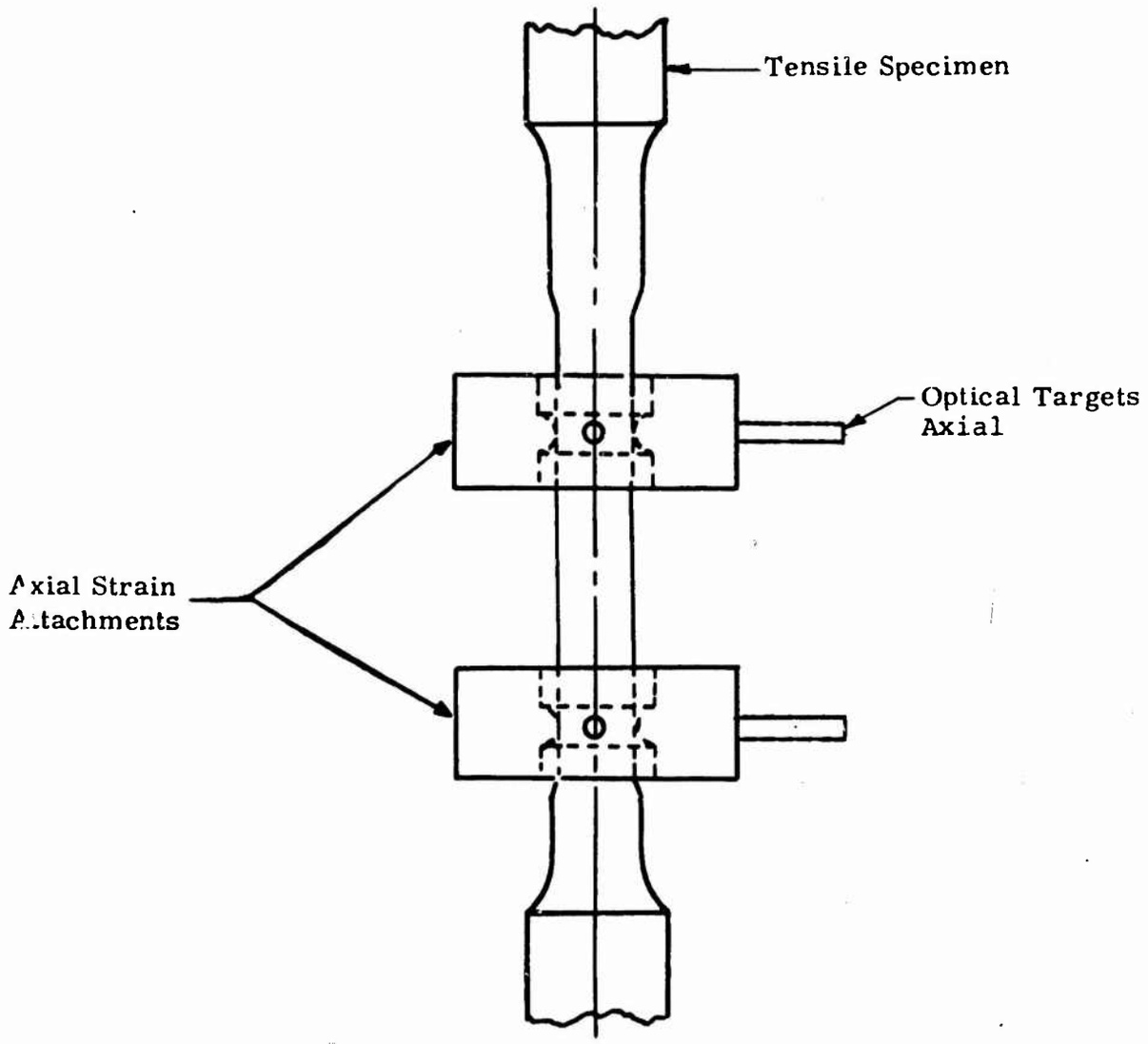

Figure 10. Location of the Flag Attachments on the Tensile Specimens

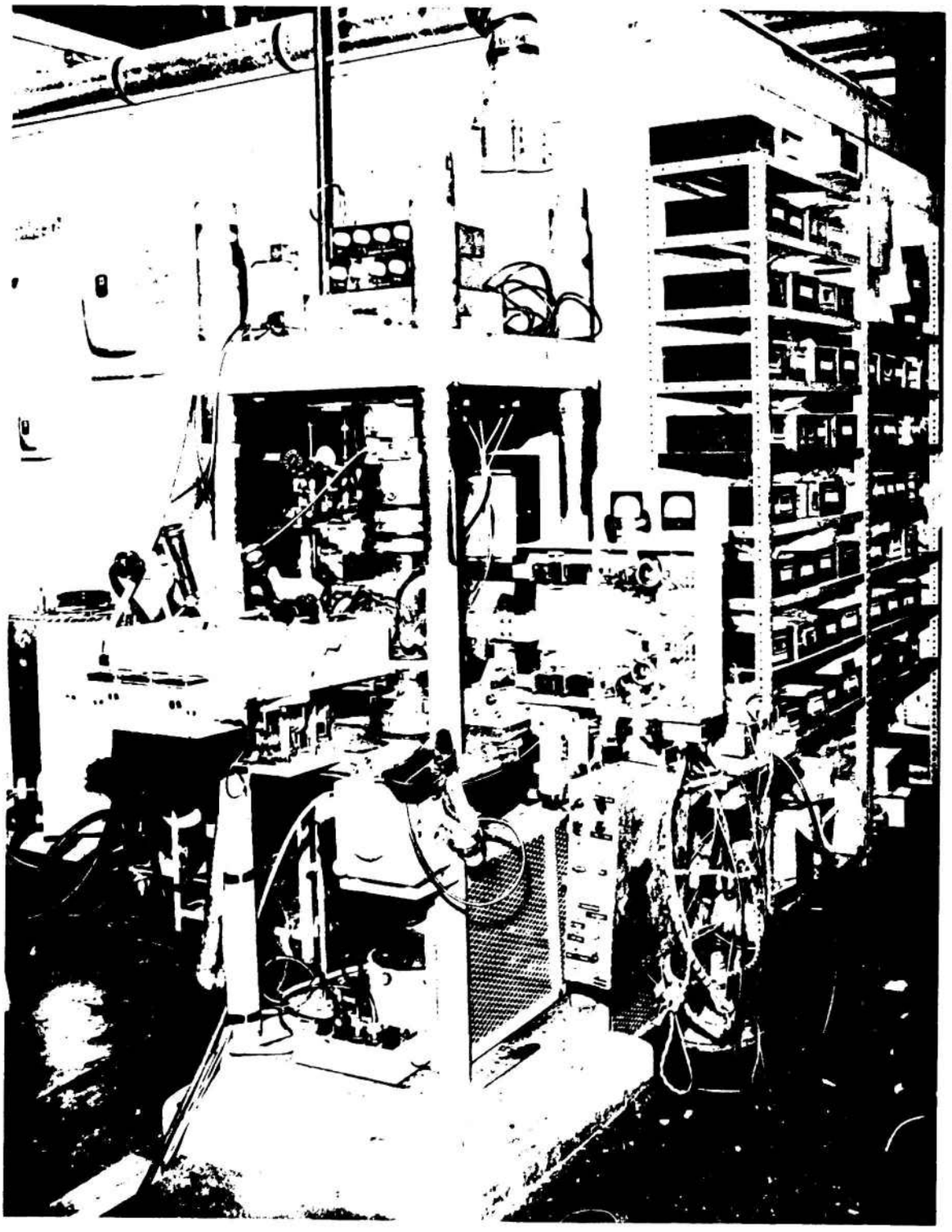

Figure 11. Picture of the Compressive Facility with Gas Bearings and Optical Strain Analyzer

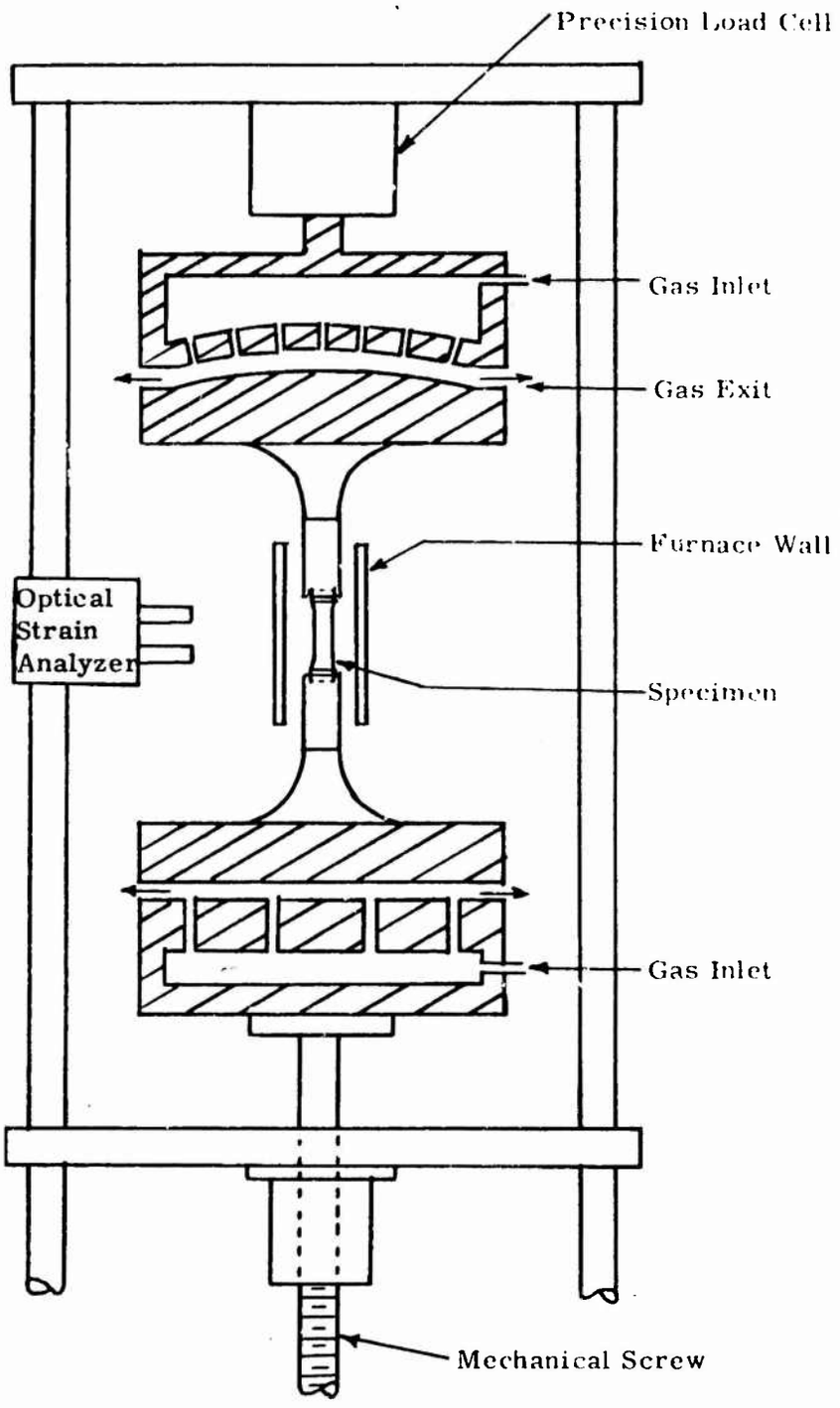

Figure 12. Schematic Arrangement of Gas-Bearing Universals, Specimen, and Load Train

The load frame is similar to most standard frames. It was designed to carry a maximum load of 100,000 pounds and to support the furnace, optical strain analyzers, and other related equipment.

Gas bearings are installed at each end of the load train to permit precise alignment of the loading train to the specimen. The upper bearing is spherical on a radius of 6.5 inches. This radius is the distance from the top of the specimens to the spherical bearing surface. The load train, not the specimen, shifts to maintain radial alignment. The lower bearing is flat and is about 6 inches in diameter. The lower bearing permits transverse alignment of the load train. The gas bearings are floated for only a small initial amount of load so that precise alignment of the load train can be attained.

The load train near the furnace consists of the specimen loaded on each side by graphite and water-cooled steel push rods. The graphite push rods are counter-bored to permit insertion of a pyrolytic graphite disc which serves as a heat dam and to align the specimen to the center-line of the load train. Extreme care is exercised in the preparation of all parts of the load train to ensure concentricity of the mating parts to less than 0.0005 inch.

The 50-ton jack is a power screw type. The mechanical drive system consists of a gear reducer driven by a Louis Allis Synchro-Spede Unit (300-3000 rpm). The gear reducer is connected to the Synchro-Spede Unit through a chain coupling and to the 50-ton jack by a single roller chain and sprocket system. Different load rates are obtained by adjustment of the variable speed setting on the Synchro-Spede and by changeout of sprockets on the gear reducer and screw jack.

The specimen configurations are presented in Figure 2. Two configurations were required for these evaluations, one (Figure 2a) for specimens oriented along the longitudinal axis of the frustums and one for specimens in the hoop or circumferential direction. The configuration shown in Figure 2a is a modification of our standard compressive specimen. The dumbbell shape is used to minimize the influences of end restraint and permit homogeneous deformation in the gage section. The gage section is 0.500 in. diameter by 1.20 in. long and the strain targets are placed one inch apart as shown in Figure 13.

A special set-up was required to make strain measurements on the small specimen shown in Figure 2b because of the reduced length of the gage section. Offset strain targets were used. They are shown schematically in Figure 14.

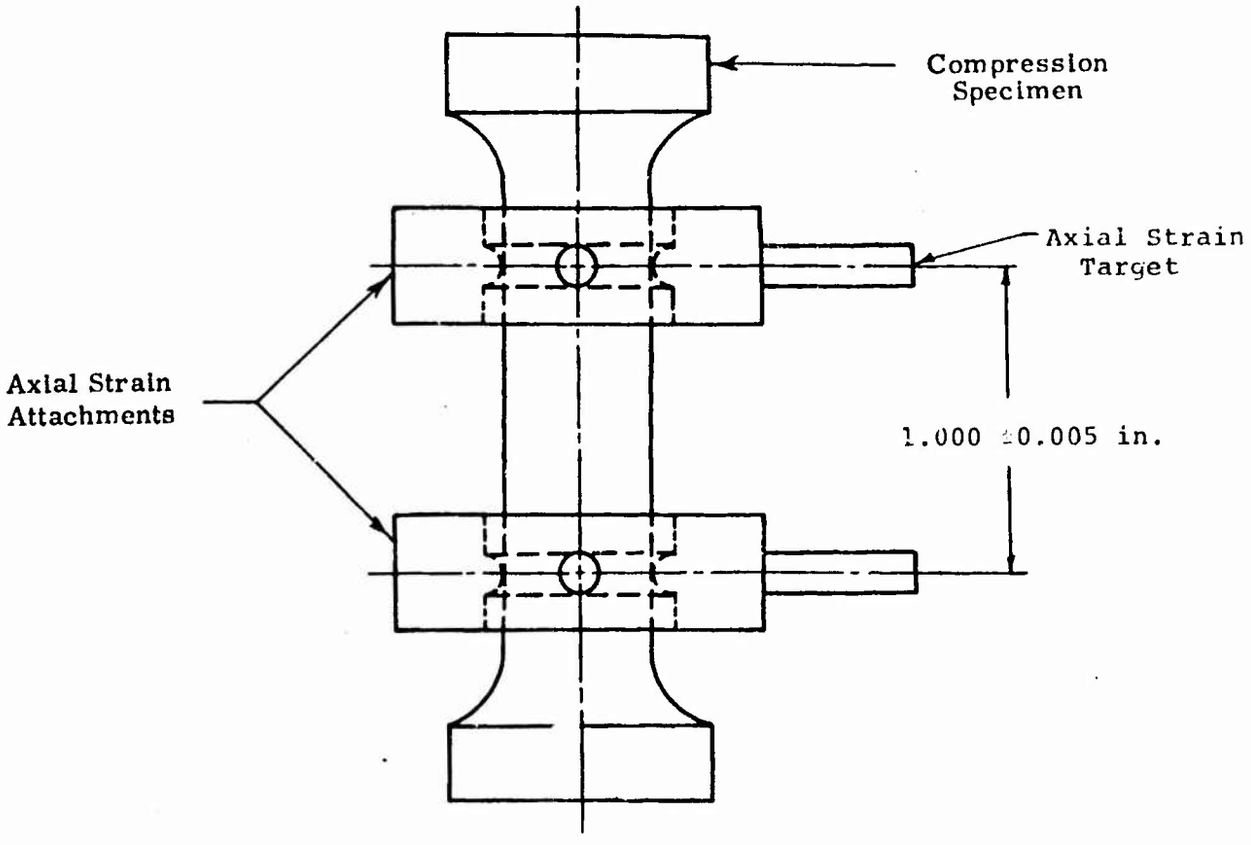

Figure 13. Location of the Flag Attachments on the Compressive Specimen

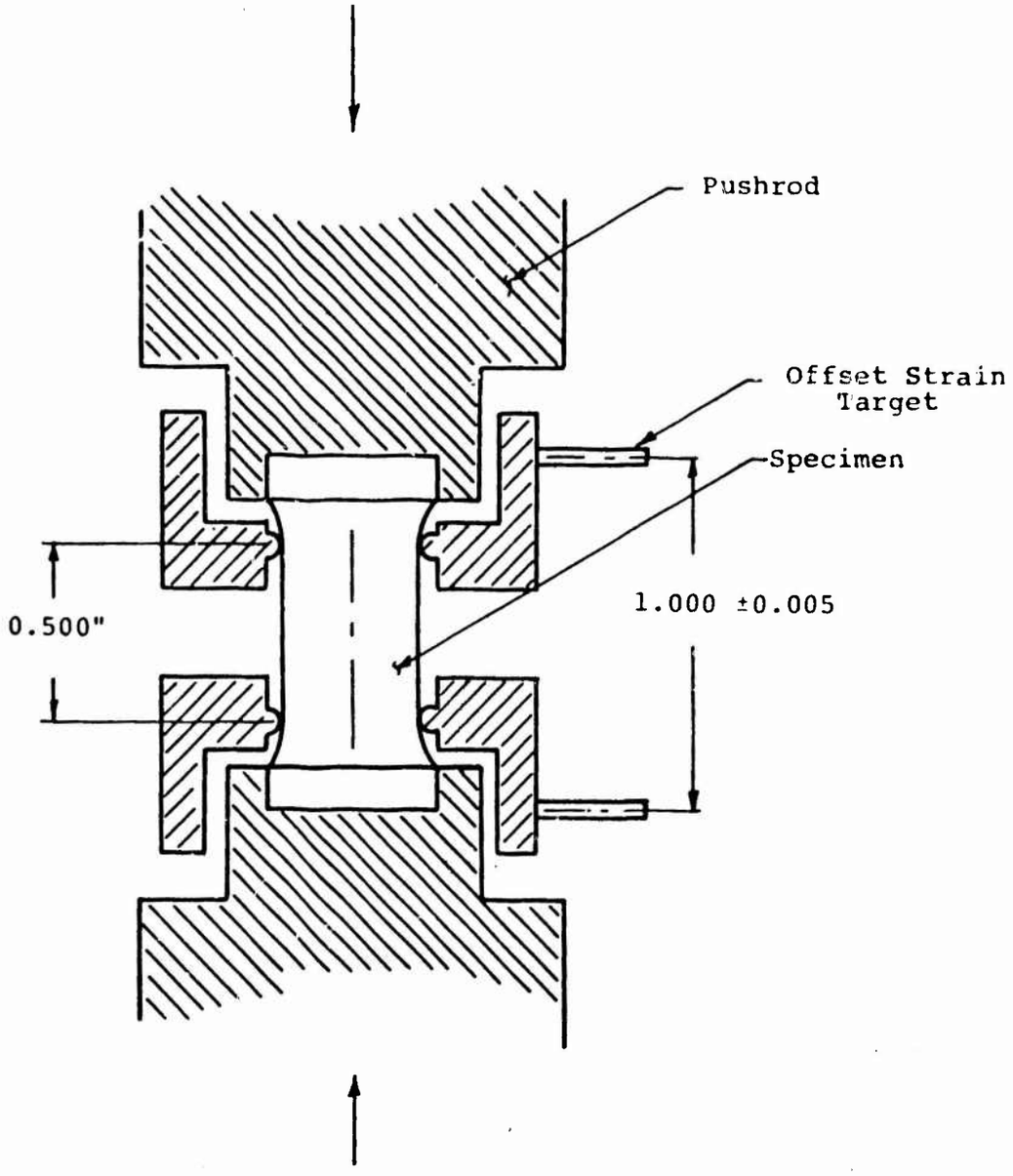

Figure 14. Schematic of Load Train and Offset Strain Targets for Circumferential Compressive Specimens

The furnace, optical strain measuring equipment and instrumentation used for the compressive evaluation were essentially the same as that employed for the tensile evaluations and therefore will not be redescribed here.

Flexure

A cross sectional schematic of the apparatus used to determined the ultimate strength and the initial elastic modulus in flexure is shown in Figure 15. Radiant heating of the specimen is provided by the high temperature furnace utilizing resistance heating of a graphite element. The furnace is similar to the furnace described earlier. The other components consist of water cooled journals, a load train, a mechanical drive system, a deflection measurement system, and instrumentation for the continuous recording of load and deflection. A third span or four point loading system was used. Figure 16 is a schematic showing the nominal dimensions of the loading setup.

The load train was designed primarily to the recommendations of ASTM C 78-59. It consists of several components, primarily (1) a stainless steel drive shaft, (2) a graphite push rod, (3) a graphite flexural arm, (4) the specimen, (5) an adapter block, (6) a graphite loading rod, (7) a stainless steel spacer, and (8) a load cell. The main objectives of the load train design were to provide precision alignment and to eliminate friction within the load train.

The stainless steel drive shaft is internally threaded to receive the threaded shaft of the gear reducer. The drive shaft is not permitted to rotate, hence the rotation of the gear reducer shaft causes the drive shaft to move in the journal. The movement of the drive shaft in turn causes the load to be transmitted to the specimen by the push rod and flexural arm. The push rod is mated to the flexural arm by a spherical socket which prevents any application of torque to the specimen. The flexural arm contains two 3/8" radius slots which hold two slotted graphite rods 3/8" diameter by 7/8" long. The specimen is contacted on the opposite side by two knife edges positioned in slots within the adapter block. The knife edges and the slotted rods within the flexural arm are easily replaceable when damaged. The load is transmitted to the load cell by way of the adapter block, a graphite push rod, and a stainless steel spacer. A ball joint is employed at the load cell.

The following steps were taken to ensure good alignment and to eliminate friction in the load train. Both journals were machined to close tolerances and good surface finishes and were precisely aligned (within 0.010") before being secured into position. The push rods were machined to close fits in the journals. All mating

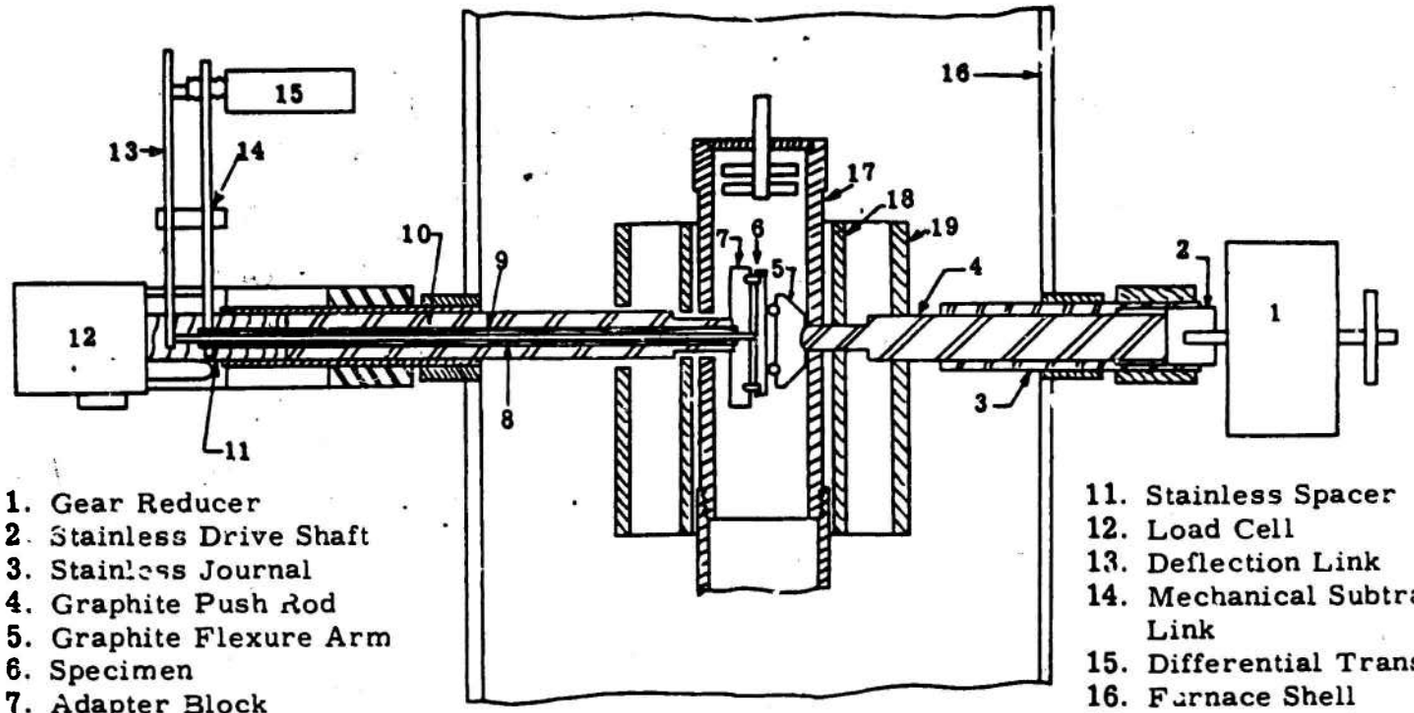

1. Gear Reducer
2. Stainless Drive Shaft
3. Stainless Journal
4. Graphite Push Rod
5. Graphite Flexure Arm
6. Specimen
7. Adapter Block
8. Deflection Rod
9. Compensating Tube
10. Graphite Push Rod
11. Stainless Spacer
12. Load Cell
13. Deflection Link
14. Mechanical Subtraction Link
15. Differential Transformer
16. Furnace Shell
17. Resistance Element
18. Protector Tube
19. Furnace Liner

Figure 15. Schematic of the High Temperature Flexure Apparatus

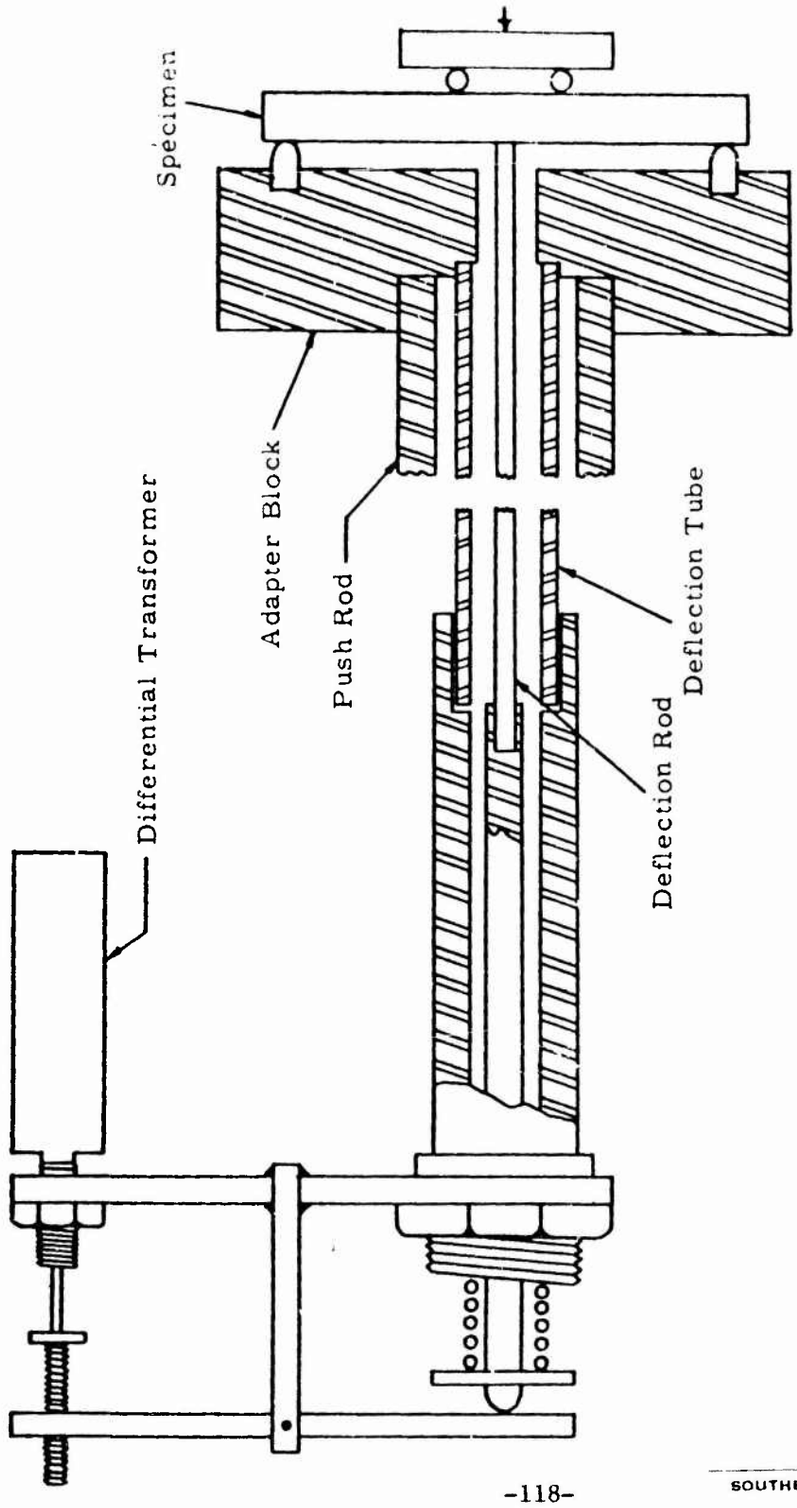

Figure 16. Schematic of Deflection Measurement System

parts were machined flat and perpendicular (with the exception of the ball joints). The static friction was measured and found to be less than one pound.

The mechanical drive system consists of a gear reducer that is chain-driven by a variable speed electric motor. The electric drive is a 3/4 horsepower Bodine Type J56 with a Type SH-257E speed control. The motor and control unit are capable of a speed range of 10-1725 rpm.

The deflection measurement system shown in Figure 16 was designed to monitor the motion of the midpoint of the flexural specimen while compensating for any relative movement of the specimen and load train components. A 1/8" diameter graphite rod (deflection rod) presses against the midpoint of the specimen. The small rod is spring loaded and moves in a graphite tube (compensating tube) which is also spring loaded. The compensating tube extends into the center of the adapter block and acts as a reference for the movement of the deflection rod. Both the graphite deflection rod and tube are fitted into similar parts of stainless steel in the cooler extremity of the furnace. A differential transformer is connected to the deflection tube through a linkage such that the entire differential transformer moves with the deflection tube. A deflection lever is attached to the transformer linkage with a pivot at its midpoint. Thus, as the specimen deflects, the deflection rod moves the deflection lever and causes an equal movement of the plunger of the differential transformer. The differential transformer transmits a signal to an X-Y recorder that is proportional to the midpoint deflection. If the adapter block or load train shift in either direction, the deflection tube and the differential transformer move the same amount, and no change in deflection is transmitted to the recorder.

The deflection as measured by this system is corrected for the deformation of the knife edges in the adapter block and the deformation of the adapter block due to bending. The correction is established at room temperature on a Tinius-Olsen universal testing machine and adjusted for the variation of elastic modulus with temperature of the flexural block. Since the adapter block is massive in comparison with the specimen, its deformation is small in relation to that of the specimen. The correction is less than 10 percent for most specimen configurations and is negligible for specimens of small cross section.

Calibration of the deflection measurement system is made by use of a specially designed calibrator employing a precision micrometer dial. Load is measured by a Baldwin SR-4 load cell which is calibrated against dead weights. These calibrations are checked at regular intervals and are found to be highly consistent. Continuous signals from the load cell and differential transformer are received and plotted by a Moseley X-Y recorder yielding a load-deflection curve. Load rates or deflection rates can be controlled utilizing simultaneous readout of load or deflection on a time recorder.

DATA AND RESULTS

The results of the tensile, compressive and flexural evaluations are shown in Tables 1, 2 and 3 respectively. In general, both the strengths and moduli from all the evaluations were scattered and the properties appeared to be quite dependent on location of the specimen in the frustums. Some general trends were shown for the material as presented in Figure 17. Here the tensile and flexural strengths are plotted versus temperature. The strengths increased about 25 percent from room temperature to 500°F, remained essentially constant to 1000°F and increased about 15 percent from 1000°F to 1500°F. The compressive results were too scattered to show any trends. The moduli stayed relatively constant throughout the temperature range.

Referrring to Table 1 the following observations can be made:

1. The tensile strength of the material in the forward section was greater than in the aft section in Frustum No. 1.

2. The tensile moduli were equal in the forward and aft sections.

3. The tensile strength in the forward section of Frustum No. 1 was greater than the tensile strength in the forward section of Frustum No. 2.

4. The tensile modulus in the forward section of Frustum No. 1 was greater than the tensile modulus in the forward section of Frustum No. 2.

Table 1

Results of the Tensile Evaluations

Loading Direction	Temperature °F	Stress Rate psi/min	Specimen Number	Ultimate Tensile Strength psi	Initial Elastic Modulus 10^6 psi	Total Strain to Fracture in./in.	Remarks
Axial	70	10,000	1-AT-0-A	4130	2.70	------	Cycled at ~3400 psi one time
			1-AT-0-F	6470	2.79	~0.003	Fractured in the radius
			2-AT-0-F1	3200	2.97	0.0010	
			2-AT-0-F2	4120	3.50	0.0013	
				4480	2.99		
	500	10,000	1-AT-5-A	5450	2.65	0.0023	Fractured in the radius
			1-AT-5-F	6620	2.75	0.0024	Cycled to ~5200 psi
			2-AT-5-F	4360	4.00	0.0012	Fractured in the radius
				5480	3.13		
	1000	10,000	1-AT-10-A	5120	2.85	~0.0018	
			1-AT-10-F	6750	2.51	------	
			2-AT-10-F	5200	3.50	0.0015	
				5690	2.95		

Table 2

Results of Compressive Evaluations

Loading Direction	Temperature °F	Stress Rate psi/min	Specimen Number	Ultimate Compressive Strength psi	Initial Elastic Modulus 10^6 psi	Remarks
Axial	70	10,000	1-AC-0-A	14,900	2.43	
			1-AC-0-M	14,880	3.01	
			2-AC-0-A	12,320	1.63	
			2-AC-0-F	11,120	3.14	
				13,300	2.55	
	500	10,000	1-AC-5-A	14,190	2.00	
			1-AC-5-M	13,640	3.69	
			2-AC-5-A	13,480	1.83	
				13,770	2.51	
	1000	10,000	1-AC-10-A	16,190	3.16	
			1-AC-10-M	17,450	3.69	
			2-AC-10-A	14,440	2.73	
				16,030	3.19	
	1500	10,000	1-AC-15-A	17,490	2.48	
			1-AC-15-M	18,290	3.65	
			2-AC-15-A	13,040	3.63	
				16,270	3.25	
	1800	10,000	2-AC-20-A	18,240	1.77	
	2000		1-AC-20-A			These specimens were heated to ~2000°F at which point they became dimensionally unstable (contracted). No compressive runs were made.
			1-AC-20-M			
Circumferential	70	10,000	1-CC-0-M	6,180	----	
			1-CC-0-F	9,670	3.42	
			2-CC-20-M	10,700	2.59	
			2-CC-0-F	8,750	3.75	
				8,830	3.25	
	500	10,000	1-CC-5-F	11,230	3.97	
			1-CC-5-M	9,380	3.80	
			2-CC-5-M	------	----	Failed under the weight of the top gas-bearing (15 lbs, ~120 psi)
				10,300	3.89	
	1000	10,000	1-CC-10-F	13,750	2.50	
			1-CC-10-M	5,700	2.03	
			2-CC-10-M	2,670	0.80	
				7,370	1.78	
	1500	10,000	1-CC-15-F	16,000	3.97	
			1-CC-15-M	9,250	2.30	
			2-CC-15-M	14,200	2.37	
				13,150	2.88	
	1800	10,000	1-CC-20-M	11,130	2.25	
			1-CC-20-F	>22,000	1.41	The push-rod failed
					1.83	

Table 3

Results of Flexural Evaluations

Loading Direction	Temperature °F	Stress Rate psi/min	Specimen Number	Modulus of Rupture psi	Flexural Modulus of Elasticity 10^6 psi	Remarks
Axial	70	10,000	2-AF-0-F1	3770	1.74	
			2-AF-0-A	3280	1.67	
			2-AF-0-F2	3800	1.76	
			2-AF-0-A	5150	2.26	
				4000	1.86	
	500	10,000	1-AF-5-A	3640	1.83	
			2-AF-5-A	6640	1.99	
			2-AF-5-F	4400	2.08	
				4890	1.97	
	1000	10,000	1-AF-10-A	4900	2.16	
			2-AF-10-A	4140	1.65	
			2-AF-10-F	5460	1.83	
				4830	1.88	
	1500	10,000	1-AF-15-A	7160	1.84	
			2-AF-15-A	5170	1.70	
			2-AF-15-F	5000	2.17	
				5780	1.90	

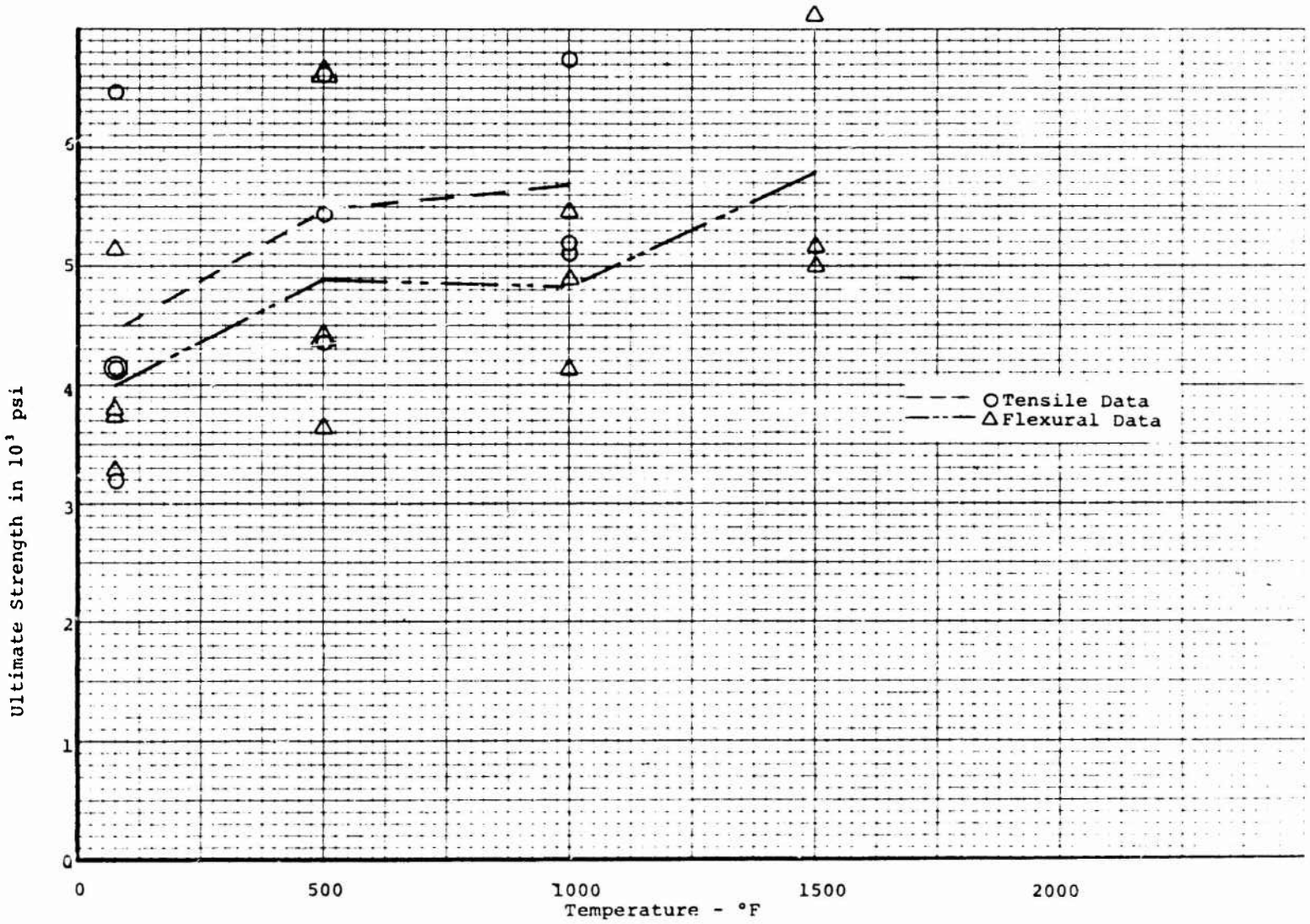

Figure 17. Ultimate Strength in Tension and Flexure versus Temperature for Material AS3DC

Table 3

Results of Flexural Evaluations

Loading Direction	Temperature °F	Stress Rate psi/min	Specimen Number	Modulus of Rupture psi	Flexural Modulus of Elasticity 10^6 psi	Remarks
Axial	70	10,000	2-AF-0-F1	3770	1.74	
			2-AF-0-A	3280	1.67	
			2-AF-0-F2	3800	1.76	
			2-AF-0-A	5150	2.26	
				4000	1.86	
	500	10,000	1-AF-5-A	3640	1.83	
			2-AF-5-A	6640	1.99	
			2-AF-5-F	4400	2.08	
				4890	1.97	
	1000	10,000	1-AF-10-A	4900	2.16	
			2-AF-10-A	4140	1.65	
			2-AF-10-F	5460	1.83	
				4830	1.88	
	1500	10,000	1-AF-15-A	7160	1.84	
			2-AF-15-A	5170	1.70	
			2-AF-15-F	5000	2.17	
				5780	1.90	

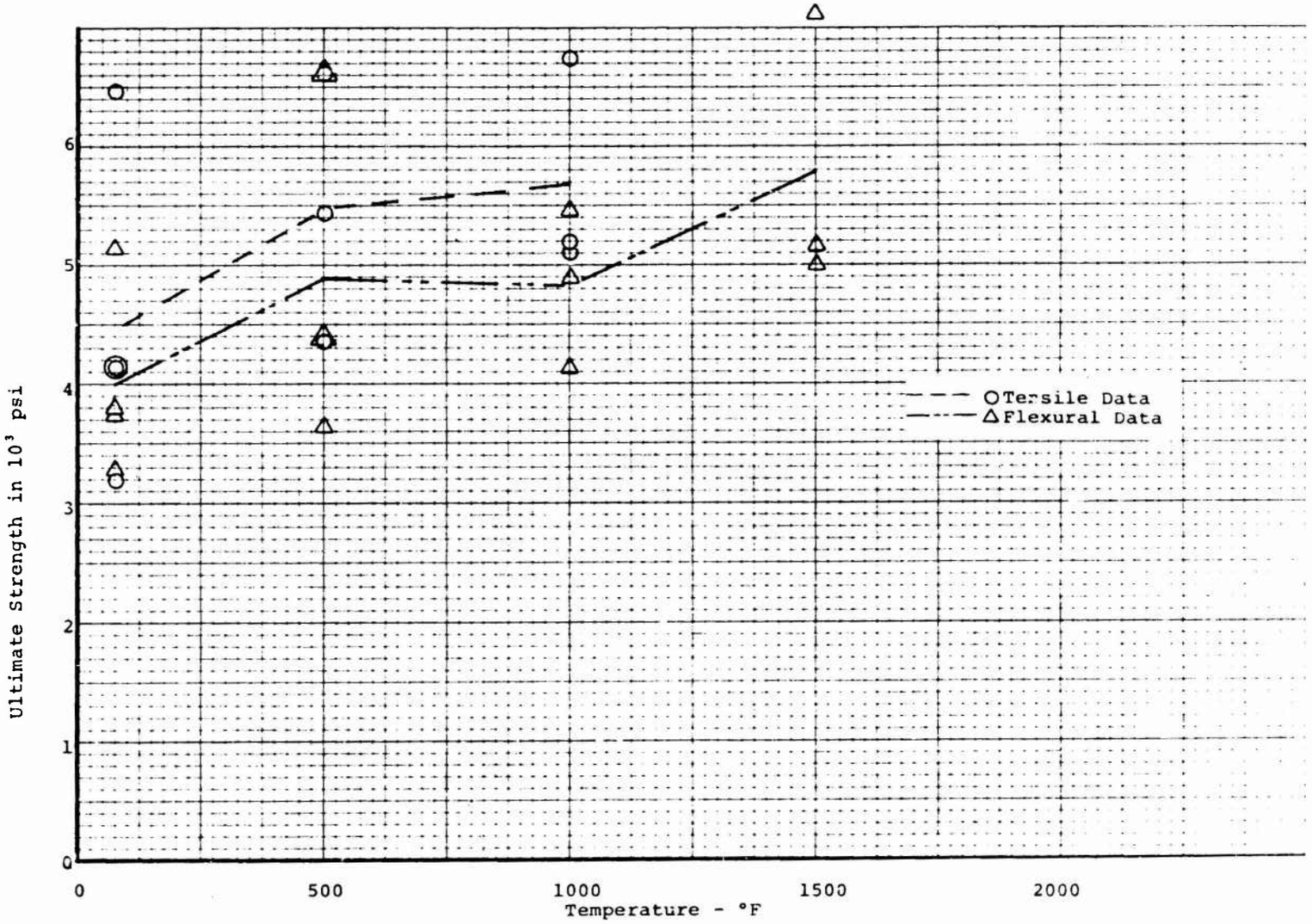

Figure 17. Ultimate Strength in Tension and Flexure versus Temperature for Material AS3DC

Observations 1 and 2 indicate that there was a strength gradient in Frustum No. 1 but that the modulus was constant. Observations 3 and 4 suggest that Frustum No. 1 was superior to Frustum No. 2 if the failure mode was buckling.

From Table 3 (compressive data) the observations were:

1. The axial compressive strengths in the mid and aft sections were equal for Frustum No. 1.

2. The axial compressive moduli were higher in the mid section than in the aft section of Frustum No. 1.

3. The circumferential compressive strengths in the forward section were higher than in the mid section of Frustum No. 1.

4. The axial compressive strengths in the aft section of Frustum No. 1 were greater than the compressive strengths in the aft section of Frustum No. 2.

Thus property gradients and differences between the two frustums were also evidenced in the compressive data as well as the tensile data. Two very low compressive strengths (2670 psi and ~120 psi) were recorded for the mid section of Frustum No. 2.

No trends or differences were shown by the flexural data. In general the flexural strengths were about 10 percent lower than the tensile strengths. Usually materials which show non linear behavior as this one did in flexure give higher flexural strengths than tensile strengths. One odd point was that failures in the room temperature flexural specimens were not visibly obvious although a definite ultimate load value was recorded during the run. After the specimens were removed from the loading fixture there were no visible signs of failure other than a slight bow. Preliminary radiographs were not revealing as to where failure occurred within the specimen.

Submitted by:
H. Stuart Starrett
H. Stuart Starrett, Head
Solid Mechanics Section

Approved by:
C. D. Pears
C. D. Pears, Head
Mechanical Engineering Division

A-246-2491-I
(3:1:12)
klr

APPENDIX IV

AVCO TEN MEGAWATT ARC JET TURBULENT WEDGE TEST RESULTS

I. OBJECTIVE

Four (4) specimens were tested in the Avco, Systems Division, Ten Megawatt (10 MW) Arc Facility (Reference 1) for Philco-Ford Corporation. All specimens were in the form of flat plates which were exposed to a supersonic, arc heated, exhaust jet.

Two (2) two-dimensional (rectangular) nozzle designs having nominal Mach numbers of 2.0 and 2.5 were utlized in the test program. The rectangular nozzles were designed using the method of characteristics as described by Puckett (Reference 2) using a constant value of the isentropic exponent equal to 1.2. The Mach 2 nozzle is 1.0 inch wide with a height at the throat of 0.8 inches and a height at the exit of 1.56 inches, resulting in a area ratio of 1.95. The Mach 2.5 nozzle is also 1.0 inch wide but has a height at the throat of 0.46 inches and a height at the exit of 1.62 inches resulting in a area ratio of 3.52.

This report describes the results of calibration and specimen tests which were conducted during the week of 25 May 1970. Mr. John Stetson of Philco-Ford Corporation witnessed all tests.

II. DISCUSSION

A. GENERAL

For the purpose of studying turbulent flow ablation, a flat plate turbulent ablation test has been designed and is referred to as a supersonic two-dimensional wedge test. This test configuration is depicted schematically in Figure 1. In all cases the specimens (Figure 2) were placed at an angle along the smaller edge of the exit nozzle. By placing the specimen at a small angle to the flow a shock wave and therefore an unfavorable pressure gradient is produced which tends to make laminar boundary layer transition to turbulent definite. In addition, it also helps to maintain relatively constant flow conditions over the greater portion of the specimen surface providing the specimen surface does not recede severely. If the specimen were aligned with the flow, the surface would recede away from the edge of the jet resulting in a less severe environment with a large region of separated flow. Of course, if the angle chosen is too large the reflection of the shock from the jet boundary may impinge on the test surface resulting in non-uniform test conditions. Too large an angle might also induce boundary layer separation at the leading edge. For the case at hand, the sample inclination angle was based upon a combination of factors. These included heat flux level, distribution of heat flux and pressure during exposure. Based on these considerations an angle of 10 degrees was chosen for the Mach 2 tests and 15 degrees for the Mach 2.5 tests.

Data gathered during the test program included:

a) Flow field properties: enthalpy, stagnation pressure, and gas flow rates.

b) Sample heat flux and pressure distribution data.

c) Pre and post test sample photographs.

d) Motion pictures of the heated surface of each test.

e) Sample brightness temperature history.

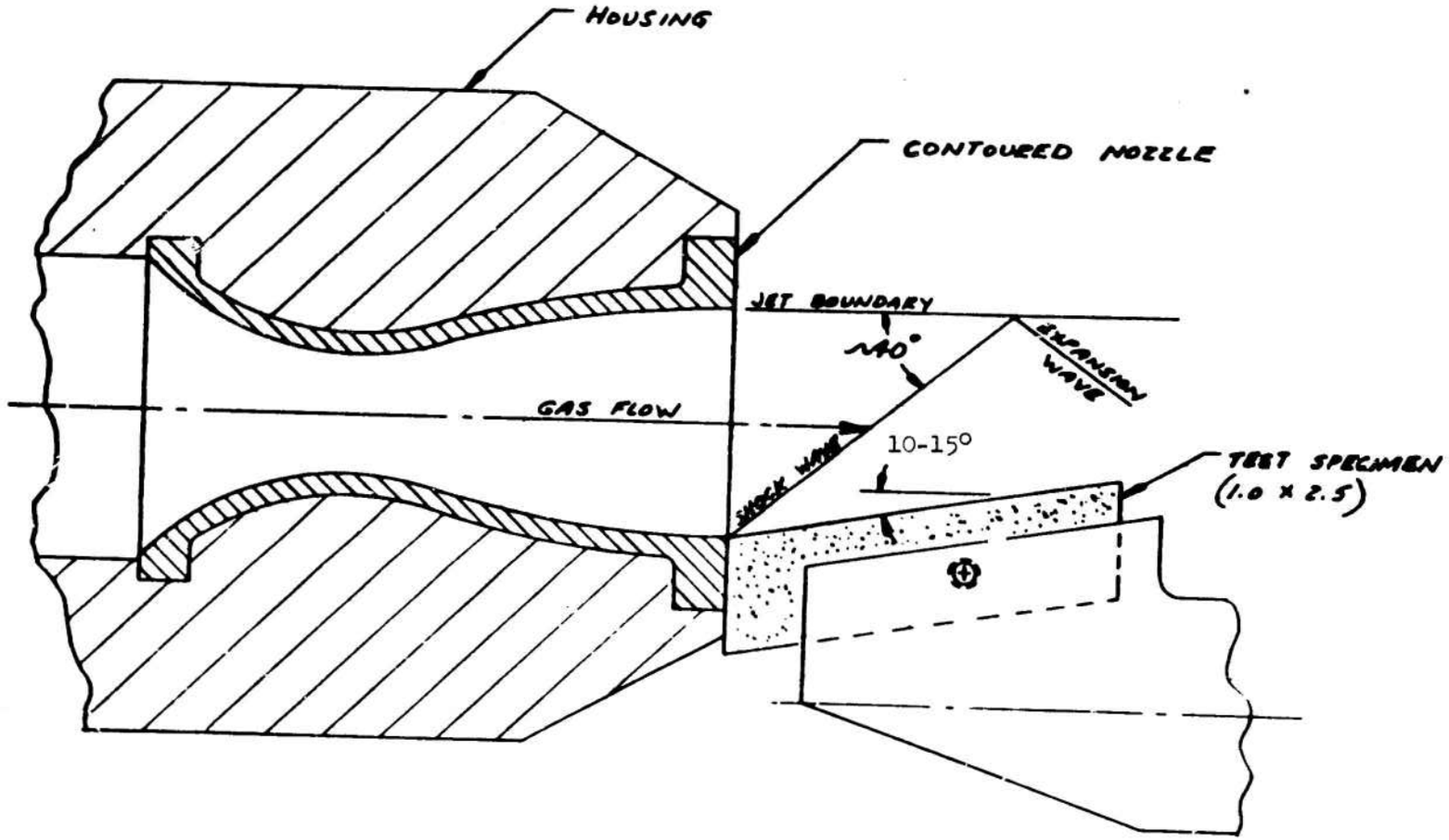

FIGURE 1 2-D WEDGE TEST CONFIGURATION AND FLOW PATTERN

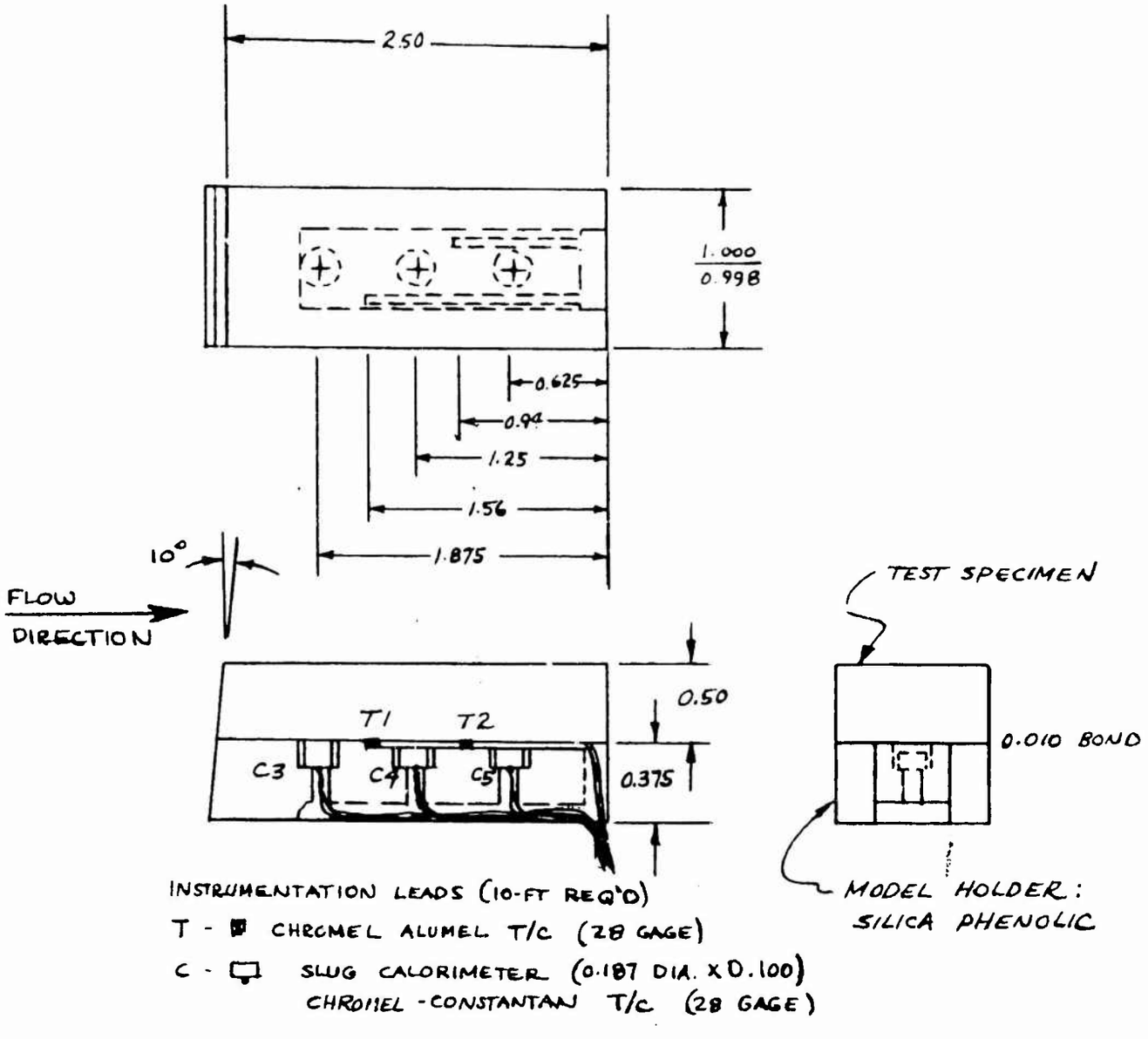

FIGURE 2. WEDGE MODEL - AS-1 ABLATION TEST

The average enthalpy of the gas stream produced by the facility was determined from the sonic flow theory of Winovich (Reference 3) as discussed in Reference 1. Measurement of gas enthalpy on the centerline of the exhaust jet with an enthalpy probe (Reference 4) has shown that the method employed in calculating the reported average enthalpy is not seriously in error.

The brightness temperature and total radiation of all specimens tested in the program was measured with a calibrated high resolution recording optical pyrometer (Thermodot TD9F) operating at a wavelength of 0.8μ and a Eppley thermopile respectively. The pyrometer field of view was a circular area having a diameter of 0.12 inch for these particular experiments. The center of the field of view was located at $1\frac{1}{2}$ inches from the leading edge of the specimen along the centerline. The spot diameter of the thermopile was 0.4 inches at the same location.

Pre and post test measurements of sample dimensions and weight were made for each sample. The nominal sample dimensions and weight were made for each sample. The nominal sample dimensions are given in Figure 2.

Still photographs of the samples before test are presented in Figures 3 to 5.

In addition, motion picture coverage of the tests was provided by Avco. A Bell and Howell, 64 frame per second, motion picture camera was used for all tests. The films have been submitted to Philco-Ford Corporation for study and retention. In general the films show quite clearly the ablation and flow phenomena of each sample.

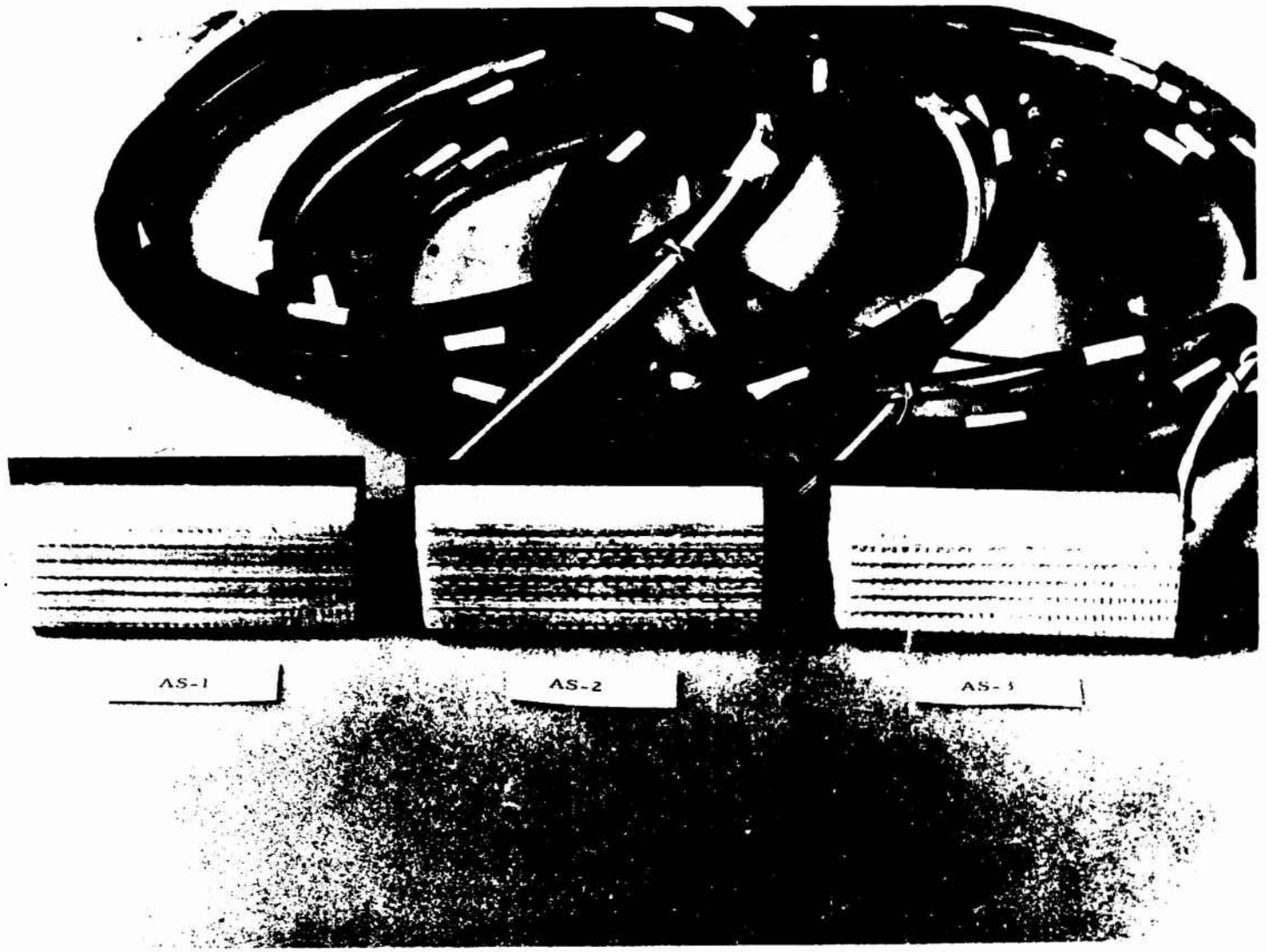

FIGURE 3 PRE TEST OVERALL VIEW OF TEST SAMPLES AS-1, AS-2 AND AS-3

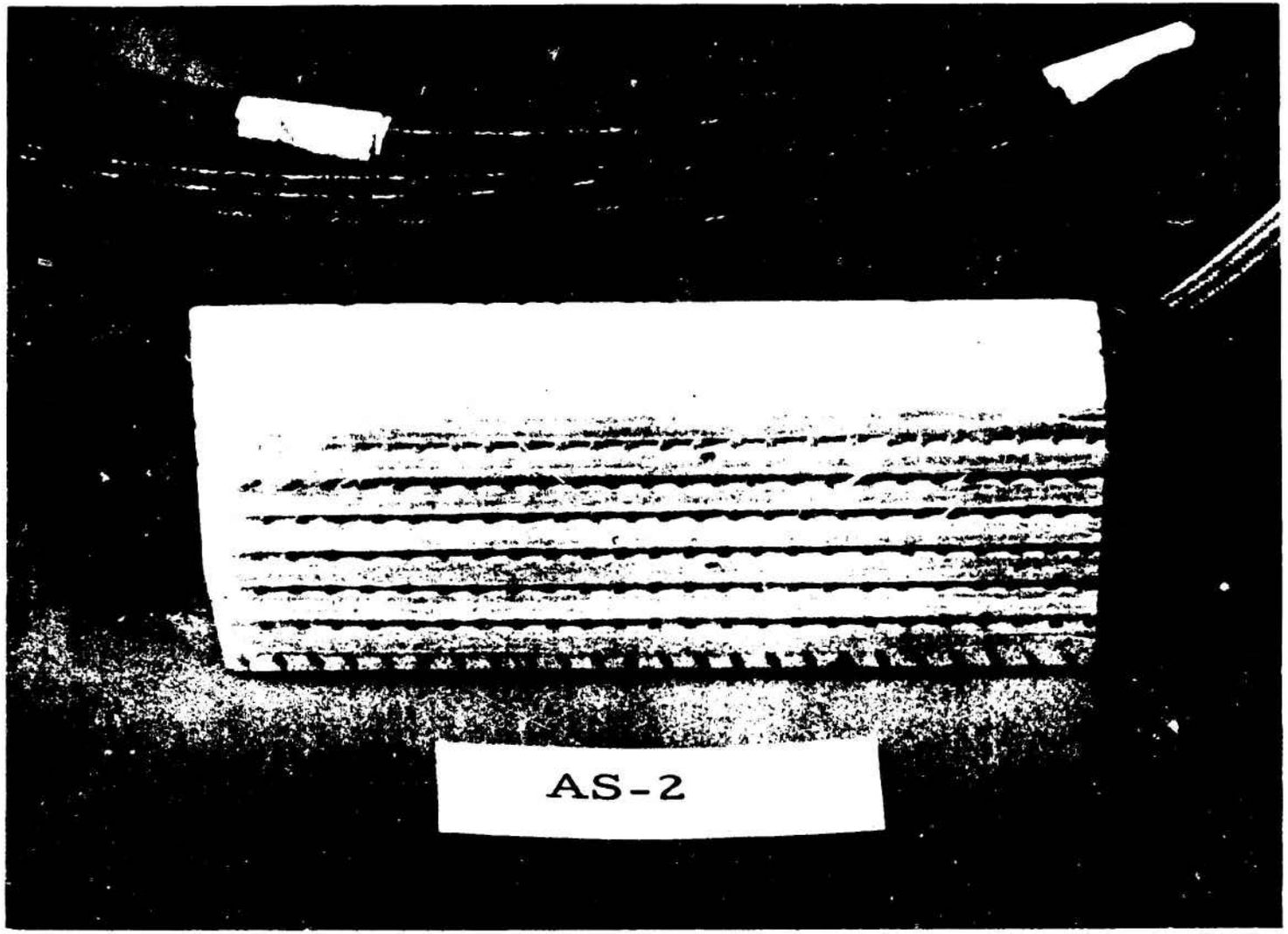

FIGURE 4 PRE TEST CLOSE-UP SURFACE VIEW OF TEST SAMPLE AS-2

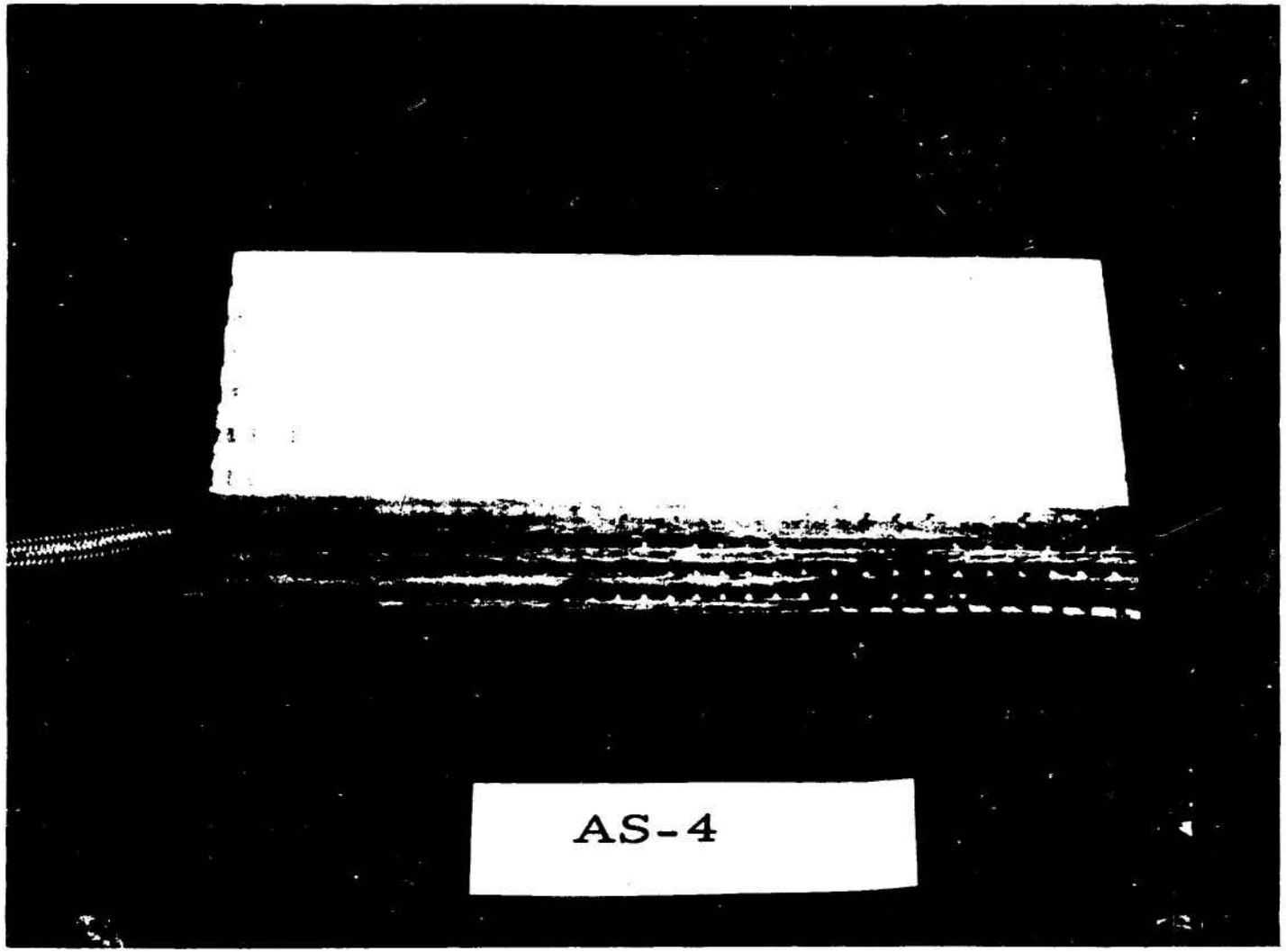

FIGURE 5 PRE TEST CLOSE-UP SURFACE VIEW OF TEST SAMPLE AS-4

B. TEST RESULTS

1. Calorimeter Measurements

Test conditions were determined by means of an instrumented copper block which was the same size and shape as the specimen. Figure 6 presents a schematic view of the Avco calorimeter assembly in the 10 MW Arc Facility. Figure 7 shows the calorimeter assembled to the 10 MW Arc exit nozzle.

A good deal of effort was previously devoted to finding the proper plenum pressure for the operating condition which results in nearly shock free flow. It was generally found that the isentropic pressure ratio for $\gamma = 1.2$ corresponding to the nozzle area ratio was about the best choice.

Conditions at the edge of the boundary layer on the specimen are found by solving the equation

$$M_2^2 = \frac{M_1^2[(\gamma+1)\xi + (\gamma-1)] - 2(\xi^2-1)}{\xi[(\gamma-1)\xi + (\gamma+1)]} \qquad (1)$$

for $\gamma = 1.2$, where ξ is the static pressure ratio across the oblique shock and M_1 is the design Mach number of the nozzle. The static pressure on the specimen is obtained by averaging the two readings for each condition. Knowing the total enthalpy, the static pressure, and the Mach number, other properties of the flow are found from the Mollier diagram for air with the use of an auxiliary scale solving the equation $U_e = \sqrt{2\Delta h}$, as described by Vincenti (Reference 5).

The mean value of the shear stress is obtained from Reynolds analogy,

$$\bar{\tau} = (q_{cw})_c \, u_e/h_s$$

where $(q_{cw})_c$ is the average measured heat flux value and h_s is the gas enthalpy.

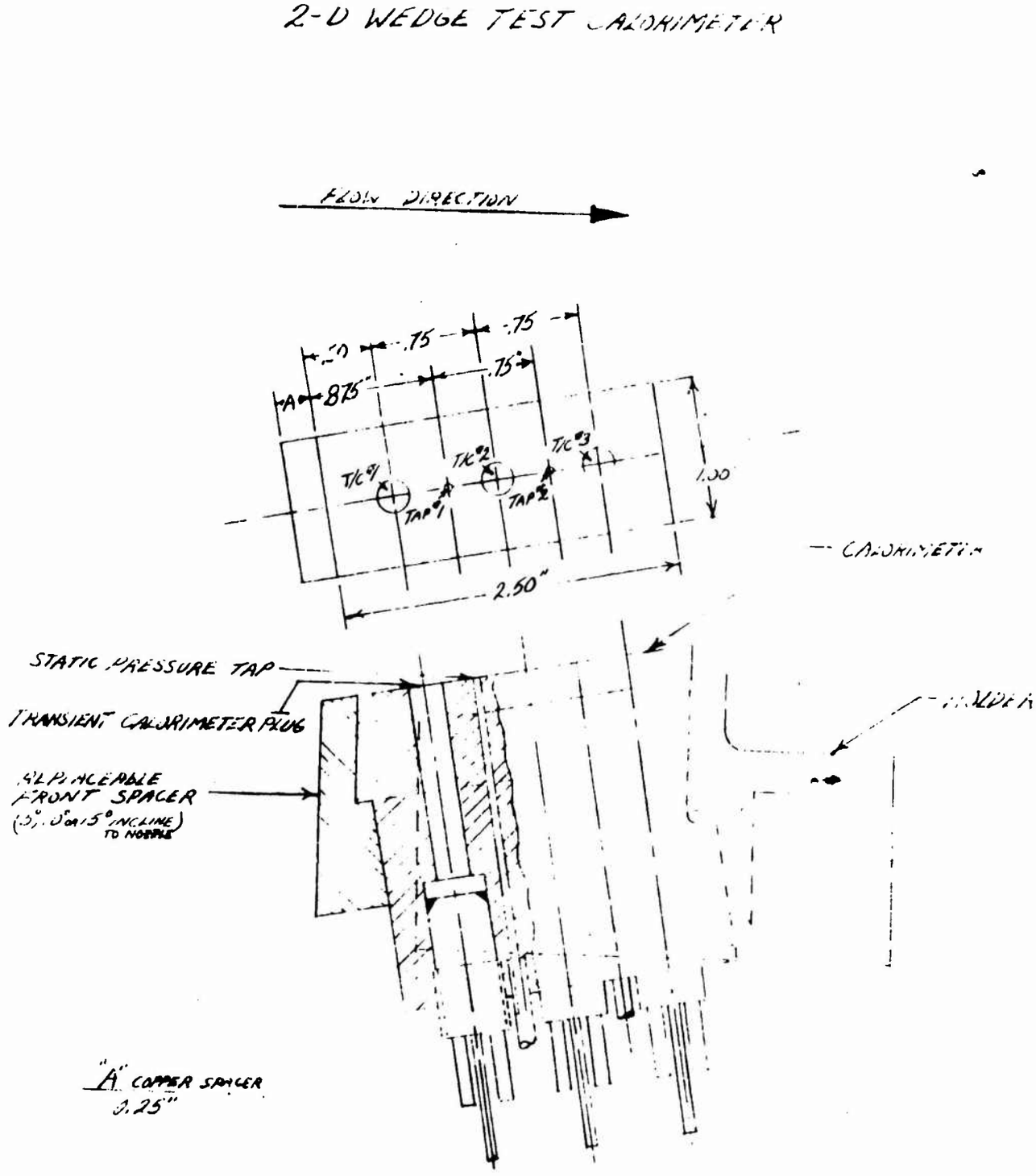

FIGURE 6 2D WEDGE TEST CALORIMETER

FIGURE 7 2D WEDGE CALORIMETER ASSEMBLED TO 10 MW ARC EXIT NOZZLE

The cold wall heat flux distribution on the Avco model (Table I) was obtained by means of three Avco null point transient calorimeters (Reference 6) from which pseudo surface temperature response data was obtained. These data were then reduced to cold wall values using a one-dimensional heat conduction program (Reference 7) using temperature variable material (OFHC copper) properties. Arc operating parameters for each calorimeter experiment are included in Table I. Heat flux data were obtained for inclination angles of 10 and 15 degrees. As is evident from the data presented in Table I, weak flow disturbances appear to be present on some of the calorimeter bodies. The disturbances are primarily the result of weak shock waves (generated in the exhaust nozzle) impinging on the body.

In addition to the heat flux measurements, surface static pressure measurements were also taken using the Avco calorimeter model (Figure 6) and are reported in Table I.

2. Material Test Results

A series of four (4) specimen tests were conducted using the turbulent (two-dimensional flow) wedge configuration, illustrated in Figure 7. Data gathered in this test sequence are presented in Tables II and III. Illustrated in Figures 8 to 13 are the transient data recorded to measure, respectively internal material temperature, true surface temperature (assuming a spectral emittance) and surface radiation. Copies of the digital and graphical plots of the internal material temperature data have been submitted to Philco-Ford Corporation for study and retention. Figures 14 to 17 present the surface recession data obtained from a Nikon 35 mm variable frame rate camera used to obtain profile films of the specimen surface. Through the use of a split filter technique it is possible to obtain a clear image of the heated specimen surface and a reference surface on the sample holder. The film is reduced

TABLE I

CALIBRATION TEST RESULTS

RUN NO.	WEDGE INCLINATION ANGLE	TOTAL ENTHALPY		PLENUM PRESSURE ATMS	AIR FLOW RATE LB/SEC	CALIBRATION OF TEST ENVIRONMENT					
						DISTANCE FROM LEADING EDGE, INCHES					
						PRESSURE, ATMS		HEAT FLUX, BTU/FT^2-SEC			
		H/RT_o	BTU/LB			1.125	1.875	0.75	1.50	2.25	AVG.
9121	10°	238	8060	7.71	0.330	1.30	0.96	1221	976	855	1017
9125	15°	118	4000	20.75	0.691	2.10	1.55	914	800	836	850

TABLE II

ARC PARAMETERS AND TEST ENVIRONMENT

RUN NO.	SAMPLE NO.	GAS ENTHALPY		TEST TIME SEC.	HEAT FLUX $\dot{q}_{cw}$ ~BTU/FT^2-SEC	SHEAR STRESS LB/FT^2	GAS MASS FLOW LB/SEC	PLENUM PRESSURE ATM	POWER TO THE AIR MW	NOZZLE THROAT SIZE INCH	NOZZLE MACH NO.
		H/RT_o	BTU/LB								
9116	AS-1	118	4000	10.06	850	58	0.697	20.98	2.94	0.464 x 1.0	2.50
9117	AS-2	118	4000	10.03	850	58	0.697	20.93	2.94	0.464 x 1.0	2.50
9122	AS-3	245	8300	10.00	1050	40	0.330	7.77	2.89	0.8 x 1.0	2.00
9123	AS-4	245	8300	9.98	1050	40	0.330	7.77	2.89	0.8 x 1.0	2.00

TABLE III

ABLATIVE PERFORMANCE

RUN NO.	SAMPLE NO.	SAMPLE DESCRPTION	WEIGHT GRAMS			THICKNESS* INCHES			PEAK** TEMPERATURE °R		ASSUMED SPECTRAL EMITTANCE	TOTAL EMITTANCE	RADIANT HEAT FLUX	RECESSION RATE
			PRE	POST	LOSS	PRE	POST	LOSS	T_b	T_T	$\lambda = 0.8\mu$		$\dot{q}_{cw}$ ~BTU/FT^2-SEC	S ~IN/SEC
9116	AS-1	Quartz fiber	103.4	100.9	2.5	0.873	0.730	0.143	4290	4730	0.50	0.31	73	0.01477
9117	AS-2	Quartz fiber	106.8	104.5	2.3	0.868	0.800	0.068	4110	4510	0.50	0.35	68	0.01127
9122	AS-3	Quartz fiber	104.8	98.0	6.8	0.871	0.716	0.155	4440	4910	0.50	0.31	87	0.01549
9123	AS-4	Quartz fiber	106.5	99.2	7.3	0.874	0.740	0.134	4420	4890	0.50	0.33	90	0.01488

* Measurement taken 1½" from leading edge along specimen centerline.

** Pyrometer focussed 1½" from leading edge on centerline viewing a spot diameter of 0.12 inch.

FIGURE 8 RECORDED INTERNAL TEMPERATURE DATA - TEST SAMPLE AS-1

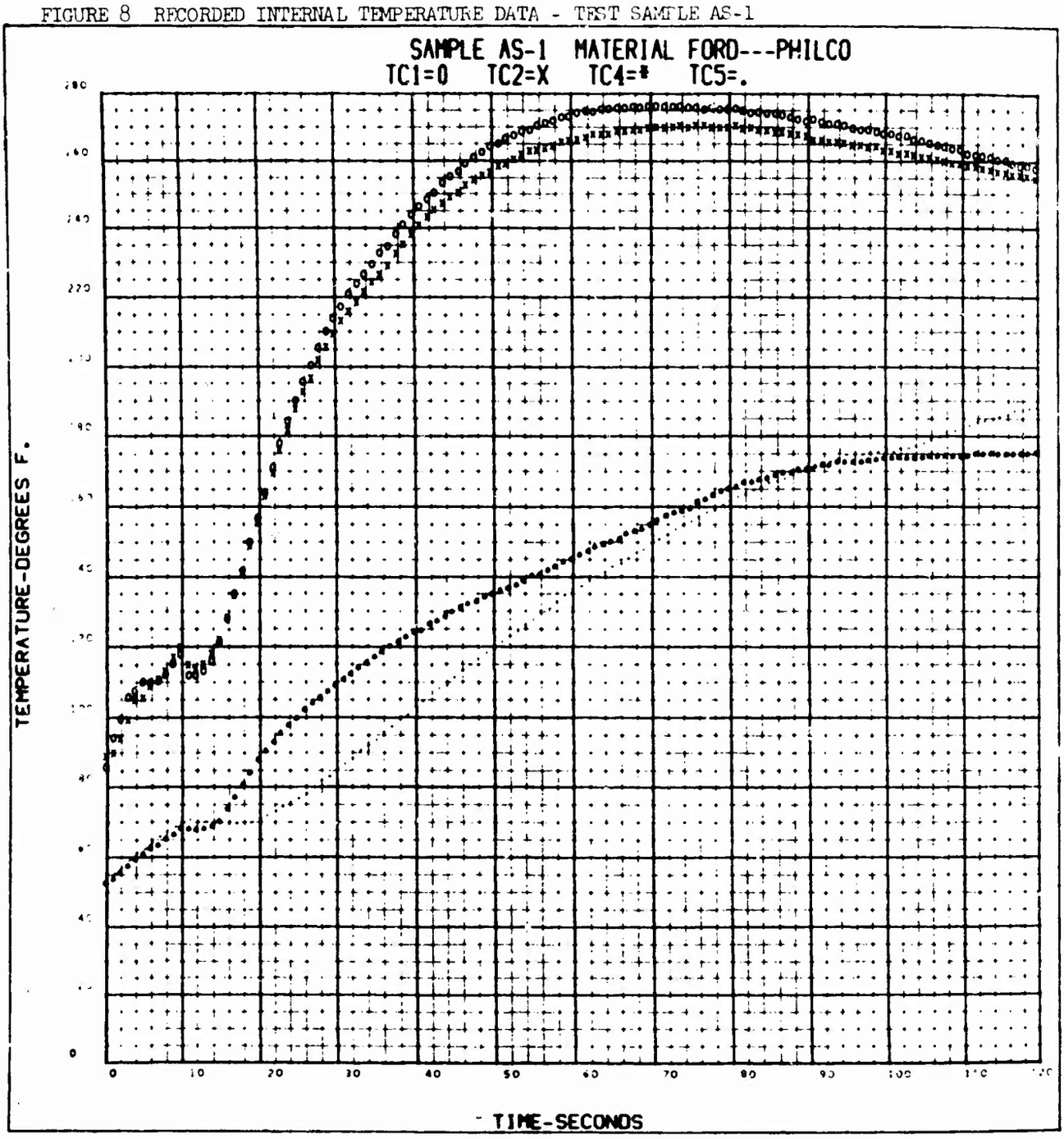

FIGURE 9 RECORDED INTERNAL TEMPERATURE DATA - TEST SAMPLE AS-2

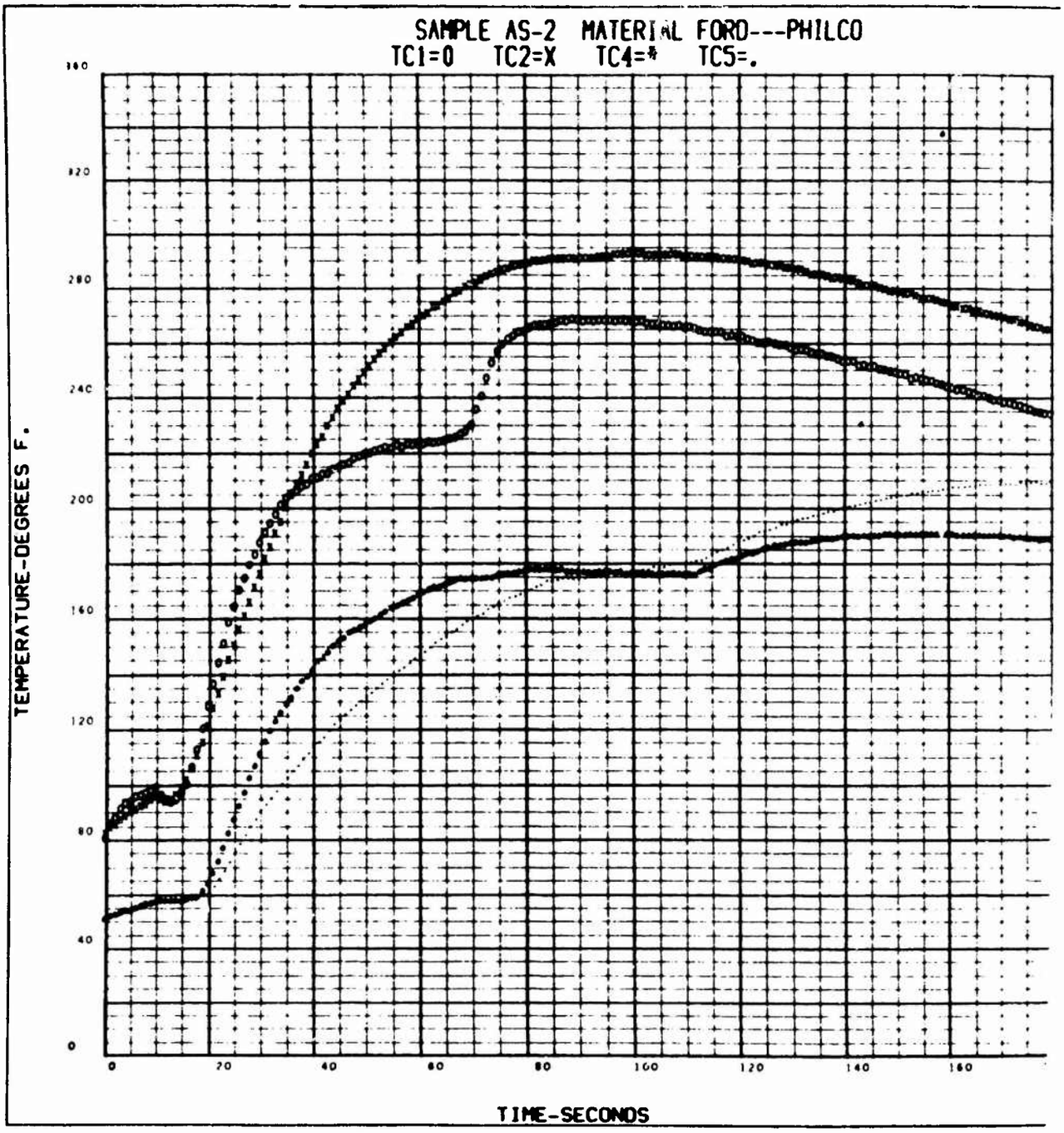

FIGURE 10 RECORDED INTERNAL TEMPERATURE DATA - TEST SAMPLE AS-3

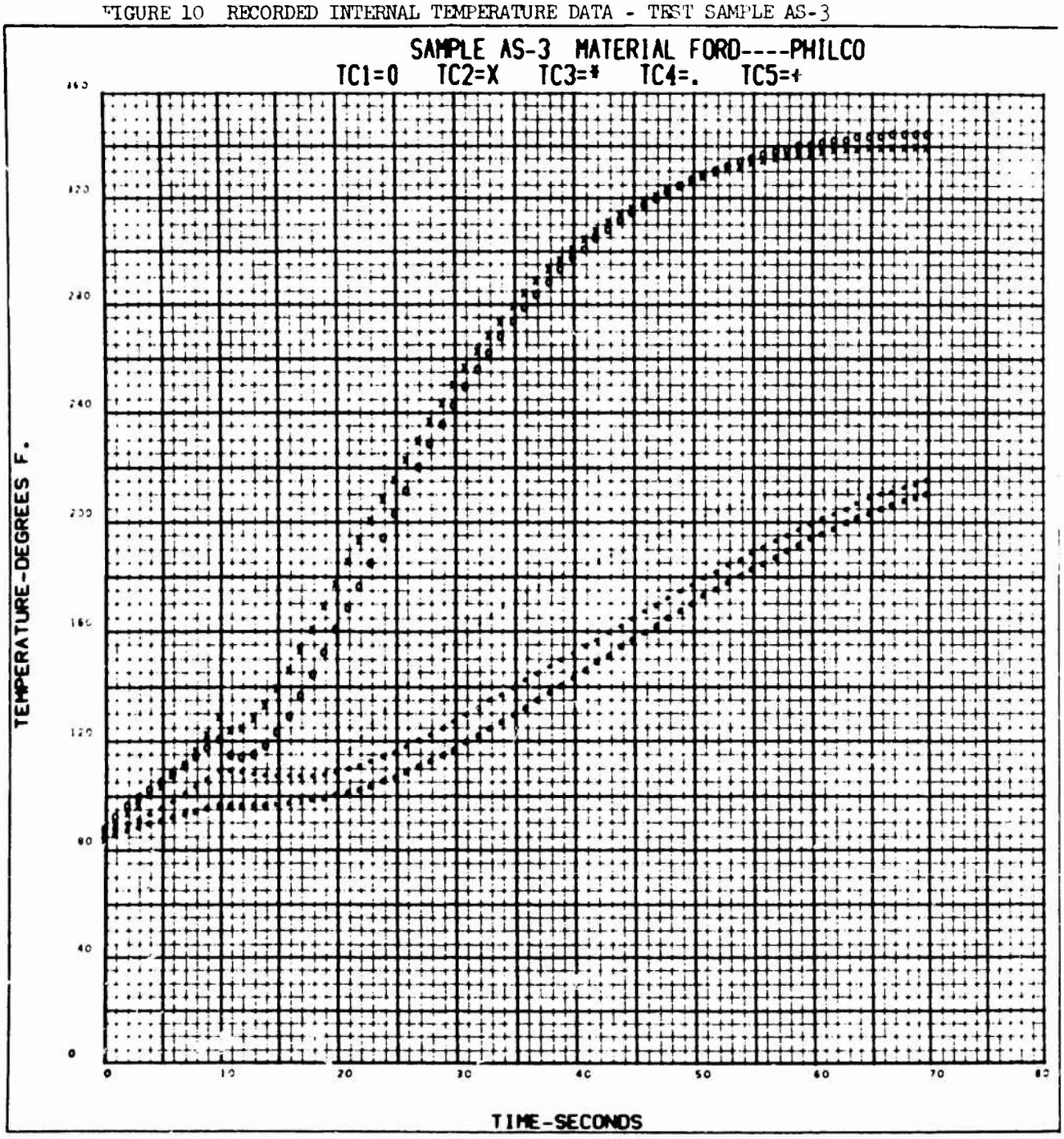

FIGURE 11 RECORDED INTERNAL TEMPERATURE DATA - TEST SAMPLE AS-4

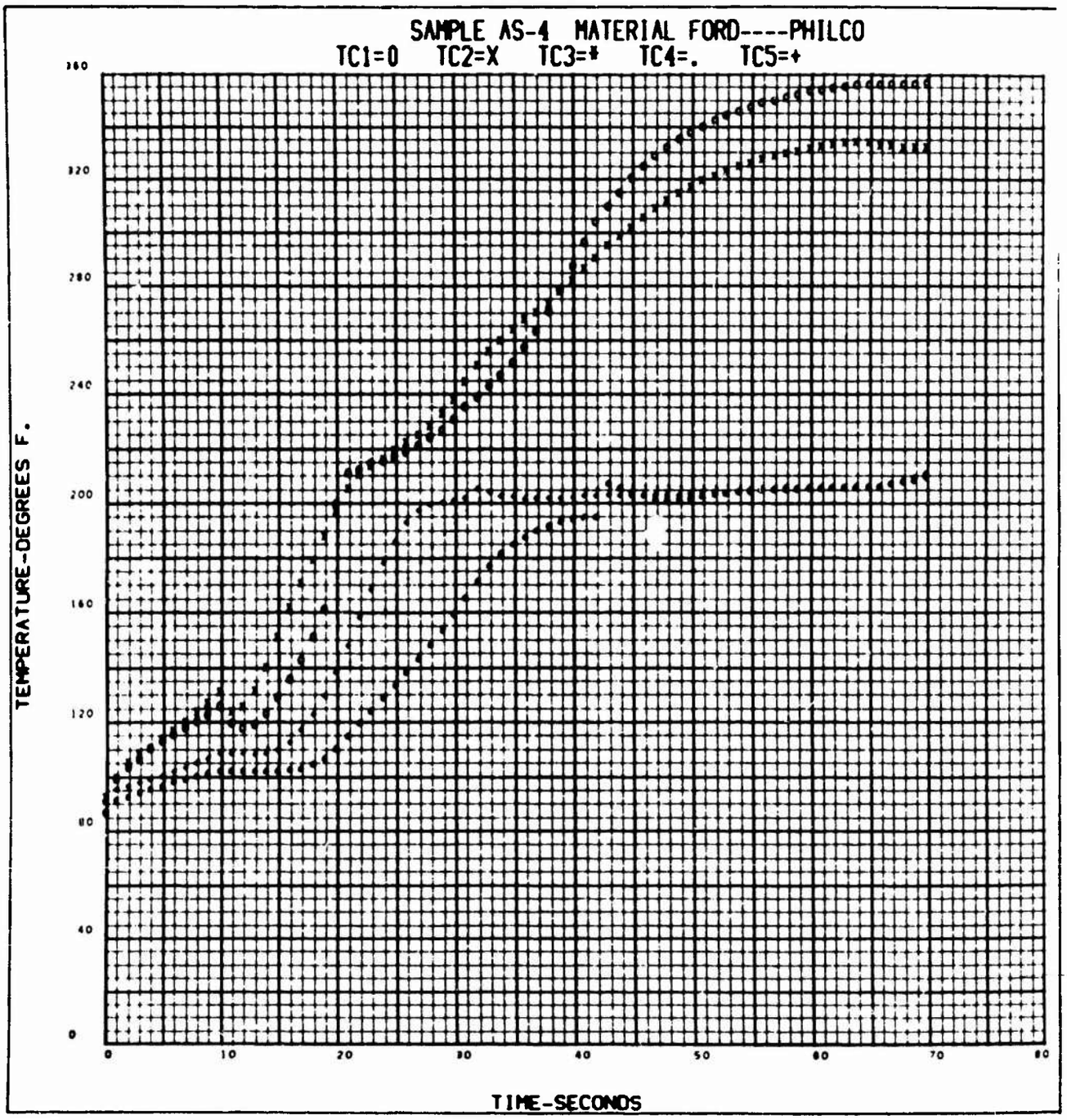

FIGURE 12
TRUE SURFACE TEMPERATURE

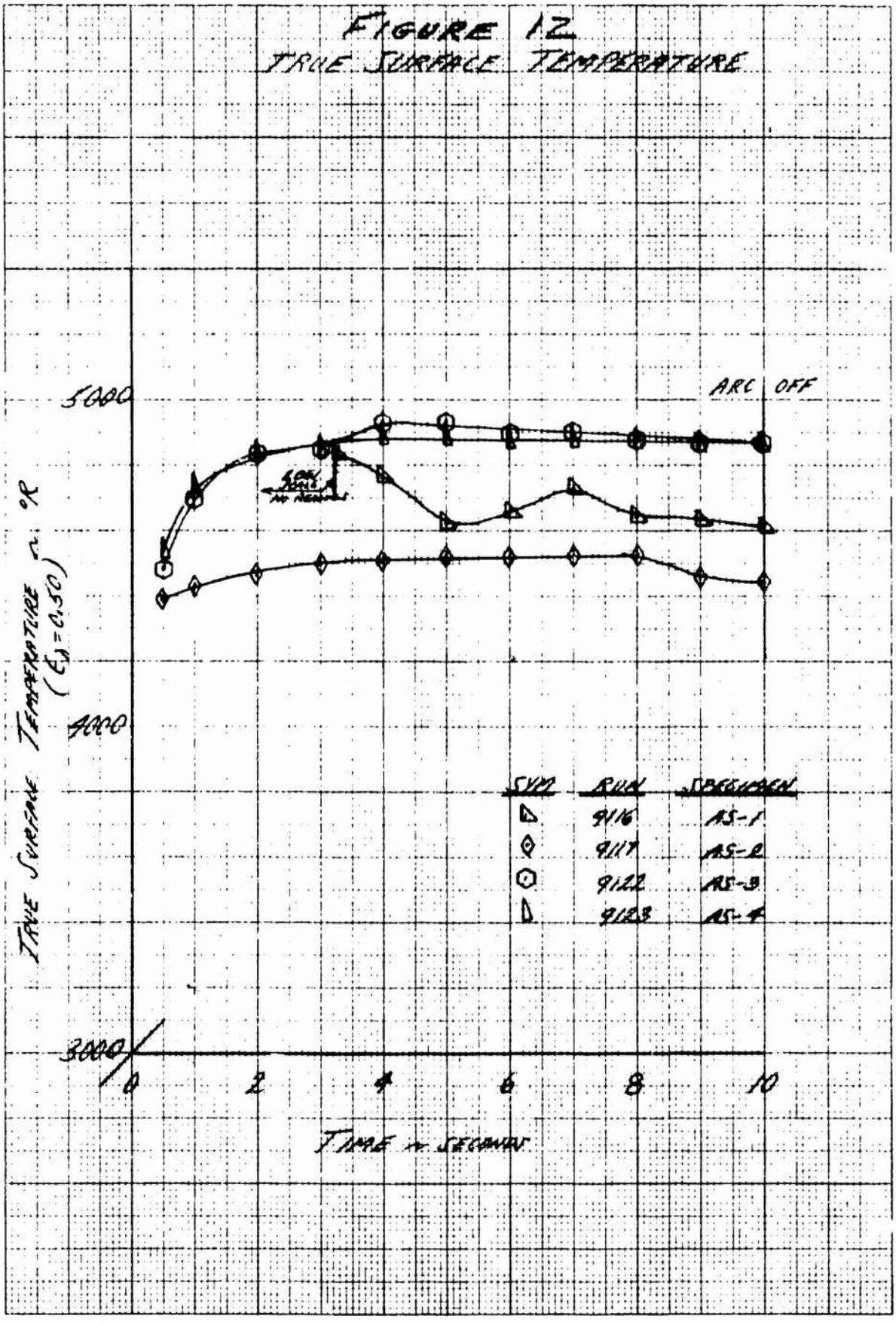

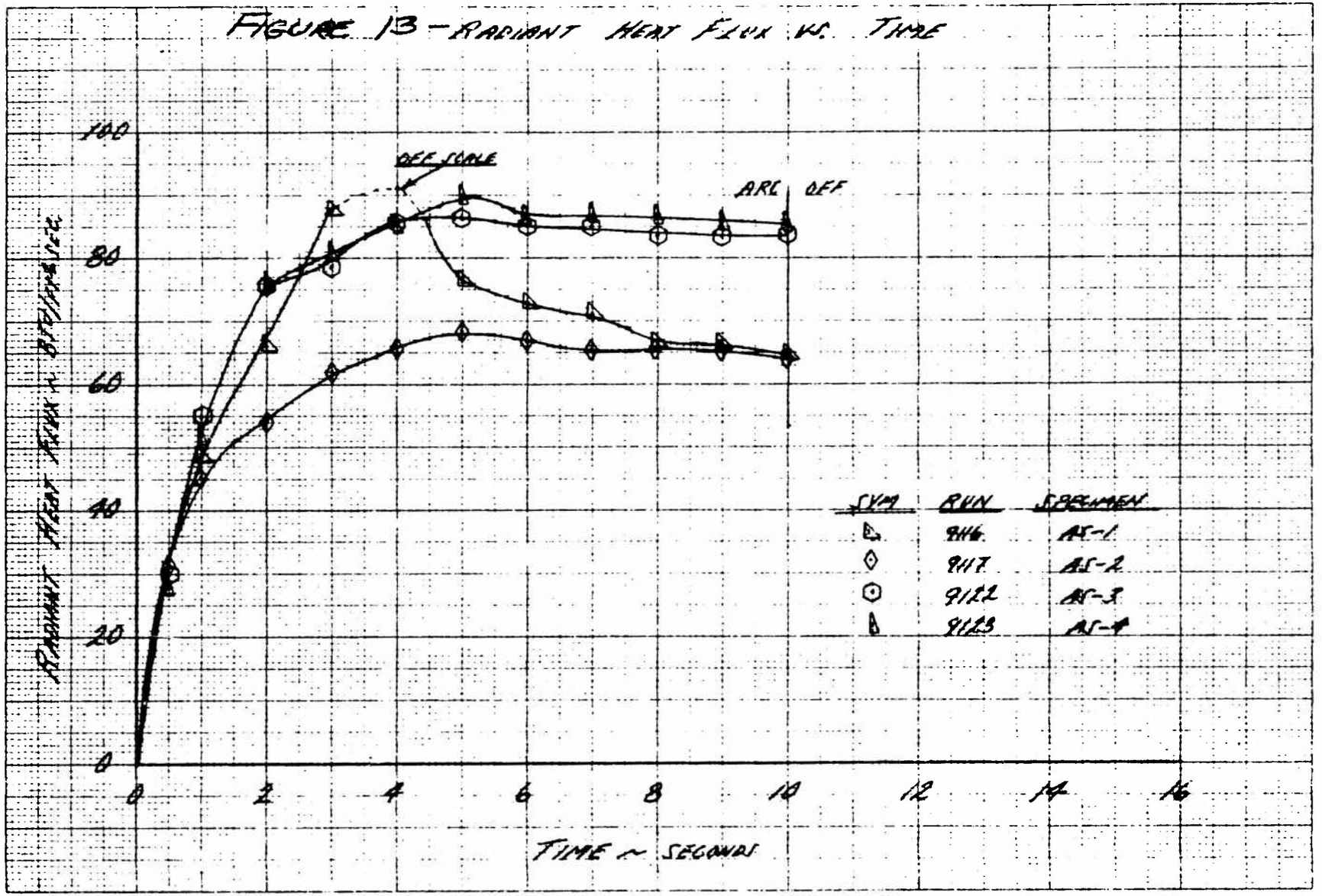
FIGURE 13 - RADIANT HEAT FLUX VS. TIME
RADIANT HEAT FLUX - BTU/ft²-sec
100
80
60
40
20
0
OFF SCALE
ARC OFF
0
2
4
6
8
10
12
14
16
TIME - SECONDS
SYM
RUN
SPECIMEN
9116
AS-1
9117
AS-2
9122
AS-3
9123
AS-4

using a Telecomputing Corporation film reader by placing the hairline along the surface of the downstream specimen half. Readings so obtained are entered into a special program to obtain a least mean squares fit recession rate as shown in Figures 14 to 17.

Figures 18 to 21 present the post test photographs taken of each specimen. In all cases the samples ablated relatively smoothly.

FIGURE 14 SURFACE RECESSION DATA - TEST SPECIMEN AS-1

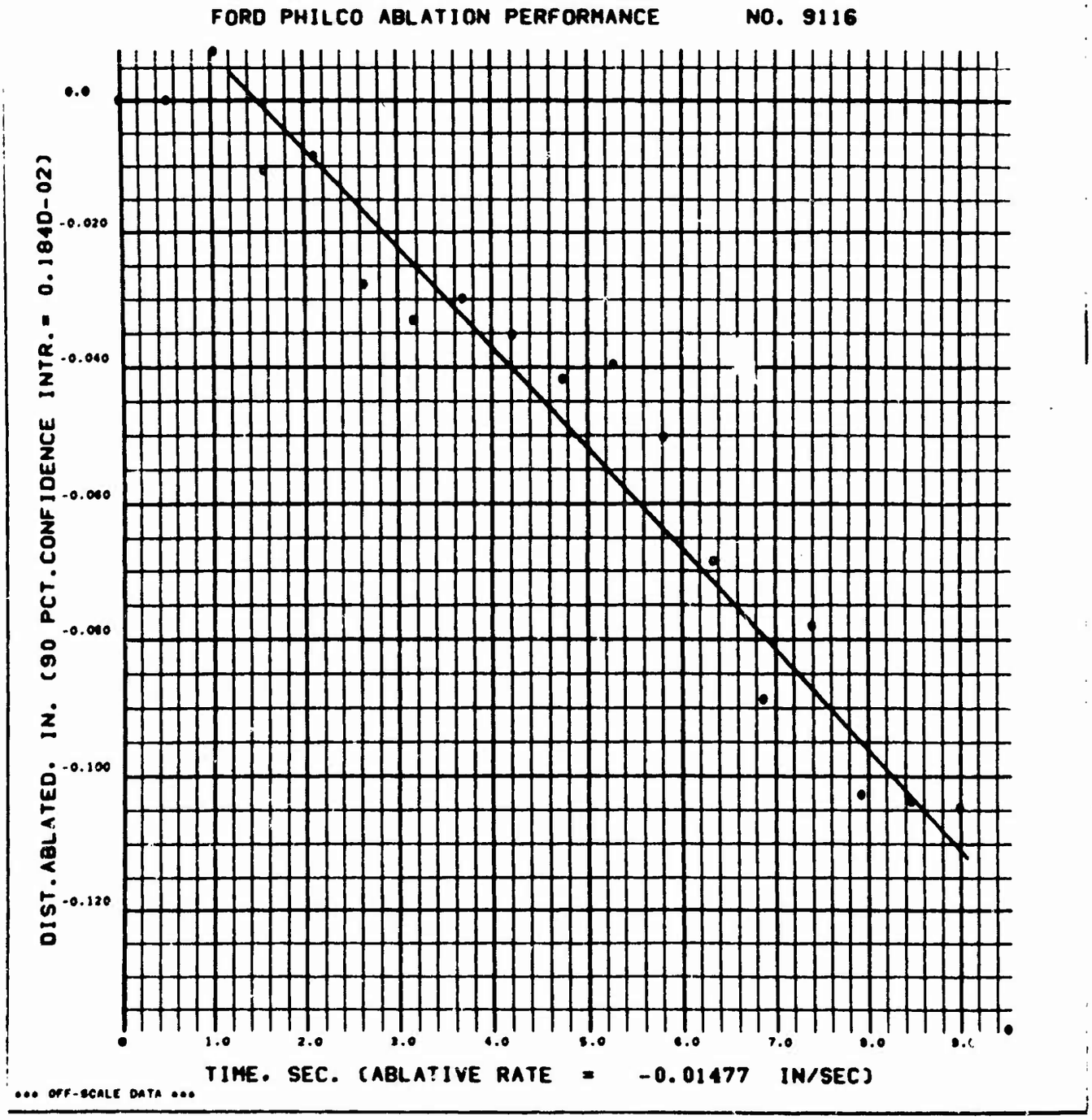

FIGURE 15 SURFACE RECESSION DATA - TEST SPECIMEN AS-2

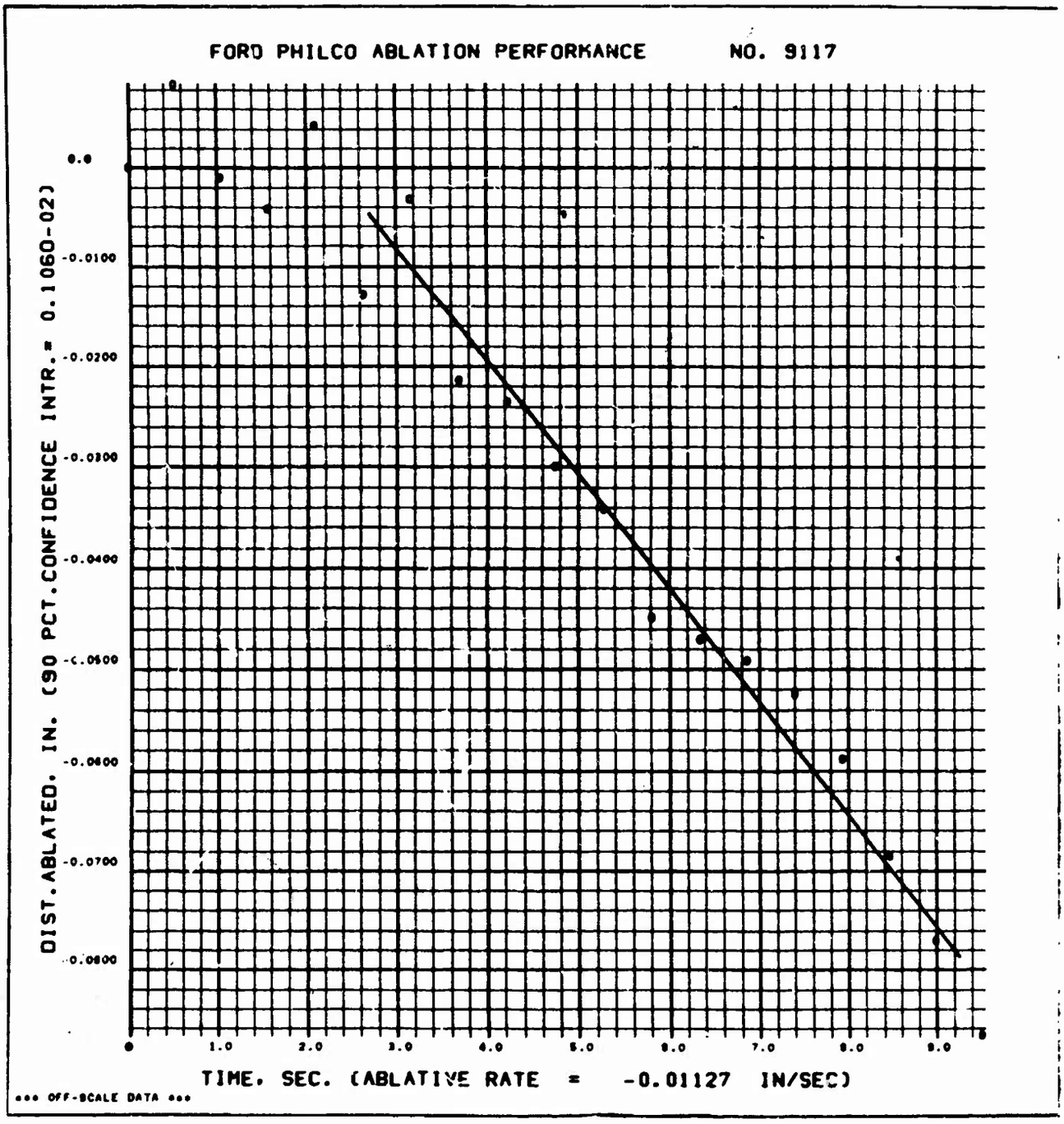

FIGURE 16 SURFACE RECESSION DATA - TEST SPECIMEN AS-3

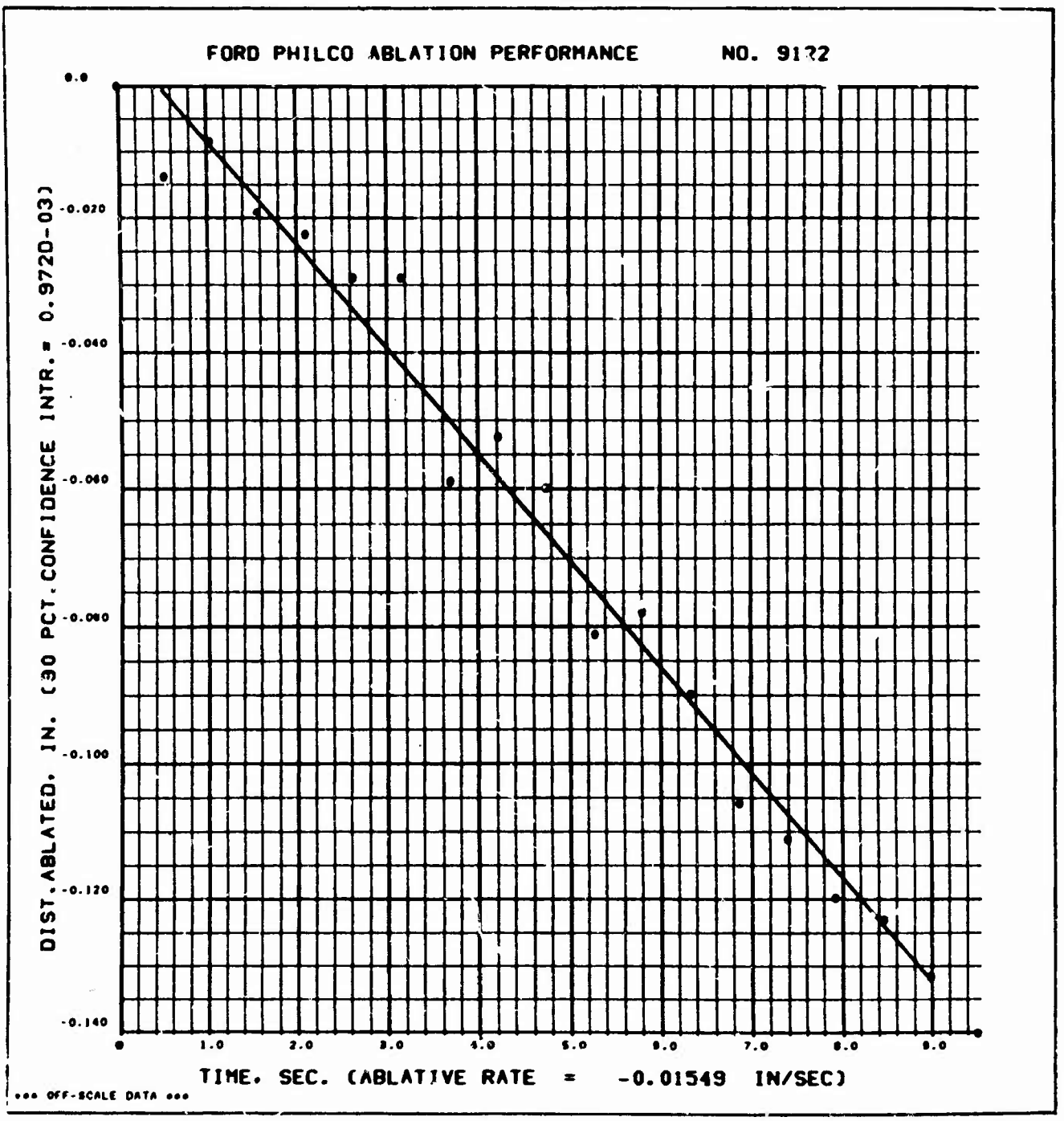

FIGURE 17 SURFACE RECESSION DATA - TEST SPECIMEN AS-4

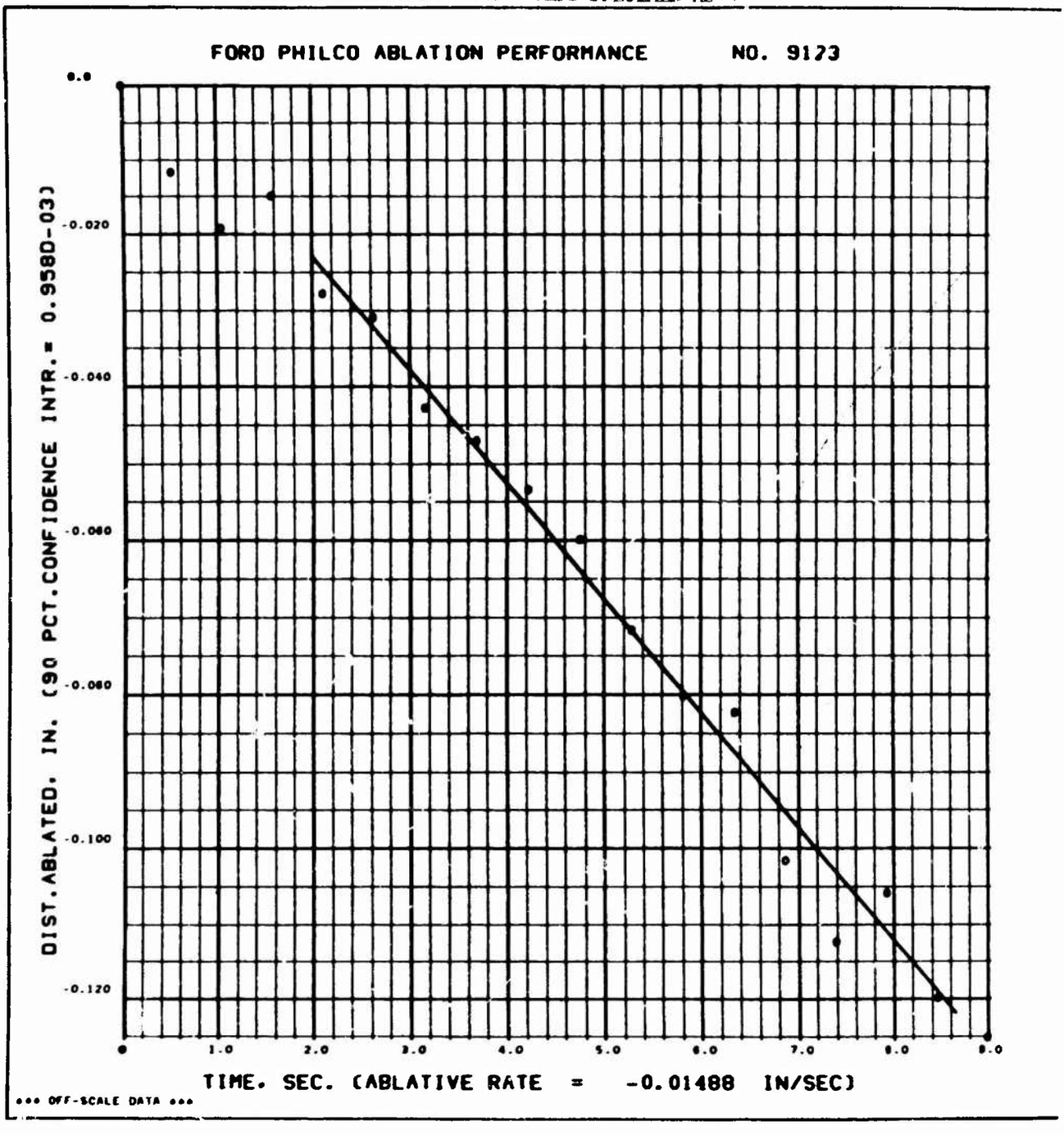

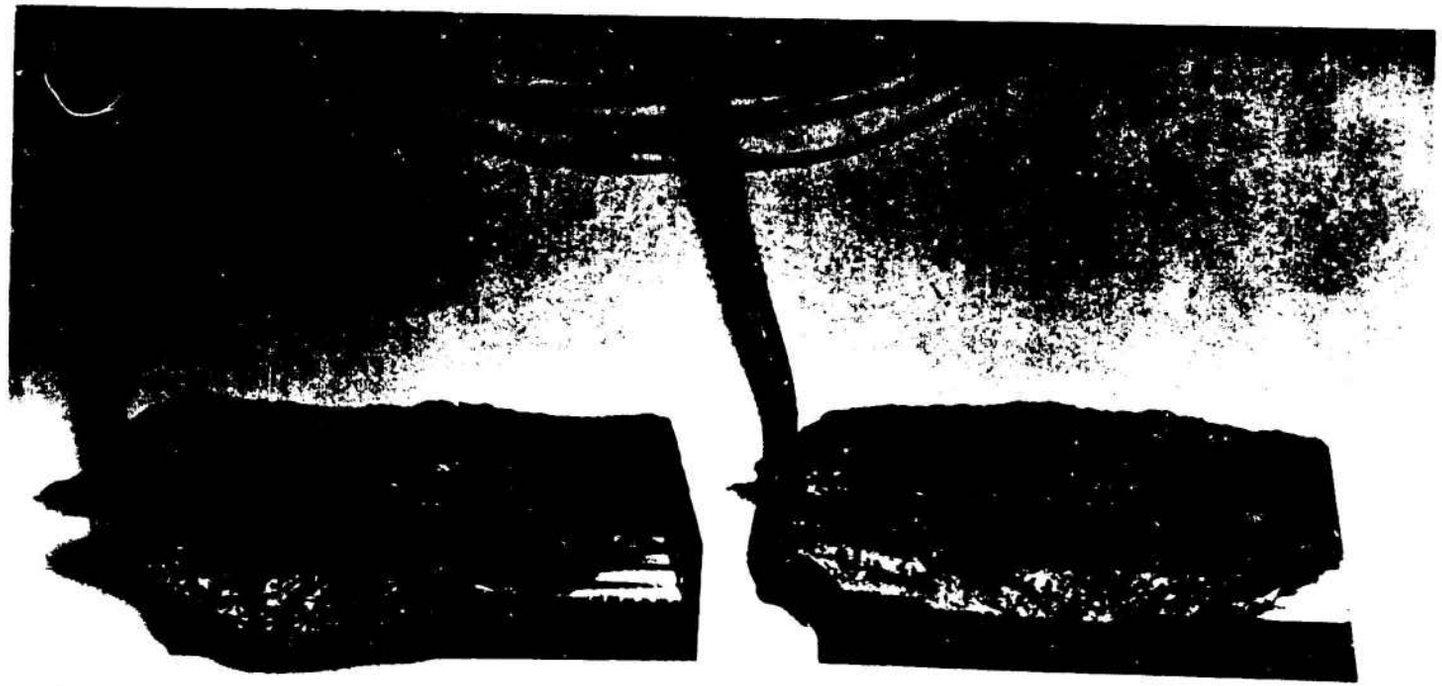

FIGURE 18 POST TEST VIEW OF TESTED SPECIMENS AS-1 AND AS-2

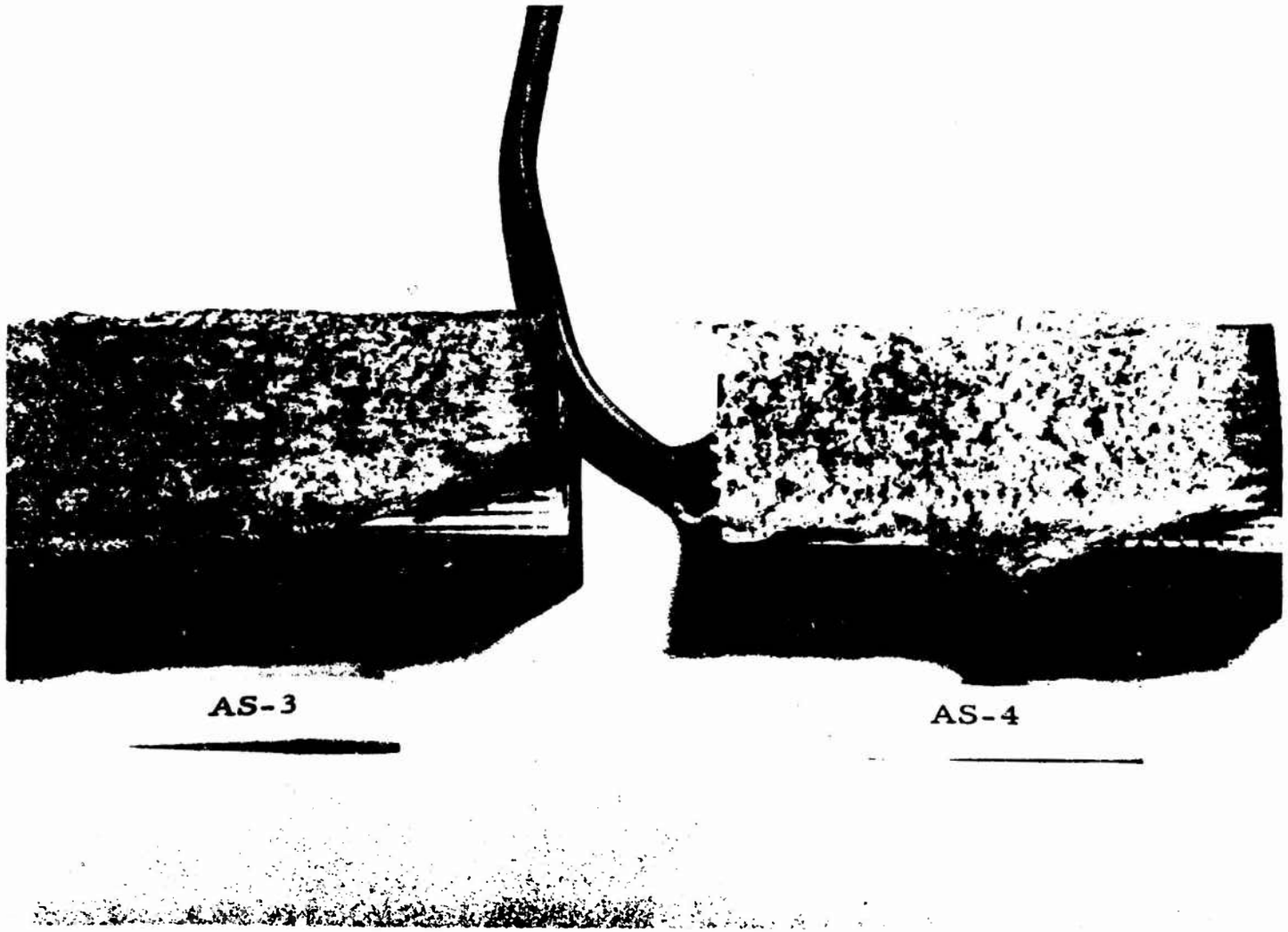

FIGURE 19 POST TEST VIEW OF TESTED SPECIMENS AS-3 AND AS-4

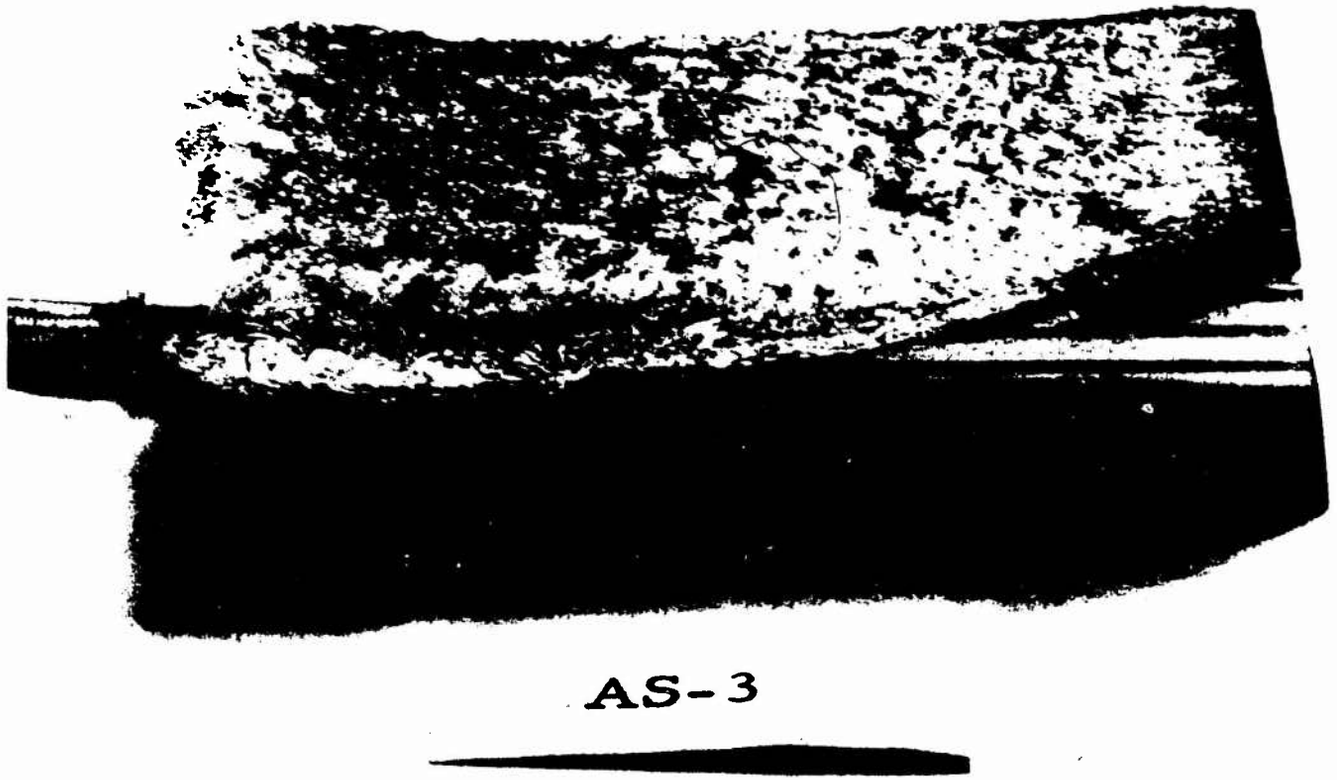

FIGURE 20 POST TEST CLOSE-UP VIEW OF TEST SPECIMEN AS-3

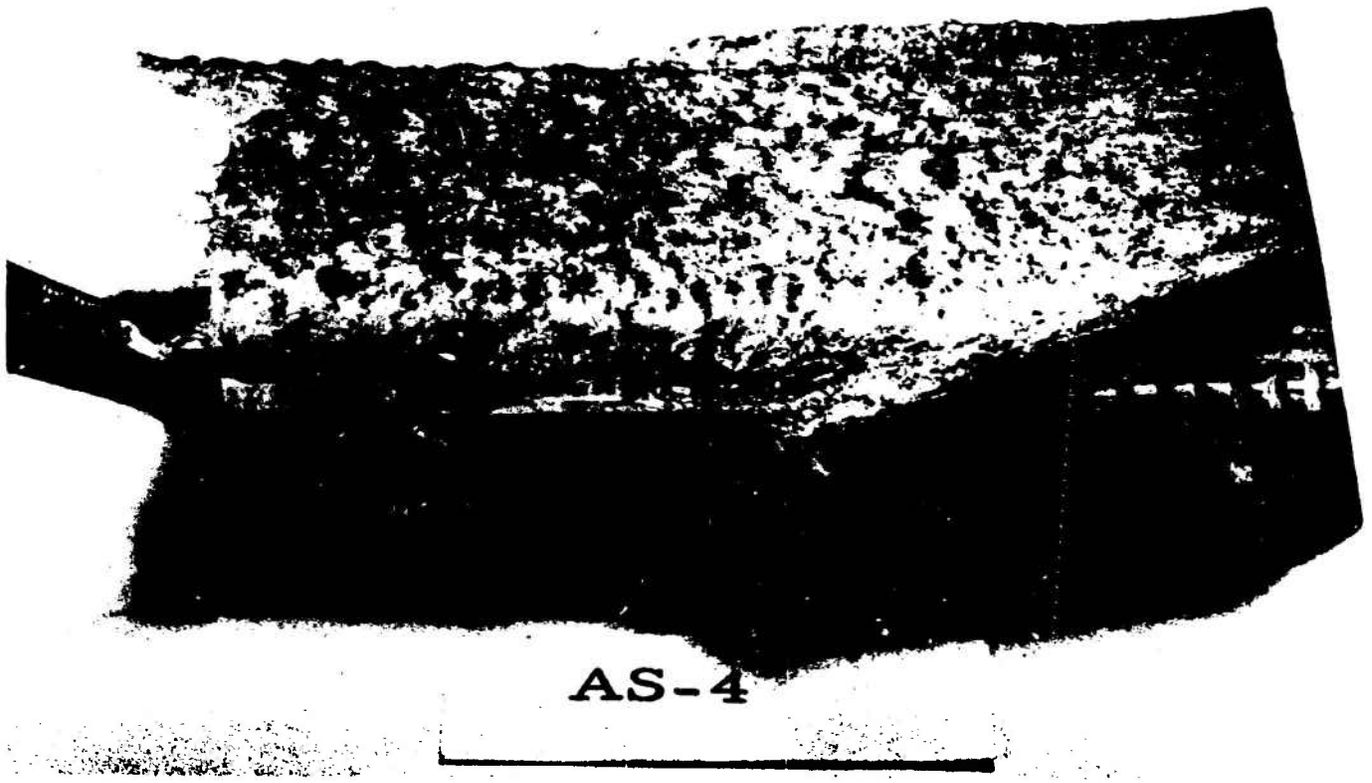

FIGURE 21 POST TEST CLOSE-UP VIEW OF TEST SPECIMEN AS-4

REFERENCES

1. "Avco Hyperthermal Simulation Capabilities", Avco Systems Division, AVSD-0006-70-CA, 15 January 1970.
2. Puckett, A. E., "Supersonic Nozzle Design", Journal of Applied Mechanics, December 1946.
3. Winovich, W., "On the Equilibrium Sonic-Flow Method for Evaluating Electric-Arc Air Heater Performance", NASA TND-2132, March 1964.
4. Cilmi, P. et al., "Ablation Test Results on Materials Evaluated in the Avco 10 MW Arc Facility for Sandia Corporation", Avco Report R720-67-96, 14 August 1967.
5. Vincenti, W. G. and C. J. Kruger, Jr., "Introduction to Physical Gas Dynamics", John Wiley, New York, 1965, p. 185.
6. O'Connor, T. J. and J. V. Morgida, "Null Point Transient Calorimeters, Theoretical Concepts and Theoretical Results", ISA Preprint No. 16.5-2-66, October 1966.
7. Beck J. V. and H. Wolfe, "Digital Program to Calculate Surface Heat Fluxes from Internal Temperatures in Heat Conducting Bodies", AVCO/RAD-TR-62-27, August 1962.

DYNATECH

Report on

THE THERMAL CONDUCTIVITY AND SPECIFIC HEAT OF AS-3D QUARTZ

For: Philco-Ford Corporation
Aeronutronic Division
Newport Beach, California 92663

I. DETAILS OF SAMPLES

The material supplied for evaluation over the temperature range 100 to 1100C was stated to be AS-3D quartz, a silica impregnated quartz fiber material having a composition of 99.8 SiO_2, 0.1% heavy metallic oxides and 200 ppm alkali.

The thermal conductivity sample was in the form of a cylinder 25.4 mm diameter and 25.4 mm long having a small hole 2 mm diameter drilled to the centre approximately 3 mm from each flat surface. It had a density of 1500 Kg m^{-3}. The specific heat sample was in the form of a slab 63 mm square and 12.7 mm thick with a hole 3 mm diameter drilled at the corners of the central 38 mm square. It had a density of 1554 Kg m^{-3}.

II. TEST PROCEDURES

(a) Thermal Conductivity

For the purposes of the test fine gauge thermocouples were insulated with twin bore protective tubing and cemented tightly into the holes in the sample. The sample was placed between two similar samples of known thermal conductivity with the same type of thermocouple instrumentation. To minimize contact resistance between each surface a thin layer of palladium foil was placed between them. The composite specimen was placed between the plates of an upper heater and a lower heat sink and a reproducible load was applied to the top of the complete system. A guard tube which could be heated in several positions along its length was placed around the system and the whole of the interspace and surrounds filled with a good heat insulating powder. By means of suitable adjustments to the power in the various heaters and of the cold sink temperature, a steady

distribution was maintained in the system and undue radial heat loss prevented by keeping the guard tube temperature gradient matched closely to that of the sample. At equilibrium conditions the temperatures at various points on the sample and guard were evaluated from thermocouple readings and the heat flow in the specimen derived in terms of that flowing through each reference sample.

The thermal conductivity was calculated from a knowledge of the mean energy, the temperature difference across the sample and the known dimensions. Measurements were made at regular temperature intervals between 100C and as close as possible to 1100C. Near the end of the equilibrium period of the test at the highest temperature one of the heater windings on the guard failed and it was not possible to obtain a reliable repeat point on cooling after attaining the highest temperature. However, at the end of the test the sample was examined and no change in appearance or significant change of weight was noted.

(b) Heat Capacity

For the purpose of the test, the sample was weighed and then tightly enclosed in a polished electrically heated container which was suspended inside a massive nickel plated and polished copper adiabatic cylindrical jacket mounted inside a further heavily insulated jacket. The whole assembly was evacuated and then cooled to a uniform temperature somewhat below the lowest mean temperature at which data was required. At steady conditions a controlled rate continuous power input was supplied to the heater on the sample container. By utilizing the output of a multi-junction differential thermopile the power to the jacket heater was automatically controlled so that the temperature of the jacket was equal to that of the sample thus allowing negligible heat transfer from the sample to its surroundings. From observations of the power input to the heater and a continuous record of sample temperature variation with time, a record of the sample and container enthalpy change with temperature was obtained.

The specific heat of the test sample was derived from a knowledge of its weight together with the above record of the total enthalpy change with temperature and a similar one for the sample container alone.

Following the thermal conductivity tests the 25 mm diameter sample was fitted with a thermocouple and then suspended by a thin wire inside the central uniform zone of a vertical furnace maintained at a steady temperature. Below the furnace opening was a large copper receiving vessel which contained a multi-junction thermopile and the whole was well insulated inside a massive water jacket. Radiation screens between the furnace and receiver insured that the receiver did not receive any radiant heat from the furnace.

A period of at least one hour was allowed for the sample to stabilize at a particular temperature. During this time the temperature of the sample was monitored regularly. In addition any small temperature rise in the receiver was noted during the stabilization period by taking regular readings of the output of the multi-junction thermopile. When time equilibrium conditions had been attained the thermocouple in the sample was released and the sample dropped quickly and carefully into the large calibrated copper receiver. Successive reading of the temperature of the receiver were then taken at rapid intervals until the maximum temperature had been reached and the resultant cooling curve well defined. The measurement was repeated at least once to ensure reproducibility.

The specific heat of the material was calculated from the enthalpy change derived from the rise in temperature of the receiver and the mass of the sample.

Measurements were made at successive increasing temperature intervals between approximately 300 and 1050C. From the results of these measurements an enthalpy versus drop temperature curve was obtained and this was combined with one obtained from the adiabatic calorimeter measurements. By differentiating the resultant curve the specific heat was derived between 300 and 1100C.

III. RESULTS

The results obtained for the particular samples tested are given in Table I, and II for the thermal conductivity and heat capacity respectively. The density of the thermal conductivity sample had fallen to 1445 Kg m^{-3} at the conclusion of all tests.

DYNATECH

TABLE I

Thermal Conductivity of a Sample of AS-3D Quartz

Mean Temperature, C	Thermal Conductivity W m^{-1} deg^{-1}
100	0.7
200	0.76
300	0.83
400	0.91
500	0.99
600	1.1
700	1.22
800	1.38
900	1.60
1000	1.75
1100	1.95

Reference: PFD-4

Date: June 16, 1970

DYNATECH

TABLE II

Specific Heat of AS-3D Quartz

Mean Temperature, C	Specific Heat J Kg^{-1} deg K^{-1}
50	690
100	770
200	890
300	960
400	1005
500	1055
600	1090
700	1120
800	1145
900	1180
1000	1205
1100	1225

Reference: PFD-4

Date: June 16, 1970

APPENDIX VI

MIT-LABORATORY FOR INSULATION RESEARCH AS-3DC LETTER REPORT

MASSACHUSETTS INSTITUTE OF TECHNOLOGY

LABORATORY FOR INSULATION RESEARCH

PROFESSOR A. R. VON HIPPEL, *Director* CAMBRIDGE, MASSACHUSETTS 02139

June 26, 1970

Mr. T. M. Place
Supervisor, Ceramics
Advanced Development Operation
Philco
Ford Road
Newport Beach, Calif. 92663

Dear Mr. Place:

The attached tabulation lists our measurements on samples mentioned in your letter of June 5. The data on the disk samples are not completely independent of the speed measurements and room humidity.

Yours truly,

W. B. Westphal

W. B. Westphal

cc: Dr. H. Tanner
Air Force Materials Lab. (MAYE)

Sample 1-XB-O-M

Density 1.653 g/cm^3

8.52 GHz	T°C	κ	tan δ
As received, Face 1 up	25	2.919	.0062
Face 2 up	25	2.956	.0064
After vacuum oven			
80°C, 10 days			
Face 2 up	25	2.938	.00162
Face 1 up	25	2.895	.00169
	115	2.89	.0012
	246	2.89	.0006
	357	2.90	.0005
	438		.0006
	535		.0008
	608		.0010
	710		.0014
	805		.0020
	908		.0026
	972		.0028
	1000		.0031*
	25	2.89	.00042

25°C		Hz				
Sample 1-VH-O-M-1		10^5	10^6	10^7	7.5×10^7	1.8×10^8
As received, density 1.536 g/cm^3	κ	2.779	2.777	2.777	2.775	2.772*
	10^4 tan δ	4.6	8.3	6.4	13.4	17*
After 18 hrs. vacuum oven 80°C	κ			2.77	2.77	2.77*
	10^4 tan δ			4.6	9.1	11.5*
Sample 1-VH-O-M-2						
As received	κ	2.722		2.720	2.72	2.72*
	10^4 tan δ	4.9		5.9	13.0	17*
After 18 hrs. vacuum oven 80°C	κ				2.72	2.72*
	10^4 tan δ				6.4	8.5*

* Extrapolated values.

838-593P
870-3749

PACIFIC SPECTROCHEMICAL LABORATORY, INC. AS-3DC LETTER REPORT

PACIFIC SPECTROCHEMICAL LABORATORY, INC.

CHEMICAL AND SPECTROGRAPHIC ANALYSIS

RESEARCH

2558 Overland Avenue

Los Angeles, California 90064

P.O. No. SVB27101
Shipper No. ARD-93798
Attn: T. M. Place RL/110

April 27, 1970

Report of semiquantitative spectrographic analysis, and HF distillation for determination of lower limits for alkali metals, of sample submitted by

Philco-Ford Corporation
Aeronutronic Division
Ford Road
Newport Beach, California 92663

	Silica Fiber AS-3DC-1
SiO_2-	Remainder
MgO-	0.0021%
Fe_2O_3-	0.0070
Al_2O_3-	0.0059
CuO-	0.00014
Ag_2O-	0.00031
CaO-	0.0020
Cr_2O_3-	0.0016
Strontium-	1.2 p.p.m.
Sodium-	not detected less than 5.0
Potassium-	not detected less than 5.0
Barium-	not detected less than 5.0
Lithium-	not detected less than 2.0

Respectfully submitted,

PACIFIC SPECTROCHEMICAL LABORATORY, INC.

838-5939
870-3749

PACIFIC SPECTROCHEMICAL LABORATORY, INC.

CHEMICAL AND SPECTROGRAPHIC ANALYSIS

RESEARCH

2558 Overland Avenue

Los Angeles, California 90064

P.O. No. SVB27101
Shipper No. ARD-94633
Attn: T. M. Place RL/110

May 12, 1970

Report of semiquantitative speccrographic analysis, and HF distillation for determination of lower limits for alkali metals, of samples submitted by

Philco-Ford Corporation
Aeronutronic Division
Ford Road
Newport Beach, California 92663

	Silica Fiber-AS-3DC-2 -	
	Side	End
SiO_2-	Remainder	---------
B_2O_3-	0.011%	0.048%
MgO-	0.0023	0.0045
Fe_2O_3-	0.0093	0.020
CuO-	0.00016	0.00014
Al_2O_3-	0.031	0.023
ZrO_2-	0.032	0.025
NiO-	0.00030	0.0010
CaO-	0.0020	0.0040
Cr_2O_3-	0.00050	0.0054
Sodium-	94. p.p.m.	330. p.p.m.
Strontium-	0.19	3.1
Barium-	not detected less than 3.0	54.
Lithium-	not detected less than 1.0	trace less than 2.0
Potassium-	not detected less than 4.0	not detected less than 8.0

Respectfully submitted,

PACIFIC SPECTROCHEMICAL LABORATORY, INC.

838-5939
870-3748

PACIFIC SPECTROCHEMICAL LABORATORY, INC.

CHEMICAL AND SPECTROGRAPHIC ANALYSIS

RESEARCH

2558 Overland Avenue

Los Angeles, California 90064

P.O. No. SVB27101
Shipper No. ARD-95070
Attn: T. M. Place RL/110

June 5, 1970

Report of semiquantitative spectrographic analysis, and HF distillation for determination of lower limits for alkali metals, of samples submitted by

Philco-Ford Corporation
Aeronutronic Division
Ford Road
Newport Beach, California 92663

	Silica Sample
	Trim 7-AS-3DC-1
SiO_2-	Remainder
MgO-	0.0012%
Fe_2O_3-	0.0086
Al_2O_3-	0.020
CuO-	0.00037
TiO_2-	0.0022
CaO-	0.0013
Sodium-	120. p.p.m.
Strontium-	1.8
Barium-	trace
	less than 2.0
Lithium-	not detected
	less than 0.50
Potassium-	not detected
	less than 2.0

Respectfully submitted,

PACIFIC SPECTROCHEMICAL LABORATORY, INC.

PACIFIC SPECTROCHEMICAL LABORATORY, INC.

CHEMICAL AND SPECTROGRAPHIC ANALYSIS

RESEARCH

2558 Overland Avenue

Los Angeles, California 90064

P.O. No. SVB27101
Shipper No. ARD-95103
Attn: R. M. Place RL/110

June 10, 1970

Report of semiquantitative spectrographic analysis, and HF distillation for determination of lower limits for alkali metals, of samples submitted by

Philco-Ford Corporation
Aeronutronic Division
Ford Road
Newport Beach, California 92663

Silica Fiber AS-3DC-3 -

	End sample	Center sample
SiO_2-	Remainder	----------
MgO-	0.0026%	0.0028%
Fe_2O_3-	0.019	0.017
Al_2O_3-	0.0064	0.010
CuO-	0.00023	0.00028
Ag_2O-	0.00011	0.00014
NiO-	0.0014	0.0015
CaO-	0.0022	0.0026
Cr_2O_3-	0.0021	0.0025
Sodium-	87. p.p.m.	50. p.p.m.
Barium-	trace	trace
	less than 2.0	------
Lithium-	trace	trace
	less than 0.50	-----
Potassium-	not detected	-------
	less than 2.0	------
Strontium-	0.65	0.37

Respectfully submitted,

PACIFIC SPECTROCHEMICAL LABORATORY, INC.

838-5939
870-3749

PACIFIC SPECTROCHEMICAL LABORATORY, INC.

CHEMICAL AND SPECTROGRAPHIC ANALYSIS
RESEARCH
2558 Overland Avenue
Los Angeles, California 90064

P.O. No. SVB27101
Shipper No. ARD-95160
Attn: T. M. Place RL/110

June 15, 1970

Report of semiquantitative spectrographic analysis, and HF distillation for determination of lower limits for alkali metals, of samples submitted by

Philco-Ford Corporation
Aeronutronic Division
Ford Road
Newport Beach, California 92663

Fused Silica Sample

Trim F-2 2 AF-0-F-1

SiO_2-	Remainder
MgO-	0.0021%
Fe_2O_3-	0.011
Al_2O_3-	0.013
CuO-	0.00016
TiO_2-	0.0027
ZrO_2-	0.0020
CaO-	0.0013
Cr_2O_3-	0.00057
Sodium-	58. p.p.m.
Barium-	3.0
Strontium-	0.36
Lithium-	not detected less than 0.50
Potassium-	not detected less than 2.0

Respectfully submitted,

Hal W. Johnson

PACIFIC SPECTROCHEMICAL LABORATORY, INC.

838-5939
870-3749

PACIFIC SPECTROCHEMICAL LABORATORY, INC.

CHEMICAL AND SPECTROGRAPHIC ANALYSIS
RESEARCH
2538 Overland Avenue
Los Angeles, California 90064

P.O. No. G66610
Shipper No. ARD-95263
Attn: T. M. Place RL/110

June 19, 1970

Report of semiquantitative spectrographic analysis, and HF distillation for determination of lower limits for alkali metals, of samples submitted by

Philco-Ford Corporation
Aeronutronic Division
Ford Road
Newport Beach, California 92663

Fused silica samples -

	Trim F-1-5	Trim F-2-2
SiO_2-	Remainder --------	
CaO-	0.0021%	0.0021%
ZrO_2-	0.0031	0.0019
TiO_2-	0.0020	0.0037
Ag_2O-	0.00036	0.000077
CuO-	0.00061	0.00033
Al_2O_3-	0.022	0.027
Fe_2O_3-	0.016	0.012
MgO-	0.0021	0.0014
Sodium-	91. p.p.m.	46. p.p.m.
Barium-	4.6	3.2
Strontium-	0.78	0.52
Lithium-	Not detected ------ less than 0.50 ----	
Potassium-	not detected ------ less than 2.0 -----	

Respectfully submitted,

PACIFIC SPECTROCHEMICAL LABORATORY, INC.

APPENDIX VIII

DRAWING WDL 20-B03880, 3D QUARTZ CONICAL BILLET

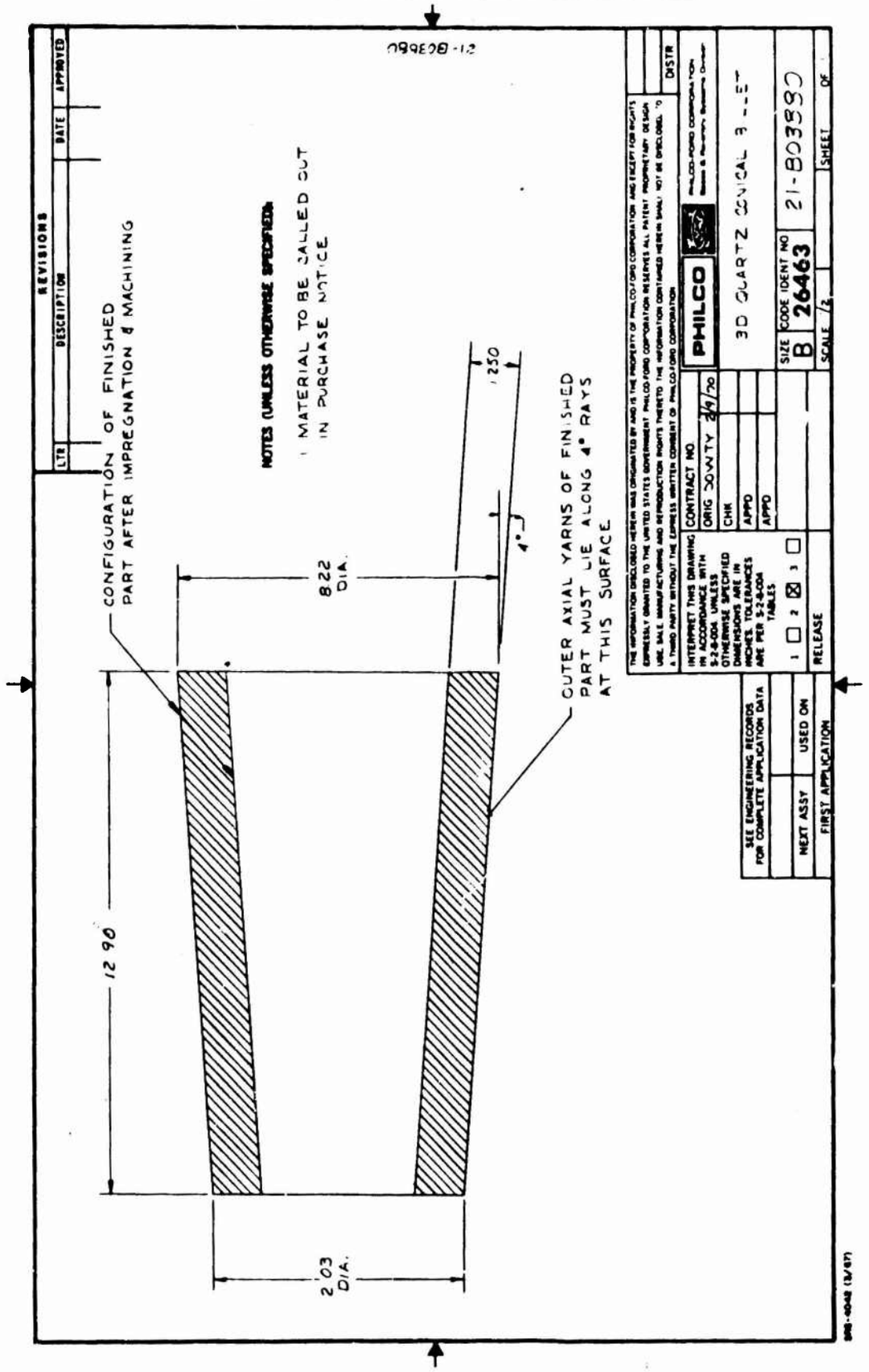

REFERENCES

1. Letter from Pacific Spectrochemical Laboratory, Inc., Los Angeles, California, to T. M. Place, Shipper No. ARD-93798, dated 27 April 1970.

2. Letter from Pacific Spectrochemical Laboratory, Inc., Los Angeles, California, to T. M. Place, Shipper No. ARD-94633, dated 12 May 1970.

3. Letter from Pacific Spectrochemical Laboratory, Inc., Los Angeles, California, to T. M. Place, Shipper No. ARD-95103, dated 10 June 1970.

4. Letter from Pacific Spectrochemical Laboratory, Inc., Los Angeles, California, to T. M. Place, Shipper No. ARD-95070, dated 5 June 1970.

5. Letter from Pacific Spectrochemical Laboratory, Inc., Los Angeles, California, to T. M. Place, Shipper No. ARD-95263, dated 19 June 1970.

6. Letter from Pacific Spectrochemical Laboratory, Inc., Los Angeles, California, to T. M. Place, Shipper No. ARD-95160, dated 15 June 1970.

7. Place, T. M. and Bridges, D. W., "Fabric Reinforced Silica Composites." Paper presented at the Pacific Coast Regional Meeting of the American Ceramic Society, Seattle, Wash., October 15-17, 1969.

8. Stetson, J. R., and Miyazawa, E. T., "Antenna Window Turbulent Q* Test Report," D. R. No. 6041, 3 October 1969.

9. Stetson, J. R., "1-D Quartz 'Rug' Antenna Window Turbulent-Wedge Ablation Test Analysis," D. R. No. 6056, 11 March 1970.

10. Linde, D. B., et al, "Final Report, Hardened Antenna Window Development Program," SAMSO-TR-70-241 , Philco-Ford Corporation (to be published).

11. "Re-Entry Antenna Windows," Philco-Ford Technical Report AFML-TR-70-78, 20 May 1970.

-172- intentionlly left blank

PRECEDING PAGE BLANK - NOT FILMED

UNCLASSIFIED

Security Classification

DOCUMENT CONTROL DATA - R&D

(Security classification of title, body of abstract and indexing annotation must be entered when the overall report is classified)

1 ORIGINATING ACTIVITY (Corporate author)
Philco-Ford Corporation
Western Development Laboratories Division
Ford Road, Newport Beach, California 92663

2a REPORT SECURITY CLASSIFICATION
UNCLASSIFIED

2b GROUP

3 REPORT TITLE
Re-entry System Environmental Protection (RESEP) Advanced 3D Fabrication Techniques, Final Technical Report

4 DESCRIPTIVE NOTES (Type of report and inclusive dates)
Technical Report - Final

5 AUTHOR(S) (Last name, first name, initial)
Hirasuna, A. R., Damoth, M. L., Harrington, N. M., Stetson, J. R.

6 REPORT DATE	7a TOTAL NO OF PAGES	7b NO OF REFS
August 1970	-186-	11

8a CONTRACT OR GRANT NO.	9a ORIGINATOR'S REPORT NUMBER(S)
F04701-68-C-0183 C/O No. 10	WDL Publication No. UG-4851
b. PROJECT NO.	
c	9b OTHER REPORT NO(S) (Any other numbers that may be assigned this report)
d	SAMSO-TR-70-367

10 AVAILABILITY/LIMITATION NOTICES This document may be further distributed by any holder only with specific prior approval of the Space and Missile Systems Organization (SMYSE), Norton AFB, California 92409.

11 SUPPLEMENTARY NOTES The distribution of this report is limited because it contains technology requiring strict approval of all disclosures by SAMSO.

12 SPONSORING MILITARY ACTIVITY
Space and Missile Systems Organization
Deputy for Re-entry Systems
Air Force Systems Command
Norton Air Force Base, California

13 ABSTRACT

This final report is the culmination of a 16 week effort, the Advanced 3D Fabrication Techniques Program (A(3D)FT), executed by Philco-Ford Corporation. The fundamental objective of A(3D)FT was to prove the feasibility of fabricating a relatively large, cone-frustum shaped, ablative, antenna window from a 3D quartz yarn reinforced, silica material. This material, AS-3DC, is a further development of AS-3DX which was developed on previous programs. AS-3DX antenna windows are small and fabricated from simple, block-shape billets. The large, cone frustum-shaped, antenna window developed here represent a substantial advance in the state of the art.

The program objectives were successfully fulfilled. Three full-scale AS-3DC frusta were woven, impregnated, machined, and the resulting parts characterized. The data indicate a superior ceramic antenna window material would ultimately result. Areas for improvement were identified and recommendations made for any subsequent development of the material.

This report documents all the tasks which were accomplished. A design data package is included. The design data are representative of AS-3DC in its initial phase of development and improvement is a certainty for subsequent AS-3DC frusta (unclassified).

DD FORM 1 JAN 64 1473

UNCLASSIFIED

Security Classification

14 KEY WORDS	LINK A		LINK B		LINK C	
	ROLE	WT	ROLE	WT	ROLE	WT

INSTRUCTIONS

1. ORIGINATING ACTIVITY: Enter the name and address of the contractor, subcontractor, grantee, Department of Defense activity or other organization *(corporate author)* issuing the report.

2a. REPORT SECURITY CLASSIFICATION: Enter the overall security classification of the report. Indicate whether "Restricted Data" is included. Marking is to be in accordance with appropriate security regulations.

2b. GROUP: Automatic downgrading is specified in DoD Directive 5200.10 and Armed Forces Industrial Manual. Enter the group number. Also, when applicable, show that optional markings have been used for Group 3 and Group 4 as authorized.

3. REPORT TITLE: Enter the complete report title in all capital letters. Titles in all cases should be unclassified. If a meaningful title cannot be selected without classification, show title classification in all capitals in parenthesis immediately following the title.

4. DESCRIPTIVE NOTES: If appropriate, enter the type of report, e.g., interim, progress, summary, annual, or final. Give the inclusive dates when a specific reporting period is covered.

5. AUTHOR(S): Enter the name(s) of author(s) as shown on or in the report. Enter last name, first name, middle initial. If military, show rank and branch of service. The name of the principal author is an absolute minimum requirement.

6. REPORT DATE: Enter the date of the report as day, month, year, or month, year. If more than one date appears on the report, use date of publication.

7a. TOTAL NUMBER OF PAGES: The total page count should follow normal pagination procedures, i.e., enter the number of pages containing information.

7b. NUMBER OF REFERENCES: Enter the total number of references cited in the report.

8a. CONTRACT OR GRANT NUMBER: If appropriate, enter the applicable number of the contract or grant under which the report was written.

8b, 8c, & 8d. PROJECT NUMBER: Enter the appropriate military department identification, such as project number, subproject number, system numbers, task number, etc.

9a. ORIGINATOR'S REPORT NUMBER(S): Enter the official report number by which the document will be identified and controlled by the originating activity. This number must be unique to this report.

9b. OTHER REPORT NUMBER(S): If the report has been assigned any other report numbers *(either by the originator or by the sponsor)*, also enter this number(s).

10. AVAILABILITY/LIMITATION NOTICES: Enter any limitations on further dissemination of the report, other than those imposed by security classification, using standard statements such as:

(1) "Qualified requesters may obtain copies of this report from DDC."

(2) "Foreign announcement and dissemination of this report by DDC is not authorized."

(3) "U. S. Government agencies may obtain copies of this report directly from DDC. Other qualified DDC users shall request through

_____."

(4) "U. S. military agencies may obtain copies of this report directly from DDC. Other qualified users shall request through

_____."

(5) "All distribution of this report is controlled. Qualified DDC users shall request through

_____."

If the report has been furnished to the Office of Technical Services, Department of Commerce, for sale to the public, indicate this fact and enter the price, if known.

11. SUPPLEMENTARY NOTES: Use for additional explanatory notes.

12. SPONSORING MILITARY ACTIVITY: Enter the name of the departmental project office or laboratory sponsoring *(paying for)* the research and development. Include address.

13. ABSTRACT: Enter an abstract giving a brief and factual summary of the document indicative of the report, even though it may also appear elsewhere in the body of the technical report. If additional space is required, a continuation sheet shall be attached.

It is highly desirable that the abstract of classified reports be unclassified. Each paragraph of the abstract shall end with an indication of the military security classification of the information in the paragraph, represented as *(TS)*, *(S)*, *(C)*, or *(U)*

There is no limitation on the length of the abstract. However, the suggested length is from 150 to 225 words.

14. KEY WORDS: Key words are technically meaningful terms or short phrases that characterize a report and may be used as index entries for cataloging the report. Key words must be selected so that no security classification is required. Identifiers, such as equipment model designation, trade name, military project code name, geographic location, may be used as key words but will be followed by an indication of technical context. The assignment of links, rules, and weights is optional

GPO 885-551